



Development and Semi-Automated Analysis of an *in vitro* Dissemination Model
for Myeloma Cells Interacting with Mesenchymal Stromal Cells

Entwicklung und semi-automatisierte Analyse eines *in vitro* Modells
für die Disseminierung von Myelomzellen in Interaktion mit mesenchymalen Stromazellen

Doctoral Thesis for a Doctoral Degree

at the

GRADUATE SCHOOL OF LIFE SCIENCES,
JULIUS-MAXIMILIANS-UNIVERSITÄT WÜRZBURG,
SECTION BIOMEDICINE

submitted by

Martin Kuric

from

Bad Neustadt a.d. Saale

Würzburg, 2024

Submitted on:
Office stamp

Members of the *Promotionskomitee*:

Chairperson: Prof. Dr. Uwe Gbureck
Primary Supervisor: Prof. Dr. rer. nat. Regina Ebert
Supervisor (Second): Prof. Dr. med. Franziska Jundt
Supervisor (Third): Prof. Dr. rer. nat. Torsten Blunk

Date of Public Defense:

Date of Receipt of Certificates:

This work was conducted at the Department of Musculoskeletal Tissue Regeneration (Bernhard-Heine-Centre for Locomotive Research), University of Würzburg from 08.04.2018 to 31.03.2024 under the supervision of Prof Dr. rer. nat. Regina Ebert.

Acknowledgements

I hereby thank these persons in no particular order:

Doris Schneider for her assistance in laboratory work.

Regina Ebert for her support and guidance. Her patience made plotastic possible.

My partner, Marie-Nicole Kobsar for her encouragement throughout the whole PhD process.

My family for their support and encouragement throughout my complete academic education.

Summary

This thesis integrates biomedical research and data science, focusing on an *in vitro* model for studying myeloma cell dissemination and a Python-based tool, `plotastic`, for semi-automated analysis of multidimensional datasets. Two major challenges are addressed: (1) understanding the early steps of myeloma dissemination and (2) improving data analysis efficiency to address the complexity- and reproducibility bottlenecks currently present in biomedical research.

In the experimental component, primary human mesenchymal stromal cells (hMSCs) are co-cultured with INA-6 myeloma cells to study cell proliferation, attachment, and detachment via time-lapse microscopy. Key findings reveal that detachment often follows cell division, predominantly driven by daughter cells. Novel separation techniques were developed to isolate myeloma subpopulations for further characterization by RNAseq, cell viability, and apoptosis assays. Differential expression of adhesion and retention factors upregulated by INA-6 cells correlates with patient survival. Overall, this work provides insights into myeloma dissemination mechanisms and identifies genes that potentially counteract dissemination through adhesion, which could be relevant for the design of new therapeutics.

To manage complex data, a Python-based software named `plotastic` was developed that streamlines analysis and visualization of multidimensional datasets. `plotastic` is built on the idea that statistical analyses are performed based on how the data is visualized. This approach not only simplifies data analysis, but semi-automates analysis in a standardized statistical protocol. The thesis becomes a case study as it reflects on the application of `plotastic` to the *in vitro* model, demonstrating how the software facilitates rapid adjustments and refinements in data analysis and presentation. Such efficiency is crucial for handling semi-big data transparently, which —despite being manageable— is complex enough to complicate analysis and reproducibility.

Together, this thesis illustrates the synergy between experimental methodologies and advanced data analysis tools. The *in vitro* model provides a robust platform for studying myeloma dissemination, while `plotastic` addresses the need for efficient data analysis. Combined, they offer a comprehensive approach to handling complex experiments, advancing both cancer biology and research practices, in support of exploratory and transparent analysis of challenging phenomena.

Zusammenfassung

Diese Doktorarbeit integriert biomedizinische Forschung und Datenwissenschaften und konzentriert sich auf ein *in vitro*-Modell zur Untersuchung der Dissemination von Myelomzellen sowie ein Python-basiertes Werkzeug, *plotastic*, zur semi-automatisierten Analyse multidimensionaler Datensätze. Zwei Hauptprobleme werden bearbeitet: (1) das Verständnis der frühen Schritte der Myelomdissemination und (2) die Verbesserung der Effizienz der Datenanalyse, um die derzeit in der biomedizinischen Forschung vorhandenen Engpässe bezüglich Komplexität und Reproduzierbarkeit zu adressieren.

Im experimentellen Teil werden primäre menschliche mesenchymale Stromazellen (hMSCs) mit INA-6-Myelomzellen kokultiviert, um Zellproliferation, Anhaftung und Ablösung mittels Zeitraffer-Mikroskopie zu untersuchen. Zentrale Erkenntnisse zeigen, dass die Ablösung oft auf die Zellteilung folgt und vorwiegend von Tochterzellen angetrieben wird. Neue Trennungstechniken wurden entwickelt, um Myelom-Subpopulationen für weitere Charakterisierungen durch RNAseq, Zellviabilität und Apoptose-Assays zu isolieren. Die differentielle Expression von Adhäsions- und Retentionsfaktoren, die durch INA-6 Zellen hochreguliert werden, korreliert mit dem Überleben der Patienten. Insgesamt liefert diese Arbeit Einblicke in die Mechanismen der Myelomdissemination und identifiziert Gene, die potenziell die Dissemination durch Adhäsion konterkarieren könnten, was für die Entwicklung neuer Therapeutika relevant sein könnte.

Zur Verwaltung komplexer Daten wurde eine Python-basierte Software namens *plotastic* entwickelt, welche die Analyse und Visualisierung multidimensionaler Datensätze optimiert. *plotastic* basiert auf der Idee, dass statistische Analysen basierend darauf durchgeführt werden, wie die Daten visualisiert werden. Dieser Ansatz vereinfacht nicht nur die Datenanalyse, sondern automatisiert sie auch teilweise in einem standardisierten statistischen Protokoll. Die Arbeit wird zu einer Fallstudie, da sie die Anwendung von *plotastic* auf das *in vitro*-Modell reflektiert und zeigt, wie die Software schnelle Anpassungen und Verfeinerungen in der Datenanalyse und -präsentation erleichtert. Eine solche Effizienz ist entscheidend für den transparenten Umgang mit Semi-Big-Data, die trotz ihrer Handhabbarkeit komplex genug ist, um die Analyse und Reproduzierbarkeit zu erschweren.

Zusammengefasst veranschaulicht diese Dissertation die Synergie zwischen experimentellen Methoden und fortgeschrittenen Werkzeugen der Datenanalyse. Das *in vitro*-Modell bietet eine robuste Plattform für die Untersuchung der Myelomdissemination, während *plotastic* den Bedarf an effizienter Datenanalyse adressiert. Zusammen bieten sie einen umfassenden Ansatz für die Bearbeitung komplexer Experimente, fördern sowohl die Krebsbiologie als auch die Forschungspraktiken und unterstützen die explorative und transparente Analyse herausfordernder Phänomene.

Contents

Summary / Zusammenfassung	ii
Abbreviations	vi
Introduction	1
Multiple Myeloma and Other Monoclonal Gammopathies	2
Dissemination of Myeloma Cells	3
Retention of Myeloma Cells in the Bone Marrow	4
Release of Myeloma Cells from the Bone Marrow	5
MSCs: Mesenchymal Stromal (Stem) Cells	6
Molecular Interactions between MSCs Myeloma Cells	8
Multidimensional Data in Biomedical Research	11
Nontransparencies in Biomedical Data Analyses	12
Semi-Big Data: Big Enough to Cause Problems	13
The Shortcomings of Common Biomedical Analysis Tools	14
Modern Standards of Software Development	16
What makes Python an “Easy” Programming Language?	18
The Potential of Python Data Science Packages for Biomedicine	23
Aims	26
Chapter 1: Modelling Myeloma Dissemination <i>in vitro</i>	27
Abstract	27
Introduction	28
Materials and Methods	30
Results	34
Discussion	50
Chapter 2: Semi-Automating Data Analysis with <code>plotastic</code>	54
Abstract	54
Introduction	55
Statement of Need	57
Example	58
Overview	60
Discussion	62
Summarising Discussion	67
How Exploratory Live-Cell Imaging Transformed the Research Focus	67
Potential and Challenges of Image Cytometry	69
Technical Considerations for Image Cytometry	71
Conclusion 1: Harnessing Automation and Image Cytometry for Advanced Insights into INA-6 and hMSC Dynamics	72
Novel Methods of Isolating Adhering Subpopulations	74
Dynamic Regulation of Adhesion Factors During Dissemination	74
Subsets of Adhesion Factors Contribute To Different Steps of Adhesion	76
What Triggers Release: One Master Switch, Many Small Switches, or is it just Random?	76
Outlook: High-Value Research Topics for Myeloma Research Arising from this Work	77
Conclusion 1: Cancer & Myeloma & Dissemination is bad	78

Semi-Automation was Critical for Establishing <i>in vitro</i> Methods	79
plotastic Exceled in Re-Doing Statistical Analyses and Plots	81
Conclusion 2: Demonstrating the Advantages of Semi-Automation in Biomedical Research Methodologies	83
References	85
Appendices	104
A Supplementary Data & Methods	104
A.1 Figures	104
A.2 Tables	123
A.3 Materials & Methods	131
B Documentation of plotastic	147
B.1 Class Diagram	148
B.2 Readme	151
B.3 Example Analysis “qpcr”	164
C Submission Forms & Documents	171
C.1 Author Contributions	171
C.2 Affidavit	178
C.3 Usage of Generative AI and Other Software	180
C.4 Curriculum Vitae	184

Abbreviations

aMM	asymptomatic Multiple Myeloma	2
BM	Bone Marrow	2
BMME	Bone Marrow Microenvironment	3
BMPC	Bone Marrow Plasma Cell	5
BMSC	Bone Marrow Stromal Cell	4
CM	hMSC-conditioned medium	30
CM-INA6	MSC-Conditioned-Medium-treated INA-6	44
CAM	Cell Adhesion Molecule	4
CLI	Command Line Interface	64
ECM	Extracellular Matrix	4
EMT	Epithelial-Mesenchymal Transition	3
FACS	Fluorescence-Activated Cell Sorting	70
GUI	Graphical User Interface	64
hMSC	human Mesenchymal Stromal Cell	7
LLM	Large Language Model	64
MA	MSC-adhering	39
MSC	Mesenchymal Stromal Cell	6
MGUS	Monoclonal Gammopathy of Undetermined Significance	2
MM	Multiple Myeloma	2
MMR	Multiple Myeloma Relapse	3
MBD	Multiple Myleoma related Bone Disease	9
nMA	non-MSC-adhering	39
OS	Overall Survival	47
PCL	Plasma Cell Leukemia	2
PFS	Progression-Free Survival	47
SP	Solitary Plasmacytoma	2
SASP	Senescence-Associated Secretory Phenotype	9

Introduction

Multiple Myeloma and Other Monoclonal Gammopathies

Multiple Myeloma (MM) is a hematological malignancy characterized by the clonal expansion of malignant plasma cells primarily within multiple sites of the Bone Marrow (BM). This cancer arises from plasma cells, the antibody-producing cells of the immune system, which undergo malignant transformation resulting in uncontrolled growth and disruption of normal bone marrow function (P. Yang et al., 2022). The prevalence of multiple myeloma has tripled across both Europe and USA from 1980 to 2014 due to an ageing population (Ocias et al., 2016; Turesson et al., 2018). For 2024, 35780 new MM cases and 12540 deaths are estimated for the USA alone (Siegel et al., 2024).

To understand the progression of a healthy plasma cell to MM, one can review other *monoclonal gammopathies*. These are defined by the presence of monoclonal immunoglobulin in the blood serum which is indicative of abnormal plasma cell clones overexpressing the same type of dysfunctional antibody. (Kyle, 1997; Fermand et al., 2018). When no further disease manifestations are present, the condition is termed *Monoclonal Gammopathy of Undetermined Significance* (MGUS), which is the most commonly diagnosed monoclonal gammopathy (Kyle, 1997). MGUS has a 1-5 % annual risk of progression to MM (Rajkumar et al., 2014).

To distinguish MM from other monoclonal gammopathies, diagnosis of MM requires not only identification of a minimum of clonal plasma cells, but also a *myeloma defining event* which is evidence of malignancy or end-organ damage, such as hypercalcemia, renal insufficiency, anemia, or bone lesions (Rajkumar et al., 2014). A localized smaller¹ mass of clonal plasma cells together with a singular primary bone lesion is diagnosed as Solitary Plasmacytoma (SP). SP can progress to MM in 32 % of cases with a median follow-up of 9.7 years (Thumallapally et al., 2017; S. Gao et al., 2024). Studies from Kyle (1997) show that SP cases are rare, constituting only 2.5 % of monoclonal gammopathy diagnoses, whereas MM represent 18 %. Another rare precursor of MM is *smouldering* or *asymptomatic Multiple Myeloma* (aMM), representing 3 % of monoclonal gammopathies (Kyle, 1997). aMM is diagnosed when no myeloma defining event is detected, although the quantities of clonal plasma cells or monoclonal protein align with respective criteria for MM diagnosis. (Rajkumar et al., 2014). Recent reports show that if left untreated, 72 % of aMM patients progress to MM, whereas early treatment can lower the progression rate to 11 % within up to 7.6 years until last follow-up² (Abdallah et al., 2024; Mateos María-Victoria et al., 2013). MM itself can progress to advanced stages, such as *extramedullary involvement/disease* which describes colonization of soft tissues outside the bone marrow (Bladé et al., 2022), but also Plasma Cell Leukemia (PCL) which is characterized by high

¹Rajkumar et al. (2014): “Solitary plasmacytoma with 10 % or more clonal plasma cells is regarded as multiple myeloma. [...] If bone marrow has less than 10 % clonal plasma cells, more than one bone lesion is required to distinguish [MM] from solitary plasmacytoma with minimal marrow involvement.”

²For non-high risk aMM patients, treatment lowered MM progression rate to 9 %, compared to 31 % for untreated patients (within up to 6.7 and 7.6 years of follow-up, respectively). For high-risk aMM patients, treatment lowered aMM progression rate to 11 %, compared to 72 % for untreated patients (within up to 5.2 years of follow-up and median time to progression of 2.2 years, respectively) (Abdallah et al., 2024).

levels of circulating plasma cells (Jung & Lee, 2022). However, the most common cause of death is renal failure during the MM stage, caused by excess immunoglobulins or hypercalcemia due to bone degradation (Kundu et al., 2022).

With a 5-year survival rate of 50% (Turesson et al., 2018), MM can be considered incurable and deadly. MM relapses within the first year in 16% of patients [Multiple Myeloma Relapse (MMR)], others face relapse at a later time or only continued response to treatment (Majithia et al., 2016). Although treatments have improved, the age-adjusted mortality rate of MM has decreased from 1999 to 2020 by only -1.6% (Doddi & Rashid, 2024). Engelhardt et al. (2024) describes the current standard care for transplant-eligible newly diagnosed MM patients as follows: Induction with a CD38 antibody, proteasome inhibitor, immunomodulatory drug, and dexamethasone, potentially followed by bone marrow transplantation and lenalidomide maintenance (Rajkumar & Kumar, 2020). A major challenge to these treatments is the continued cycle of remission and relapse, with each relapse generally being harder to treat (Podar & Leleu, 2021). Development of such resistance is well described in the literature, often arising from the intraclonal genetic heterogeneity within the myeloma cell population and the protective niche provided by the Bone Marrow Microenvironment (BMME) (Solimando et al., 2022).

Dissemination of Myeloma Cells

As the name suggests, *multiple* myeloma involves spreading of clonal plasma cells in multiple sites within the body, a process that's described with the term *dissemination*. Although a single large plasmacytoma is still classified as MM (Rajkumar et al., 2014), the presence of multiple tumor lesions within the BM is very common. More than one or 25 such lesions predict poor prognosis for asymptomatic and symptomatic MM patients, respectively (Kastritis et al., 2014; Mai et al., 2015). Additionally, MM cells can disseminate to extramedullary sites of virtually any tissue, highlighting MM as a systemic disease with potential multi-organ impact (Rajkumar & Kumar, 2020; Bladé et al., 2022). Hence, dissemination is a major contributor to MM progression and poor prognosis, enabling MM cells to colonize new niches that favor survival, quiescent states or are less accessible for therapy, especially with high subclonal heterogeneity (Forster & Radpour, 2022; Keats et al., 2012).

Dissemination of MM is reminiscent of *metastasis*, a term typically associated with solid tumors describing the spread of cancer cells to distant sites. However, it substantially differs from metastasis due to the hematological or “liquid” nature of MM. Long-lived plasma cells originate from migratory B-cells, negating the need for extensive transformative processes such as Epithelial-Mesenchymal Transition (EMT), which is required for escaping tightly connected solid tissues to enter the bloodstream (Ribatti et al., 2020). Although referred to as “liquid tumor”, MM cells still accumulate as distinct foci within the bone marrow, somewhat mirroring the localized growth of solid tumors. This characteristic has led to MM being proposed as a model for studying solid “micrometastases” (Ghobrial, 2012), highlighting its unique blend of liquid and solid tumor properties and providing insights

into the mechanisms of cancer dissemination and colonization of new niches.

The exact mechanism of MM dissemination is not entirely understood. Nevertheless, attempts to structure this process have been made by Zeissig et al. (2020), describing MM dissemination in five steps:

1. Retention in the BM
2. Release from the BM
3. Intravasation
4. Extravasation
5. Colonization.

According to Zeissig et al. (2020), MM dissemination begins with MM cells overcoming retention and adhesion within the BMME. Following release, MM cells undergo *intravasation* into the bloodstream, where they can circulate before extravasating into new BM sites. This migration is directed by chemokines and growth factors produced by BM cells. For instance, CXCL12 and IGF-1 are critical in guiding MM cells back to the BM, a process called *homing* (Vande Broek et al., 2008). In the BM they can *colonize* and form new tumor foci.

The review by Zeissig et al. (2020) implies a sequential order of such steps, yet direct proof of this is lacking. Still, the review provides a framework that integrates multiple complex research topics into one coherent context. For instance, Zeissig et al. (2020) states that two adhesive processes are critical for successful dissemination: Lowered adhesion to the BM, but increased adhesion to the endothelium to initiate extravasation (Asosingh et al., 2001; Mrozik et al., 2015). This alone implies stringent separation of different adhesive processes during the dissemination process. Given that Cell Adhesion Molecules (CAMs) have become attractive targets for treating MM (Bou Zerdan et al., 2022; Katz, 2010), such detailed understanding of cell adhesion is crucial for developing successful therapies.

Retention of Myeloma Cells in the Bone Marrow

According to Zeissig et al. (2020), overcoming retention and adhesion to the BME is critical to MM dissemination. Retention of plasma cells to the BME is mediated by multiple mechanisms, which are categorized here into *direct adhesion*, *soluble survival factors* and *chemotaxis*. A fourth notable mechanism is the physical boundary that is bone tissue and Extracellular Matrix (ECM), which could become important for MM dissemination once degradation of bone tissue has progressed.

Direct adhesion of MM cells to the BM is mediated through ECM components and cell adhesion to other BM resident cells like osteoblasts, osteoclasts and Bone Marrow Stromal Cells (BMSCs) (Teoh & Anderson, 1997; Bou Zerdan et al., 2022). ECM components include fibronectin, collagens, and proteoglycans such as decorin (Hu et al., 2021; Huang et al., 2015; Katz, 2010; Kibler et al., 1998). BMSCs are vital in this niche, supporting cell adhesion through CAMs but also by secretion of (ECM)

components (Katz, 2010). Such adhesion acts both as physical anchorage but also provides signaling cues for growth, survival, and drug resistance (Chauhan et al., 1996). A classic example is the binding of MM cell integrins to VCAM-1 on BMSCs, such as $\alpha 4\beta 1$ (VLA-4) (Bou Zerdan et al., 2022). Since direct adhesion promotes both retention and tumour growth, it could play an ambiguous role during MM dissemination.

Soluble survival factors contribute to BM retention, since plasma cells can not survive outside the bone marrow without them. For example, deleting BCMA — a receptor for survival factors — leads to loss of Bone Marrow Plasma Cells (BMPCs) due to unsustained maintenance of cell survival (O'Connor et al., 2004). Soluble survival factors include IL-6, IGF-1, BAFF, APRIL, and VEGF, although IGF-1 has proven to be the primary survival factor (Sprynski et al., 2009). These signals are secreted by BMSCs and adipocytes (Kibler et al., 1998; García-Ortiz et al., 2021). *Chemotaxis* is also crucial for BM retention (T. R. Ullah, 2019). CXCL12 and CXCL8 are soluble chemotactic signals produced by BMSCs and attract MM cells, but also primes their cytoskeleton and integrins for adhesion (Aggarwal et al., 2006; Alsayed et al., 2007). Roccaro et al. (2015) demonstrated that inhibiting CXCR4 — the receptor of CXCL12 — with the monoclonal antibody Ulocuplumab decreased MM cell homing to the BM and reduced dissemination via factors associated with EMT. Consequently, CXCL12/CXCR4 signaling has emerged as a promising target of several treatments aiming at preventing myeloma cell migration, as reviewed by Ito et al. (2021) who conclude a need for further studies to develop combined therapies explicitly against tumor cell dissemination.

Together, BMSCs play a critical role in MM retention, providing direct adhesion, soluble survival factors, and chemotactic signals.

Release of Myeloma Cells from the Bone Marrow

Zeissig et al. (2020) describes the release of myeloma cells from the BMME as all steps required for overcoming bone marrow retention, but also putative triggers leading to migration out of the BME. To the author's knowledge, release of MM cells is the least understood among disseminative processes. Still, in order to gain understanding of how MM dissemination is initiated, one can summarize reports that could be involved.

Studies suggest that CAMs expression indeed plays a role in MM dissemination. For instance, studies demonstrate that circulating MM cells exhibit reduced levels of integrin $\alpha 4\beta 1$, in contrast to those located in the BM (Paiva et al., 2013, 2011). Given that dissemination can be induced in mice by overexpressing the CAM shedding protease heparanase (Y. Yang et al., 2005), it seems reasonable that dynamic loss of adhesive strength is causing release of MM cells from the BM. Another useful comparison is that of CAMs expression at different disease stages, indicative of their role in disease progression, which in turn could serve as a proxy for disseminative potential. For example, Terpos et al.

(2016) reported an increase in adhesion molecule expression of ICAM-1 and VCAM-1 in patients with MM compared to those with MGUS and aMM. However, Pérez-Andrés et al. (2005) reported that CD40 is downregulated in PCL patients, hence, different CAMs could serve ambiguous roles in MM progression. Together, the regulation of CAMs can depend on both momentary microenvironmental factors, but also on the stage of the disease, while the specific stimuli regulating their expression are not fully defined. A study from Akhmetzyanova et al. (2020) presents CD138 (*aka* Syndecan-1) as a potential *switch* between adhesion and release, as mice treated with CD138 blocking antibodies exhibited rapid mobilization of MM cells from the BM to peripheral blood, confirming that alterations in adhesion molecule expression are sufficient to cause MM cell release. Brandl et al. (2022) builds on that finding, showing that JAM-C inversely correlates with CD138 expression while promoting MM progression in a mouse model.

Another often overlooked requirement for MM cell release is the need for independence from essential growth and survival signals provided by BMSC. Autocrine signaling has been proposed as a key mechanism through which myeloma cells gain independence from essential survival factors such as IL-6 (Frassanito et al., 2001; Urashima et al., 1995). Autocrine signaling could also disrupt responsiveness to Mesenchymal Stromal Cell (MSC)-derived chemotactic signals, since MM cells from BM biopsies were shown to express CXCL12 under hypoxic conditions induced by HIF-2 α (Martin et al., 2010). Since MM niches turn increasingly hypoxic and circulating myeloma cells upregulate hypoxia associated genes, hypoxia is a promising factor for understanding the release of MM (Garcés et al., 2020).

The degradation of bone tissue could also play a critical role in myeloma cell release by eliminating adhesive anchorage within the ECM, considering that ECM is remodeled even at the MGUS stage Glavey et al. (2017). This degradation is part of a ‘vicious cycle’ that is well described in osteotropic cancer types and is the key pathway of bone destruction, dissolving bone-resident growth factors like TGF- β that further drive tumor growth (Harada et al., 2021; Siclari et al., 2007; Wang et al., 2019). Notably, it is reasonable to assume that bone destruction drives dissemination by removing physical barriers, yet such concept was not proven yet.

In summary, the release of MM cells from the BM is a complex process that involves dynamic regulation of CAMs, autocrine signaling, and hypoxia, but also the degradation of bone tissue. These processes are not fully understood and require further investigation to formulate strategies that prevent uncontrolled spread of MM cells and support modern therapies.

MSCs: Mesenchymal Stromal (Stem) Cells

The previous sections mentioned MSCs several times as BMSCs, being a crucial component of the BMME in the context of multiple myeloma (Mangolini & Ringshausen, 2020). Before discussing their

role in MM specifically, it is important to understand what an MSC is and what impact this cell type has on biomedical research.

Explaining what an MSC is, can be challenging. MSCs are derived from multiple different sources, serve a wide array of functions and are always isolated as a heterogenous group of cells. This makes it particularly challenging to find a consensus on their exact definition, nomenclature, exact function and *in vivo* differentiation potential. Therefore, the following paragraphs provide a brief overview of the biology of MSCs set within a historical context.

MSCs first gained popularity as a stem cell. Stem cells lay the foundation of multicellular organisms. Embryonic stem cells orchestrate the growth and patterning during embryonic development, while adult stem cells are responsible for regeneration during adulthood. The classical definition of a stem cell is that of a relatively undifferentiated cell that divides asymmetrically, generating one daughter cell with maintained stemness, and one differentiated daughter cell (Cooper, 2000; Shenghui et al., 2009). Because of their significance in biology and regenerative medicine, stem cells have become a prominent subject in modern research. human Mesenchymal Stromal Cells (hMSCs) have been presented as promising candidate in the context of regeneration, given that they feature also intriguing immunomodulatory capabilities, easy isolation and *in vitro* expansion, and safety for both autologous and allogeneic transplantation (I. Ullah et al., 2015).

Mesenchyme first appears in embryonic development during gastrulation. There, cells that are committed to a mesodermal fate, lose their cell junctions and exit the epithelial layer in order to migrate freely. This process is called epithelial-mesenchymal transition (Tam & Beddington, 1987; Nowotschin & Hadjantonakis, 2010). Hence, the term mesenchyme describes non-epithelial embryonic tissue differentiating into mesodermal lineages such as bone, muscles and blood. Interestingly, it was shown nearly twenty years earlier that cells within adult bone marrow seemed to have mesenchymal properties as they were able to differentiate into bone tissue (A. J. Friedenstein et al., 1966; A. Friedenstein & Kuralesova, 1971; Bianco, 2014). This was the origin of the “*mesengenic process*”-hypothesis: This concept states that mesenchymal stem cells serve as progenitors for multiple mesodermal tissues (bone, cartilage, muscle, marrow stroma, tendon, fat, dermis and connective tissue) during both adulthood and embryonic development (A. Caplan, 1991; A. I. Caplan, 1994). The mesenchymal nature of these cells (termed bone marrow stromal cells: BMSCs) was confirmed later when they were shown to differentiate into adipocytic (fat) and chondrocytic (cartilage) lineages (Pittenger et al., 1999). Since then, the term “*mesenchymal stem cell*” (MSC) has grown popular as an adult multipotent precursor to a couple of mesodermal tissues. MSCs derived from bone marrow (BMSCs) were shown to differentiate into osteocytes, chondrocytes, adipocytes and cardiomyocytes (Gronthos et al., 1994; Muruganandan et al., 2009; Xu et al., 2004). Most impressively, these cells also exhibited ectodermal and endodermal differentiation potential, as they produced neuronal cells, pancreatic cells and hepatocytes (Barzilay et al., 2009; Wilkins et al., 2009; Gabr et al., 2013; Stock et al., 2014).

It was later established that cultures with MSC-like properties can be isolated from ‘*virtually every post-natal organs and tissues*’, and not just bone marrow (da Silva Meirelles et al., 2006). However, depending on which tissue they originated from, MSCs can differ greatly in their transcription profile and *in vivo* differentiation potential (Jansen et al., 2010; Sacchetti et al., 2016).

Since MSCs are a heterogenous group of cells, they were defined by their *in vitro* characteristics. A minimal set of criteria are the following (Dominici et al., 2006): First, MSCs must be plastic adherent. Second, they must express or lack a set of specific surface antigens (positive for CD73, CD90, CD105; negative for CD45, CD34, CD11b, CD19). Third, MSCs must differentiate to osteoblasts, adipocytes and chondroblasts *in vitro*. Together, MSCs exhibit diverse differentiation potentials and can be isolated from multiple sources of the body.

Today, the potential in MSCs lies not their stemness, but rather in their immunomodulatory capabilities, which could be the reason why conventionally the ‘S’ in MSC stands for *Stromal* instead of *Stem*. Although, MSCs are not yet established in routine clinical practice — despite thousands of clinical trials covering most of the human body’s organs —, they still are among the most studied cell types and are topic of vast research (Abdelrazik, 2023). MSCs are valued for their very high treatment tolerance, but also as an adaptive platform for modifications to improve their therapeutic effects (D’souza et al., 2015). For example, Chen & Zhou (2022) boldly announced the translation of modified MSCs into the clinical practice of treating ischemic strokes, whereas Moñivas Gallego & Zurita Castillo (2024) conclude that *further studies are needed*, a statement that’s ubiquitous in publications on MSCs based therapies³. Still, many fields of research benefit from this vast general understanding of MSCs biology, including this work and the study of the BMME in the context of cancer pathologies such as MM.

Molecular Interactions between MSCs Myeloma Cells

As mentioned in previous sections, MSCs are key drivers of MM progression through mediating retention and survival of MM cells in the bone marrow through e.g. cell adhesion and chemoattraction (Zeissig et al., 2020). However, BMSCs play a far more complex role in the overall pathology of MM (Mangolini & Ringshausen, 2020). Since bone tissue represents a sturdy physical barrier that MM cells might have to overcome to disseminate, it is crucial to revisit the impact that myeloma cells leave on the BMME.

In healthy bone tissue, there’s an equilibrium between bone formation and degradation to maintain turnover, repair and remodelling. (Väänänen, 1993): Mesenchymal stromal cells (BMSCs) differentiate into bone forming osteoblasts, while bone degrading osteoclasts are derived from hematopoietic stem

³Abdelrazik (2023): “*Altogether, the articles published in this Special Issue raise more questions than they answer, given that most of the conclusions carry the statement ‘further studies are needed’.*”

cells. Myeloma cells shift the equilibrium of bone turnover towards degradation, leading to Multiple Myleoma related Bone Disease (MBD) (Hideshima et al., 2007). MBD is present in 80% of patients at diagnosis and is characterized by osteolytic lesions, osteopenia and pathological fractures (Terpos et al., 2018).

MM cells establish this shift in bone turnover on multiple levels: They directly stimulate osteoclast activity by secreting MIP1 α (Oba et al., 2005), but also indirectly through reprogramming BMSCs by having them produce osteoclast stimulating factor RANKL (Tsubaki et al., 2020). This is mediated by NF- κ B signaling, a pathway that's crucial for MM pathology which is activated through direct cell-cell contact between myeloma cells and BMSCs via e.g. VCAM1 (Cippitelli et al., 2023; Roy et al., 2018). NF- κ B is activated in both myeloma cells and BMSCs, but with different outcomes: In myeloma cells, NF- κ B transduces survival signaling (Roy et al., 2017). BMSCs however react with stress-induced senescence and secretion of multiple factors that drive MM pathology, such as RANKL and components of the Senescence-Associated Secretory Phenotype (SASP) (Chauhan et al., 1996; Fairfield et al., 2020).

Another fundamental factor contributing to bone destruction is the suppression of osteogenic differentiation of BMSCs by myeloma cells: MM cells secrete DKK1, which inhibits Wnt signaling that otherwise induces the key osteogenic transcription factor RUNX2 (Gaur et al., 2005; Qiang et al., 2008; F. Zhou et al., 2013). Instead, BMSCs are driven towards the adipogenic lineage MM by VCAM1 signaling, with MM cells stabilizing the adipogenic transcription factor PPAR- γ (Dotterweich et al., 2016; Liu et al., 2020). Furthermore, MM inhibit osteogenic differentiation of BMSCs on an epigenetic level (Allegra et al., 2022). Key mediator GFI1, a zinc finger protein activated by TNF- α which recruits the chromatin modifier HDAC1 to the promoter of RUNX2 (D'Souza et al., 2011; Adamik et al., 2017). Intriguingly, the same group was able to prevent activation of GFI1 and rescue osteogenic differentiation by inhibition of p62, an adapter protein involved in autophagy that bridges several signaling pathways, including NF- κ B (Adamik et al., 2018). Teramachi et al. (2016) previously treated mice with the same inhibitor XRK3F2, which resulted in bone formation restricted to MM containing bones. This approach is intriguing, since NF- κ B has remained an untreatable target given its ubiquitous role in cell survival. However, a review by Verzella et al. (2022) clearly disagrees with this notion⁴, shifting the focus onto upstream activators and downstream effectors of NF- κ B signaling, a principle that was exemplified by the work of Adamik et al. (2018) on the GFI1/p62 interface. This requires a thorough characterization of the transcriptional programs elicited by NF- κ B signaling in MM cells and BMSCs, especially during direct cell adhesion.

Overall, MSCs are pivotal within the BMME, serving both structural and responsive roles in MM. NF- κ B signaling, essential in MSC-myeloma interactions, plays a crucial role in myeloma survival and MSC function modification (Cippitelli et al., 2023; Roy et al., 2018). Direct contact is necessary to ac-

⁴Verzella et al. (2022): “Collectively, this bulk of evidence demonstrates that the safe and cancer-selective inhibition of the NF- κ B pathway is clinically achievable and promises profound benefit to patients with NF- κ B-driven cancers”

tivate these pathways, exacerbating MM pathology. Targeting components of NF- κ B signaling offers therapeutic potential, aiming to disrupt key interactions and inhibit myeloma progression. Deeper molecular understanding of the MSC–Myeloma interactions could lead to therapies that effectively target a cancer microenvironment that's driving MM progression.

Multidimensional Data in Biomedical Research

As modern biosciences advance, researchers increasingly encounter datasets that are influenced by a variety of independent variables, such as time, dosage, and environmental conditions. These variables introduce multidimensional complexity into datasets, challenging traditional analysis methods. For instance, cell adhesion studies, which are crucial for understanding cellular interactions and cancer metastasis, often require analyses across multiple time points and varying adhesion molecule concentrations, demonstrating a time-dependent variability that significantly impacts biological interpretations (Rebl et al., 2010; McKay et al., 1997; Bolado-Carrancio et al., 2020).

Multidimensional data encompass datasets where multiple *independent variables* (here referred to as *factors*) can influence one *dependent variables* (*outcomes*) (Krzewinski & Savig, 2013). In biomedicine, dependent variables are often continuous (intervals or ratios), whereas independent variables are often categorical (ordinal or nominal), respectively. Categorical variables comprise discrete values called categories or *levels*, which are assigned to experimental conditions or measurement modalities, for example the factor ‘*time*’ could comprise three levels: ‘0 h’, ‘24 h’, and ‘48 h’. Such setups are attractive, because they are compatible with common hypothesis tests, such as ANOVA etc. (Motulsky, 2018): If the levels of one factor are associated with a different outcome, that factor is considered to have an influence on the dependent variable. Multiple factors address multiple hypotheses, including the influence from each individual factor, but also potential interactions between factors. This makes it crucial to design analysis strategies that can reveal the true structure and value of the data (Krzewinski & Savig, 2013).

A primary example of multidimensional data is multiplex RT-qPCR, where the expression levels of various genes are measured across different samples under varying conditions (Bustin, 2014). Here, the dependent variable is typically the fold change expression values derived from $\Delta\Delta Ct$ calculations (Brankatschk et al., 2012). The independent variables include the genes being measured and the experimental conditions under which the samples are processed.

Microscopy data further illustrate the complexity of multidimensional datasets (Rueden et al., 2017). In this context, the dependent variable might be a quantifiable feature, such as cell count or morphological metrics extracted from image analyses. The independent variables can expand immensely to include factors such as well-plate coordinates in a 96-well plate, Z-positions in confocal microscopy, and time points in time-lapse studies.

Lastly, big-data aggregation tools like Metascape provide a rich source of multidimensional data by integrating various dependent variables, such as gene expression fold changes and associated *p*-values, with independent variables spanning gene identifiers, gene ontology terms, and ontology classes derived from multiple databases (Y. Zhou et al., 2019). Despite the provision of summarized graphical outputs, the raw data often remain in complex, nested formats within Excel sheets, posing significant

challenges for hypothesis-driven research.

This extensive integration of multiple dimensions requires sophisticated visualization and analysis techniques. While basic statistical visualizations suffice for one- or two-dimensional data, more complex data sets necessitate advanced techniques, which allow researchers to visualize and interact with data in ways that elucidate the underlying patterns and relationships (Dunn et al., 2017). However, the gap between available visualization tools and the needs of clinicians or biologists without extensive bioinformatics training remains wide, emphasizing the need for intuitive, user-friendly tools that bridge this knowledge gap and enhance the accessibility of complex data analyses (Dunn et al., 2017).

Nontransparencies in Biomedical Data Analyses

The advent of advanced technologies in biosciences has ushered in an era of *big data*, characterized by unprecedented volumes and complexities of data (Bubendorf, 2001; A. Yang et al., 2017; Ekmekci et al., 2016). This rise has been paralleled by significant challenges in data analysis, particularly impacting the reproducibility of scientific research. Studies such as the Baker (2016) survey revealed that more than 70 % of researchers have tried and failed to reproduce another scientist's experiments, highlighting a reproducibility crisis that questions the reliability of scientific findings (Begley & Ioannidis, 2015; Ioannidis, 2005).

Reproducibility is considered foundational to scientific research, ensuring that findings are reliable and verifiable. Still, its meaning requires precise definition (Goodman et al., 2016). The common understanding of scientific reproduction implies not only that detailed information is provided to enable independent repetition (*transparency*), but also that time and effort is invested into repeating the experiments (*corroboration*). However, since modern biomedical journals are demanding novelty research, and since experiments have become highly specialized and time-intensive, repeating someone else's work is considered neither interesting⁵ nor possible for most publications (Flier, 2022; Peng, 2011). Hence, the meaning of reproducibility is confined to *transparency*, a concept that has been applied to many fields, including clinical trials (Goodman et al., 2016; Committee on Strategies for Responsible Sharing of Clinical Trial Data et al., 2015).

Nevertheless, there is a surprising amount of evidence for nontransparencies in biomedical data analyses: For Microarray-based miRNA profiling, raw data was not reported in more than 40 % of 127 articles, making independent verification impossible (Witwer, 2013). The same study also found that re-analysis of data often times did not support the original conclusions. Furthermore, 44 % of 233 preclinical articles describe statistical tests insufficiently, while few don't describe them at all (Gosselin, 2021). Another study reviewed 147 papers in the field of optometrics and found that

⁵Flier (2022): “There are no scientists with the interest, resources, or incentives to “repeat” or confirm this vast sea of published work, so whether the findings they report are reproducible will simply never be assessed.”

91 % did not discuss their rationale of correcting p -values for multiple comparisons (e.g. Bonferroni correction) (Armstrong, 2014). However, given that the exact use of multiple comparisons corrections has been under debate for decades, it is reasonable to assume that researchers lack the confidence to report their technique in detail (Perneger, 1998; Moran, 2003; Sullivan & Feinn, 2021). In general, p -values are target of extreme scrutiny and also the cause of many arguments, which themselves are of questionable statistical reasoning⁶ (Leek & Peng, 2015). Additionally, statistical illiteracy is a well-known problem among clinicians (Lakhli et al., 2023). Among biomedical researchers, 77 % state that they have not received formal training in data literacy, including visualization and public deposition of data, although they understand its high relevance (Federer et al., 2016). Correspondingly, it has been communicated that there is a lack of intuitive tools to embed computational work into publications, but also a lack of bioinformaticians to translate computation into clinics (Mesirov, 2010; Smith et al., 2018; Gómez-López et al., 2019). Therefore, nontransparencies in biomedical analyses are not only caused by a habit⁷ of insufficient reporting, but could be exacerbated by the confusions caused by currently available methodologies and the lack of proper training.

Semi-Big Data: Big Enough to Cause Problems

Recent advances in big data analysis have significantly improved the standardization of both raw data availability and processing pipelines (Gomez-Cabrero et al., 2014). Particularly in RNAseq analysis, automation and the use of sophisticated software have established standards that enhance reproducibility across studies. For example, tools such as STAR and HISAT for sequence alignment, and Cufflinks and DESeq for differential expression analysis, rely on scripts that standardize processing steps to produce repeatable and verifiable results (Dobin et al., 2013; Kim et al., 2015; Trapnell et al., 2012; Love et al., 2014). These frameworks not only automate data handling but also ensure that data analysis protocols are followed consistently, reducing human error and variability between different users or laboratories.

However, this level of standardization and automation has not been mirrored in the analysis of *semi-big data*. Semi-big data, as introduced in this thesis, describes datasets that are on the cusp of manageability: substantial enough to overwhelm manual analysis methods yet not sufficiently large or uniform to justify the heavy computational frameworks developed for big data. Such data are frequently generated in experiments like automated microscopy or multiplex qPCR, where the scale and complexity of the data can vary significantly depending on the experimental design and objectives (Krzywinski & Savig, 2013).

⁶Leek & Peng (2015): “Arguing about the P value is like focusing on a single misspelling, rather than on the faulty logic of a sentence”

⁷Peng (2011): “[...] old habits die hard, and many will be unwilling to discard the hours spent learning existing systems.”

Researchers often revert to basic tools such as *Microsoft Excel* for analyzing these semi-big datasets (Incerti et al., 2019). While Excel provides familiarity and immediate accessibility, it lacks the sophisticated data handling capabilities necessary for efficient and error-free processing of complex (multi-dimensional) datasets. This reliance on manual methods not only makes the analysis laborious and prone to mistakes but also significantly impedes the reproducibility of research findings. The time and effort required to replicate analyses done manually mean that validating findings from semi-big data can be prohibitively challenging for peer reviewers and other researchers in the field.

Given these challenges, there is a critical need for developing new tools and frameworks specifically tailored for semi-big data. These tools should bridge the gap between the simplicity of user-friendly software like Excel and the robust, script-based automation seen in big data frameworks. By providing standardized, repeatable, and easy-to-use methods for handling complex datasets, such tools could significantly enhance the reliability and efficiency of research involving semi-big data, ultimately supporting broader scientific inquiry and verification.

The Shortcomings of Common Biomedical Analysis Tools

Interactive software systems commonly used for exploratory data analysis in biomedical research often lack mechanisms to track and reproduce the researcher's actions systematically. Even when analysis is performed using scripting languages, the integration of results from multiple packages without a coherent record of the commands and code used undermines reproducibility. This practice can obscure analysis, making it difficult, if not impossible, for other researchers to replicate the results (Leek & Peng, 2015; Peng, 2011; Mesirov, 2010; Localio et al., 2018).

A particularly illustrative example is *GraphPad Prism*, a tool ubiquitously employed across biomedical disciplines for statistical analysis. Despite its widespread use, it does contribute to data analysis nontransparencies due to *Prism*'s closed-source nature and the common journal practice of not requiring detailed methodological transparency in its usage, a practice that is common in biostatistics literature (Gosselin, 2021; Localio et al., 2018). Furthermore, *GraphPad Prism* still requires manual data entry and lacks the robustness and automation necessary for handling multidimensional or semi-big data. Although, *GraphPad Prism* is compatible “*multiple variable tables*”—similar to long-form tables known from Wickham (2014)—, but does not automatically graph these kinds of tables, but only user specified subsets (*GraphPad Prism 10 User Guide*, 2024).

Moreover, *Microsoft Excel*, another staple in data processing in biomedicine, is notoriously inadequate for handling multidimensional data and complex statistical analyses. Its limitations include poor error tracking, absence of change documentation (audit trails), and a propensity for introducing errors that often go unnoticed, such as converting gene names to dates (Ziemann et al., 2016). To compensate for these shortcomings, *Microsoft* has recently integrated a Python interpreter into

Excel, allowing researchers to automate tasks and analyze data efficiently and correctly (Excel, 2023).

Indeed, many common tools in biomedicine allow for scripting or automation to handle semi-big data more effectively. For example, *Fiji/ImageJ*, a popular image processing platform, supports extensive macro and scripting capabilities (Rueden et al., 2017). These features enable researchers to automate batch processing of image data, streamlining tasks that would otherwise require laborious manual input. Similarly, *PyMOL*, a leading tool in protein structural biology, utilizes Python scripting to automate complex tasks, allowing for detailed molecular modeling and visualization that are reproducible and scalable across datasets (*PyMOL*, 2024; Rigsby & Parker, 2016).

Although automation scripts used in tools like *Fiji/ImageJ* and *PyMOL* improve transparency for publishing singular data analysis pipelines, they still face challenges that can impede their reproducibility (Peng, 2011; Sandve et al., 2013): These scripts sometimes require specialized software environments, where setting up dependencies and configurations can be complex enough to discourage replication efforts. Additionally, these scripts do not always provide comprehensive outputs of intermediate steps, which is crucial for verifying and understanding the progression of data analysis (Sandve et al., 2013).

On the other hand, when scripts are designed to be more generalized and distributed—for instance, as a *Fiji/ImageJ* plugin or a standalone application—they can make substantial contributions to scientific research by enabling other researchers to apply these tools to their own data sets (Narzt et al., 1998; Wilkinson et al., 2016). However, this approach also comes with its own set of challenges (Sandve et al., 2013). These generalized tools often lack comprehensive user-manuals (*documentation*) and are not thoroughly tested across different platforms or data sets, which can lead to unexpected errors that can not be fixed by the user. Moreover, even when these tools are available, they frequently suffer from low adoption rates, meaning that few people are familiar with the details of such tools, further decreasing the confidence and reproducibility in the final results.

Given these complexities, there is a pressing need for new analytical tools specifically designed for semi-big data. These tools must strike a balance between the ease of use found in basic software and the robust, analytical capabilities of more sophisticated systems. By providing standardized workflows, comprehensive documentation, and ensuring cross-platform compatibility, these tools can significantly enhance reproducibility. They not only allow researchers to perform analyses more efficiently but also ensure that these analyses are robust, transparent, and easily verifiable by the broader scientific community.

This thesis presents a software environment developed in Python, designed to bridge this gap. It demonstrates that even minimal coding skills can be leveraged to create powerful tools that standardize and accelerate the analysis of semi-big data, ultimately fostering more reproducible and trustworthy scientific research.

Modern Standards of Software Development

A main reason to write software is to define reusable instructions for task automation (Narzt et al., 1998). The complexity of software code makes it prone to errors, which can prevent its usage by persons other than the author himself. This is a problem for the general scientific community, as the software is often essential for reproduction (Sandve et al., 2013). Hence, modern journals aim to enforce standards to software development, including software written and used by biological researchers (Smith et al., 2018). Here, we provide a brief overview of the standards utilized by `plotastic` that ensure its reliability and reproducibility by the scientific community (Peng, 2011).

Modern software development is a long-term commitment of maintaining and improving code after initial release (Boswell & Foucher, 2011). Hence, it is good practice to write the software such that it is *scalable*, *maintainable* and *usable*. *Scalability* or, to be precise, *structural scalability* means that the software can easily be expanded with new features without major modifications to its architecture (Bondi, 2000). This is achieved by writing the software in a modular fashion, where each module is responsible for a single function. *Maintainability* means that the software can easily be fixed from bugs and adapted to new requirements (Kazman et al., 2020). This is achieved by writing the code in a clear and readable manner, and by writing tests that ensure that the code works as expected (Boswell & Foucher, 2011). *Usability* is hard to define (Brooke, 1996), yet one can consider a software as usable if the commands have intuitive names and if the software's manual, termed *documentation*, is up-to-date and easy to understand for new users with minimal coding experience. A software package that has not received an update for a long time (approx. one year) could be considered abandoned. Abandoned software is unlikely to be fully functional, since it relies on other software (dependencies) that has changed in functionality or introduce bugs that were not expected by the developers of all dependencies. Together, software that's scalable, maintainable and usable requires continuous changes to its codebase. There are best practices that standardize the continuous change of the codebase, including version control, continuous integration (often referred to as CI), and software testing.

Version control is a system that records changes to the codebase line by line, documenting of the detailed history of the codebase, including the person and timepoint of every change. This is required to isolate new and experimental features into newer versions and away from the stable version that's known to work. The most popular version control system is Git, which is considered the industry standard for software development (Chacon & Straub, 2024). Git can use GitHub.com as a platform to store and host codebases in the form of software repositories. GitHub's most famous feature is called "pull request". A pull request is a request from anyone registered on GitHub to include changes to the codebase (as in "*please pull this into your main code*"). One could see pull requests as the identifying feature of the open source community, since it exposes the codebase to potentially thousands of independent developers, reaching a workforce that is impossible to achieve with closed

source models used by paid software companies.

Continuous integration (CI) is a software development practice in which developers integrate code changes into a shared repository several times a day (Duvall et al., 2007). Each integration triggers the test suite, aiming to detect errors as soon as possible. The test suite includes building the software, setting up an environment for the software to run, and then executing the programmed tests, ensuring that the software runs as a whole. Continuous integration is often used together with software branches. Branches are independent copies of the codebase that are meant to be merged back into the original code once the changes are finished. Since branches accumulate multiple changes over time, this can lead to minor incompatibilities between the branches of all developers (integration conflicts), which is something that CI helps to prevent.

Continuous integration especially relies on a thorough software testing suite. Software testing is the practice of writing code that checks if the codebase works as expected (Myers et al., 2011). The main type of software testing is unit testing, which tests the smallest units of the codebase (functions and classes) in isolation (Listing 1). Software testing is automated by specialized frameworks that execute the tests and report the results, a popular example being `pytest`, which is utilized by `plotastic` (Krekel et al., 2004).

Listing 1: Example of an arbitrary Python function and its respective unit test function. The first function simply returns the number 5. The second function tests if the first function indeed returns the number 5. The test function is named with the prefix “`test_`” and is placed in a file that ends with the suffix “`_test.py`”. Testing frameworks such as `pytest` scan the repository for files that end with “`_test.py`” and execute the functions that start with “`test_`”. Note that code after “`#`” is considered a comment and won’t be executed.

```
1 # Define a function called "give_me_five" that returns the number 5
2 def give_me_five():
3     return 5
4 # Define a test function asserting that "give_me_five" returns 5
5 def test_give_me_five():
6     assert give_me_five() == 5
```

The quality of the software testing suite is measured by the code coverage, the precision of the tests, and the number of test-cases that are checked. The code coverage is the percentage of the codebase that is called by the testing functions, which should be as close to 100% as possible, although it does not measure how well the code is tested. The precision of the test is not a measurable quantity, but it represents if the tests truly checks if the code works as expected. The number of test-cases is the number of different scenarios that are checked by the testing functions, for example testing every possible option or combinations of options for functions that offer multiple options.

Together, the standards of software development, including version control, continuous integration, and software testing, ensure that the software is scalable, maintainable, and usable. This is especially important for software that is used by the scientific community, as it ensures that the software is working as expected at defined versions years after publishing scientific results.

What makes Python an “Easy” Programming Language?

Here, we provide a general overview of the Python programming language, explaining terms like “*type*”, “*method*”, etc., in order to prepare readers without prior programming experience for the following chapters. We also describe the design principles of Python to lay out the key concepts that differentiate Python compared to other programming languages. A more detailed tutorial on Python that’s specialized for bioscientists is found in Ekmekci et al. 2016

Languages such as Python are considered “*high-level*”, which means that it is designed to be easy to read and write, but also independent of hardware by hiding (“*abstracting*”) underlying details (*The Python Language Reference*, 2024). A key principle of Python is the emphasis on implementing a syntax that is concise and close to human language (Listing 2, Listing 3).

Listing 2: Example of readable Python code. This one-line code returns the words (string) “Hello, World!” when executed. The command is straightforward and easy to understand.

```
1 print("Hello, World!")
2 // Expected output: Hello, World!
```

Listing 3: Example of less readable code written in the low-level programming language C. This code is doing exactly the same as the Python code in Listing 2, but is harder to understand because more steps are needed, including the import of a library stdio.h and the definition of a function called main. Note that C uses // to begin comment sections.

```
1 #include <stdio.h>           // Import functions for standard input & output
2 int main() {                  // Define a function called 'main'
3     printf("Hello, World!");
4     return 0;
5 }
6 // Expected output: Hello, World!
```

Furthermore, Python is an *interpreted* language, which means that the code is executed line by line. This makes coding easier because the programmer can see the results of the code immediately

after writing it, and error messages point to the exact line where the error occurred (Listing 4). This is in contrast to *compiled* languages, where the code has to be compiled into machine code before it can be executed. The advantage of compiled languages is that the code runs faster, because the machine code is optimized for the hardware.

Listing 4: Example of an error message. Since Python is case-sensitive, the error is caused by misspelling the variable name `hi` as `Hi`. The error message begins with the type of error (`NameError`), followed by a traceback that shows the sequence of function calls that led to the error. The traceback located the source of the error in the file `errormessage.py` and points to the line that caused the error. Finally, the error message explains the error, stating that '`Hi`' is undefined.

```
1 hi = "Hello World" # Define a variable 'hi' with the value "Hello World"
2 print(Hi)           # Print the value of the undefined variable 'Hi'
3
4 # Expected Output:
5 # -----
6 # NameError                                     Traceback (most recent call last)
7 # File /Users/martinkuric/Documents/errormessage.py:2
8 #     1 hi = "Hello World"
9 # ----> 2 print(Hi)
10
11 # NameError: name 'Hi' is not defined
```

Python automates tasks that would otherwise require an advanced understanding of computer hardware, like the need for manual allocation of memory space. This is achieved by using a technique called "*garbage collection*", which automatically frees memory space that is no longer needed by the program. This is a feature that is not present in low-level programming languages like C or C++, that were designed to maximize control over hardware.

Another hallmark of Python is its *dynamic typing system*. In Python the type is inferred automatically during code execution (Listing 5). This is in contrast to *statically* typed languages like C, where the type of a variable has to be declared explicitly and cannot be changed during code execution (Listing 6) (*The Python Language Reference*, 2024).

Listing 5: Example of dynamic typing in Python. The variable "`a`" is assigned the value `5`, which is of type `integer`. The variable "`a`" is then overwritten with the value "`Hello, World!`", which is of type `string`. Python allows dynamic re-assignment of variables with different types. Note that code after "`#`" is considered a comment and won't be executed.

```
1 a = 5 # Type integer
2 a = 5.0 # Type float
3 a = 'Hello, World!' # Type string
4 a = True # Type boolean
5 a = False # Type boolean
6 a = [1, 2, 3] # Type list of integers
7 a = {'name': 'Regina'} # Type dictionary
```

Dynamic typing makes Python a very beginner-friendly language, since one does not have to keep track of the type of each variable. However, this also makes Python a slower language, because the interpreter has to check the type of each variable during code execution. Also, developing code with dynamic typing systems is prone to introducing bugs (`TypeError`), because it allows unexperienced

Listing 6: Example of static typing in C. The variable “a” is declared as an integer (`int`), and can only store integers. The variable “a” is then assigned the value 5, which is an integer. The variable “a” is then assigned the value ‘Hello, World!’, which is a string. This results in a compilation error, because the variable “a” can only store integers. Note that code after “//” is considered a comment and won’t be executed.

```
1 int a; // Declare type as integer
2 a = 5;
3 a = 'Hello, World!'; // Compilation error!
```

developers to convert variables from one type to another without noticing, leading to unexpected behavior. Hence, larger Python projects require disciplined adherence to programming conventions. One such convention is *type hinting*, which is a way to explicitly note the type of a variable. Type hinting does not have an effect on the code, but it makes the code more readable and understandable for other developers, and allows for development environments to detect type errors before execution (Listing 7) (van Rossum et al., 2014).

Listing 7: Example of type hints used in Python. Explicitly stating the type of the variable is optional and does not change the behavior of the code, but behaves exactly as shown in Listing 5.

```
1 a: int = 5
2 a: str = 'Hello, World!'
```

To make Python as easy as possible, python packages aim to reduce the amount of code that has to be written by the user. For example, the package `matplotlib` is a plotting library where every command is written such that the user immediately understands its purpose, like plotting a line or labeling an axis (Listing 8). Hence `matplotlib` code is a sequence of simple function calls, where the state of the plot is modified and saved in the background line by line.

Listing 8: Example of using pre-written functions of a Python package. The functions of the package `matplotlib.pyplot` become accessible by importing the package as `plt`, where `plt` serves as an alias (or rather shortcut) to access the functions of the package. Then, two arbitrary lists are defined, `x` and `y`. These datapoints are plotted (scatterplot) using the function `plot`. The plots x- and y-axes are then labeled and saved as an image. The code is written in a sequence of function calls, where the state of the plot is saved in the background. The plot is then displayed using the function `show`.

```
1 import matplotlib.pyplot as plt # Make functions accessible via plt
2 x = [1, 2, 3, 4, 5]           # Define arbitrary x values
3 y = [1, 4, 9, 16, 25]         # Define arbitrary y values
4 plt.plot(x, y)                # Plot x against y
5 plt.xlabel('Timepoint')        # Add a label to the x axis
6 plt.ylabel('Foldchange')       # Add a label to the y axis
7 plt.title('Gene Expression')   # Add a title above the plot
8 plt.savefig('plot.png')        # Save plot as image onto harddrive
9 plt.show()                     # Show the plot preview
```

However, when no pre-written functions or packages are available, Python offers the tools of a general purpose programming language to write and deploy custom code easily. Programming styles can be classified into two main paradigms: *functional* and *object-oriented* programming, which can be understood as different ways to structure code. Python supports both paradigms. In *functional*

programming, the code is written in a way that the program is a sequence of function calls, where each function call returns a value that is used in the next function call (Listing 9). This approach is useful when multiple actions have to be performed on the same data and the structure of the data is relatively simple, for example a string of a DNA sequence.

Listing 9: Example of functional programming in Python. The code defines a function called “find_restriction_site” that finds the position of a restriction site in a DNA sequence. The function “cut” uses the function “find_restriction_site” to cut the sequence at the restriction site. To execute both functions, we first define an arbitrary DNA sequence and then call the function cut passing the sequence as an argument.

```
1 def find_restriction_site(sequence: str): # Define a function
2     return sequence.find('GCGC')           # Find the position of 'GCGC'
3
4 def cut(sequence: str):                  # Define another function
5     position = find_restriction_site(sequence) # Use the function above
6     return sequence[:position]            # Cut sequence at the position
7
8 seq1 = 'TGAGCTGAGCTGATGCGCTATTTAGGCG' # Define an arbitrary sequence
9 seq1_cut = cut(seq1)                   # Cut the sequence
10 print(seq1_cut)                      # Show the result
11 # Expected output: GCGCTATTTAGGCG
```

When the data itself gains in complexity, for example when storing not just the gene sequence, but also the promoter sequence, an *object-oriented* approach is more suitable (Listing 10). Object-oriented programming is a programming paradigm that uses objects and classes. An object is a collection of both data and functions, and a class is a blueprint for creating objects. The data of an object is stored as *attributes*. Functions that are associated with an object are called *methods*. A major benefit of using an object oriented versus a functional approach is that the data itself is programmable, enabling the programmer to define the behavior of the data through methods. This is achieved by using ‘self’ to reference the objects themselves inside the class. self can be understood as “*this object*”, and is a placeholder for objects that are to be created from the blueprint. self is required to access attributes and methods before specific objects are created in order to program how the objects are to be changed when calling methods.

When designing software, both functional and object oriented programming can be used together, where object oriented programming is often used to design the program’s overall architecture, and functional programming is used to implement the algorithms of the program’s features. This allows for scalability of the software, as every single class is extended through the addition of new methods.

Furthermore, classes can be expanded in their functionalities through *inheritance* (Listing 11). Inheritance is a feature of object-oriented programming that allows a class to access every attribute and method of a parent class. For example, one could extend the class “Gene” with a class “mRNA”, by writing a class “mRNA” that inherits from the class “Gene”.

Listing 10: Example of object oriented programming in Python. The class is called “Gene” and acts as a blueprint to create Gene objects. Gene has four methods, “`__init__`”, “`find_promoter`”, “`find_restriction_site`” and “`cut`”. The method “`__init__`” is called when creating (“initializing”) an object, which fills the object with user-defined data. The parameter “`self`” is a placeholder for the objects that are to be created. “`find_promoter`” is a method that finds the position of the promoter in the gene and is called during object initialization.

```

1 class Gene:                                # Define a Gene class
2     def __init__(self, sequence: str):      # Define how a Gene object is created
3         self.sequence: str = sequence        # Save sequence as attribute
4         self.promoter: str = self.find_promoter() # Automatically find promoter
5         # Add further Gene attributes here
6     def find_promoter(self):            # Define how to find the promoter
7         return self.sequence.find('TATA')
8     def find_restriction_site(self):    # Define how to find restriction site
9         return self.sequence.find('GCGC') # Find the position of 'GCGC'
10    def cut(self):                  # Define how to cut the DNA sequence
11        position = self.find_restriction_site() # Call the method above
12        return self.sequence[position:] # Cut the gene at the position
13
14 gene1 = Gene(sequence='TGAGCTGAGCTGATGCGCTATTTAGGCG') # Create Gene object
15 print(gene1.cut())                      # Cut gene and show result
16 # Expected output: GCGCTATATTAGGCG

```

Listing 11: Example of inheritance in Python. The class “mRNA” inherits from the class “Gene”, and has two methods, “`__init__`” and “`find_stopcodon`”. “`find_stopcodon`” loops through a list of stop codons (for `x` in `list`): For each stop codon, the position is found. If a codon wasn’t found, the `.find()` method returns -1, which leads to a different print message. Note that `f""` formats strings to include variables.

```

1 class mRNA(Gene):          # Define the mRNA class, inheriting from Gene class
2     def __init__(self, sequence: str):  # Define how an mRNA object is created
3         super().__init__(sequence)    # Get attributes from parent class
4         self.sequence = self.sequence.replace('T', 'U') # Replace T with Uracil
5     def find_stopcodons(self):       # Define how to find stop codons
6         for stopcodon in ['UGA', 'UAA', 'UAG']: # Loop over stop codons
7             position: int = self.sequence.find(stopcodon) # Find the position
8             if position == -1:           # If position is -1, codon wasn't found
9                 print(f'{stopcodon} not found') # Message if not found
10            else:                   # If position isn't -1, codon was found
11                print(f'{stopcodon} found at {position}')
12
13 mRNA1 = mRNA(sequence='TGAGCTGAGCTGATGCGCTATTTAGGCG') # Create an mRNA object
14 mRNA1.find_stopcodons()                      # Show the position of stop codons
15 # Expected outputs:
16 # UGA found at 0
17 # UAA not found
18 # UAG found at 24

```

Together, Python is not just beginner-friendly, but also well respected for its ease in development, which is why it is widely used in professional settings for web development, data analysis, machine learning, biosciences and more (Ekmekci et al., 2016; Rayhan & Gross, 2023).

The Potential of Python Data Science Packages for Biomedicine

Python includes a vast number of built-in packages used for basic data-types, software development, simple math operations, etc., (*The Python Language Reference*, 2024). Still, Python relies on packages developed by its users to provide specialized tools for data analysis. A Python package consists of multiple Python *modules*, where each module is a text-file with a .py ending containing Python code. Famous examples of such packages are pytorch and tensorflow, that are used to build models of artificial intelligence, including *ChatGPT* (Paszke et al., 2019; Abadi et al., 2016; Radford et al., 2019). Here, we outlay the most important packages used for plotastic in Chapter 2 and present examples how these packages are utilized in modern biomedical research.

Interactive Python: The standard Python interface is insufficient for data science, because it lacks the tools to quickly and conveniently visualize and explore data. IPython can be understood as an enhanced version of the standard Python interpreter, designed to improve the interactivity of Python code execution (Perez & Granger, 2007). IPython introduces features like rich media support to display graphics, but also helps users to use correct python data types through dynamic type introspection, detecting errors in the code. This functionality is akin to what *MATLAB* and *RStudio* provide through their advanced graphical user interfaces and extensive debugging tools. IPython is most often utilized in the form of *Jupyter Notebooks*.

Jupyter: Jupyter is an evolution of IPython, introducing the *Jupyter notebook* format, which has the file-ending .ipynb (Kluyver et al., 2016). Jupyter Notebooks are documents that combine both code and text structured as *code cells* and *markdown cells*, respectively. Markdown cells allow the author to provide additional information with text formatting, for example structuring the document with headings and subheadings, adding hyperlinks, images and mathematical formulas. Code cells can be executed individually, displaying the output directly below the cell. This allows for an interactive exploration of data, but also makes Jupyter Notebooks a very human-readable format that outlays data analysis in a clear manner with precise and reproducible documentation of all data processing steps. Another major benefit of Jupyter Notebooks are interchangeable *Kernels*, allowing the execution of code in different programming languages, such as R, Julia, and C++ (Giorgi et al., 2022). Today, Jupyter Notebooks have become a standard format compatible with collaborative platforms like *Google Colab* and *JupyterLab*, but also professional software development tools like *VS Code*, and *PyCharm*. For biomedical research, Jupyter Notebooks are a powerful solution for improving reproducibility: They elegantly combine both documentation and code execution into a concise presentation of the data analysis process, hence being an intuitive tool to both capture and embed computational work directly into papers, a requirement postulated by Mesirov (2010). Jupyter notebooks are increasingly found in the supplemental of modern publications of both bioinformatics and wet-lab research (Taskiran et al., 2024; Bosch-Queralt et al., 2022; Howe & Chain, 2015).

NumPy: Central processing units (CPU) usually execute one instruction on one data point at a time. For manipulating tabular data, this is inefficient as the same instruction must be repeatedly loaded for every data point. NumPy accelerates the mathematical capabilities of Python by enabling large-scale operations on multi-dimensional arrays and matrices with high efficiency (Harris et al., 2020). One key feature of NumPy is the implementation of “vectorization” or SIMD (Single Instruction, Multiple Data) instructions. SIMD allows multiple data points to be processed simultaneously, significantly speeding up operations that are inherently parallelizable, such as matrix addition or multiplication. NumPy’s syntax and functional approach to array manipulation have set a standard for matrix computation, influencing the design of advanced AI frameworks such as PyTorch and mlx, which mirrors several of NumPy’s functionalities to facilitate ease of use for those familiar with NumPy (Paszke et al., 2019; Hannun et al., 2023). This standardization has made NumPy an attractive tool not only in genomics (Ding et al., 2023), but also for modern clinical applications like imaging technologies and augmented-reality in surgery (Thompson et al., 2020).

Pandas: Tables are the most common way to store experimental results. Pandas extends Python with a tabular datatype, called `DataFrame`, which allows for easy data manipulation with integrated indexing (Mckinney, 2011). The intuitive interface of Pandas can be likened to *Microsoft Excel*; however, it is vastly more powerful due to its speed, functionality, and ability to handle larger datasets, e.g. by running efficient numpy vectorization in the background. Unlike *Excel*, Pandas enables automation by summarizing processing commands into scripts, documenting each step, and ensuring reproducibility. Pandas is used in biomedicine for data wrangling, data cleaning, and data analysis, as it allows for the integration of multiple data sources into a single table (Santos et al., 2020).

matplotlib: `matplotlib` is a plotting library that provides a wide range of static, animated, and interactive plots and graphs (Listing 8) (Hunter, 2007). It serves as the foundation for many visualization tools and is particularly valued for its flexibility and customization options. For example, Pandas uses `matplotlib` to plot column datapoints directly from a `DataFrame` object, creating histograms or scatter plots, which is useful for preliminary data analysis and checking data distributions. However, `matplotlib` uses a low-level syntax, hence plots generated by `matplotlib` can be cumbersome to format and customize.

seaborn: While the low-level syntax of `matplotlib` is valued for its flexibility, formatting publication grade plots can be laborious, and its inconsistent syntax can make it difficult to remember the correct commands for different plot types. `seaborn` is a high-level interface on top of `matplotlib` that offers a more intuitive and highly standardized syntax across a wide array of plot types (Waskom, 2021). `seaborn` also integrates closely with Pandas data structures: It automatically groups data-points, calculates measures of both central tendency (e.g. mean, median) and variance (e.g. standard deviation), and displays them into the plot (e.g. error bars). This completely replaces manual calculation of descriptive statistics. `seaborn` also offers intuitive grouping (*facetting*) of data points, which

simplifies the creation of complex visualizations involving multidimensional data, making it easier to reveal patterns and relationships via color encoding, faceting, and automated statistical fits. This is particularly useful in biomedical research for visualizing and understanding complex datasets, such as large quantities of protein data (Krzywinski & Savig, 2013; Weiss, 2022). `seaborn` could indirectly contribute to improving reproducibility in biomedical research by making visualizations of complex data very accessible through an easy and standardized syntax.

Pingouin: Integrating both data visualization and statistical analysis is beneficial for researchers who wish to conduct advanced statistical analysis without switching between different software environments. `Pingouin` is designed to be a user-friendly statistical tool that offers a straightforward syntax for performing statistical tests, which are commonly implemented in R (Vallat, 2018). Unlike R, `Pingouin` integrates seamlessly within the Python ecosystem, which allows combining data manipulation, analysis, and visualization all in one platform. This improves reproducibility by reducing the number of software tools required to analyze data. Despite its potential to streamline the data analysis process, `Pingouin` has not been widely adopted by biomedical research, yet. One example of a study that utilized `Pingouin` is the work of Kelly et al. (2023) in the field of Patient Public Involvement (PPI), producing an ethical matrix that allows for the inclusion of stakeholder opinion in medical research design. This lack of `Pingouin`'s adoption in biomedicine could be due to recent development and the dominance of R in the field. However, since Python offers multiple benefits over R in syntax, software development, runtime performance and integration with other tools (like including performant C++ code), `Pingouin` is an attractive standard for future statistical analyses in biomedicine (Gorelick & Ozsvald, 2020).

statannotations: While `seaborn` and `matplotlib` offer a wide range of statistical plots, they lack the ability to automatically annotate plots with *p*-values often abbreviated by stars. `statannotations` is a package that extends `seaborn` by providing an interface to add statistical annotations to plots, but also perform simple statistical tests (Charlier et al., 2022). It is limited to only pairwise comparisons such as t-tests and can not perform omnibus tests like ANOVA.

Together, these python packages form the backbone of modern data analysis in Python, often times combining software from different languages to accelerate certain features, while retaining the ease of use and readability that Python is known for. This is particularly advantageous in the field of biomedicine, where the requirements of modern data analysis are often complex and require a high degree of flexibility and customization.

Aims

This PhD thesis is designed to bridge significant gaps in the understanding and analysis of myeloma cell behavior and the handling of complex biomedical datasets. The specific aims are as follows:

- Develop an *in vitro* model to elucidate the mechanisms of myeloma cell dissemination in interaction with mesenchymal stromal cells (hMSCs), focusing particularly on:
 - Observing and quantifying cell proliferation, attachment, and detachment dynamics using time-lapse microscopy.
 - Isolating and characterizing distinct myeloma subpopulations interacting with hMSCs to understand differential gene expression related to cell adhesion and patient survival.
- Design and implement a Python-based software tool, `plotastic`, to facilitate the analysis of multidimensional datasets generated in biomedical research. This tool will aim to:
 - Streamline the data analysis process, making it more efficient and reproducible.
 - Integrate visualization and statistical analysis capabilities to ensure that data analysis protocols are aligned with the ways in which data is visualized.
 - Provide a case study demonstrating the application of `plotastic` in the analysis of *in vitro* dissemination experiments, emphasizing the tool's ability to handle semi-big data and enhance reproducibility.
- Synthesize the findings from the experimental and software development components to advance the understanding of myeloma dissemination and improve research practices in biomedical data analysis.

These aims are crafted to address both the biological and technical challenges in current cancer research methodologies and data science applications in biomedicine, fostering advancements that could lead to novel therapeutic strategies and more robust scientific inquiries.

Chapter 1: Modelling Myeloma Dissemination *in vitro*

Abstract

Multiple myeloma involves early dissemination of malignant plasma cells across the bone marrow; however, the initial steps of dissemination remain unclear. Human bone marrow-derived mesenchymal stromal cells (hMSCs) stimulate myeloma cell expansion (e.g., IL-6) and simultaneously retain myeloma cells via chemokines (e.g., CXCL12) and adhesion factors. Hence, we hypothesized that the imbalance between cell division and retention drives dissemination. We present an *in vitro* model using primary hMSCs co-cultured with INA-6 myeloma cells. Time-lapse microscopy revealed proliferation and attachment/detachment dynamics. Separation techniques (V-well adhesion assay and well plate sandwich centrifugation) were established to isolate MSC-interacting myeloma subpopulations that were characterized by RNAseq, cell viability and apoptosis. Results were correlated with gene expression data ($n = 837$) and survival of myeloma patients ($n = 536$). On dispersed hMSCs, INA-6 saturate hMSC-surface before proliferating into large homotypic aggregates, from which single cells detached completely. On confluent hMSCs, aggregates were replaced by strong heterotypic hMSC-INA-6 interactions, which modulated apoptosis time-dependently. Only INA-6 daughter cells (nMA-INA6) detached from hMSCs by cell division but sustained adherence to hMSC-adhering mother cells (MA-INA6). Isolated nMA-INA6 indicated hMSC-autonomy through superior viability after IL-6 withdrawal and upregulation of proliferation-related genes. MA-INA6 upregulated adhesion and retention factors (CXCL12), that, intriguingly, were highly expressed in myeloma samples from patients with longer overall and progression-free survival, but their expression decreased in relapsed myeloma samples. Altogether, *in vitro* dissemination of INA-6 is driven by detaching daughter cells after a cycle of hMSC-(re)attachment and proliferation, involving adhesion factors that represent a bone marrow-retentive phenotype with potential clinical relevance.

Statement of Significance

Novel methods describe *in vitro* dissemination of myeloma cells as detachment of daughter cells after cell division. Myeloma adhesion genes were identified that counteract *in vitro* detachment with potential clinical relevance.

Introduction

Multiple myeloma arises from clonal expansion of malignant plasma cells in the bone marrow (BM). At diagnosis, myeloma cells have disseminated to multiple sites in the skeleton and, in some cases, to “virtually any tissue” (Bladé et al., 2022; Rajkumar et al., 2014). However, the mechanism through which myeloma cells initially disseminate remains unclear. Dissemination is a multistep process involving invasion, intravasation, intravascular arrest, extravasation, and colonization (Zeissig et al., 2020). To initiate dissemination, myeloma cells overcome adhesion, retention, and dependency on the BM microenvironment, which could involve the loss of adhesion factors such as CD138 (Akhmetzyanova et al., 2020; García-Ortiz et al., 2021). BM retention is mediated by multiple factors: First, chemokines (CXCL12 and CXCL8) produced by mesenchymal stromal cells (MSCs), which attract plasma cells and prime their cytoskeleton and integrins for adhesion (Aggarwal et al., 2006; Alsayed et al., 2007). Second, myeloma cells must overcome the anchorage and physical boundaries of the extracellular matrix (ECM), consisting of e.g. fibronectin, collagens, and proteoglycans such as decorin (Hu et al., 2021; Huang et al., 2015; Katz, 2010; Kibler et al., 1998). Simultaneously, ECM provides signals inducing myeloma cell cycle arrest or progression the cell cycle (Hu et al., 2021; Katz, 2010). ECM is also prone to degradation, which is common in several osteotropic cancers, and is the cause of osteolytic bone disease. This is driven by a ‘vicious cycle’ that maximizes bone destruction by extracting growth factors (EGF and TGF- β) that are stored in calcified tissues (Glavey et al., 2017). Third, direct contact with MSCs physically anchors myeloma cells to the BM (Zeissig et al., 2020; Sanz-Rodríguez et al., 1999). Fourth, to disseminate to distant sites, myeloma cells require, at least partially, independence from essential growth and survival signals provided by MSCs in the form of soluble factors or cell adhesion signaling (García-Ortiz et al., 2021; Chatterjee et al., 2002; Hideshima et al., 2007). For example, the VLA4 (Myeloma)-VCAM1 (MSC)-interface activates NF- κ B in both myeloma and MSCs, inducing IL-6 expression in MSCs. The independence from MSCs is then acquired through autocrine survival signaling (Frassanito et al., 2001; Urashima et al., 1995). In short, anchorage of myeloma cells to MSCs or ECM is a ‘double-edged sword’: adhesion counteracts dissemination, but also presents signaling cues for growth, survival, and drug resistance (Solimando et al., 2022).

To address this ambiguity, we developed an *in vitro* co-culture system modeling diverse adhesion modalities to study dissemination, growth, and survival of myeloma cells and hMSCs. Co-cultures of hMSCs and the myeloma cell line INA-6 replicated tight interactions and aggregate growth, akin to “microtumors” in Ghobrial’s metastasis concept (Ghobrial, 2012). We characterized the growth conformations of hMSCs and INA-6 as homotypic aggregation *vs.* heterotypic hMSC adherence and their effects on myeloma cell survival. We tracked INA-6 detachments from aggregates and hMSCs, thereby identifying a potential “disseminated” subpopulation lacking strong adhesion. We developed innovative techniques (V-well adhesion assay and well plate sandwich centrifugation) to separate weakly and strongly adherent subpopulations for the subsequent analysis of differential gene expression and

cell survival. Notably, our strategy resolves the differences in gene expression and growth behavior between cells of one cell population in “direct” contact with MSCs. In contrast, previous methods differentiated between “direct” and “indirect” cell-cell contact using transwell inserts (Dziadowicz et al., 2022). To evaluate whether genes mediating adhesion and growth characteristics of INA-6 were associated with patient survival, we analyzed publicly available datasets (Seckinger et al., 2017, 2018).

Materials and Methods

See Appendix A.3 for a complete method list and description.

Ethics Statement

Primary human MSCs were collected with the written informed consent of all patients. The procedure was conducted in accordance with recognized ethical guidelines (Helsinki Declaration) and approved by the local Ethics Committee of the University of Würzburg (186/18).

Cultivation and Co-Culturing of primary hMSCs and INA-6

Primary human MSCs were obtained from the femoral head of 34 non-myeloma patients (Appendix A: Tab. 1: 21 male and 13 female, mean age 68.9 ± 10.6) undergoing elective hip arthroplasty. The INA-6 cell line (*DSMZ Cat# ACC-862, RRID:CVCL_5209*, link) was initially isolated from a pleural effusion sample obtained from an 80-year-old male with multiple myeloma (Burger, Günther, et al., 2001; Gramatzki et al., 1994). hMSCs were not tested for mycoplasma, whereas stocks of INA-6 were tested in this study (Appendix A: Tab. 1) using the *Venor GeM OneStep* kit (Minerva Biolabs, Berlin, Germany). For each co-culture, hMSCs were seeded 24 h before INA-6 addition to generate the hMSC-conditioned medium (CM). INA-6 cells were washed with PBS, resuspended in MSC medium, and added to hMSCs so that the co-culture comprised 33% (v/v) of CM gathered directly from the respective hMSC donor. The co-cultures were not substituted for IL-6 (Chatterjee et al., 2002).

Cell Viability and Apoptosis Assay

Cell viability and apoptosis rates were measured using *CellTiter-Glo Luminescent Cell Viability Assay* and *Caspase-Glo 3/7 Assay*, respectively (Promega GmbH, Mannheim, Germany).

Automated Fluorescence Microscopy

Microscopic images were acquired using an Axio Observer 7 (Zeiss) with a COLIBRI LED light source and motorized stage top using 5x and 10x magnification. The tiled images had an automatic 8–10% overlap and were not stitched.

Live Cell Imaging

hMSCs (stained with PKH26) were placed into an ibidi Stage Top Incubation System and equilibrated to 80 % humidity and 5 % CO₂. INA-6 (2×10^3 cells/cm²) were added directly before the start of acquisition. Brightfield and fluorescence images of up to 13 mm² of the co-culture area were acquired every 15 min for 63 h. Each event of interest was manually analyzed and categorized into defined event parameters.

V-well Adhesion Assay

INA-6 cells were arrested during mitosis by two treatments with thymidine, followed by nocodazole. Arrested INA-6 were released and added to 96 V-well plates (10⁴ cells/cm²) on top of confluent hMSCs and adhered for 1–3 h. The co-culture was stained with calcein-AM (Thermo Fisher Scientific, Darmstadt, Germany) before non-adherent INA-6 were pelleted into the tip of the V-well (555 g, 5–10 min). MSC-adhering INA-6 cells were manually detached by rapid pipetting. The pellet brightness was measured microscopically and the pellet was isolated by pipetting.

Cell Cycle Profiling by Image Cytometry

Isolated INA-6 cells were fixed in 70 % ice-cold ethanol, washed, resuspended in PBS, distributed in 96-well plates, and stained with Hoechst 33342. The plates were scanned at 5x magnification. A pre-trained convolutional neural network (Intellesis, Zeiss) was fine-tuned to segment the scans into single nuclei and exclude fragmented nuclei. Nuclei were filtered to exclude extremes of size and roundness. The G0/G1 frequency was determined by Gaussian curve fitting.

Well Plate Sandwich Centrifugation (WPSC)

hMSCs were grown to confluence in 96-well plates coated with collagen I (rat tail; Corning, NY, USA). INA-6 cells were added and the cells were allowed to adhere for 24 h. A second plate (“catching plate”) was attached upside down to the top of the co-culture plate. That “well plate sandwich” was turned around and the content of the co-culture plate was centrifuged into the catching plate three times (40 s at 110 g) while gently adding 30 µL of medium in between centrifugation steps. Non-MSC-adhering INA-6 cells were collected from the catching plate, whereas MSC-adhering INA-6 cells were isolated by digesting the co-culture with accutase. For RNA sequencing (RNAseq), all samples were purified using anti-CD45 magnetic-assisted cell sorting (Miltenyi Biotec B.V. & Co. KG, Bergisch Gladbach).

RNA Isolation

RNA was isolated using the *NucleoSpin RNA II Purification Kit* (Macherey-Nagel) according to the manufacturer's instructions. RNA was isolated from INA-6 cells co-cultured with a unique hMSC donor ($n = 5$ for RNA sequencing, $n = 11$ for qPCR).

RNA sequencing, Differential Expression, and Functional Enrichment Analysis

RNA sequencing (RNaseq) was performed at the Core Unit Systems Medicine, University of Würzburg. mRNA was enriched with polyA beads. Fastq files were aligned to the GRCh38 reference genome using STAR (*RRID:SCR_004463*, link) and raw read counts were generated using HTseq (*RRID:SCR_005514*, link) (Anders et al., 2015; Dobin et al., 2013; Zerbino et al., 2018). Differential gene expression was analyzed using edgeR in R (version 3.6.3) (*RRID:SCR_012802*, link). Functional enrichment analysis was performed using Metascape (*RRID:SCR_016620*, link) (Y. Zhou et al., 2019).

RT-qPCR

RNA (1 µg) was reverse transcribed using *SuperScript IV reverse transcriptase* (Thermo Fisher Scientific). qPCR was performed using 10 µL *GoTaq qPCR Master Mix* (Promega), 1:10 diluted cDNA, and 5 pmol of primers obtained from Biomers.net or Qiagen (Appendix A: Tab. 3).

Statistical Analysis

Inferential statistics were performed using Python (IPython, *RRID:SCR_001658*, link) (3.10) packages *pingouin* (0.5.1) and *statsmodels* (0.14.0) (Vallat, 2018; Seabold & Perktold, 2010). The figures were plotted using *plotastic* (0.0.1) (Kuric & Ebert, 2024). Normality (for $n \geq 4$) and sphericity were ensured using Mauchly's and Shapiro-Wilk tests, respectively. Data points were Log₁₀ transformed to convert the scale from multiplicative to additive or to fulfill sphericity requirements. $p = 0.05 > * > 0.01 > ** > 10^{-3} > *** > 10^{-4} > ****$. p -values were either adjusted (*p*-adj) or not adjusted (*p*-unc) for family wise error rate. Power calculations were not performed to determine the sample size.

Patient Cohort, Analysis of Survival and Expression

Survival and gene expression data were obtained as previously described (Seckinger et al., 2017, 2018) and are available at the European Nucleotide Archive (ENA) under accession numbers PRJEB36223 and PRJEB37100. The expression level was categorized into "high" and "low" using *maxstat* (Maximally selected Rank Statistics) thresholds (Hothorn & Lausen, n.d.).

Data Availability Statement

A detailed description of the methods is provided in the Supplementary Material section. Raw tabular data and examples of analyses and videos are available in the github repository, link. Raw RNAseq data are available from the NCBI Gene Expression Omnibus (GEO) (*RRID:SCR_005012*, link) (GSE261423). Microscopy data are available at BioStudies (EMBL-EBI) (*RRID:SCR_004727*, link) (S-BIAD1092).

Results

INA-6 Cells Saturate hMSC-Interaction to Proliferate into Aggregates

hMSCs are isolated as a heterogeneous cell population. To analyze whether INA-6 cells could adhere to every hMSC, we saturated hMSCs with INA-6. A seeding ratio of 1:4 (hMSC:INA-6) resulted in the occupation of $93 \pm 6\%$ of single hMSCs by one or more INA-6 cells within 24 hours after INA-6 addition, escalating to 6% after 48 hours (Fig. 1A, B). Therefore, most hMSCs provide an interaction surface for INA-6 cells.

INA-6 exhibits homotypic aggregation when cultured alone, a phenomenon observed in some freshly isolated myeloma samples (up to 100 cells after 6 hours) (Kawano et al., 1991; Okuno et al., 1991). Adding hMSCs at a 1:1 ratio led to smaller aggregates after 24 hours (size 1–5 cells), all of which were distributed over $52 \pm 2\%$ of all hMSCs (Fig. 1A, B). Intriguingly, INA-6 aggregation was notably absent when grown on confluent hMSCs, and occurred only when heterotypic interactions were limited to 0.2 hMSCs per INA-6 cell (Fig. 1C). We concluded that INA-6 cells prioritize heterotypic over homotypic interactions.

To monitor the formation of such aggregates, we conducted live-cell imaging of hMSC/INA-6 co-cultures for 63 hours. We observed that INA-6 cells adhered long after cytokinesis, constituting $55 \pm 12\%$ of all homotypic interactions between 13 hours and 26 hours, increasing to more than 75% for the remainder of the co-culture (Fig. 1D). Therefore, homotypic INA-6 aggregates were mostly formed by cell division.

Apoptosis of INA-6 Depends on Ratio Between Heterotypic and Homotypic Interaction

Although direct interaction with hMSCs has been shown to enhance myeloma cell survival through NF- κ B signaling (Hideshima et al., 2007), the impact of aggregation on myeloma cell viability during hMSC interaction remains unclear. To address this, we measured the cell viability (ATP) and apoptosis rates of INA-6 cells growing as homotypic aggregates compared to those in heterotypic interactions with hMSCs by modulating hMSC density (Fig. 1E). To equalize the background signaling caused by soluble MSC-derived factors, all cultures were incubated in hMSC-conditioned medium and the results were normalized to INA-6 cells cultured without direct hMSC contact (Fig. 1E, left).

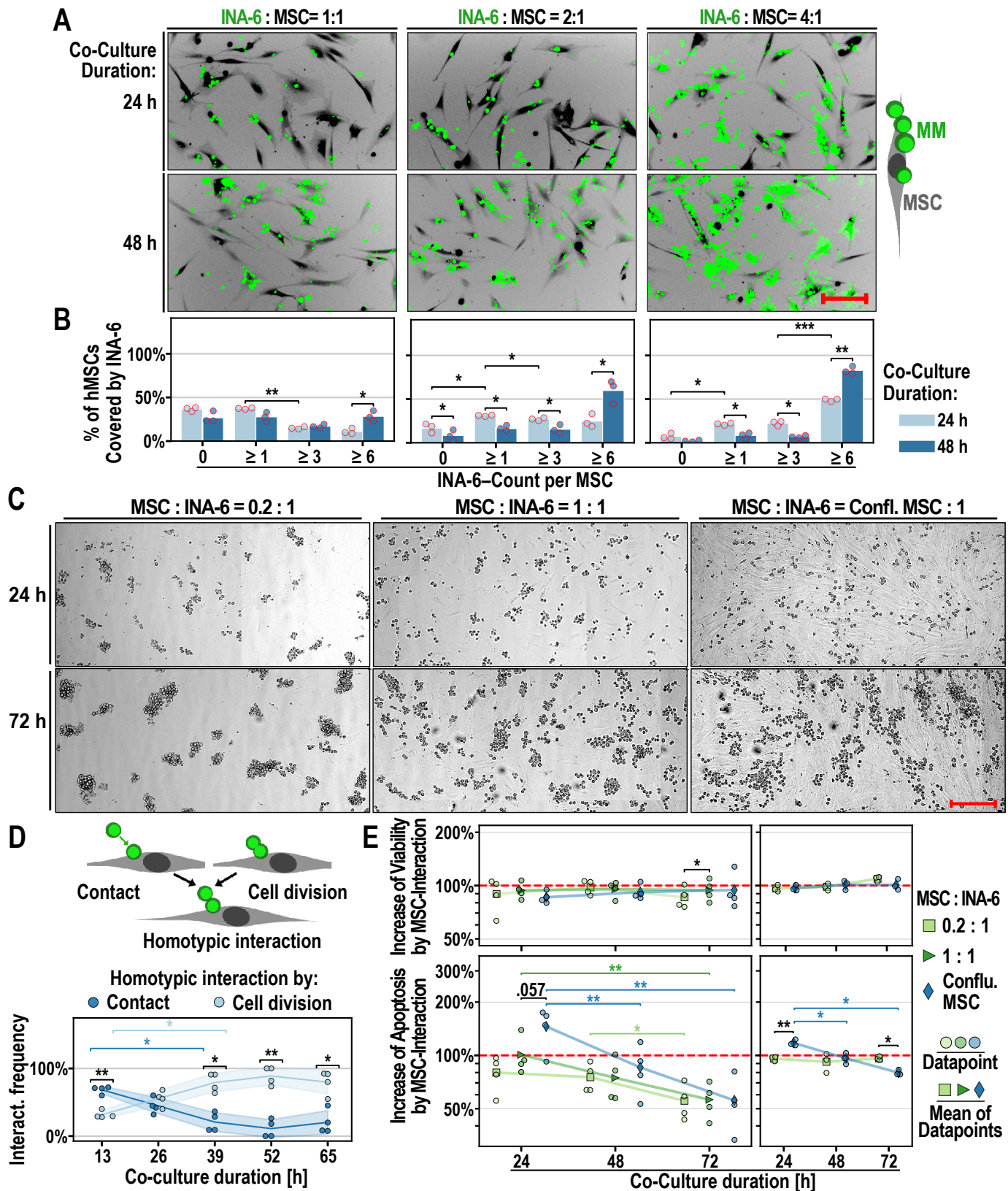


Figure 1: INA-6 growth conformations and survival on hMSCs. **A:** Interaction of INA-6 (green) with hMSCs (black, negative staining) at different INA-6 densities (constant hMSC densities). Scale bar = 200 μ m. **B:** Frequency of single hMSCs (same as A) that are covered by INA-6 of varying group sizes. Technical replicates = three per datapoint; 100 single hMSCs were evaluated per technical replicate. – continued on next page

Figure 1: continued from previous page – **C:** Interaction of INA-6 with hMSCs at different hMSC densities (constant INA-6 densities). Scale bar = 300 µm. **D:** Two types of homotypic interaction: Attachment after cell contact and sustained attachment of daughter cells after cell division. Datapoints represent one of four independent time-lapse recordings, each evaluating 116 interaction events. **E:** Effects of hMSC-density on the viability (ATP, top) and apoptosis (Caspase3/7 activity, bottom). INA-6:MSC ratio = 4:1; Technical replicates = four per datapoint; **E left:** Signals were measured in INA-6 washed off from hMSCs and normalized by INA-6 cultured in MSC-conditioned medium (= red line) ($n = 4$). **E right:** Signals were measured in co-cultures and normalized by the sum of the signals measured in hMSC and INA-6 cultured separately (= red line) ($n = 3$). **Statistics:** Paired t-test, two-factor RM-ANOVA. Datapoints represent independent co-cultures with hMSCs from three (A, B, D, E right), four (E left) unique donors. Confl. = Confluent.

INA-6 viability (ATP) was not affected by the direct adhesion of hMSCs at any density. However, apoptosis rates decreased over time [$F(2, 6) = 23.29, p\text{-unc} = 1.49 \times 10^{-3}$] (Two-factor RM-ANOVA), interacting significantly with MSC density [$F(4, 12) = 6.98, p\text{-unc} = 3.83 \times 10^{-3}$] For example, 24 hours of adhesion to confluent MSCs increased apoptosis rates by 1.46 ± 0.37 fold, while culturing INA-6 cells on dispersed hMSCs (ratio 1:1) did not change the apoptosis rate (1.01 ± 0.26 fold).

We presumed that sensitive apoptotic cells might have been lost when harvesting INA-6 cells from hMSCs. Hence, we measured survival parameters in the co-culture and in hMSC and INA-6 cells cultured separately (Fig. 1E, right). We defined MSC interaction effects when the survival measured in the co-culture differed from the sum of the signals measured from INA-6 and hMSCs alone. RM-ANOVA confirmed that adherence to confluent MSCs increased apoptosis rates of INA-6 cells 24 hours after adhesion and decreased after 72 hours [$F(2, 4) = 26.86, p\text{-unc} = 4.80 \times 10^{-3}$] (interaction between MSC density and time, Two-factor RM-ANOVA), whereas INA-6 cells were unaffected when grown on dispersed hMSCs. In summary, the growth conformation of INA-6 cells, measured as the ratio between homotypic aggregation and heterotypic MSC interactions, affected apoptosis rates of INA-6 cells.

Single INA-6 Cells Detach Spontaneously from Aggregates of Critical Size

Using time-lapse microscopy, we observed that $26 \pm 8\%$ of INA-6 aggregates growing on single hMSCs spontaneously shed INA-6 cells (Fig. 2A, B; Supplementary Video 1). Notably, all detached cells exhibited similar directional movements, suggesting entrainment in convective streams generated by temperature gradients within the incubation chamber. INA-6 predominantly detached from other INA-6 cells or aggregates (Fig. 2C), indicating weaker adhesive forces in homotypic interactions than in heterotypic interactions. The detachment frequency increased after 52 hours, when most aggregates that shed INA-6 cells were categorized as large (greater than 30 cells) (Fig. 2D). Since approximately 10-20 INA-6 cells already fully covered a single hMSC, we suggest that myeloma cell detachment depended not only on hMSC saturation but also required a minimum aggregate size. Interestingly, INA-6 detached mostly as single cells, independent of aggregate size categories [$F(2, 6) = 4.68, p\text{-unc} = 0.059$] (Two-factor RM-ANOVA) (Fig. 2E), showing that aggregates remained mostly stable

despite losing cells.

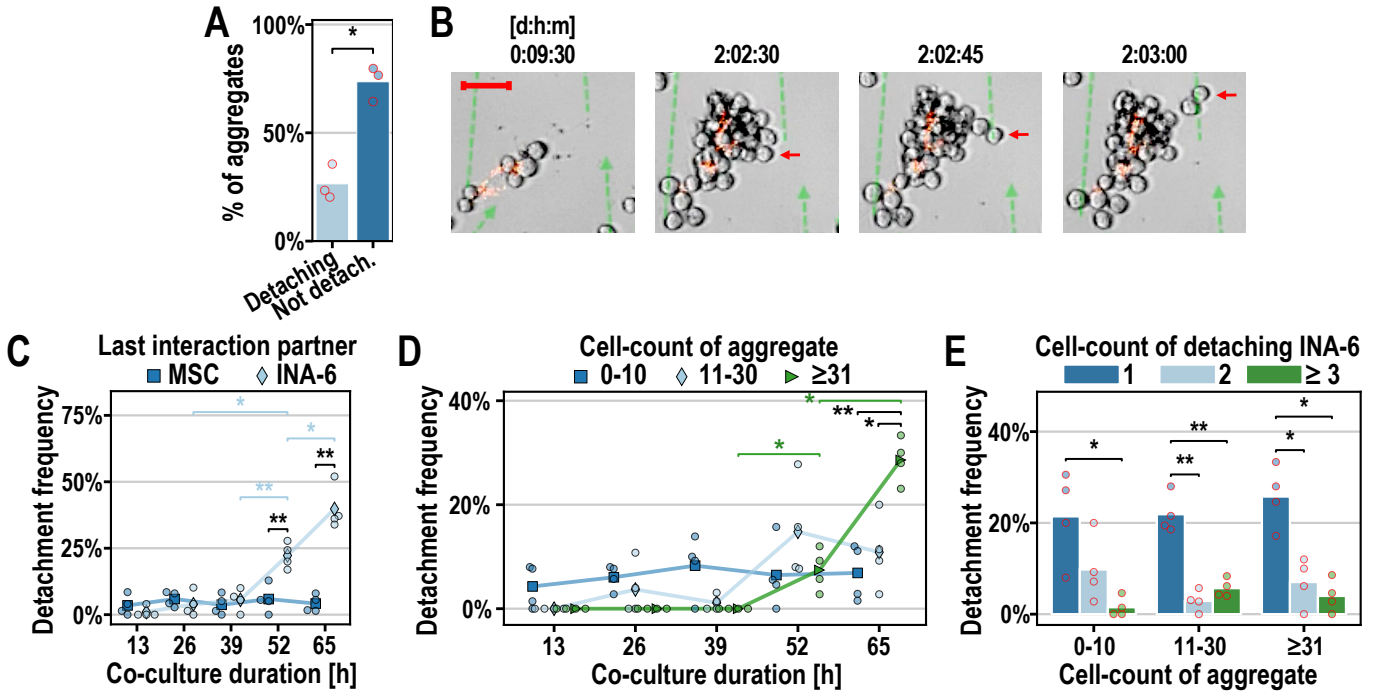


Figure 2: Time-lapse analysis of INA-6 detachment from INA-6 aggregates and hMSCs. **A:** Frequency of observed INA-6 aggregates that did or did not lose INA-6 cell(s). 87 aggregates were evaluated per datapoint. **B:** Example of a “disseminating” INA-6 aggregate growing on fluorescently (PKH26) stained hMSC (from A-D). Dashed green lines are trajectories of detached INA-6 cells. Scale bar = 50 μ m. **C-E:** Quantitative assessment of INA-6 detachments. 45 detachment events were evaluated per datapoint. Seeding ratio INA-6:MSC = 4:1. **C:** Most INA-6 cells dissociated from another INA-6 cell and not from an hMSC [$F(1, 3) = 298$, $p\text{-unc} = 4.2 \times 10^{-4}$]. **D:** Detachment frequency of aggregate size categories. **E:** Detachment frequency of INA-6 cells detaching as single, pairs or more than three cells. **Statistics:** (A): Paired-t-test; (C-E): Paired-t-test, Two-factor RM-ANOVA; Datapoints represent three (A) or four (C-E) independent time-lapse recordings of co-cultures with hMSCs from two (A) or three (C-E) unique donors.

Cell Division Generates a Daughter Cell Detached from hMSC

We suspected that cell division drives detachment because we observed that MSC-adhering INA-6 cells could generate daughter cells that “roll over” the mother cell (Fig. 3A; Supplementary Video 2). We recorded and categorized the movement of INA-6 daughter cells in confluent hMSCs after cell division. Half of all INA-6 divisions yielded two daughter cells that remained stationary, indicating hMSC adherence (Fig. 3B, C; Supplementary Video 3). The other half of division events generated one hMSC-adhering cell and one non-hMSC-adhering cell, which rolled around the MA-INA6 cell for a median time of 2.5 hours post division ($Q_1 = 1.00$ hour, $Q_3 = 6.25$ hours) until it stopped and re-adhered to the hMSC monolayer (Fig. 3D; Supplementary Video 2, Supplementary Video 4). Thus, cell division establishes a time window in which one daughter cell can detach.

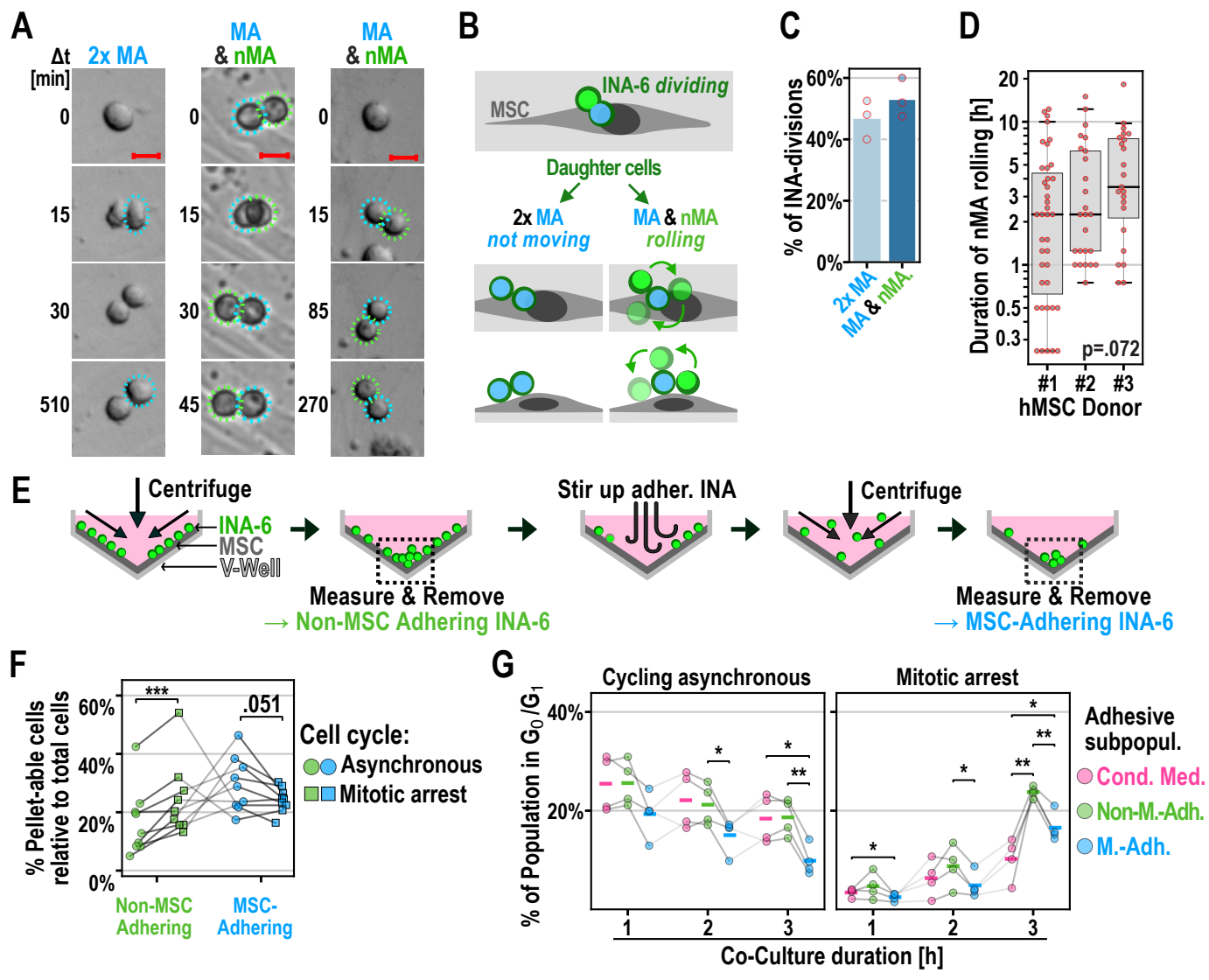


Figure 3: Detachment of INA-6 daughter cells after Cell Division. **A-D:** INA-6 divisions in interaction with confluent hMSCs. Seeding ratio INA-6:MSC = 4:20. **A:** Three examples of dividing INA-6 cells generating either two MA, or one MA and one nMA daughter cells as described in (G). Dashed circles mark mother cells (white), MA cell (blue), and first position of nMA cell (green). Scale bar: 20 μ m. **B:** Cell division of MSC-adhering (MA) mother cell can yield one mobile non-MSC-adhering (nMA) daughter cell. **C:** Frequencies of INA-6 pairs defined in (A, B) per observed cell division. 65 divisions were evaluated for each of three independent time-lapse recordings. **D:** Rolling duration of nMA cells after division did not depend on hMSC donor [$H(2) = 5.250$, $p\text{-unc} = .072$]. Datapoints represent single nMA-cells after division. **E-G:** Adhesive and cell cycle assessment of MSC-interacting INA-6 subpopulations using the V-Well assay. **E:** Schematic of V-Well Assay (see Appendix A: Fig. 1 for detailed analysis). MSC-interacting subpopulations were separated by subsequent centrifugation and removal of the pellet. The pellet size was quantified by its total fluorescence brightness. Adhering subpopulations were resuspended by rough pipetting. **F:** Relative cell pellet sizes of adhesive INA-6 subpopulations that cycle either asynchronously or were synchronized at mitosis. Gray lines in-between points connect dependent measurements of co-cultures ($n = 9$) that shared the same hMSC-donor and INA-6 culture. Co-cultures were incubated for three different durations (1 h, 2 h and 3 h after INA-6 addition). Time points were pooled, since time did not show an effect on cell adhesion [$F(2, 4) = 1.414$, $p\text{-unc} = 0.343$] Factorial RM-ANOVA shows an interaction between cell cycle and the kind of adhesive subpopulation [$F(1, 8) = 42.67$, $p\text{-unc} = 1.82 \times 10^{-4}$]. Technical replicates = 4 per datapoint. **G:** Cell cycles were profiled in cells gathered from the pellets of four independent co-cultures ($n = 4$) and the frequency of G0/G1 cells are displayed depending on co-culture duration (see Appendix A: Fig. 3 for cell cycle profiles). Four technical replicates were pooled after pelleting. **Statistics:** (D): Kruskal-Wallis H-test. (F): Paired t-test, (G): Paired t-test, two-factor RM-ANOVA. Datapoints represent INA-6 from independent co- cultures with hMSCs from three unique donors.

To validate that cell division reduced adhesion, we measured both the size and cell cycle profile of the nMA-INA6 and MA-INA6 populations using an enhanced V-well assay (method described in Fig. 3E, Appendix A: Fig. 1, 2). For comparison, we fully synchronized and arrested INA-6 cells at mitosis and released their cell cycle immediately before addition to the hMSC monolayer, rendering them more likely to divide while adhering. Mitotic arrest significantly increased the number of nMA-INA6 cells and decreased the number of MA-INA6 cells (Fig. 3F). Furthermore, the nMA-INA6 population contained significantly more cells cycling in the G0/G1 phase than the MA-INA6 population, both in synchronously and asynchronously cycling INA-6 (Fig. 3G, Appendix A: Fig. 3, 4). The number of nMA-INA6 INA-6 cells increased due to a higher cell division frequency. Taken together, we showed that INA-6 detach from aggregates by generating one temporarily detached daughter cell after cell division, a process that potentially contributes to the initiation of dissemination.

RNAseq of Non-MSC-Adhering and MSC-Adhering Subpopulations

To characterize the subpopulations separated by WPSC, we conducted RNAseq, revealing 1291 differentially expressed genes between nMA-INA6 *vs.* CM-INA6, 484 between MA-INA6 *vs.* CM-INA6, and 195 between MA-INA6 *vs.* nMA-INA6. We validated RNAseq and found that the differential expression of 18 genes correlated with those measured with qPCR for each pairwise comparison (Fig. 4C-E, Appendix A: Fig. 5): nMA-INA6 *vs.* CM-INA6 [$\rho(16) = .803$, $p = 6.09 \times 10^{-5}$], MA-INA6 *vs.* CM-INA6 [$\rho(16) = .827$, $p = 2.30 \times 10^{-5}$], and MA-INA6 *vs.* nMA-INA6 [$\rho(16) = .746$, $p = 3.74 \times 10^{-4}$] (Spearman's rank correlation). One of the 18 genes (*MUC1*) measured by qPCR showed a mean expression op-

posite to that obtained by RNAseq (nMA-INA6 *vs.* CM-INA6), although the difference was insignificant (Fig. 4C). For nMA-INA6 *vs.* CM-INA6, the difference in expression measured by qPCR was significant for only two of the 11 genes (*DKK1*, *OPG*), whereas the other genes (*DKK1*, *OPG*, *BCL6*, *BMP4*, *BTG2*, *IL10RB*, *IL24*, *NOTCH2*, *TNFRSF1A*, *TRAF5*) only confirmed the tendency measured by RNAseq (Fig. 4C–E). For MA-INA6 *vs.* CM-INA6, qPCR validated the significant upregulation of seven genes (*DKK1*, *OPG*, *BCL6*, *BMP4*, *BTG2*, *IL10RB*, *IL24*, *NOTCH2*, *TNFRSF1A*, *TRAF5*, *TGM2*, *DCN*, *LOX*, *MMP14*, *MMP2*, *CXCL12*, *CXCL8*), whereas the downregulation of *BMP4* was insignificant.

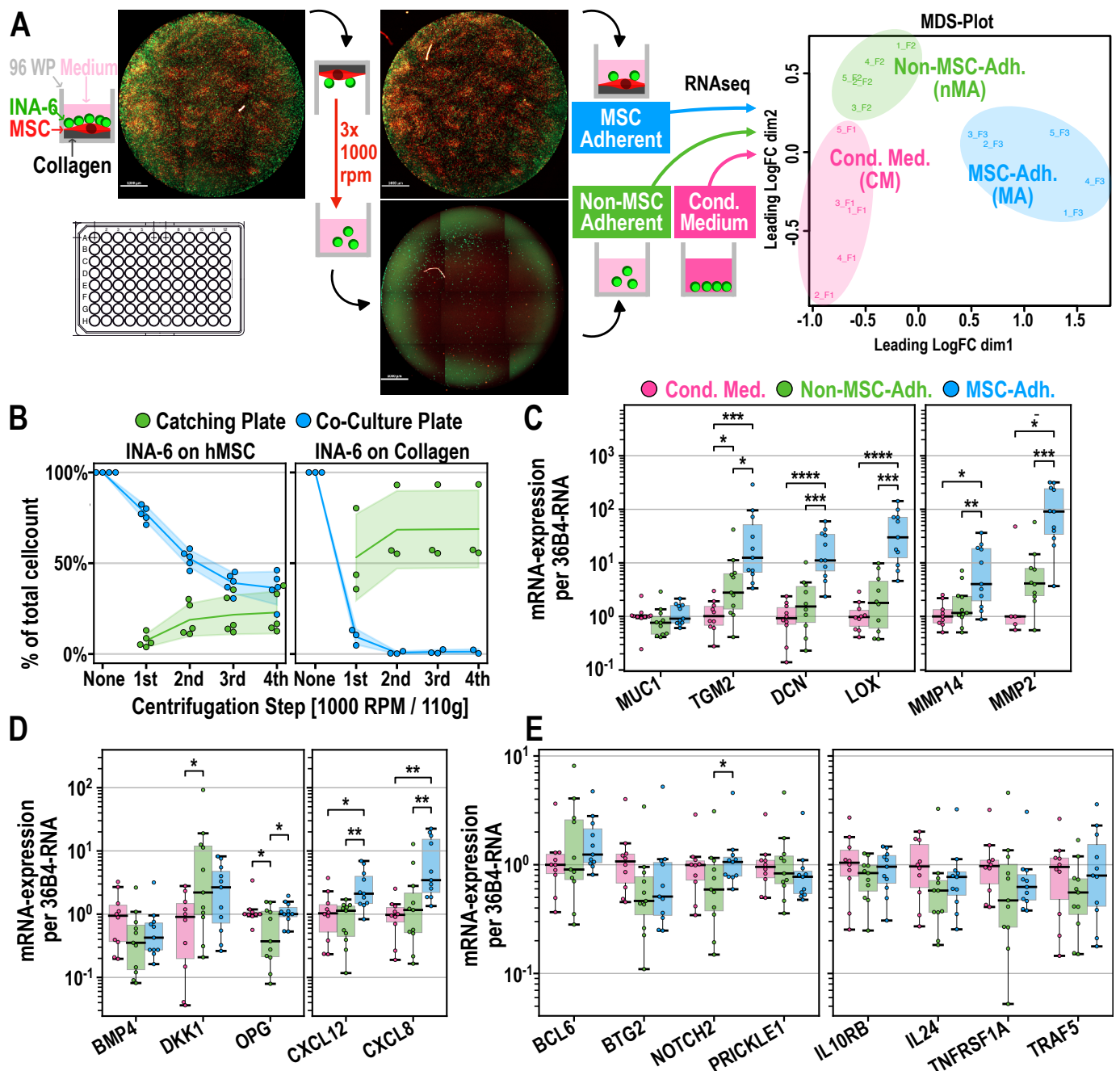


Figure 4: Separation and gene expression of INA-6 subpopulations. **A:** Schematic of “Well-Plate Sandwich Centrifugation” (WPSC) separating nMA- from MA-INA6. A co-culture 96-well plate is turned upside down and attached on top of a “catching plate”, forming a “well-plate sandwich”. nMA-INA6 cells are collected in the catching plate by subsequent rounds of centrifugation and gentle washing. MA-INA6 are enzymatically dissociated from hMSCs or by rough pipetting. Subsequent RNAseq of MSC-interacting subpopulations reveals distinct expression clusters [right, multidimensional scaling plot (MDS) ($n = 5$)]. **B:** Separation was microscopically tracked after each centrifugation step. **C-E:** RT-qPCR of genes derived from RNAseq results. Expression was normalized to the median of CM-INA6. Samples include those used for RNAseq and six further co-cultures ($n = 11$; non-detects were discarded). **C:** Adhesion factors, ECM proteins, and matrix metalloproteinases. **D:** Factors involved in bone remodeling and bone homing chemokines. **E:** Factors involved in (immune) signaling. **Statistics:** (C-E): Paired t-test. Datapoints represent the mean of three (B-E) technical replicates. INA-6 were isolated from independent co-cultures with hMSCs from five (A, B), nine (C-E) unique donors.

Non-MSC-Adhering INA-6 and MSC-Adhering INA-6 Have Distinct Expression Patterns of Proliferation or Adhesion, Respectively

To functionally characterize the unique transcriptional patterns in nMA-INA6 and MA-INA6, we generated lists of genes that were differentially expressed *vs.* the other two subpopulations [termed nMA *vs.* (MA & CM) and MA *vs.* (nMA & CM)]. Functional enrichment analysis was performed, and the enriched terms were displayed as ontology clusters (Fig. 5A). nMA-INA6 upregulated genes enriched with loosely connected term clusters associated with proliferation (e.g., “positive regulation of cell cycle”). MA-INA6 upregulated genes enriched with tightly connected term clusters related to cell adhesion and the production of ECM factors (e.g., “cell-substrate adhesion”). Similar ontology terms were enriched in the gene lists obtained from pairwise comparisons nMA *vs.* CM, MA *vs.* CM, and MA *vs.* nMA (Fig. 5B). In particular, nMA *vs.* CM (but not MA *vs.* CM) upregulated genes that were enriched with “G1/S transition”, showing that WPSC isolated nMA-INA6 daughter cells after cell division.

To check for similarities between lists of differentially expressed genes from hMSC-interacting subpopulations, we performed enrichment analysis on gene lists from the overlaps (“ \cap ”) between all pairwise comparisons (Fig. 5B, Appendix A: Fig. 6), and showed the extent of these overlaps in circos plots (Fig. 5C). The overlap between MA *vs.* CM and nMA *vs.* CM showed neither enrichment with proliferation- nor adhesion-related terms but with apoptosis-related terms. A direct comparison of MSC-interacting subpopulations (MA *vs.* nMA) showed a major overlap with MA *vs.* CM (Fig. 5C, middle). This overlap was enriched with terms related to adhesion but not proliferation. Hence, MA-INA6 and nMA-INA6 mostly differed in their expression of adhesion genes.

To assess whether nMA-INA6 and MA-INA6 were regulated by separate transcription factors, we examined the enrichment of curated regulatory networks from the TRRUST database (Fig. 5B, bottom). All the lists were enriched for p53 regulation. E2F1 regulation was observed only in genes upregulated in nMA *vs.* CM and downregulated in MA *vs.* nMA. Genelists involving MA-INA6 were enriched in regulation by subunits of NF- κ B (NFKB1/p105 and RELA/p65) and factors of immediate

early response (SRF, JUN). Correspondingly, NF- κ B and JUN are known to regulate the expression of adhesion factors in multiple myeloma and B-cell lymphoma, respectively (Blonska et al., 2015; Tai et al., 2006).

Taken together, MSC-interacting subpopulations showed unique regulatory patterns, focusing on either proliferation or adhesion.

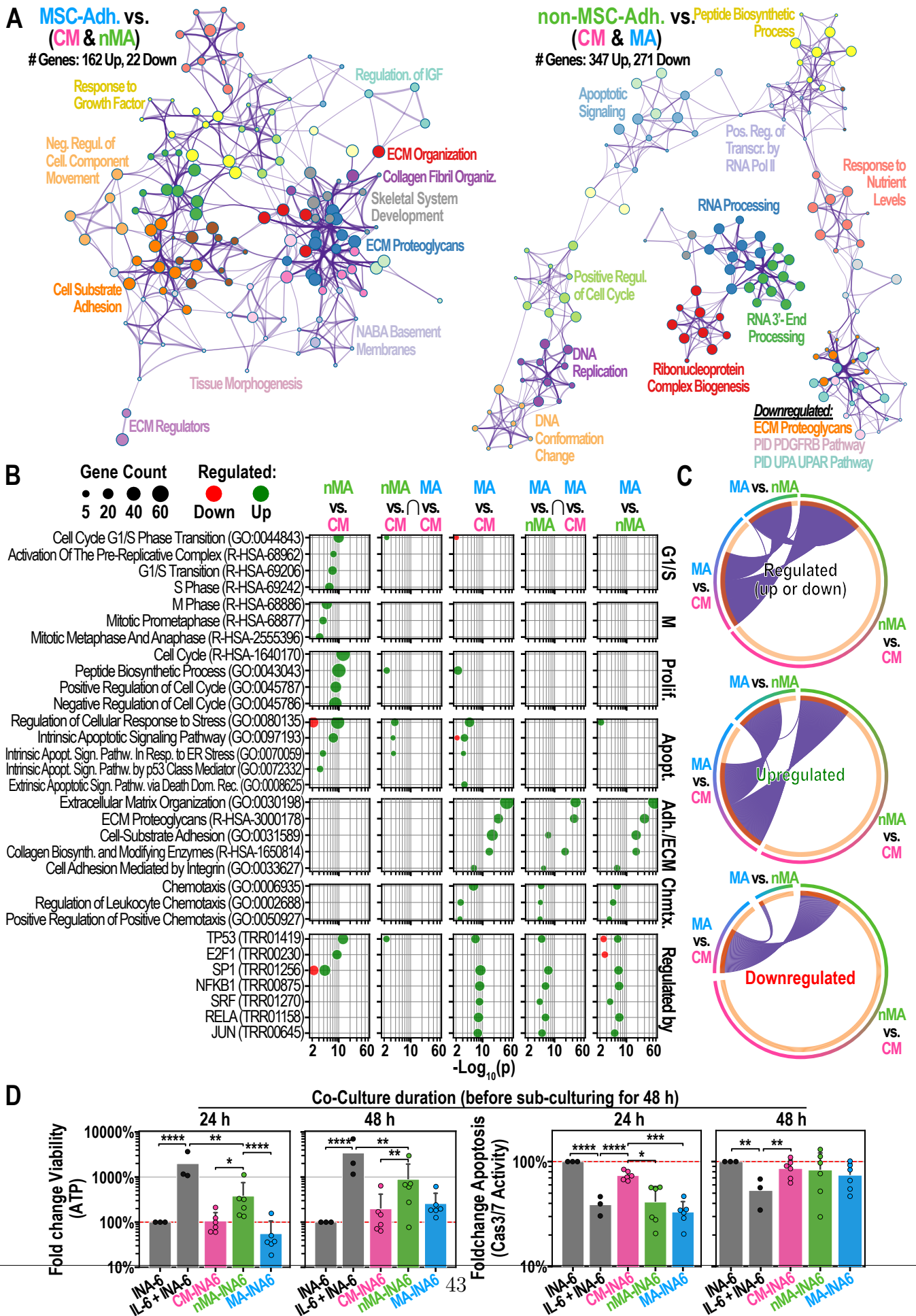


Figure 5: Functional analysis of MSC-interacting subpopulations (**A-C**): Functional enrichment analysis of differentially expressed genes (from RNAseq) using Metascape. **A:** Gene ontology (GO) cluster analysis of gene lists that are unique for MA (left) or nMA (right) INA-6. Circle nodes represent subsets of input genes falling into similar GO-term. Node size grows with the number of input genes. Node color defines a shared parent GO-term. Two nodes with a similarity score > 0.3 are linked. **B:** Enrichment analysis of pairwise comparisons between MA subpopulations and their overlaps (arranged in columns). GO terms were manually picked and categorized (arranged in rows). Raw Metascape results are shown in Appendix A: Fig. 6. For each GO-term, the p-values (x-axis) and the counts of matching input genes (circle size) were plotted. The lowest row shows enrichment of gene lists from the TRRUST-database. **C:** Circos plots by Metascape. Sections of a circle represent lists of differentially expressed genes. Purple lines connect same genes appearing in two gene lists. \cap : Overlapping groups, MA: MSC-adhering, nMA: non-MSC-adhering, CM: MSC-Conditioned Medium. **D:** INA-6 were co-cultured on confluent hMSC for 24 h or 48 h, separated by WPSC and sub-cultured for 48 h under IL-6 withdrawal ($n = 6$), except the control (IL-6 + INA-6) ($n = 3$). Signals were normalized (red line) to INA-6 cells grown without hMSCs and IL-6 ($n = 3$). **Statistics:** (D): Paired t-test, two-factor RM-ANOVA. Datapoints represent the mean of four technical replicates. INA-6 were isolated from independent co-cultures with hMSCs from six unique donors.

nMA-INA6 and MA-INA6 Show Increased Apoptosis Signaling Mediated by ER-Stress, p53 and Death Domain Receptors

As previously stated, apoptosis rates increased in INA-6 cells grown on confluent hMSCs compared with MSC-Conditioned-Medium-treated INA-6 (CM-INA6) cells after 24 hours of co-culture (Fig. 1D). Since this setup was similar to that used to separate hMSC-interacting subpopulations using WPSC, we looked for enrichment of apoptosis-related terms (Fig. 5B). “Regulation of cellular response to stress” and “intrinsic apoptotic signaling pathway (in response to ER-stress)” are terms that were enriched in nMA *vs.* CM, MA *vs.* CM and their overlap. We also found specific stressors for either nMA-INA6 (“intrinsic apoptotic signaling pathway by p53 class mediator”) or MA-INA6 (“extrinsic apoptotic signaling pathway via death domain receptor”). Therefore, apoptosis may be driven by ER stress in both nMA-INA6 and MA-INA6, but also by individual pathways such as p53 and death domain receptors, respectively.

nMA-INA6 and MA-INA6 Regulate Genes Associated with Bone Loss

Myeloma cells cause bone loss by degradation and dysregulation of bone turnover via *DKK1* and *OPG* (Standal et al., 2002; Van Valckenborgh et al., 2004; F. Zhou et al., 2013). RNAseq of hMSC-interacting subpopulations showed enrichment with functional terms “skeletal system development” and “ossification” (Fig. 5A, Appendix A: Fig. 6), as well as the regulation of *MMP2*, *MMP14*, *DKK1*, and *OPG*. Validation by qPCR (Fig. 4C, D) showed that MA-INA6 significantly upregulated both *MMP14* and *MMP2* compared with either nMA-INA6 or CM-INA6. The expression of *DKK1*, however, was upregulated significantly in nMA-INA6 (and not significantly upregulated in MA-INA6), while *OPG* was significantly downregulated only in nMA-INA6.

Together, hMSC-interacting subpopulations might contribute to bone loss through different mechanisms: MA-INA6 expression of matrix metalloproteinases and nMA-INA6 cells via paracrine signal-

ing.

MA-INA6 Upregulate Collagen and Chemokines Associated with Bone Marrow Retention

Retention of myeloma cells within the bone marrow is mediated by adhesion to the ECM (e.g., collagen VI) and the secretion of chemokines (*CXCL8* and *CXCL12*), potentially counteracting dissemination (Alsayed et al., 2007; Katz, 2010). RNAseq of hMSC-interacting subpopulations showed that genes upregulated in MA-INA6 were enriched with collagen biosynthesis and modifying enzymes, as well as chemotaxis and chemotaxis-related terms (Fig. 5B). Using qPCR, we validated the upregulation of collagen crosslinkers (*LOX* and *TGM2*), collagen-binding *DCN*, and chemokines (*CXCL8* and *CXCL12*) in MA-INA6 compared with both nMA-INA6 and CM-INA6 (Fig. 4D). Therefore, MA-INA6 can provide both an adhesive surface and soluble signals for the retention of malignant plasma cells in the bone marrow.

nMA-INA6 Show Highest Viability During IL-6 Withdrawal

Although RNAseq did not reveal IL-6 induction in any WPSC-isolated subpopulation, nMA-INA6 upregulated *IGF-1* 1.35-fold [RNAseq, nMA vs. (MA & CM)], which was shown to stimulate growth in CD45+ and IL-6 dependent myeloma cell lines such as INA-6, implying increased autonomy for nMA-INA6 (40). To test the autonomy of hMSC-interacting INA-6 subpopulations, we isolated them using WPSC after 24 hours and 48 hours of co-culture, sub-cultured them for 48 hours under IL-6 withdrawal, and measured both viability and apoptosis (Fig. 5D). Among the subpopulations, nMA-INA6 was the most viable. Compared to MA-INA6, nMA-INA6 increased cell viability by 8 or 4 fold when co-cultured for 24 hours or 48 hours, respectively [Hedges *g* of $\text{Log}_{10}(\text{Fold Change}) = 2.31$ or 0.82]. However, the difference was no longer significant after 48 hours of co-culture, probably because nMA-INA6 adhered to the hMSC layer (turning into MA-INA6) during prolonged co-culture, which could also explain why the viability of MA-INA6 cell subcultures increased with prolonged co-culture. Nevertheless, nMA-INA6 did not achieve the same viability as that of INA-6 cells cultured with IL-6. Despite the differences in viability, subcultures of hMSC-interacting subpopulations did not show any differences in caspase 3/7 activity when co-cultured for 48 hours (Fig. 5D, right).

Overall, among the hMSC-interacting subpopulations, nMA-INA6 had the highest chance of surviving IL-6 withdrawal.

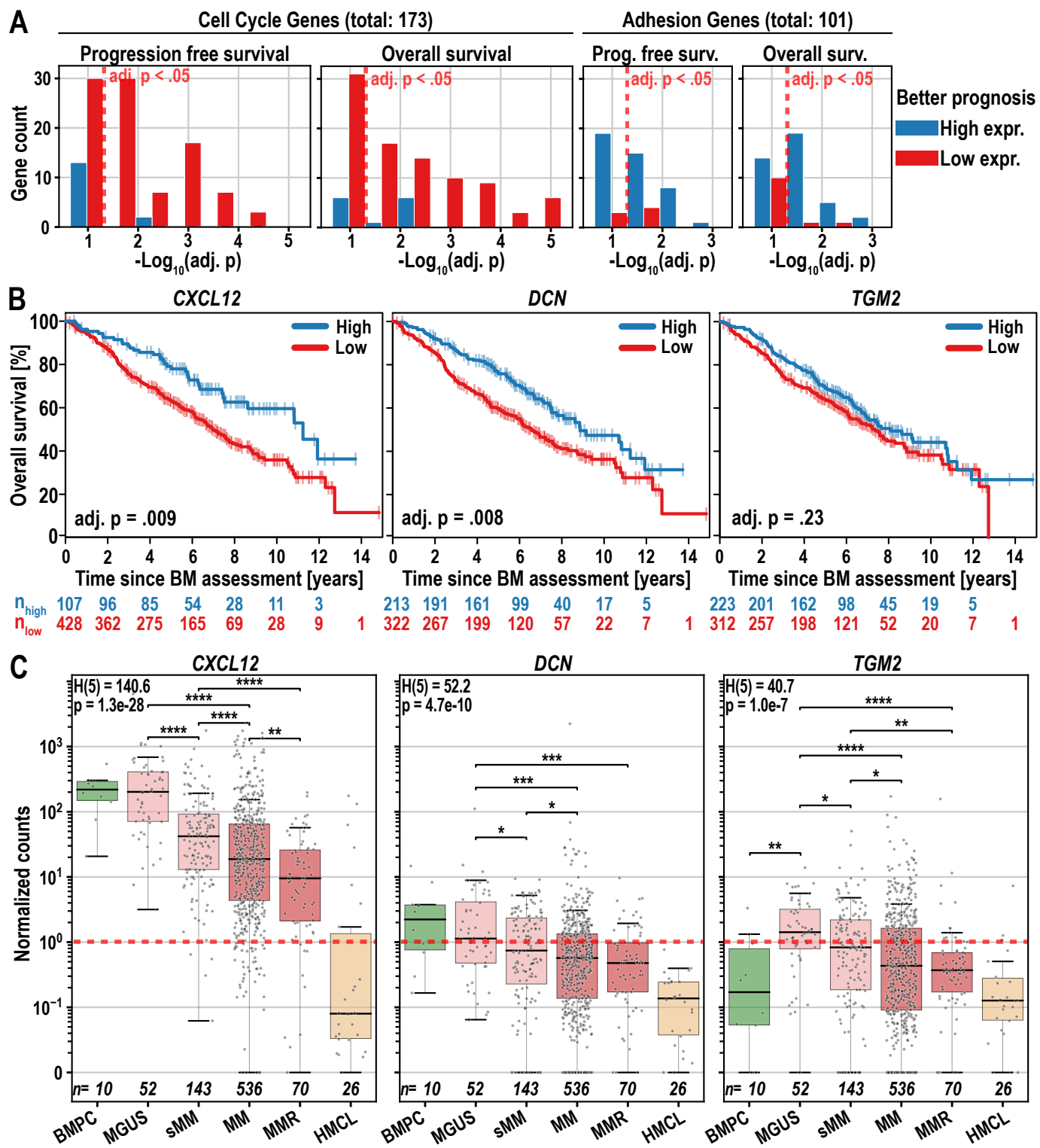


Figure 6: Survival of patients with multiple myeloma regarding the expression levels of adhesion and bone retention genes. **A:** p-value distribution of genes associated with patient survival ($n = 535$) depending on high or low expression levels. Red dashed line marks the significance threshold of $p\text{-adj} = 0.05$. Histogram of p -values was plotted using a bin width of $-\log_{10}(0.05)/2$. Patients with high and low gene expression were delineated using maximally selected rank statistics (maxstat). **B:** Survival curves for three genes taken from the list of adhesion genes shown in (A), maxstat thresholds defining high and low expression were: *CXCL12*: 81.08; *DCN*: 0.75; *TGM2*: 0.66 normalized counts. **C:** Gene expression (RNAseq, $n = 873$) measured in normalized counts (edgeR) of *CXCL12*, *DCN* in Bone Marrow Plasma Cell (BMPC), Monoclonal Gammopathy of Undetermined Significance (MGUS), smoldering Multiple Myeloma (sMM), Multiple – *continued on next page*

Figure 6: *continued from previous page* – Myeloma Relapse (MMR), Human Myeloma Cell Lines (HMCL). The red dashed line marks one normalized read count. **Statistics:** (A, B): Log-rank test; (C): Kruskal-Wallis, Mann-Whitney U Test. All p -values were corrected using the Benjamini-Hochberg procedure.

Genes Upregulated by MA-INA6 are Associated with an Improved Disease Prognosis

To relate the adhesion of MA-INA6 observed *in vitro* to the progression of multiple myeloma, we assessed patient survival [$n = 535$, Seckinger et al. (2017, 2018)] depending on the expression level of 101 genes, which were upregulated in MA *vs.* (nMA & CM) and are part of the ontology terms “Extracellular matrix organization,” “ECM proteoglycans,” “cell-substrate adhesion,” and “negative regulation of cell-substrate adhesion” (Fig. 6A, Appendix A: Tab. 2). As a reference, we generated a list of 173 cell cycle-related genes that were upregulated by nMA *vs.* (MA & CM).

As expected, longer patient survival was associated with low expression of the majority of cell cycle genes [71 or 68 genes for Progression-Free Survival (PFS) or Overall Survival (OS)]. Only a few cell cycle genes (two for PFS and seven for OS) were associated with survival when highly expressed. Intriguingly, adhesion genes showed an inverse pattern: a large group of adhesion genes (24 for PFS and 26 for OS) was significantly associated with improved survival when highly expressed, whereas only a few genes (two for PFS and four for OS) improved survival when expressed at low levels (Tab. 1). We concluded that the myeloma-dependent expression of adhesion factors determined in our *in vitro* study correlates with improved patient survival.

Expression of Adhesion- or Retention-related Genes (*CXCL12*, *DCN* and *TGM2*) is Decreased During Progression of Multiple Myeloma

To examine how the disease stage affects the adhesion and bone marrow retention of myeloma cells *in vitro*, we analyzed the expression of *CXCL12* in healthy plasma cell (BMPC) cohorts of patients at different disease stages and in myeloma cell lines (HMCL) [described in Seckinger et al. (2018)] (Fig. 6C). We also included *DCN* and *TGM2* since both are suggested to inhibit metastasis in different cancers by promoting cell-matrix interactions (Hu et al., 2021; Tabolacci et al., 2019). In accordance

with independent reports (Huang et al., 2015; Bao et al., 2013), high expression of *CXCL12* and *DCN* by myeloma cells was associated with improved overall survival (adj. $p = .009$ and $.008$, respectively) (Fig. 6B).

Table 1: Adhesion and ECM genes (shown in Fig. 6A) were filtered by their association with patient survival (p -adj. < 0.01) and were categorized as continuously downregulated during disease progression. The complete list is presented in Appendix A: Tab. 2. Bone Marrow Plasma Cells (BMPC), Monoclonal Gammopathy of Undetermined Significance (MGUS), smoldering Multiple Myeloma (sMM), Multiple Myeloma (MM), and Multiple Myeloma Relapse (MMR). p-unc: unadjusted p-values; p-adj: p-values adjusted using the Benjamini-Hochberg method with 101 genes.

Regulation during disease progression	Gene	Ensemble ID	Progression Free / Overall Survival	Better Prognosis with high/low expression	Association of expression with survival	
					[p-unc]	[p-adj]
Not Downregulated (or overall low expression)	CCNE2	ENSG00000175305	Overall	low	5.34E-04	8.64E-03
	MMP2	ENSG00000087245	Prog. Free	high	2.29E-05	2.32E-03
	OSMR	ENSG00000145623	Prog. Free	high	5.67E-04	7.15E-03
Continuously Downregulated (BMPC > MGUS > sMM > MM > MMR)	AXL	ENSG00000167601	Overall	high	3.64E-05	1.84E-03
	COL1A1	ENSG00000108821	Prog. Free	high	3.03E-04	4.37E-03
			Overall	high	5.93E-04	8.64E-03
	CXCL12	ENSG00000107562	Prog. Free	high	1.16E-04	2.93E-03
			Overall	high	6.48E-04	8.64E-03
	CYP1B1	ENSG00000138061	Overall	high	6.84E-04	8.64E-03
	DCN	ENSG00000011465	Overall	high	2.47E-04	8.33E-03
	LRP1	ENSG00000123384	Overall	high	4.34E-04	8.64E-03
	LTBP2	ENSG00000119681	Prog. Free	high	9.03E-05	2.93E-03
	CYP1B1	ENSG00000138061	Overall	high	6.84E-04	8.64E-03
	DCN	ENSG00000011465	Overall	high	2.47E-04	8.33E-03
	LRP1	ENSG00000123384	Overall	high	4.34E-04	8.64E-03
	LTBP2	ENSG00000119681	Prog. Free	high	9.03E-05	2.93E-03
	MFAP5	ENSG00000197614	Prog. Free	high	2.43E-04	4.09E-03
	MMP14	ENSG00000157227	Prog. Free	high	6.93E-05	2.93E-03
	MYL9	ENSG00000101335	Prog. Free	high	1.46E-04	2.95E-03
			Overall	high	1.56E-05	1.57E-03

CXCL12 is expressed by BMPCs (median = 219 normalized counts), but its expression levels are significantly lower from MGUS to relapsed multiple myeloma (MMR) (median = 9 normalized counts in MMR and absent expression in most HMCL). *DCN* (but not *TGM2*) was weakly expressed in BMPCs ($Q_1 = 0.7$, $Q_3 = 3.7$, normalized counts), whereas *TGM2* was weakly expressed only in

patients with monoclonal gammopathy of undetermined significance (MGUS) ($Q_1 = 0.4$, $Q_3 = 4.1$ normalized counts). The median and upper quartiles of both *DCN*- and *TGM2* decreased continuously after each stage, ending at $Q_3 = 0.9$ and $Q_3 = 0.6$, respectively, in MMR. 49 of the 101 adhesion genes (Fig. 6A) followed a similar pattern of continuous downregulation in the advanced stages of multiple myeloma (Appendix A: Fig. 7 and 8), of which 19 genes were associated with longer PFS when they were highly expressed. The other 52 (out of 101) adhesion genes that were not downregulated across disease progression (or were expressed at a level too low to make that categorization) contained only five genes that were associated with longer PFS at high expression (Tab. 1, Appendix A: Tab. 2).

Together, the expression of adhesion or bone marrow retention-related markers (*CXCL12*, *DCN*, and *TGM2*) is reduced or lost at advanced stages of multiple myeloma, which could enhance dissemination and reduce retention in the BM microenvironment.

Discussion

In this study, we developed an *in vitro* model to investigate the attachment/detachment dynamics of INA-6 cells to/from hMSCs and established methods to isolate the attached and detached intermediates nMA-INA6 and MA-INA6. Secondly, we characterized a cycle of (re)attachment, division, and detachment, linking cell division to the switch that causes myeloma cells to detach from hMSC adhesion (Fig. 7). Thirdly, we identified clinically relevant genes associated with patient survival, where better or worse survival was based on the adherence status of INA-6 to hMSCs.

INA-6 cells emerged as a robust choice for studying myeloma dissemination *in vitro*, showing rapid and strong adherence, as well as aggregation exceeding MSC saturation. The IL-6 dependency of INA-6 enhanced the resemblance of myeloma cell lines to patient samples, with INA-6 ranking 13th among 66 cell lines (Sarin et al., 2020). Despite variations in bone marrow MSCs between multiple myeloma and healthy states, we anticipated the robustness of our results, given the persistent strong adherence and growth signaling from MSCs to INA-6 during co-cultures (Dotterweich et al., 2016).

We acknowledge that INA-6 cells alone cannot fully represent the complexity of myeloma aggregation and detachment dynamics. However, the diverse adhesive properties of myeloma cell lines pose a challenge. We reasoned that attempting to capture this complexity within a single publication would not be possible. Our focus on INA-6 interactions with hMSCs allowed for a detailed exploration of the observed phenomena, such as the unique aggregation capabilities that facilitate the easy detection of detaching cells *in vitro*. The validity of our data was demonstrated by matching the *in vitro* findings with the gene expression and survival data of the patients (e.g., *CXCL12*, *DCN*, and *TGM2* expression, $n = 873$), ensuring biological consistency and generalizability regardless of the cell line used. The protocols presented in this study offer a cost-efficient and convenient solution, making them potentially valuable for a broader study of cell interactions. We encourage optimizations to meet the varied adhesive properties of the samples, such as decreasing the number of washing steps if the adhesive strength is low. We caution against strategies that average over multiple cell lines without prior understanding their diverse attachment/detachment dynamics, such as homotypic aggregation. Such detailed insights may prove instrumental when considering the diversity of myeloma patient samples across different disease stages (Kawano et al., 1991; Okuno et al., 1991).

The intermediates, nMA-INA6 and MA-INA6, were distinct but shared similarities in response to cell stress, intrinsic apoptosis, and regulation by p53. Unique regulatory patterns were related to central transcription factors: E2F1 for nMA-INA6; and NF- κ B, SRF, and JUN for MA-INA6. This distinction may have been established through antagonism between p53 and the NF- κ B subunit RELA/p65 (Wadgaonkar et al., 1999; Webster & Perkins, 1999). Similar regulatory patterns were found in transwell experiments with RPMI1-8226 myeloma cells, where direct contact with the MSC cell line HS5 led to NF- κ B signaling and soluble factors to E2F signaling (Dziadowicz et al., 2022).

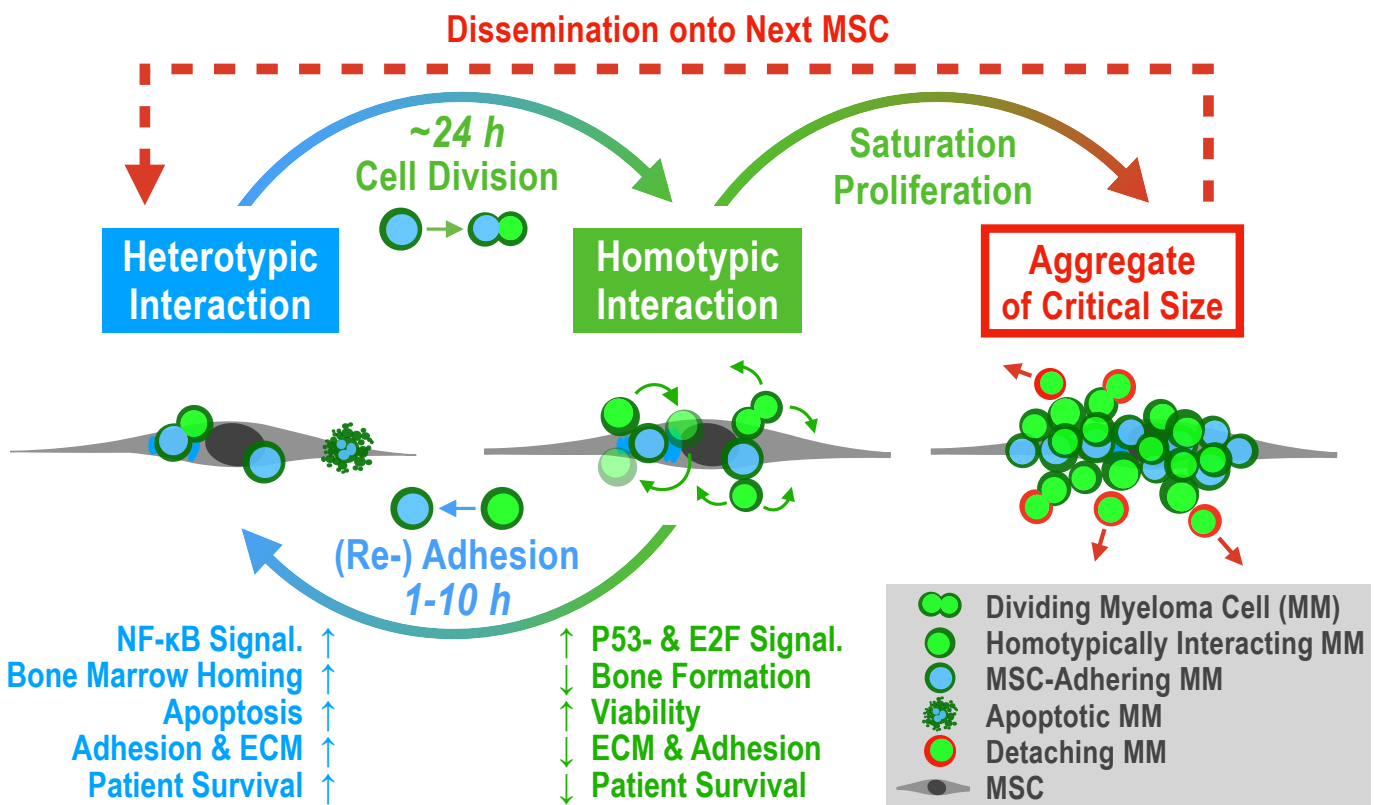


Figure 7: Proposed model of “Detached Daughter Driven Dissemination” (DDDD) in aggregating multiple myeloma. **Heterotypic Interaction:** Malignant plasma cells colonize the bone marrow microenvironment by adhering to an MSC (or osteoblast, ECM, etc.) to maximize growth and survival through paracrine and adhesion mediated signaling, even if contact may trigger initial apoptosis. Gene expression will focus on establishing a strong anchor within the bone marrow, but also on attracting other myeloma cells (via secretion of ECM factors and CXCL12/CXCL8, respectively). **Cell Division:** Cell fission can generate one daughter cell that no longer adheres to the MSC (nMA). **Homotypic Interaction:** If myeloma cells have the capacity to grow as aggregates, the daughter cell stays attached to their MSC-adhering mother cell (MA). **Re-Adhesion:** The daughter cell “rolls around” the mother cell until it re-adheres to the MSC. Our model estimates the rolling duration to be 1–10 h long. **Proliferation & Saturation:** We estimate that a single myeloma cell covers one MSC completely after roughly four population doublings. When heterotypic adhesion is saturated, subsequent daughter cells benefit from a homotypic interaction, since they stay close to growth-factor secreting MSCs and focus gene expression on proliferation (e.g. driven by E2F) and not adhesion (driven by NF- κ B). **Critical Size:** Homotypic interaction is weaker than heterotypic interaction, and each cell fission destabilizes the aggregate. Hence, detachment of myeloma cells may depend mostly on aggregate size. **Dissemination:** After myeloma cells have detached, they gained a viability advantage through IL-6-independence (with unknown duration), which enhances their survival outside of the bone marrow and allows them to spread throughout the body.

The first subpopulation, nMA-INA6, represented proliferative and disseminative cells; They drove detachment through cell division, which was regulated by E2F, p53, and likely their crosstalk (Polager & Ginsberg, 2009). nMA-INA6 upregulate cell cycle progression genes associated with worse prognosis, because proliferation is a general risk factor for an aggressive disease course (Hose et al., 2011). Additionally, nMA-INA6 survived IL-6 withdrawal better than CM-INA6 and MA-INA6, implying their ability to proliferate independently of the bone marrow (Bladé et al., 2022). Indeed, xenografted INA-6 cells developed autocrine IL-6 signaling but remained IL-6-dependent after explan-

tation (Burger, Günther, et al., 2001). The increased autonomy of nMA-INA6 cells can be explained by the upregulation of *IGF-1*, being the major growth factor for myeloma cell lines (Sprynski et al., 2009). Other reports characterized disseminating cells differently: Unlike nMA-INA6, circulating myeloma tumor cells were reported to be non-proliferative and bone marrow retentive (Garcés et al., 2020). In contrast to circulating myeloma tumor cells, nMA-INA6 were isolated shortly after detachment and therefore these cells are not representative of further steps of dissemination, such as intravasation, circulation or intravascular arrest (Zeissig et al., 2020). Furthermore, Brandl et al. described proliferative and disseminative myeloma cells as separate entities, depending on the surface expression of CD138 or JAM-C (Akhmetzyanova et al., 2020; Brandl et al., 2022). Although CD138 was not differentially regulated in nMA-INA6 or MA-INA6, both subpopulations upregulated JAM-C, indicating disease progression (Brandl et al., 2022).

Furthermore, nMA-INA6 showed that cell division directly contributed to dissemination. This was because INA-6 daughter cells emerged from the mother cell with distance to the hMSC plane in the 2D setup. A similar mechanism was described in an intravasation model in which tumor cells disrupt the vessel endothelium through cell division and detach into blood circulation (Wong & Searson, 2017). Overall, cell division offers key mechanistic insights into dissemination and metastasis.

The other subpopulation, MA-INA6, represented cells retained in the bone marrow; MA-INA6 strongly adhered to MSCs, showed NF- κ B signaling, and upregulated several retention, adhesion, and ECM factors. The production of ECM-associated factors has recently been described in MM.1S and RPMI-8226 myeloma cells (Maichl et al., 2023). Another report did not identify the upregulation of such factors after direct contact with the MSC cell line HS5; hence, primary hMSCs may be crucial for studying myeloma-MSC interactions (Dziadowicz et al., 2022). Moreover, MA-INA6 upregulated adhesion genes associated with prolonged patient survival and showed decreased expression in relapsed myeloma. As myeloma progression implies the independence of myeloma cells from the bone marrow (Bladé et al., 2022; Sarin et al., 2020), we interpreted these adhesion genes as mediators of bone marrow retention, decreasing the risk for dissemination and thereby potentially prolonging patient survival. However, the overall impact of cell adhesion and ECM on patient survival remains unclear. Several adhesion factors have been proposed as potential therapeutic targets (Brandl et al., 2022; ?). Recent studies have described the prognostic value of multiple ECM genes, such as those driven by NOTCH (Maichl et al., 2023). Another study focused on ECM gene families, of which only six of the 26 genes overlapped with our gene set (Appendix A: Tab. 2) (Evers et al., 2023). The expression of only one gene (*COL4A1*) showed a different association with overall survival than that in our cohort. The lack of overlap and differences can be explained by dissimilar definitions of gene sets (homology *vs.* gene ontology), methodological discrepancies, and cohort composition.

In summary, our *in vitro* model provides a starting point for understanding the initiation of dissemination and its implications for patient survival, providing innovative methods, mechanistic

insights into attachment/detachment, and a set of clinically relevant genes that play a role in bone marrow retention. These results and methods might prove useful when facing the heterogeneity of disseminative behaviors among myeloma cell lines and primary materials.

Chapter 2: Semi-Automating Data Analysis with `plotastic`

Abstract

`plotastic` addresses the challenges of transitioning from exploratory data analysis to hypothesis testing in Python’s data science ecosystem. Bridging the gap between `seaborn` and `pingouin`, this library offers a unified environment for plotting and statistical analysis. It simplifies the workflow with user-friendly syntax and seamless integration with familiar `seaborn` parameters (`y`, `x`, `hue`, `row`, `col`). Inspired by `seaborn`’s consistency, `plotastic` utilizes a `DataAnalysis` object to intelligently pass parameters to `pingouin` statistical functions. Hence, statistics and plotting are performed on the same set of parameters, so that the strength of `seaborn` in visualizing multidimensional data is extended onto statistical analysis. In essence, `plotastic` translates `seaborn` parameters into statistical terms, configures statistical protocols based on intuitive plotting syntax and returns a `matplotlib` figure with known customization options and more. This approach streamlines data analysis, allowing researchers to focus on correct statistical testing and less about specific syntax and implementations.

Introduction

The reproducibility crisis in research highlights a significant challenge in contemporary biosciences, where a substantial portion of studies faces reproducibility issues (Baker, 2016; Begley & Ioannidis, 2015; Gosselin, 2021). One critical yet often overlooked aspect contributing to this crisis is data management. The literature most often refers to *big data* as the main challenge (Gomez-Cabrero et al., 2014). However, these challenges are also present in smaller datasets, which the author refers to as *semi-big data*. This term describes datasets that – while not extensive enough to necessitate advanced computational tools typically reserved for *big data* – are sufficiently large to render manual analysis very time-intensive. Semi-big data is often generated by methods like automated microscopy or multiplex qPCR, which produce volumes of data that are manageable on a surface level, but pose substantial barriers for in-depth, manual reproducibility (Bustin, 2014; Incerti et al., 2019). This is further complicated by the complexity inherent in multidimensional datasets (Krzywinski & Savig, 2013): Modern biosciences describe processes (e.g. cell-adhesion) that are highly dependent on multiple experimental parameters (factors), like ‘*time*’ or ‘*kinds of treatments*’ (Rebl et al., 2010; McKay et al., 1997). Manually grouping the data by multiple factors (facetting) is challenging and error-prone, especially when the data is not structured in a way that is immediately compatible with statistical tests. Without a clearly documented data analysis protocol and standardized data formats, analysis of multidimensional data becomes nontransparent and too overwhelming for reproduction (Bustin, 2014).

The evolving standards in data analysis advocate for the standardization of analytical pipelines, rationalization of sample sizes, and enhanced infrastructure for data storage, addressing some of these challenges (Goodman et al., 2016; Wilkinson et al., 2016). However, these advancements can place undue pressure on researchers, particularly those with limited training in statistics, underscoring the need for intuitive, user-friendly analytical tools (Federer et al., 2016; Lakhli et al., 2023; Armstrong, 2014; Gómez-López et al., 2019; Leek & Peng, 2015).

In this context, `plotastic` emerges as a tool designed to democratize access to sophisticated statistical analysis, offering a user-centric interface that caters to researchers across varying levels of statistical proficiency. `plotastic` simplifies inferential statistics building on a simple idea: Statistical analyses are often performed based on how the data is visualized. For example, the results of a qPCR are categorized by gene; hence, both ANOVA and plot can be accomplished in parallel for every gene independently and automatically. This principle is not only intuitive but also statistically sound, because the parameters that structure the figure (e.g. facetting) are often times re-used for statistical testing (e.g. independent variables or factors). By integrating robust statistical methodologies within an accessible framework, `plotastic` could contribute to enhancing the reproducibility of research in the biosciences (Gomez-Cabrero et al., 2014).

plotastic key design feature is centralizing the facetting parameters utilized by seaborn into a `DataAnalysis` object. `seaborn` uses the parameters `x`, `hue`, `col`, `row` as arguments for many plotting functions. These parameters lay out the structure of the plot, such as which data points are shown on the x-axis, what categories are highlighted by color (`hue`), and how data is grouped into separate plots (by columns and/or rows). By centralizing these parameters, plotastic ensures that all subsequent analysis steps do not require the user to re-specify these parameters, automating not only statistical analysis, but also all edits applied to the plot, such as *p*-value annotations.

The user-centric approach of plotastic distinguishes itself from the fully automated pipelines used for big data, which are designed to handle extensive computational tasks. Instead, plotastic focuses on ease-of-use and structures its commands to enable an interactive review of intermediate outputs, a concept the author refers to as *semi-automation* (Tab. 1).

Table 1: Key Principles of Semi-Automation and their Implementation in Plotastic

No.	Principle	Implementation in plotastic
1	Standardized input: The data to-be-analyzed follows a strict standardized format. The user should be able to convert their data into that format.	Long-format pandas <code>DataFrames</code> are used as input
2	Automation over flexibility: If there is an obvious way to do things, automate it and minimize user input. User options should be added with good reason. Avoid situations where the user is asked to pass the same parameter twice. This reduces the risk of human error, confusion and time spent on configuration.	E.g. passing the parameter “subject” once makes the rest of the pipeline switch automatically to the paired versions of statistical tests.
3	Out of the box functionality: The software’s default configuration should provide acceptable (but potentially sub-optimal) results. Beginners should be invited to experiment without the need to learn custom configurations. Options are still available to allow feature-rich adaptions according to the needs of both data and user.	Default tests are standard unpaired t-tests and ANOVA
4	Focus on intermediate outputs: The user composes the analysis pipeline using smaller commands that are each designed to provide human-readable output of an intermediate result. Each step is a stage to control quality, allowing quick error detection and troubleshooting.	Processing steps are separated into main steps: assumption tests, factor analysis, post-hoc analysis and plotting
5	Highly useful error messages: Never leave the user hanging. Tell him what went wrong <i>and</i> what the software was expecting.	E.g.: <code>ValueError: User passed 'subect' as subject, please choose one of ['subject', 'event', 'region']</code>

The need for plotastic in this specific project is described in detail in the summarizing discussion, since this chapter focuses on the software itself. In short, two main challenges arose that led to the development of plotastic: The first is the author’s need for a tool that could handle the complex, multidimensional data generated by e.g. qPCR experiments. These experiments involved the analysis of multiple outcomes across multiple genes, timepoints, method variations, cell-types, biological replicates, technical replicates etc., resulting in datasets with about 2970 datapoints spread over four dimensions: three subpopulations, one timepoint, eleven biological replicates, and three

technical replicates. Such complexity was necessary, since establishing new methods required extensive controls and creative variation of the experimental setup. Data analysis had to be automated somehow, since the lab-work itself was already time-intensive. The second challenge was to accept the potential of plot-configured statistical analyses. The author believes that the way data is visualized is often the way it should be analyzed, e.g. accomplishing both plot and ANOVA in parallel for every gene when showing qPCR results. This vision is not limited to biomedical application, but a general principle that could benefit the scientific community overall. Making `plotastic` a generalized tool was a conscious decision to maximize its adoption rate and ensure its long-term relevance and quality, of which biomedical research will also benefit.

Statement of Need

Python's data science ecosystem provides powerful tools for both visualization and statistical testing. However, the transition from exploratory data analysis to hypothesis testing can be cumbersome, requiring users to switch between libraries and adapt to different syntaxes. `seaborn` has become a popular choice for plotting in Python, offering an intuitive interface. Its statistical functionality focuses on descriptive plots and bootstrapped confidence intervals (Waskom, 2021). The library `pingouin` offers an extensive set of statistical tests, but it lacks integration with common plotting capabilities (Vallat, 2018). `statannotations` integrates statistical testing with plot annotations, but uses a complex interface and is limited to pairwise comparisons (Charlier et al., 2022).

`plotastic` addresses this gap by offering a unified environment for plotting and statistical analysis. With an emphasis on user-friendly syntax and integration of familiar `seaborn` parameters, it simplifies the process for users already comfortable with `seaborn`. The library ensures a smooth workflow, from data import to hypothesis testing and visualization.

Example

The following code demonstrates how plotastic analyzes the example dataset “fmri”, similar to Waskom (2021) (Fig. 1).

```
1 ### IMPORT PLOTASTIC
2 import plotastic as plst
3
4 # IMPORT EXAMPLE DATA
5 DF, _dims = plst.load_dataset("fmri", verbose = False)
6
7 # EXPLICITLY DEFINE DIMENSIONS TO FACET BY
8 dims = dict(
9     y = "signal",      # y-axis, dependent variable
10    x = "timepoint",   # x-axis, independent variable (within-subject factor)
11    hue = "event",     # color, independent variable (within-subject factor)
12    col = "region"     # axes, grouping variable
13 )
14 # INITIALIZE DATAANALYSIS OBJECT
15 DA = plst.DataAnalysis(
16     data=DF,           # Dataframe, long format
17     dims=dims,         # Dictionary with y, x, hue, col, row
18     subject="subject", # Datapoints are paired by subject (optional)
19     verbose=False,     # Print out info about the Data (optional)
20 )
21 # STATISTICAL TESTS
22 DA.check_normality() # Check Normality
23 DA.check_sphericity() # Check Sphericity
24 DA.omnibus_rm_anova() # Perform RM-ANOVA
25 DA.test_pairwise()    # Perform Posthoc Analysis
26
27 # PLOTTING
28 DA
29 .plot_box_strip()    # Pre-built plotting function initializes plot
30 .annotate_pairwise(  # Annotate results from DA.test_pairwise()
31     include="__HUE") # Use only significant pairs across each hue
32
33 )
```

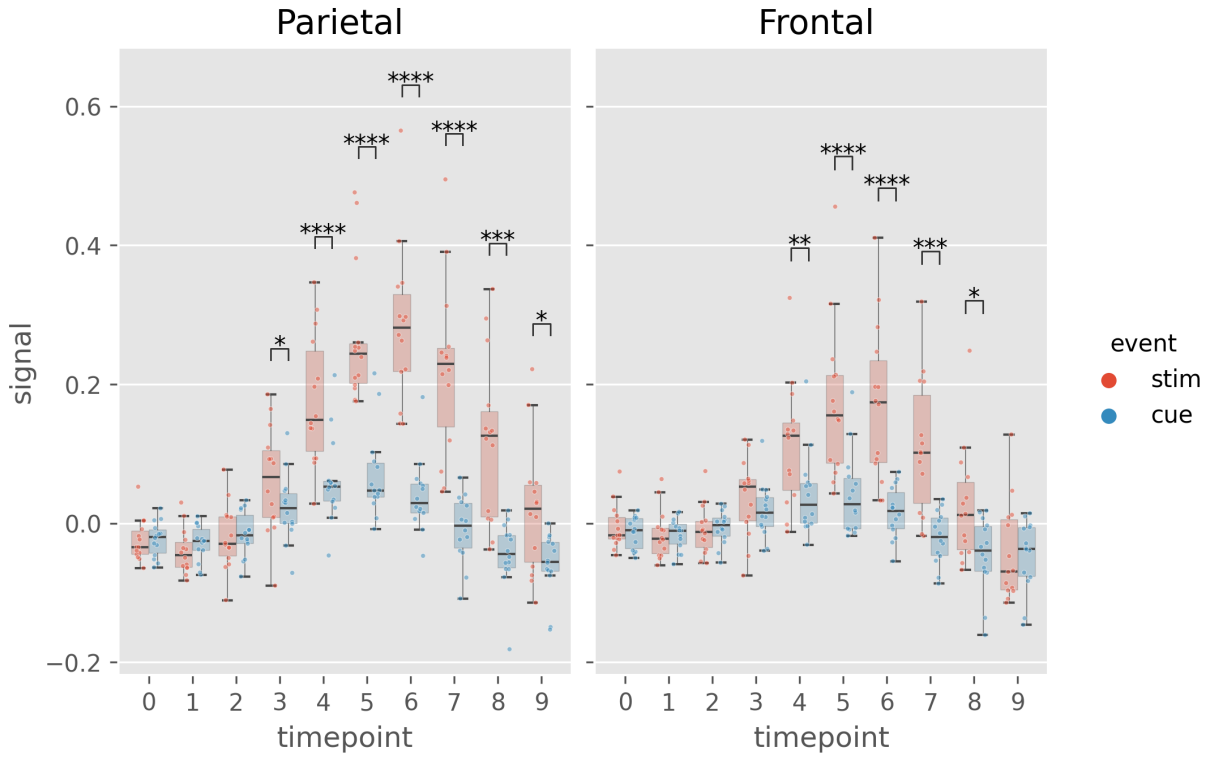


Figure 1: Example figure of plotastic (version 0.1). Image style was set by `plt.style.use('ggplot')`

Table 2: Results from `DA.check_sphericity()`. plotastic assesses sphericity after grouping the data by all grouping dimensions (hue, row, col). For example, `DA.check_sphericity()` grouped the ‘fmri’ dataset by “region” (col) and “event” (hue), performing four subsequent sphericity tests for four datasets.

‘region’, ‘event’	spher	W	chi2	dof	pval	group count	n per group
‘frontal’, ‘cue’	True	3.26e+20	-462.7	44	1	10	[14]
‘frontal’, ‘stim’	True	2.45e+17	-392.2	44	1	10	[14]
‘parietal’, ‘cue’	True	1.20e+20	-452.9	44	1	10	[14]
‘parietal’, ‘stim’	True	2.44e+13	-301.9	44	1	10	[14]

Table 3: Results of `DA.omnibus_rm_anova()`. plotastic performs one two-factor RM-ANOVA per axis (grouping the data by row and col dimensions) using x and hue as the within-factors. For this example, `DA.omnibus_rm_anova()` grouped the ‘fmri’ dataset by “region” (col), performing two subsequent two-factor RM-ANOVAs. Within-factors are “timepoint” (x) and “event” (hue). For conciseness, GG-Correction and effect sizes are not shown.

‘region’	Source	SS	ddof1	ddof2	MS	F	p-unc	stars
‘parietal’	timepoint	1.583	9	117	0.175	26.20	3.40e-24	****
‘parietal’	event	0.770	1	13	0.770	85.31	4.48e-07	****
‘parietal’	timepoint * event	0.623	9	117	0.069	29.54	3.26e-26	****
‘frontal’	timepoint	0.686	9	117	0.076	15.98	8.28e-17	****
‘frontal’	event	0.240	1	13	0.240	23.44	3.21e-4	***
‘frontal’	timepoint * event	0.242	9	117	0.026	13.031	3.23e-14	****

Overview

The functionality of `plotastic` revolves around a seamless integration of statistical analysis and plotting, leveraging the capabilities of `pingouin`, `seaborn`, `matplotlib` and `statannotations` (Vallat, 2018; Waskom, 2021; Hunter, 2007; Charlier et al., 2022). It utilizes long-format `pandas` `DataFrames` as its primary input, aligning with the conventions of `seaborn` and ensuring compatibility with existing data structures (Wickham, 2014; Team, 2020; McKinney, 2010).

`plotastic` was inspired by `seaborn` using the same set of intuitive and consistent parameters (`y`, `x`, `hue`, `row`, `col`) found in each of its plotting functions (Waskom, 2021). These parameters intuitively delineate the data dimensions plotted, yielding ‘faceted’ subplots, each presenting `y` against `x`. This allows for rapid and insightful exploration of multidimensional relationships. `plotastic` extends this principle to statistical analysis by storing these `seaborn` parameters (referred to as dimensions) in a `DataAnalysis` object and intelligently passing them to statistical functions of the `pingouin` library. This approach is based on the impression that most decisions during statistical analysis can be derived from how the user decides to arrange the data in a plot. This approach also prevents code repetition and streamlines statistical analysis. For example, the `subject` keyword is specified only once during `DataAnalysis` initialisation, and `plotastic` selects the appropriate paired or unpaired version of the test. Using `pingouin` alone requires the user to manually pick the correct test and to repeatedly specify the `subject` keyword in each testing function.

In essence, `plotastic` translates plotting parameters into their statistical counterparts. This translation minimizes user input and also ensures a coherent and logical connection between plotting and statistical analysis. The goal is to allow the user to focus on choosing the correct statistical test (e.g. parametric vs. non-parametric) and worry less about specific implementations.

At its core, `plotastic` employs iterators to systematically group data based on various dimensions, aligning the analysis with the distinct requirements of tests and plots. Normality testing is performed on each individual sample, which is achieved by splitting the data by all grouping dimensions and also the `x-axis` (`hue`, `row`, `col`, `x`). Sphericity and homoscedasticity testing is performed on a complete sampleset listed on the `x-axis`, which is achieved by splitting the data by all grouping dimensions (`hue`, `row`, `col`) (Tab. 2). For omnibus and posthoc analyses, data is grouped by the `row` and `col` dimensions in parallel to the `matplotlib` axes, before performing one two-factor analysis per axis using `x` and `hue` as the within/between-factors. (Tab. 3).

`DataAnalysis` visualizes data through predefined plotting functions designed for drawing multi-layered plots. A notable emphasis within `plotastic` is placed on showcasing individual datapoints alongside aggregated means or medians. In detail, each plotting function initializes a `matplotlib` figure and axes using `plt.subplots()` while returning a `DataAnalysis` object for method chaining. Axes are populated by `seaborn` plotting functions (e.g., `sns.boxplot()`), leveraging automated ag-

gregation and error bar displays. Keyword arguments are passed to these `seaborn` functions, ensuring the same degree of customization. Users can further customize plots by chaining `DataAnalysis` methods or by applying common `matplotlib` code to override `plotastic` settings. Figures are exported using `plt.savefig()`.

`plotastic` also focuses on annotating statistical information within plots, seamlessly incorporating p-values from pairwise comparisons using `statannotations` (Charlier et al., 2022). This integration simplifies the interface and enables options for pair selection in multidimensional plots, enhancing both user experience and interpretability.

For statistics, `plotastic` integrates with the `pingouin` library to support classical assumption and hypothesis testing, covering parametric/non-parametric and paired/non-paired variants. Assumptions such as normality, homoscedasticity, and sphericity are tested. Omnibus tests include two-factor RM-ANOVA, ANOVA, Friedman, and Kruskal-Wallis. Posthoc tests are implemented through `pingouin.pairwise_tests()`, offering (paired) t-tests, Wilcoxon, and Mann-Whitney-U.

To sum up, `plotastic` stands as a unified and user-friendly solution catering to the needs of researchers and data scientists, seamlessly integrating statistical analysis with the power of plotting in Python. It streamlines the workflow, translates `seaborn` parameters into statistical terms, and supports extensive customization options for both analysis and visualization.

Discussion

As awareness of the complexities associated with multidimensional data in biomedical research increases, there is a growing demand for tools that not only simplify analysis but also enhance its intuitiveness and effectiveness (Dunn et al., 2017). `plotastic` is designed to meet this demand by seamlessly integrating data visualization with inferential statistics, making sophisticated statistical methods accessible to researchers of all expertise levels. This integration could be pivotal as it allows the visualization of data —how it is grouped and presented— to directly guide the statistical analysis, reducing the need for in-depth statistical knowledge and ensuring that the analyses are intuitively aligned with the visual aspects of the data. This approach could not only simplify the analytical process but also enhance the transparency and reproducibility of research findings.

Statistical Features: A detailed list of implemented and planned features is provided on the GitHub page of the project (Kuric, 2024). `plotastic` is comprehensive in its current scope, incorporating a robust suite of statistical tests that cater to a wide range of research needs. It includes assumption tests for normality, homoscedasticity, and sphericity, alongside classical statistical tests such as ANOVA and t-tests, available in both parametric and non-parametric forms, as well as paired and unpaired variants. However, its reliance on the `pingouin` library means that `plotastic` is subject to the same limitations as `pingouin` itself. For instance, it does not yet support survival analysis tools like log-rank tests and Kaplan-Meier plots, which are critical for certain biomedical applications. While there are external packages that offer these capabilities, integrating them into `plotastic` could significantly expand its utility and provide a more unified user experience (Davidson-Pilon, 2019).

One known issue in `plotastic` is its handling of multiple testing corrections. Currently, `plotastic` might not correctly apply these corrections when the data is split across different facets with their own y-axes (facetted by `row` and `col` keywords), which can lead to potentially incorrect statistical inferences. This is a fixable issue, and plans are in place to address it in upcoming versions to ensure that corrections for multiple testing are appropriately applied across the complete dataset. Additionally, bivariate analysis tools like correlation and regression are not yet implemented, since `plotastic` focused on data with a categorical x-axis, which is more common in biomedical research.

Plotting Features: The plotting capabilities of `plotastic` employ all of `seaborn`'s non-facetgrid plotting functions (e.g. `sns.boxplot()`), which include a wide range of plot types but may not cover all possible visualizations (Waskom, 2021). Future versions could expand the range of specialized plots, for example QQ-plots. `plotastic` focuses on offering both high- and low-level plotting configuration: `Multiplots` automate overlaying multiple plot types, which is extremely useful for displaying raw data points alongside aggregated statistics (barplots, boxplots, etc.), a feature that can be cumbersome to implement manually. Low-level plotting configuration is supported just like in `seaborn`, since `plotastic` uses `matplotlib` as its backend. This level of flexibility is unique to `plotastic`, serving

both beginners and advanced users.

Plot Annotation: Annotating statistical results into plots (e.g. *** above barplots) is a key requirement in modern biomedical journals and could be key feature why researchers choose proprietary software like *GraphPad Prism* over other solutions. `plotastic` automates this process as well, making it a strong competitor to other statistical software. This is especially useful for re-arranging plots, since the statistical annotations are automatically updated when the plot is re-drawn. This feature is unique to `plotastic` and could be a key selling point for the software.

Software Testing: The development of `plotastic` adheres to modern software engineering principles to ensure reliability and maintainability. The project utilizes continuous integration practices, which means that with every change to the codebase, a comprehensive test suite is automatically run to identify potential bugs and ensure that new contributions do not disrupt existing functionalities. This test suite covers approximately 79 % of the testable lines of code, a statistic tracked automatically by an independent service called `codecov`, highlighting a strong commitment to software quality (*Codecov*, 2024).

No Official Support for Interactive Plots: Interactive plots are a popular feature in modern data visualization tools, allowing users to explore data dynamically, e.g. hovering over data points to display additional information, or zooming in on specific regions of a plot. Python has several libraries that support interactive plotting, such as `plotly` and `bokeh` (Inc., 2015; Bokeh Development Team, 2018). The ability to include interactive 3D figures into .pdf articles without commercial software have been around for over a decade (Barnes et al., 2013). `plotastic` could also support interactive plotting through its `matplotlib` backend, but there are no plans to officially support this feature.

Documentation: Documentation serves as a critical resource for enhancing user experience and adoption, especially for software aimed at users with varying levels of expertise. Currently, `plotastic`'s documentation is focused on basic functionalities. These include detailed installation instructions, example analyses using five test datasets from `seaborn` that are commonly used in teaching statistics, guidelines on dimension switching with commands like `DataAnalysis.switch()`, and tutorials on constructing and configuring plots, annotating statistical data, and utilizing multiplot capabilities.

However, the documentation of `plotastic` could be significantly enhanced. Currently, it lacks a dedicated website, relying instead on GitHub-hosted Jupyter notebooks. While useful, these notebooks are not the most user-friendly or maintainable format for documentation as they can be challenging to navigate and don't update synchronously with software changes. A more robust approach would involve leveraging services like `Read the Docs` or `Sphinx` to generate and host documentation directly from the codebase (*Read the Docs*, 2024; *Sphinx*, 2024). This would not only ensure that the documentation remains up-to-date with the latest software developments but also provide a more

accessible and navigable user experience, meeting the expectations of users who prefer a dedicated website for software documentation.

Usability for Non-Statisticians: `plotastic` aims to make statistical analysis more accessible to researchers without extensive statistical training by intuitively mapping plotting concepts to statistical operations. To the author's knowledge, this approach is unique to `plotastic` and has great potential to make statistics easier and educational for non-statisticians. Still, the software requires responsible and self-critical usage, as emphasized by the thorough disclaimer on its GitHub page regarding the software's statistical robustness, (Kuric, 2024). The disclaimer highlights that while `plotastic` can facilitate gaining practical experience with statistics and provide a preliminary analysis, it is not a substitute for professional statistical consultation. It is designed to aid users in generating publication-grade figures and performing statistical tests, provided they have a basic understanding of the procedures involved or have their results verified by a statistician. To enhance usability for non-statisticians, `plotastic` could incorporate a system to suggest appropriate statistical tests based on data characteristics, like parametric tests for normally distributed data. This feature would guide users in selecting the correct tests, thereby augmenting the tool's functionality and broadening its appeal. Additionally, the GitHub page provides critical guidelines for responsible statistical practice, urging users to document their work in detail, understand the limitations of the tests applied, and consult professionals to validate their findings, ensuring that `plotastic` supports but does not replace thorough statistical analysis (Sandve et al., 2013; Kuric, 2024).

Usability for Non-Programmers: Despite the advantages of `plotastic`, its adoption among non-programmers in biomedicine may be challenging due to its reliance on a Command Line Interface (CLI), which is less intuitive for those accustomed to Graphical User Interface (GUI). However, the integration of Large Language Models (LLMs), such as ChatGPT, presents a compelling case for embracing CLI. Indeed, ChatGPT is believed to potentially revolutionize medical research (Ruk-sakulpiwat et al., 2023).

Unlike GUIs, CLIs are highly compatible with text-based AI technologies, which can significantly lower the barrier to entry. In fact, both ChatGPT-3.5 and 4 demonstrate impressive performance in python (Arefin et al., 2023). This is a game changer, since researchers can now use similar tools as programmers and are only limited by their methodological expertise to formulate a correct prompt (Qureshi et al., 2023)⁸. For instance, when a software is not working as intended, users of a GUI are likely to be stuck without help or further research. Users of a CLI however, could utilize ChatGPT to ask for code-corrections or explanations of the code line-by-line, but also for advice on how to proceed with a statistical analysis and how to implement new features (e.g. editing a plot). Attempts to integrate AI into GUIs however have proven challenging (D. Gao et al., 2024).

⁸Kelleher (2024): “*You can now recognize and learn the language of almost anything with structure, and you can translate it to anything with structure — so text-protein, protein-text. [...] Everybody is a programmer, and the programming language of the future is called ‘human.’*”

Still, ChatGPT requires responsible use, as it is not sufficient as a standalone tool for statistical analysis (Ordak, 2023). It should also be noted that `plotastic` is not yet known to ChatGPT, but could be included in future versions, depending on the popularity of `plotastic`.

Overall, the transition to a new data analysis software, especially one that incorporates coding, presents a learning curve. However, the advantages of `plotastic` in terms of analytical clarity, speed, and depth are anticipated to outweigh these initial challenges.

Adoption and Open-Source Contributions: The adoption rate of `plotastic` is a critical factor for its sustainability, particularly in the open-source environment where community contributions can significantly support the author in improving and maintaining the software. Since its publication in the Journal of Open Source Software on March 9, 2024, `plotastic` has garnered attention with 41 visits and 8 *stars* (similar to a ‘like’ on social media platforms) on its GitHub page. This level of engagement, while modest, shows initial interest and potential for growth. Active involvement from the community is essential for ongoing improvements; hence, efforts are being made to enhance the software’s documentation and structure to attract more contributors: `plotastic`’s GitHub page shows a detailed outline of the software’s architecture as a class diagram in unified modeling language (UML) format, helping potential contributors orient themselves within `plotastic`’s several modules and classes (shown in Appendix B.1). But further efforts are required, e.g. only few functions are documented with docstrings, which help understanding the purpose and usage of each function. Still, `plotastic` is a general-purpose data analysis software designed not only for biologists but for a broad range of scientific disciplines, making it a versatile tool with promising potential for wider adoption.

Contributions to Methodological Transparency and Biomedicine: `plotastic` standardizes statistical analysis by ensuring that it is performed alongside visual representations. This integrated approach simplifies both analysis and interpretation, facilitating smooth replication of analyses. Although it streamlines the data analysis process, it is not a complete solution to the reproducibility crisis in scientific research. Researchers must still possess a basic understanding of data analysis principles and be cautious about their reliance on scripting solutions like Python, which is less familiar to some biomedical researchers.

Statistical literacy and lack of training is a well-documented challenge among clinicians and biomedical researchers, decreasing the confidence in presenting their analyses in detail (Lakhlifi et al., 2023; Federer et al., 2016). Since `plotastic` alleviates some need for statistical knowledge by automating the configuration of statistical tests, the room for error is reduced, and the user can lay off some responsibility to the software, gaining confidence in presenting their analysis transparently.

Furthermore, `plotastic`’s compatibility with the Jupyter ecosystem leverages “*simple, intuitive ways to both capture and embed computational work directly into our papers*” as advocated by Mesirov (2010). This integration makes `plotastic` not just a tool for analysis but also a means of enhancing the accessibility and reproducibility of scientific work. As Peng (2011) suggests, the exploration

of data and analysis code may often be sufficient to verify the quality of scientific claims. This seems plausible, given that statistical tests themselves pose rigorous requirements on the data, and the results are often not interpretable without the context data. Combining `plotastic` with Jupyter Notebooks provides a compelling solution to transparently integrate and document both intermediate results and analytical processes, thus furthering scientific rigor and replicability.

Overall, `plotastic` is useful statistical tool with the potential to improve methodological transparency and reproducibility of research in biomedicine.

Summarising Discussion

The following paragraphs will discuss the previously presented chapters both in terms of how they integrate within current scientific fields, but also outlay technical and academic challenges that were faced during the course of this project. Given the broad scope of the shown topics, this discussion is structured into three main sections: Microscopy, Molecular Biology, and Data Analysis. Each section will explain key experiments that

How Exploratory Live-Cell Imaging Transformed the Research Focus

Exploratory experimentation emphasizes discovering and characterizing novel phenomena (Mättig, 2022). Exploratory cell biology often leverages emerging technologies to visualize and analyze the mechanisms of cell behavior dynamically. Such approaches allow real-time observations that can lead to unexpected insights and breakthroughs. In this project, the application of live-cell imaging proved pivotal.

Direct Observation of Complexity and Novelty: Initially, the project did not focus on *in vitro* myeloma cell dissemination. The project's research focus shifted when making the unexpected—or arguably insignificant—observation of cancer cells detaching from aggregates. This shows the transformative power of time-lapse microscopy or live cell imaging (Cole, 2014). For the author, live-cell imaging provides an observation method that's unmatched in intuition and directness. Unlike RNA sequencing, which can obscure biological processes behind cryptic data, live-cell imaging offers a clear view into the dynamic cellular events as they unfold.

Such clarity was particularly effective in revealing the detachment of cells following division, a phenomenon that might be overlooked in static analyses. Multiple parameters can be read out in parallel, such as both time and aggregate size for detachments to begin. Also, complex cellular behavior can be deduced from movement, or rather lack thereof, which was interpreted as re-attachment of INA-6 daughter cells to the hMSC monolayer. This allowed for measuring the duration of nMA-INA6 existing until re-attaching and turning into MA-INA6. This information was helpful when designing experiments to prove that dissemination is initiated by cell division, requiring precise timing to capture the detached daughter cells right after cell division. Together, live cell imaging enabled key mechanistic insights in understanding the dynamics involved in multicellular interactions by integrating the study of multiple phenomena at once.

Difficulties Connecting Observation with Academic Terminology Exploring video data begins with the search of scientific novelties. In order to correctly identify cellular phenomena relevant to the research question, a deep understanding of cell biology is required, e.g. in field of cell dynamics to read migratory behavior (Nalbant & Dehmelt, 2018). This is a challenge for both students

and experienced researchers, since finding the academically correct terms to describe observations is difficult, especially for novel phenomena or a sequence of events that can overlap. After all, cell biology is taught using textbooks, not videos. For this project in particular, the used terminology was revised frequently, being caused by the constant struggle of finding the middle-ground between the precise description of observations, the compatibility with results from other experiments, comprehensability, and memorability. Ultimately, comprehensability and memorability were prioritized to maximize adoption of the new terminology by other researchers. For instance, *non MSC adherence* was chosen over *mobile interaction*, *aggregation* over *homotypic interaction*, and *detachment event* over *in vitro metastasis*. In general, the gap between observations and their description remains a challenge in exploratory cell biology that might be overlooked. This gap could be bridged by currently available multimodal LLMs like ChatGPT-4o: These models could match recorded phenomena with descriptions and images that were amassed in the literature over decades. By doing so, researchers not only use established terminology instead of inventing new terms, but also minimize the risk of missing potential discoveries.

Why Hide Videos Behind a Download Link? A major challenge remains in how to effectively present these dynamic observations in a publishable format, as traditional scientific publications and websites are not equipped to display video data. Instead, it is common practice to assemble video frames into static figures, presumably to support both online and printed reading habits (Peras et al., 2023). Representative example videos are then relegated to supplementary data. Although supplementary data is downloaded often, most biomedical researchers favor a presentation of additional figures and tables directly on the journal’s website (Price et al., 2018). Given the increasing availability of video data⁹, embedding video content next to figures and tables on the article’s website does make a compelling case. In fact, the journal *Nature* does offer this feature already, but rarely used (*Nature Video Content*, n.d.). In the end, there is no reason to not present videos alongside figures and tables, as they can be as informative, and potentially more so. Such new standards can benefit other fields of medicine, as videos provide the best medium for first aid, medical emergency and education (D. Gupta et al., 2023).

Overall, Live-cell imaging has proven indispensable in exploratory cell biology, uncovering dynamic cellular phenomena that static analyses often miss. This is exemplified in this work, where live-cell imaging shifted the research focus by revealing unexpected cell behaviors, like detachment during division, emphasizing the need for integrating real-time observations with molecular data. By making such dynamic processes visible, live-cell imaging not only enriches our understanding but also challenges us to enhance how scientific findings are presented, advocating for greater accessibility of video data in scientific publications.

⁹The number of PubMed articles with “*live cell imaging*” doubled from 2011 to 2023.

Potential and Challenges of Image Cytometry

Quantifying microscopy data is critical for both analytic and exploratory approaches to microscopy: For instance, microscopic assessment of live/dead cells should produce bar charts presenting cell viabilities (Spaepen et al., 2011), whereas describing novel phenomena should be supported by charts proving the reproducibility of claimed observations. Microscopy data is source of vast amount and types of information: cell morphology; organelle count, shape, and distribution; membrane and lipid distribution; protein localization, DNA content, et cetera. However, leveraging this information has always been limited by the ability to extract quantitative data from microscopy images (Galbraith, 2023). This extraction process is the essence of *image cytometry*, a field that has seen significant advances by integrating machine learning for automating image analysis tasks. (A. Gupta et al., 2019). The following sections discuss the experiences gained from this project in quantifying microscopy data and outlines potentials and challenges of image cytometry.

Considering Automated Analysis for Future Live-Cell Imaging: This work would have benefited from computational automation for the analysis of live-cell imaging, for example, the task of associating INA-6 cell detachment with INA-6 aggregate size and time: Manual analysis consisted of zooming in closely and watching the time-lapse over and over again until a detachment event was found. A very tedious task that had to be repeated approx. 50 times for every one of four independent videos. Instead of manually counting the number of single INA-6 cells across time, a pixel segmentation algorithm could have been trained to detect cells and background. Single cells would be discernable from aggregates by filtering cells by size. The count of single cells would then be representative of detached cells, given that the vast majority of INA6 cells were part of aggregates.

The workload of manual video analysis motivated the purchase of Intellesis, a software package by *Zeiss* for the Zen microscopy software ecosystem. Intellesis is a machine learning-based pixel segmentation software (*Zeiss OAD Feature Extractors*, n.d.). As a feature extractor¹⁰, it uses the first convolution layers of VGG19, which is convolutional neural network¹¹ (Simonyan & Zisserman, 2015). Intellesis does not contain a deep neural network for segmentation, but instead classifies pixel features using a *random forest classifier*. Random forest is a machine learning algorithm that —for small sets of training images— performs almost as well as deep neural networks, but are computationally far less demanding (Breiman, 2001; Richardson et al., 2023). A comparable hybrid approach was also used by Qamar et al. (2023) to segment images of bacterial spores into eight

¹⁰Features are structural elements of an image, such as edges, corners, directions, colors. These features are mathematically extractable using *filters* — also referred to as *convolution kernels* —, which are functions or algorithms applied to the pixel values of an image. For instance, *gabor filters* can extract edges of one particular direction, resulting in an image of the same size as the input, but showing only edges of one direction. *Feature extraction* is the process of applying multiple filters, resulting in a stack of filtered images called a feature vector. (?A. Gupta et al., 2019)

¹¹Convolutional neural networks (CNN) are algorithms that use the output of a feature extractor¹⁰ to feed into a neural network. The network then learns to associate these feature vectors with a label, such as *cell* or *background*. This is called *supervised learning*.

distinct pixel classes using only 50 training images. Also, free alternatives to Intellesis exist, such as Ilastik (Berg et al., 2019).

Intellesis proved useful for segmenting single multi-channel images. However, live cell imaging adds another layer of complexity to image analysis: The addition of a time axis encodes the motion of objects and other image features. This concept can be described with the term *optical flow* (Niehorster, 2021). Mathematically speaking, optical flow is a vector field that describes the motion of image features¹⁰ between consecutive frames of a video. It can be used to train machine learning models on video data efficiently (Robitaille et al., 2022). Without tricks like optical flow, machine learning algorithms like Intellesis segment the video frame by frame, ignoring the feature similarities between frames. This makes segmentation computationally inefficient, but not impossible (Pylvänäinen et al., 2023).

Together, future analyses of live-cell imaging data could benefit from the use of modern machine learning based tools that have been released recently, as summarised in Pylvänäinen et al. (2023).

Image Cytometry is Precise, Fast, Flexible and Accessible: In this study, image cytometry was indispensable for validating prior cell divisions within the nMA-INA6 cell population by profiling their DNA content. The complexity of this experiment required a method capable of managing a high throughput across three subpopulations, four timepoints, and two conditions, involving up to 24 samples per trial (Appendix A.1: Fig. 3). Despite having access to automated Fluorescence-Activated Cell Sorting (FACS) equipment offered by the Core Unit FACS at the University of Würzburg, the author saw a more time- and cost-effective solution in the laboratory microscope equipped with motorized stage top and Intellesis. This setup scanned 96 different samples in 1.5 h, and resulting large scans were processed by Intellesis overnight, quantifying thousands of DNA-stained nuclei. This demonstrated that image cytometry could match the throughput and precision of FACS with modern standard microscopy equipment (Appendix A.1: Fig. 2).

The advantages of image cytometry could have of great impact for the future of cell biology: It is applicable to adherent cell cultures (Roukos et al., 2015) and provides diverse readouts like structure, brightness, size, and shape. Moreover, image cytometry's capacity to evaluate cell viability without the need for staining or expensive analytical chemicals makes it an exceptionally cost-efficient approach for drug screening, reducing operational costs to cell culturing and electricity for microscopy (Pattarone et al., 2021). However, challenges such as the need for sophisticated automation in microscopic scans, including autofocus and shading adjustments, and the computational demands of AI processing remain.

Interestingly, the author's initial unfamiliarity with image cytometry and limited experience in image processing did not prevent the effective use of this technology. This underscores the accessibility of current imaging tools to biologists without specialized training in image analysis. As confirmed by recent advancements (Nitta et al., 2023), image cytometry is becoming increasingly competitive

with established techniques like FACS. Despite its limitations, the simplicity and efficiency of image cytometry could be pivotal for its broader acceptance and integration into biological research. The exclusivity of Intellesis to Zeiss microscopes could be a major hurdle, however there are free alternatives offering the same accessibility (Berg et al., 2019).

Manual Analysis Remains Robust for Complex and Unique Phenomena: Many biologists lack the access to tools like Intellesis, or the computational expertise to automate analysis of microscopy data, often reverting to manual analysis. This project also utilized manual strategies for the detailed characterization of dynamic intercellular interactions such as attachment, aggregation, detachment, and division. This was very time-consuming and required a thoughtful categorization strategy and a disciplined, bias-free execution. However, some analysis tasks are simply unfeasable for automation. For example, this work manually counted if two INA-6 cells interacted homotypically due to coming into contact with each other, or by staying connected as two daughter cells after cell division. Automating such a task would require a very sophisticated algorithm and developing such would be unfeasable for a task that unique. Hence, manual analysis is unmatched in terms of flexibility and complexity of categorizations, when compared to computational techniques of image processing.

In summary, image cytometry significantly enhanced this project by merging the precision of FACS with the cost-efficiency of modern microscopy. Utilizing Intellesis simplified complex image analyses, making advanced cytometric techniques more accessible. While challenges like automation and software availability persist, the potential of image cytometry to advance biomedical research and discovery remains substantial.

Technical Considerations for Image Cytometry

Acquiring Accurate Image Data: In order to capture rare cellular events with a frequency sufficient for statistical analysis, this study chose high temporal resolution and spatial depth: We utilized 1 frame every 15 min, suitable for tracking cell migration (Huth et al., 2010), but too slow for intricate movements or intracellular processes. Spatial resolution is a compromise between detail and the total observed surface area. We favored the latter to allow the exploration of potentially rare events, and acquired a —somewhat arbitrarily— large surface area of up to 13 mm². Ultimately, we assessed only approx. a quarter of the acquired surface area, as that was sufficient to gather enough events for each time bin. Such extensive automated video acquisition poses high demands on microscopy equipment, including an incubation setup and motorized stage top. The total size of video files can also complicate storage, transfer and analysis. The raw video data from chapter 1 comprises 80 GB (BioStudies, n.d.); however, far more data was acquired due to protocol optimizations

and treatments not shown in this work. File size could have been reduced by acquiring in an 8-bit image format, although a larger bit-depth could be necessary for precise and/or sensitive fluorescence microscopy. Minimizing the acquired surface area could have reduced file size as well, however the meniskus of the medium led to significant shading effects that complicated the choice of the surface area for phase contrasting. Also, archiving large surface scans allows for the search of very rare events in the course of future projects. After all, HDD space is cheap, while re-acquiring data is not. Hence, exploratory live cell imaging benefits from settings that are higher-than-required, if raw data is properly documented and remain accessible.

Generating Training Datasets: In this project, considerable effort was dedicated to training the machine learning software *Intellessis* for image segmentation, particularly for fluorescent images. It was also utilized for phase contrast, yet training required far more effort in generating annotated training images. Phase contrast or brightfield images often display low contrast between cell edges and the background, complicating the task of differentiating individual cells from their surroundings. Such complexity necessitates extensive annotation of training images – a process that can be both time-consuming and demanding.

To address these challenges and enhance the efficacy of *Intellessis*, pre-processing steps could be incorporated to emphasize essential image features and reduce irrelevant ones. For instance, edge-enhancing filters are applicable to clarify cell boundaries, while median filters can suppress noise and unnecessary details while preserving edges. These filters, available within the Zen software suite, help simplify the machine learning task by focusing the algorithm's learning on pertinent features, thereby reducing the volume of data needed for effective training.

This approach streamlines the training process for *Intellessis*, enabling more efficient and accurate segmentation of complex microscopy images. By refining the feature extraction phase, the project could have improved the performance of the segmentation algorithm but also significantly cut down on the labor and frustration typically associated with preparing large sets of annotated training data.

Conclusion 1: Harnessing Automation and Image Cytometry for Advanced Insights into INA-6 and hMSC Dynamics

This study utilized live-cell imaging and image cytometry to investigate the complex interactions between INA-6 cells and hMSCs, offering significant insights into myeloma cell behavior. The findings underscored the critical role of MSC-interactions in shaping cell behavior, e.g. INA-6 cells showed a preference for heterotypic interactions with hMSCs. These techniques revealed dynamic processes, such as cell detachment and migration, which are pivotal for understanding disease mechanisms and developing therapeutic strategies.

Live-cell imaging proved instrumental in capturing real-time cellular behaviors that static methods

cannot, such as the detachment of INA-6 cells during division. This ability to directly observe dynamic processes provided a deeper understanding of the cellular mechanisms that may contribute to myeloma dissemination. However, this approach also posed challenges, including the need for extensive manual analysis and the difficulty of presenting dynamic data in traditional scientific formats, highlighting the potential benefits of integrating automated analysis tools in future research.

Image cytometry facilitated high-throughput and precise analysis of cellular interactions, despite challenges related to automation and computational demands. The integration of manual and automated techniques in this study not only enabled a comprehensive analysis but also demonstrated the accessibility and potential of these advanced imaging technologies for broader applications in biomedical research. These findings underscore the importance of adopting innovative imaging techniques to enhance our understanding of cellular dynamics and multicellular interactions.

Novel Methods of Isolating Adhering Subpopulations

In this work, innovative *in vitro* methodologies (Well Plate Sandwich Centrifugation and V-Well adhesion Assay) were developed. This was required to fill in gaps of isolating cells with minimized variability introduced by user-bias to clearly separate subpopulations and precisely quantify them.

It is evident that direct or indirect contact with MM can have different effects on both hMSCs and Myeloma cells and methods to differentiate between those are crucial for understanding the change of the BMME during MM progression (Fairfield et al., 2020; Dziadowicz et al., 2022)

cite all those methods for cell isolation! - Turning around wellplates: Doesn't allow isolation, just quantification - The author did not show all his washing experiments - Washing is very bad (data not shown): Highly dependent on user: position of cell on well bottom (border cells receive less force), position of pipette tip in well (depth, angle and position on bottom) - This motivated us to explore more reproducible methods

It's a challenge: either quantify cell population, or isolate them! - It's better to specialize in one method, than to do both poorly - Well Plate Sandwich Centrifugation is badly suited for quantification, but possible - we switched to developing V-well adhesion assay for quantification - We realized, V-well isolation allows both ultra precise quantification and isolation of small amounts of cells! - unmatched precision through centrifugation, no washing - But V-well pellets comprise only few cells requiring a lot of technical replicates and an untiring pipetting hand

The Well Plate Sandwich Centrifugation (WPSC) used two different techniques to dissociate MA-INA6 cells from the hMSC monolayer. This had no impact on the ratio of isolated MA-INA6 to nMA-INA6, since nMA-INA6 isolation was performed prior to dissociation using the same protocol consistently. We tried this to test if MACS was really necessary, after all it is costly, time-consuming, introduces an antibody bias and requires cell cold-treatment during antibody: Strong pipetting ('Wash') and repeated Accutase treatment followed by magnetic activated cell sorting ('MACS').

Dynamic Regulation of Adhesion Factors During Dissemination

One main question arises:

INA-6 was initially isolated from plasma cell leukemia as an extramedullary plasmacytoma located in the pleura from a donor of age. There is not much more information available on the background of that patient (*Two New Interleukin-6 Dependent Plasma Cell Lines Carrying a Chromosomal Abnormality Involving the IL-6 Gene Locus. Abstract Two Plasma Cell Lines, INA-6 and JK-6, Have Been Initiated and*

Continuously Cultured from Two Patients with Malignant Plasma Cell Diseases. Both Cell Lines Are EBNA Negative and Show Morphological and Immunophenotypical Features of Plasma Cells. INA-6 Expresses the CD39 and CDw75 Antigens, JK-6 Is Strongly Positive with CD38 and CD39 Antibodies. By Flow Cytometry They Were Non-Reactive with Ia Antibodies and B Cell Reagents CD19, CD20, CD21, CD22, and CD24. While INA-6 Cells Are Releasing Kappa Light Chains Only, JK-6 Cells Produce IgG Kappa. Both Cell Lines Could Only Be Initiated with IL-6 Supplemented Medium and Remained IL-6 Responsive throughout Continuous Culture. INA-6 Is Strictly Dependent on IL-6. No Spontaneously Secreted IL-6 Was Found nor Could It Be Induced by IL-1beta /TNFalpha Stimulation. Molecular Analysis with RT-PCR Revealed mRNA for the IL-6 Receptor in Both Lines. No IL-6 mRNA Was Detectable in INA-6 Cells, While in JK-6 Minute Amounts Were Observed. Cytogenetic Analysis of Both Lines Revealed, among Other Abnormalities, a Deletion (7)(P13). Interestingly, the 7p Deletion Affects the Location Of the IL-6 Gene. In Both Cell Lines, IL-6 Dependent Proliferation Could Be Inhibited by IFNalpha. IFNalpha Had Growth Regulatory Effects Only on JK-6: While High Concentrations Were Inhibitory, Low IFNalpha Amounts Were Clearly Stimulatory. A Wide Variety of Other Cytokines Including GM-CSF and IL-11 Did Not Have the Capacity to Influence Proliferation. These Plasma Cell Lines Do Not Only Allow to Further Characterize Regulatory Events in Plasma Cell Neoplasias but Also Provide Tools to Study Therapeutic Interventions., n.d.; Burger, Guenther, et al., 2001). But assuming that This is a highly advanced stage of myeloma. However, Chapter 2 shows that adhesion factors are lost during MM progression. INA-6 are highly adhesive to hMSCs.

This is a contradiction that needs to be resolved.

For example, circulating MM cells show lower levels of integrin $\alpha 4\beta 1$ compared to those residing in the BM. Furthermore, treatment with a syndecan-1 blocking antibody has been shown to rapidly induce the mobilization of MM cells from the BM to peripheral blood in mouse models, suggesting that alterations in adhesion molecule expression facilitate MM cell release (Zeissig et al., 2020).

However, INA-6 do not express adhesion factors. They do that only in hMSC presence. Hence MAINA-6 could be a smaller fraction of MM cells, specialized on preparing a new niche for the rest of the MM cells. This could be a reason why they are so adhesive.

This assumption dictates that aggressive myeloma cells gain the ability to dynamically express adhesion factors. It could be that INA-6 has gained the capability to express adhesion factors fast in order to colonize new niches, such as pleura from which they were isolated.

This shows that not just the stage of the disease, but also the location of the myeloma cells plays a role when considering adhesion factors. According to this, this thesis predicts a low expression of adhesion factors in circulating myeloma cells, but a high expression in adhesive cells, e.g. non-circulating, or rather those

indeed CD138 paper isolated cells from circulating MM cells (Akhmetzyanova et al., 2020)

indeed, temporal subclones have been identified (Keats et al., 2012).

Subsets of Adhesion Factors Contribute To Different Steps of Adhesion

- adhesion molecules during vascular involvement have these adhesion molecules: JAM-C and CD138. - NONE of Them were shown in Chapter 2 of this study, (except for JAM-B)

- One has to consider that intravasation and/or extravasation would require a different set of adhesion factors than adhesion to BM or extramedullary environments.

This has great implications for targeting adhesion factors for therapy, as it suggests that different adhesion factors should either be antagonized or agonized depending on the function of the adhesion factor. According to this assumption, adhesion factors involved in intra- and extravasation adhesion should be antagonized, while adhesion factors involved in BM adhesion —as identified in Chapter 2— should be agonized. Indeed, Adhesion factors for endothelium were shown to decrease tumour burden in mouse models (Asosingh et al., 2001; Mrozik et al., 2015)

Bou Zerdan et al. (2022): "Classically, the BMM has been divided into endosteal and vascular niches"

Together, a detailed mapping of the niches available in the bone marrow is required to understand the adhesion factors required for each niche. This is a highly complex task, as the bone marrow is a highly complex organ.

What Triggers Release: One Master Switch, Many Small Switches, or is it just Random?

Papers like Akhmetzyanova et al. (2020) make it seem as if there is one molecule that decides if a myeloma cell is circulating or not.

It's less about one clear (molecular) mechanism that decides that a myeloma cell decides to become a disseminating cell, but rather a indirect consequence of a combination of many processes. These processes are:

- Loss of adhesion factors or dynamic expression of adhesion factors
- Loss of dependency from bone marrow microenvironment
- asdf

Our thesis postulates that there is no big switch that decides if a myeloma cell detaches from the bone marrow, *it simply happens* once these processes are present.

Outlook: High-Value Research Topics for Myeloma Research Arising from this Work

As an Outlook, the Author lists research topics arising from this work that have great potential for breakthroughs in myeloma research.

Anti tumor effects of MSCs: This thesis has discussed the pro-tumor effects of MSCs. However, MSCs have also been shown to have anti-tumor effects (Galderisi et al., 2015). This work has also shown that primary hMSCs can induce apoptosis in INA-6 6 cells initially — probably through the action of death domain receptors —, but inhibit apoptosis during prolonged culturing.

This shows that hMSCs could be leveraged as a therapeutic target that could prevent myeloma progression.

Cell Division as a Mechanism for Dissemination Initiation: The author describes how the detachment of daughter cells from the mother cell after a cycle of hMSC-(re)attachment and proliferation could be a key mechanism in myeloma dissemination. This mechanism was shown in other studies of extravasation. The author sees great potential in this mechanism as a target for future research. It is probably under-researched due to requirement of sophisticated time-lapse equipment, yet the simplicity of detachment through cell division is intriguing through its simplicity. It implies asymmetric cell division. Cancer cells are known to divide asymmetrically, e.g. moving miRNAs to one daughter cell.

Lists of Adhesion Gene Associated With Prolonged Patient Survival: The author lists adhesion genes that are associated with prolonged patient survival. These genes are highly expressed in myeloma samples from patients with longer overall

At this time we could be on the verge of a new era of myeloma therapy, including bi-specific antibodies and cell based approaches (Morè et al., 2023; Engelhardt et al., 2024). Currently, available CAR-T Cell therapies (ide-cel, cilda-cel) are extremely expensive, but show complete remission rates of up to 80 % and a 18-month progression free survival rate of 66 % (Bobin & Leleu, 2022). An affordable “off-the-shelf” CAR-T Cell product could become reality since the problem of deadly graft-versus-host disease during allogeneic transplantation seems to be solvable (Qasim et al., 2017), hence, research groups and biotech companies are racing towards developing a safe allogeneic CAR-T Cell technology (Depil et al., 2020).

the list of genes could be good targets because the BM niche is highly hypoxic, car t cells are not well, but directing them to the BM niche could increase efficacy.

Conclusion 1: Cancer & Myeloma & Dissemination is bad

lorem ipsum yes yes very bad

Semi-Automation was Critical for Establishing *in vitro* Methods

In vitro research is valued for their speed at creating precise data (Moleiro et al., 2017). In this work, the development and publication of innovative *in vitro* methodologies necessitated the adoption of semi-automated data analysis tools. These novel methods introduced complexities that span multiple experimental parameters, making the results multidimensional. This demanded precise, efficient and standardized data handling capabilities which were facilitated by Python tools like `seaborn` and `plotastic` (Waskom, 2021; Kuric & Ebert, 2024).

Inherent Multidimensionality of Adhesion Studies: Cell adhesion studies often involve multiple independent parameters, posing significant analytical challenges. Two critical dimensions are particularly notable: '*Subpopulation*' and '*Time*'. Analyzing cell adhesion often involves isolation of adherent and non-adherent subpopulations, effectively introducing '*Subpopulation*' as a vital dimension in the dataset (Dziadowicz et al., 2022). This study specifically categorized cells into three levels of MSC-interaction: CM-INA6, nMA-INA6, and MA-INA6, representing INA-6 cells incubating in MSC-conditioned medium, INA-6 cells not adhering to MSCs, and INA-6 cells adhering to MSCs, respectively. Furthermore, the dynamic nature of cell adhesion processes is profoundly influenced by the factor '*Time*', making it a crucial experimental parameter for investigation (Rebl et al., 2010; McKay et al., 1997; Bolado-Carrancio et al., 2020). This work includes extensive time-lapse microscopy experiments utilizing a high time resolution (1 frame every 15 min), similar to those time resolutions used by Purschke et al. (2010). This precision was required for key mechanistic insights on hMSC-INA-6 interaction dynamics. These included identifying rolling movements of nMA-INA6 daughter cells around MA-INA6 mother cells, measuring the minimum time for INA-6 detachments to begin, and measuring the time required for daughter cells to re-attach to the hMSC monolayer, etc. Next to mechanistic insights, adhesion time played a crucial methodological role in this study as well: During the V-Well adhesion experiments, we did not know initially how long INA-6 cells required to form strong adhesion with hMSCs before pelleting nMA-INA6, but required a timepoint with hour precision to capture detachments after cell division that was accelerated through prior cell cycle synchronization at M-Phase.

The extensive faceting features of `seaborn` and `plotastic` were essential for visualizing these multidimensional datasets, allowing for quick exploration of the data (Waskom, 2021).

Further Contributions and Remedies to Multidimensional Complexity: In addition to '*Subpopulation*' and '*Time*', this study faced additional layers of complexity that were managed through semi-automated analysis.

Experiments typically involved at least three biological replicates and corresponding technical replicates. Although replicates were not treated as independent variables — instead serving for displaying variance — they can add substantially to the data management workload. In this work,

semi-automation nullified the manual burdens of handling technical replicates: pandas was used to automate aggregation of technical replicates into means after removing technical outliers thorough z-score thresholding, while the jupyter notebook format allowed for reviewing filtered data for specific data losses. The removal of technical noise was especially relevant for qPCR data, where low gene expression can lead to sudden increase in Ct value (non-detects). In fact, the decision to remove or impute non-detects is under active discussion, however, available algorithms are hard to understand for non bioinformaticians, but also do not separate biological from technical variance, which is considered bad practice by Motulsky (2018) (McCall et al., 2014; Sherina, 2020). Semi-automation also nullified the burden of handling biological replicates: The automatic aggregation of datapoints during plotting is a key feature of seaborn, on which plotastic was built. Without such automation, calculating means and standard deviations for simple barplots would have required extensive manual computation in *Microsoft Excel*, or tedious plot configurations in *GraphPad Prism* due to limited faceting functionality of multiple variable tables (*GraphPad Prism 10 User Guide*, 2024).

Replicates can expand datasets as this factor comprises a lot of levels. Similarly, the factor ‘*Gene*’ multiplied the dataset by a total of 30 genes when validating RNAseq data with RT-qPCR. With three subpopulations, one timepoint, eleven biological replicates, and three technical replicates, the qPCR dataset used in this study grew to 2970 datapoints to be statistically analyzed and visualized. This is a manageable size for manual analysis, but the effort involved illustrates the definition of semi-big data.

Methodological variability also introduced additional dimensions: The Well Plate Sandwich Centrifugation (WPSC) used two different techniques to dissociate MA-INA6 cells from the hMSC monolayer: Strong pipetting (‘*Wash*’) and repeated Accutase treatment followed by magnetic activated cell sorting (‘*MACS*’). These variations, recorded as the factor ‘*method*’, further complicated the dataset. Although this distinction is not discussed in this work — rather pooled into one group —, this showcases how protocol changes can add dimensions to the dataset that are not necessarily relevant for the biological question but essential for method optimizations and validation.

Agility During Establishment of V-Well Assay: The concept of agility in laboratory research, inspired by the Agile Manifesto’s principle of “*Responding to change over following a plan*” (*Manifesto for Agile Software Development*, 2001), is increasingly relevant in biomedical research (West, 2018; Quanbeck et al., 2022). This adaptive approach was particularly crucial during the development of the V-Well adhesion assay in this study. This experiment was planned such that the author performed fluorescent readout using microscopy and preliminary analysis, while a technical assistant prepared the samples for the next timepoint. Semi-automation accelerated the preliminary data analysis and visualization to a point that results were reviewable before the next sample timepoint was prepared and ready for fluorescent readout. This enabled immediate adjustments to the experimental protocol inbetween sample measurements, allowing for quick troubleshooting of small and avoidable

problems that are often unforeseeable when establishing new methodologies. Without such agility, these problems would have been identified after the experiment, requiring a complete re-run of a very work-intensive experiment that included cell cycle synchronization. Such an agile and adaptive work environment, facilitated by python tools and *seaborn*, proved invaluable for refining the *in vitro* methods being developed.

Additionally, the simplicity offered by *seaborn* for complex data plotting, such as the cell cycle profiling shown in Appendix A.1: Fig. 3, which required minimal code to produce a detailed series of 24 histograms, underscores the utility of semi-automation in enhancing laboratory efficiency. While this work does not quantify the full benefits of semi-automation, the author's experiences suggest potential impacts on the speed and adaptability of method development in biomedical research.

plotastic Exceled in Re-Doing Statistical Analyses and Plots

Establishing new methods of *in vitro* dissemination required not just innovative experimental protocols, but also adaptive ways to visually present complex data. This need for adaptability is crucial during the publication process, where researchers must often experiment with different ways to visually represent their findings to best convey their significance. This process typically involves frequent adjustments to how data is displayed in plots. Such adjustments become especially cumbersome when subsequent adjustments are involved. Traditional tools (*Microsoft Excel* or *Graphpad Prism*) fail at handling semi-big data, while Python packages like *seaborn* reach their limits in terms of adaptability, making the development of *plotastic* a critical step in this work.

plotastic addresses these challenges by not only automating statistics, but also by enhancing the adaptability of data visualization as well, making it easier to modify how data is presented without repetitive manual adjustments. The author saw four key steps that required streamlining through *plotastic*:

1. Re-arranging facets
2. Plotting multiple layers of different plot types
3. Statistical Re-Analysis and Re-Annotation
4. Fine-Tuning for publication grade quality

These adjustment steps made re-plotting tedious, since a change in prior steps required a complete re-work of following steps, something which *plotastic* prevented. Its key design feature is the centralized storage of facetting parameters (`x`, `hue`, `col`, `row`). These parameters define which data points are shown on the x-axis, what categories are highlighted by color (`hue`), and how data is grouped into separate plots (by columns and/or rows) into separate plots. This centralization means that once these parameters are set, they not only automate statistical analysis, but also can be automatically applied across all subsequent adjustments made to the plot. This contrasts with *seaborn*, where

changing these parameters required adjusting multiple lines of subsequent code.

Re-arranging Facets: `plotastic`'s `.switch()` method allowed for easily shifting the arrangement of plots — for example, switching the data represented on the x-axis with that represented by color — to explore different perspectives of the data quickly. This proved particularly useful when trying to find the most effective way to illustrate complex interactions or trends that might not be immediately apparent. In `seaborn`, changing facets is easy and proved useful during intermediate data analysis, but unfeasable when plots involved multiple layers, sophisticated style edits or statistical annotations, as this can require re-writing subsequent adjustments.

Plotting Multiple Layers of Different Plot Types: Modern journal standards increasingly demand the representation of individual datapoints alongside aggregated data, for example plotting datapoints above a bar- or boxplots. `seaborn` does not automate this, but can require calling two plotting functions in sequence, e.g. `sns.boxplot()` followed by `sns.swarmplot()`. This can get repetitive, as adjusting the style of these plots to match each other, e.g. defining the point size or transparency of individual data points to fit into a barplot. `plotastic` was designed for multi-layered plotting, offering single-line functions for plot combinations with pre-configured style-parameters.

Statistical Re-Analysis and Re-Annotation To the author's knowledge, `plotastic`'s capability of streamlining statistical re-analysis is unique and unmatched. `seaborn` alone can not perform this without multiple lines of `statannotations` (Charlier et al., 2022). `plotastic` automates the inclusion of statistical annotations directly into plots. This is a significant enhancement because it ensures that any statistical significance noted in the data is immediately visible and correctly updated whenever the data presentation is changed. This feature proved particularly useful during the peer review process of Kuric et al. (2024), where a reviewer asked for a complete statistical analysis of Chapter 15 D, which at that time included only paired t-tests between selected groups.

Fine-Tuning for Publication Grade Quality: `plotastic` simplified the creation of publication-quality figures by automating style adjustments that are typically manually coded with `matplotlib` when using `seaborn`. These include adjustments like angled x-axis labels or consistent visual styles across multiple figures, which are important for maintaining the professional appearance of published data.

Outlook: Could `plotastic` Address a Re-Analysis Bottleneck? Re-doing analyses and plots is often overlooked bottlenecks in the reproducibility of scientific research, although it does overlap with two principles of the FAIR-guidelines for scientific data management and stewardship: Interoperability¹² and Re-Usability (Wilkinson et al., 2016). This challenge was exemplified during this work's experiments using RT-qPCR. The field of qPCR, where reproducibility issues have been notoriously prevalent. As Bustin (2014) noted, many publications using PCR-based methods have

¹²Wilkinson et al. (2016): “Interoperability—the ability of data or tools from non-cooperating resources to integrate or work together with minimal effort.”

been seriously flawed, underscoring the need for updated approaches (Bustin et al., 2013; Ruiz-Villalba et al., 2021). Furthermore, the evolution of the $\Delta\Delta Ct$ formula over recent years highlights the dynamic nature of data analysis standards in biomedicine (Pfaffl, 2001; Ramakers et al., 2003; Ruijter et al., 2021). Despite these challenges, current data analysis infrastructures seldom facilitate a smooth revision or complete redoing of figures, which could hamper efforts to re-analyse and apply the latest techniques to existing datasets, which could be requested e.g. during peer-review (Wilkinson et al., 2016). In response, `plotastic` was specifically designed to streamline the reconfiguration and reanalysis of data visualizations. This work serves as a case study showing that —according to the author’s experiences— the manual effort involved was effectively reduced, making the task of re-analysis seem a lot more inviting, especially for handling semi-big data.

Conclusion 2: Demonstrating the Advantages of Semi-Automation in Biomedical Research Methodologies

This thesis illustrates the challenges and solutions associated with managing the inherent complexity of adhesion studies and related methodologies, such as Cell Cycle profiling. These methodologies necessitate sophisticated data handling tools to address two primary challenges: (1) the multidimensionality of semi-big data and (2) the rapid iterative loop of results evaluation and protocol adjustments, a process for which *in vitro* methods are valued.

`seaborn` and `plotastic` have been instrumental in addressing these challenges. `seaborn` facilitated the rapid processing of intermediate results during method development, while `plotastic` was crucial for crafting publication-grade analyses and figures, filling in the capabilities that `seaborn` lacks. This includes facilitating the easy (re-)design of visualizations and statistical analyses, which are critical for late-stage data processing.

Though this work does not provide empirical evidence quantifying the benefits of semi-automation, it serves as a practical case study demonstrating the transformative potential of such technologies in biomedical research. The integration of semi-automation tools streamlined complex *in vitro* methodologies, significantly enhancing operational agility. This case study bridges biomedical research with bioinformatics, highlighting how semi-automation can reduce data analysis workloads and enable researchers to focus more on exploratory research within the laboratory setting.

To the author’s experience, the gained efficiencies not only saved valuable time but also enhanced the clarity and communicative power of the research findings. This is particularly crucial in fields like myeloma dissemination, where precise and transparent data presentation is essential for advancing understanding and treatment strategies. This conclusion suggests a need for further empirical research to validate these benefits more broadly and encourage wider adoption of semi-automation tools in biomedical research.

However, adopting `plotastic` poses its own set of challenges, particularly in the realm of biomedicine where researchers may prefer graphical user interfaces (GUIs) over command-line interfaces (CLIs). While `plotastic` offers a powerful CLI that is efficient and capable of handling complex data manipulation and visualization tasks, the transition from GUIs to CLIs can be intimidating for those accustomed to more visual interaction with software. This barrier can be mitigated by the integration of tools like ChatGPT, which can facilitate the use of CLIs by offering context understanding, code assistance, and error identification.

References

- Abadi, M., Agarwal, A., Barham, P., Brevdo, E., Chen, Z., Citro, C., ... Zheng, X. (2016, March). *TensorFlow: Large-Scale Machine Learning on Heterogeneous Distributed Systems* (No. arXiv:1603.04467). arXiv. Retrieved 2024-03-07, from <http://arxiv.org/abs/1603.04467> doi: 10.48550/arXiv.1603.04467
- Abdallah, N. H., Lakshman, A., Kumar, S. K., Cook, J., Binder, M., Kapoor, P., ... Rajkumar, S. V. (2024, January). Mode of progression in smoldering multiple myeloma: A study of 406 patients. *Blood Cancer Journal*, 14(1), 1–7. Retrieved 2024-05-22, from <https://www.nature.com/articles/s41408-024-00980-5> doi: 10.1038/s41408-024-00980-5
- Abdelrazik, H. (2023, August). Mesenchymal Stem Cells: A Hope or a Hype? *International Journal of Molecular Sciences*, 24(17), 13218. Retrieved 2024-06-10, from <https://www.ncbi.nlm.nih.gov/pmc/articles/PMC10487858/> doi: 10.3390/ijms241713218
- Adamik, J., Jin, S., Sun, Q., Zhang, P., Weiss, K. R., Anderson, J. L., ... Galson, D. L. (2017, April). EZH2 or HDAC1 Inhibition Reverses Multiple Myeloma-Induced Epigenetic Suppression of Osteoblast Differentiation. *Molecular cancer research: MCR*, 15(4), 405–417. doi: 10.1158/1541-7786.MCR-16-0242-T
- Adamik, J., Silbermann, R., Marino, S., Sun, Q., Anderson, J. L., Zhou, D., ... Galson, D. L. (2018). XRK3F2 Inhibition of p62-ZZ Domain Signaling Rescues Myeloma-Induced GFI1-Driven Epigenetic Repression of the Runx2 Gene in Pre-osteoblasts to Overcome Differentiation Suppression. *Frontiers in Endocrinology*, 9, 344. doi: 10.3389/fendo.2018.00344
- Aggarwal, R., Ghobrial, I. M., & Roodman, G. D. (2006, October). Chemokines in multiple myeloma. *Experimental hematology*, 34(10), 1289–1295. Retrieved 2023-04-02, from <https://www.ncbi.nlm.nih.gov/pmc/articles/PMC3134145/> doi: 10.1016/j.exphem.2006.06.017
- Akhmetzyanova, I., McCarron, M. J., Parekh, S., Chesi, M., Bergsagel, P. L., & Fooksman, D. R. (2020). Dynamic CD138 surface expression regulates switch between myeloma growth and dissemination. *Leukemia*, 34(1), 245–256. Retrieved 2023-04-04, from <https://www.ncbi.nlm.nih.gov/pmc/articles/PMC6923614/> doi: 10.1038/s41375-019-0519-4
- Allegra, A., Casciaro, M., Barone, P., Musolino, C., & Gangemi, S. (2022, May). Epigenetic Crosstalk between Malignant Plasma Cells and the Tumour Microenvironment in Multiple Myeloma. *Cancers*, 14(11), 2597. Retrieved 2024-06-10, from <https://www.ncbi.nlm.nih.gov/pmc/articles/PMC9179362/> doi: 10.3390/cancers14112597
- Alsayed, Y., Ngo, H., Runnels, J., Leleu, X., Singha, U. K., Pitsillides, C. M., ... Ghobrial, I. M. (2007, April). Mechanisms of regulation of CXCR4/SDF-1 (CXCL12)-dependent migration and homing in multiple myeloma. *Blood*, 109(7), 2708–2717. doi: 10.1182/blood-2006-07-035857
- Anders, S., Pyl, P. T., & Huber, W. (2015, January). HTSeq—a Python framework to work with high-throughput sequencing data. *Bioinformatics (Oxford, England)*, 31(2), 166–169. doi: 10.1093/bioinformatics/btu638
- Andrews, S. (2010). *FASTQC. A quality control tool for high throughput sequence data*.
- Arefin, S. E., Heya, T. A., Al-Qudah, H., Ineza, Y., & Serwadda, A. (2023, July). *Unmasking the giant: A comprehensive evaluation of ChatGPT's proficiency in coding algorithms and data structures* (No. arXiv:2307.05360). arXiv. Retrieved 2024-05-03, from <http://arxiv.org/abs/2307.05360> doi: 10.48550/arXiv.2307.05360
- Armstrong, R. A. (2014, September). When to use the Bonferroni correction. *Ophthalmic & Physiological Optics: The Journal of the British College of Ophthalmic Opticians (Optometrists)*, 34(5), 502–508. doi: 10.1111/opo.12131
- Asosingh, K., Günthert, U., De Raeve, H., Van Riet, I., Van Camp, B., & Vanderkerken, K. (2001). A unique pathway in the homing of murine multiple myeloma cells: CD44v10 mediates binding to bone marrow endothelium. *Cancer Research*, 61(7), 2862–2865.

- Baker, M. (2016, May). 1,500 scientists lift the lid on reproducibility. *Nature*, 533(7604), 452–454. Retrieved 2024-04-22, from <https://www.nature.com/articles/533452a> doi: 10.1038/533452a
- Bao, L., Lai, Y., Liu, Y., Qin, Y., Zhao, X., Lu, X., ... Huang, X. (2013, September). CXCR4 is a good survival prognostic indicator in multiple myeloma patients. *Leukemia Research*, 37(9), 1083–1088. doi: 10.1016/j.leukres.2013.06.002
- Barnes, D. G., Vidiassov, M., Ruthensteiner, B., Fluke, C. J., Quayle, M. R., & McHenry, C. R. (2013, September). Embedding and Publishing Interactive, 3-Dimensional, Scientific Figures in Portable Document Format (PDF) Files. *PLOS ONE*, 8(9), e69446. Retrieved 2024-06-13, from <https://journals.plos.org/plosone/article?id=10.1371/journal.pone.0069446> doi: 10.1371/journal.pone.0069446
- Barzilay, R., Ben-Zur, T., Bulvik, S., Melamed, E., & Offen, D. (2009, May). Lentiviral delivery of LMX1a enhances dopaminergic phenotype in differentiated human bone marrow mesenchymal stem cells. *Stem cells and development*, 18(4), 591–601. doi: 10.1089/scd.2008.0138
- Begley, C. G., & Ioannidis, J. P. A. (2015, January). Reproducibility in science: Improving the standard for basic and preclinical research. *Circulation Research*, 116(1), 116–126. doi: 10.1161/CIRCRESAHA.114.303819
- Berg, S., Kutra, D., Kroeger, T., Straehle, C. N., Kausler, B. X., Haubold, C., ... Kreshuk, A. (2019, December). Ilastik: Interactive machine learning for (bio)image analysis. *Nature Methods*, 16(12), 1226–1232. Retrieved 2024-06-16, from <https://www.nature.com/articles/s41592-019-0582-9> doi: 10.1038/s41592-019-0582-9
- Bianco, P. (2014). "Mesenchymal" stem cells. *Annual review of cell and developmental biology*, 30, 677–704. doi: 10.1146/annurev-cellbio-100913-013132
- BioStudies. (n.d.). *BioStudies < The European Bioinformatics Institute < EMBL-EBI*. Retrieved 2024-06-12, from <https://www.ebi.ac.uk/biostudies/bioimages/studies/S-BIAD1092?key=69bafe9c-74ff-492b-9e68-bd42655c4d1b>
- Bladé, J., Beksać, M., Caers, J., Jurczyszyn, A., von Lilienfeld-Toal, M., Moreau, P., ... Richardson, P. (2022, March). Extramedullary disease in multiple myeloma: A systematic literature review. *Blood Cancer Journal*, 12(3), 1–10. Retrieved 2023-03-24, from <https://www.nature.com/articles/s41408-022-00643-3> doi: 10.1038/s41408-022-00643-3
- Blonska, M., Zhu, Y., Chuang, H. H., You, M. J., Kunkalla, K., Vega, F., & Lin, X. (2015, February). Jun-regulated genes promote interaction of diffuse large B-cell lymphoma with the microenvironment. *Blood*, 125(6), 981–991. Retrieved 2023-03-01, from <https://www.ncbi.nlm.nih.gov/pmc/articles/PMC4319238/> doi: 10.1182/blood-2014-04-568188
- Bobin, A., & Leleu, X. (2022, September). Recent advances in the treatment of multiple myeloma: A brief review. *Faculty Reviews*, 11, 28. Retrieved 2024-03-27, from <https://www.ncbi.nlm.nih.gov/pmc/articles/PMC9523543/> doi: 10.12703/r/11-28
- Bokeh Development Team. (2018). *Bokeh: Python library for interactive visualization* [Manual]. Retrieved from <https://bokeh.pydata.org/en/latest/>
- Bolado-Carrancio, A., Rukhlenko, O. S., Nikanova, E., Tsyganov, M. A., Wheeler, A., Garcia-Munoz, A., ... Kholodenko, B. N. (2020, July). Periodic propagating waves coordinate RhoGTPase network dynamics at the leading and trailing edges during cell migration. *eLife*, 9, e58165. Retrieved 2024-04-25, from <https://elifesciences.org/articles/58165> doi: 10.7554/eLife.58165
- Bondi, A. B. (2000, September). Characteristics of scalability and their impact on performance. In *Proceedings of the 2nd international workshop on Software and performance* (pp. 195–203). New York, NY, USA: Association for Computing Machinery. Retrieved 2024-03-07, from <https://dl.acm.org/doi/10.1145/350391.350432> doi: 10.1145/350391.350432
- Bosch-Queralt, M., Tiwari, V., Damkou, A., Vaculčíková, L., Alexopoulos, I., & Simons, M. (2022, March). A fluorescence microscopy-based protocol for volumetric measurement of lysolecithin lesion-associated de- and re-

- myelination in mouse brain. *STAR protocols*, 3(1), 101141. doi: 10.1016/j.xpro.2022.101141
- Boswell, D., & Foucher, T. (2011). *The Art of Readable Code: Simple and Practical Techniques for Writing Better Code*. "O'Reilly Media, Inc."
- Bou Zerdan, M., Nasr, L., Kassab, J., Saba, L., Ghossein, M., Yaghi, M., ... Chaulagain, C. P. (2022). Adhesion molecules in multiple myeloma oncogenesis and targeted therapy. *International Journal of Hematologic Oncology*, 11(2), IJH39. Retrieved 2023-02-01, from <https://www.ncbi.nlm.nih.gov/pmc/articles/PMC9136637/> doi: 10.2217/ijh-2021-0017
- Brandl, A., Solimando, A. G., Mokhtari, Z., Tabares, P., Medler, J., Manz, H., ... Beilhack, A. (2022, March). Junctional adhesion molecule C expression specifies a CD138low/neg multiple myeloma cell population in mice and humans. *Blood Advances*, 6(7), 2195–2206. Retrieved 2023-04-04, from <https://doi.org/10.1182/bloodadvances.2021004354> doi: 10.1182/bloodadvances.2021004354
- Brankatschk, R., Bodenhausen, N., Zeyer, J., & Bürgmann, H. (2012, June). Simple Absolute Quantification Method Correcting for Quantitative PCR Efficiency Variations for Microbial Community Samples. *Applied and Environmental Microbiology*, 78(12), 4481–4489. Retrieved 2023-05-27, from <https://journals.asm.org/doi/10.1128/AEM.07878-11> doi: 10.1128/AEM.07878-11
- Breiman, L. (2001, October). Random Forests. *Machine Learning*, 45(1), 5–32. Retrieved 2024-06-14, from <https://doi.org/10.1023/A:1010933404324> doi: 10.1023/A:1010933404324
- Brooke, J. (1996, January). SUS – a quick and dirty usability scale. In (pp. 189–194).
- Bubendorf, L. (2001, August). High-throughput microarray technologies: From genomics to clinics. *European Urology*, 40(2), 231–238. doi: 10.1159/000049777
- Burger, R., Guenther, A., Bakker, F., Schmalzing, M., Bernand, S., Baum, W., ... Gramatzki, M. (2001). Gp130 and ras mediated signaling in human plasma cell line INA-6: A cytokine-regulated tumor model for plasmacytoma. *The Hematology Journal: The Official Journal of the European Haematology Association*, 2(1), 42–53. doi: 10.1038/sj.thj.6200075
- Burger, R., Günther, A., Bakker, F., Schmalzing, M., Bernand, S., Baum, W., ... Gramatzki, M. (2001, January). Gp130 and ras mediated signaling in human plasma cell line INA6: A cytokine-regulated tumor model for plasmacytoma. *Hematology Journal - HEMATOL J*, 2, 42–53. doi: 10.1038/sj.thj.6200075
- Bustin, S. A. (2014, December). The reproducibility of biomedical research: Sleepers awake! *Biomolecular Detection and Quantification*, 2, 35–42. Retrieved 2024-03-18, from <https://www.sciencedirect.com/science/article/pii/S2214753515000030> doi: 10.1016/j.bdq.2015.01.002
- Bustin, S. A., Benes, V., Garson, J., Hellemans, J., Huggett, J., Kubista, M., ... Vandesompele, J. (2013, November). The need for transparency and good practices in the qPCR literature. *Nature Methods*, 10(11), 1063–1067. Retrieved 2024-05-16, from <https://www.nature.com/articles/nmeth.2697> doi: 10.1038/nmeth.2697
- Caplan, A. (1991). Mesenchymal stem cells. *Journal of orthopaedic research : official publication of the Orthopaedic Research Society*, 9(5), 641–50. Retrieved from <http://www.ncbi.nlm.nih.gov/pubmed/1870029> doi: 10.1002/jor.1100090504
- Caplan, A. I. (1994, July). The mesengenic process. *Clinics in plastic surgery*, 21(3), 429–435.
- Carlson, M. (2016). Org.Hs.eg.db. *Bioconductor*. Retrieved 2023-06-09, from <http://bioconductor.org/packages/org.Hs.eg.db/> doi: 10.18129/B9.bioc.org.Hs.eg.db
- Chacon, S., & Straub, B. (2024, March). *Git - Book*. Retrieved 2024-03-07, from <https://git-scm.com/book/de/v2>
- Charlier, F., Weber, M., Izak, D., Harkin, E., Magnus, M., Lalli, J., ... Repplinger, S. (2022, October). *Trevismd/statannotations: V0.5*. Zenodo. Retrieved 2023-11-16, from <https://zenodo.org/record/7213391> doi: 10.5281/ZENODO.7213391
- Chatterjee, M., Hönenmann, D., Lentzsch, S., Bommert, K., Sers, C., Herrmann, P., ... Bargou, R. C. (2002, November). In the presence of bone marrow stromal cells human multiple myeloma cells become independent of the

- IL-6/gp130/STAT3 pathway. *Blood*, 100(9), 3311–3318. doi: 10.1182/blood-2002-01-0102
- Chauhan, D., Uchiyama, H., Akbarali, Y., Urashima, M., Yamamoto, K., Libermann, T., & Anderson, K. (1996, February). Multiple myeloma cell adhesion-induced interleukin-6 expression in bone marrow stromal cells involves activation of NF-??B. *Blood*, 87, 1104–12. doi: 10.1182/blood.V87.3.1104.bloodjournal8731104
- Chen, H., & Zhou, L. (2022, June). Treatment of ischemic stroke with modified mesenchymal stem cells. *International Journal of Medical Sciences*, 19(7), 1155–1162. Retrieved 2024-06-10, from <https://www.ncbi.nlm.nih.gov/pmc/articles/PMC9339408/> doi: 10.7150/ijms.74161
- Cippitelli, M., Stabile, H., Kosta, A., Petillo, S., Lucantonio, L., Gismondi, A., ... Fionda, C. (2023, January). Role of NF-κB Signaling in the Interplay between Multiple Myeloma and Mesenchymal Stromal Cells. *International Journal of Molecular Sciences*, 24(3), 1823. Retrieved 2024-06-08, from <https://www.mdpi.com/1422-0067/24/3/1823> doi: 10.3390/ijms24031823
- Codecov. (2024). Retrieved 2024-05-02, from <https://github.com/codecov>
- Cole, R. (2014). Live-cell imaging. *Cell Adhesion & Migration*, 8(5), 452–459. doi: 10.4161/cam.28348
- Committee on Strategies for Responsible Sharing of Clinical Trial Data, Board on Health Sciences Policy, & Institute of Medicine. (2015). *Sharing Clinical Trial Data: Maximizing Benefits, Minimizing Risk*. Washington (DC): National Academies Press (US). Retrieved 2024-04-23, from <http://www.ncbi.nlm.nih.gov/books/NBK269030/>
- Cooper, G. M. (2000). The Cell: A Molecular Approach. 2nd Edition. *Sinauer Associates*, Proliferation in Development and Differentiation. Retrieved from <https://www.ncbi.nlm.nih.gov/books/NBK9906/>
- da Silva Meirelles, L., Chagastelles, P. C., & Nardi, N. B. (2006, June). Mesenchymal stem cells reside in virtually all post-natal organs and tissues. *Journal of cell science*, 119(Pt 11), 2204–2213. doi: 10.1242/jcs.02932
- Davidson-Pilon, C. (2019, August). Lifelines: Survival analysis in Python. *Journal of Open Source Software*, 4(40), 1317. Retrieved 2024-05-02, from <https://joss.theoj.org/papers/10.21105/joss.01317> doi: 10.21105/joss.01317
- Depil, S., Duchateau, P., Grupp, S. A., Mufti, G., & Poirot, L. (2020, March). ‘Off-the-shelf’ allogeneic CAR T cells: Development and challenges. *Nature Reviews Drug Discovery*, 19(3), 185–199. Retrieved 2024-03-27, from <https://www.nature.com/articles/s41573-019-0051-2> doi: 10.1038/s41573-019-0051-2
- Ding, W., Goldberg, D., & Zhou, W. (2023, August). PyComplexHeatmap: A Python package to visualize multimodal genomics data. *iMeta*, 2(3), e115. doi: 10.1002/imt2.115
- Dobin, A., Davis, C. A., Schlesinger, F., Drenkow, J., Zaleski, C., Jha, S., ... Gingeras, T. R. (2013, January). STAR: Ultrafast universal RNA-seq aligner. *Bioinformatics*, 29(1), 15–21. Retrieved 2023-05-27, from <https://www.ncbi.nlm.nih.gov/pmc/articles/PMC3530905/> doi: 10.1093/bioinformatics/bts635
- Doddi, S., & Rashid, M. H. (2024). Disparities in Multiple Myeloma Mortality Rate Trends by Demographic Status in the USA. *Cancer Diagnosis & Prognosis*, 4(3), 288–294. doi: 10.21873/cdp.10322
- Dominici, M., Le Blanc, K., Mueller, I., Slaper-Cortenbach, I., Marini, F., Krause, D., ... Horwitz, E. (2006). Minimal criteria for defining multipotent mesenchymal stromal cells. The International Society for Cellular Therapy position statement. *Cytotherapy*, 8(4), 315–317. doi: 10.1080/14653240600855905
- Dotterweich, J., Schlegelmilch, K., Keller, A., Geyer, B., Schneider, D., Zeck, S., ... Schütze, N. (2016, December). Contact of myeloma cells induces a characteristic transcriptome signature in skeletal precursor cells -Implications for myeloma bone disease. *Bone*, 93, 155–166. doi: 10.1016/j.bone.2016.08.006
- D’souza, N., Rossignoli, F., Golinelli, G., Grisendi, G., Spano, C., Candini, O., ... Dominici, M. (2015, August). Mesenchymal stem/stromal cells as a delivery platform in cell and gene therapies. *BMC medicine*, 13, 186. doi: 10.1186/s12916-015-0426-0
- D’Souza, S., del Prete, D., Jin, S., Sun, Q., Huston, A. J., Kostov, F. E., ... Galson, D. L. (2011, December). Gf1 expressed in bone marrow stromal cells is a novel osteoblast suppressor in patients with multiple myeloma bone disease. *Blood*, 118(26), 6871–6880. Retrieved 2024-06-08, from <https://www.ncbi.nlm.nih.gov/pmc/articles/PMC3245209/> doi: 10.1182/blood-2011-04-346775

- Dunn, W., Burgun, A., Krebs, M.-O., & Rance, B. (2017, November). Exploring and visualizing multidimensional data in translational research platforms. *Briefings in Bioinformatics*, 18(6), 1044–1056. Retrieved 2024-04-23, from <https://www.ncbi.nlm.nih.gov/pmc/articles/PMC5862238/> doi: 10.1093/bib/bbw080
- Duvall, P., Matyas, S., & Glover, A. (2007). *Continuous integration: Improving software quality and reducing risk*. Pearson Education. Retrieved from <https://books.google.de/books?id=PV9qfEdv9L0C>
- Dziadowicz, S. A., Wang, L., Akhter, H., Aesoph, D., Sharma, T., Adjerooh, D. A., ... Hu, G. (2022, January). Bone Marrow Stroma-Induced Transcriptome and Regulome Signatures of Multiple Myeloma. *Cancers*, 14(4), 927. Retrieved 2022-10-25, from <https://www.mdpi.com/2072-6694/14/4/927> doi: 10.3390/cancers14040927
- Ekmekci, B., McAnany, C. E., & Mura, C. (2016, July). An Introduction to Programming for Bioscientists: A Python-Based Primer. *PLOS Computational Biology*, 12(6), e1004867. Retrieved 2024-03-10, from <https://journals.plos.org/ploscompbiol/article?id=10.1371/journal.pcbi.1004867> doi: 10.1371/journal.pcbi.1004867
- Engelhardt, M., Kortüm, K. M., Goldschmidt, H., & Merz, M. (2024, February). Functional cure and long-term survival in multiple myeloma: How to challenge the previously impossible. *Haematologica*. doi: 10.3324/haematol.2023.283058
- Evers, M., Schreder, M., Stühmer, T., Jundt, F., Ebert, R., Hartmann, T. N., ... Leich, E. (2023, March). Prognostic value of extracellular matrix gene mutations and expression in multiple myeloma. *Blood Cancer Journal*, 13(1), 43. doi: 10.1038/s41408-023-00817-7
- Ewels, P., Magnusson, M., Lundin, S., & Käller, M. (2016, October). MultiQC: Summarize analysis results for multiple tools and samples in a single report. *Bioinformatics*, 32(19), 3047–3048. Retrieved 2023-06-09, from <https://doi.org/10.1093/bioinformatics/btw354> doi: 10.1093/bioinformatics/btw354
- Excel, M. (2023, August). *Announcing Python in Excel: Combining the power of Python and the flexibility of Excel*. Retrieved 2024-03-11, from <https://techcommunity.microsoft.com/t5/excel-blog/announcing-python-in-excel-combining-the-power-of-python-and-the/ba-p/3893439>
- Fairfield, H., Costa, S., Falank, C., Farrell, M., Murphy, C. S., D'Amico, A., ... Reagan, M. R. (2020). Multiple Myeloma Cells Alter Adipogenesis, Increase Senescence-Related and Inflammatory Gene Transcript Expression, and Alter Metabolism in Preadipocytes. *Frontiers in Oncology*, 10, 584683. doi: 10.3389/fonc.2020.584683
- Federer, L. M., Lu, Y.-L., & Joubert, D. J. (2016, January). Data literacy training needs of biomedical researchers. *Journal of the Medical Library Association : JMLA*, 104(1), 52–57. Retrieved 2024-04-24, from <https://www.ncbi.nlm.nih.gov/pmc/articles/PMC4722643/> doi: 10.3163/1536-5050.104.1.008
- Fermand, J.-P., Bridoux, F., Dispenzieri, A., Jaccard, A., Kyle, R. A., Leung, N., & Merlini, G. (2018, October). Monoclonal gammopathy of clinical significance: A novel concept with therapeutic implications. *Blood*, 132(14), 1478–1485. doi: 10.1182/blood-2018-04-839480
- Fernandez-Rebollo, E., Mentrup, B., Ebert, R., Franzen, J., Abagnale, G., Sieben, T., ... Wagner, W. (2017, July). Human Platelet Lysate versus Fetal Calf Serum: These Supplements Do Not Select for Different Mesenchymal Stromal Cells. *Scientific Reports*, 7, 5132. Retrieved 2023-05-02, from <https://www.ncbi.nlm.nih.gov/pmc/articles/PMC5506010/> doi: 10.1038/s41598-017-05207-1
- Flier, J. S. (2022). The Problem of Irreproducible Bioscience Research. *Perspectives in Biology and Medicine*, 65(3), 373–395. doi: 10.1353/pbm.2022.0032
- Forster, S., & Radpour, R. (2022, July). Molecular Impact of the Tumor Microenvironment on Multiple Myeloma Dissemination and Extramedullary Disease. *Frontiers in Oncology*, 12. Retrieved 2024-05-23, from <https://www.frontiersin.org/journals/oncology/articles/10.3389/fonc.2022.941437/full> doi: 10.3389/fonc.2022.941437
- Frassanito, M. A., Cusmai, A., Iodice, G., & Dammacco, F. (2001, January). Autocrine interleukin-6 production and highly malignant multiple myeloma: Relation with resistance to drug-induced apoptosis. *Blood*, 97(2), 483–489. doi: 10.1182/blood.v97.2.483

- Friedenstein, A., & Kuralesova, A. I. (1971, August). Osteogenic precursor cells of bone marrow in radiation chimeras. *Transplantation*, 12(2), 99–108.
- Friedenstein, A. J., Piatetzky-Shapiro, I. I., & Petrakova, K. V. (1966, December). Osteogenesis in transplants of bone marrow cells. *Journal of embryology and experimental morphology*, 16(3), 381–390.
- Gabr, M. M., Zakaria, M. M., Refaie, A. F., Ismail, A. M., Abou-El-Mahasen, M. A., Ashamallah, S. A., ... Ghoneim, M. A. (2013). Insulin-producing cells from adult human bone marrow mesenchymal stem cells control streptozotocin-induced diabetes in nude mice. *Cell transplantation*, 22(1), 133–145. doi: 10.3727/096368912X647162
- Galbraith, C. G. (2023, January). Pumping up the volume. *Journal of Cell Biology*, 222(2), e202212042. Retrieved 2024-06-14, from <https://doi.org/10.1083/jcb.202212042> doi: 10.1083/jcb.202212042
- Galderisi, U., Özcan, S., Alessio, N., Acar, M. B., Toprak, G., Onal, Z. B., & Peluso, G. (2015, October). Myeloma cells can corrupt senescent mesenchymal stromal cells and impair their anti-tumor activity. *Oncotarget*, 6(37), 39482–39492. Retrieved 2024-06-10, from <https://www.oncotarget.com/article/5430/text/> doi: 10.18632/oncotarget.5430
- Gao, D., Ji, L., Bai, Z., Ouyang, M., Li, P., Mao, D., ... Shou, M. Z. (2024, January). ASSISTGUI: Task-Oriented Desktop Graphical User Interface Automation (No. arXiv:2312.13108). arXiv. Retrieved 2024-05-16, from <http://arxiv.org/abs/2312.13108> doi: 10.48550/arXiv.2312.13108
- Gao, S., Wang, Y.-T., Ma, G.-Y., Lu, M.-Q., Chu, B., Shi, L., ... Bao, L. (2024, April). Solitary bone plasmacytoma: Long-term clinical outcomes in a single center. *Current Problems in Cancer*, 50, 101095. doi: 10.1016/j.currproblcancer.2024.101095
- Garcés, J.-J., Simicek, M., Vicari, M., Brozova, L., Burgos, L., Bezdekova, R., ... Paiva, B. (2020, February). Transcriptional profiling of circulating tumor cells in multiple myeloma: A new model to understand disease dissemination. *Leukemia*, 34(2), 589–603. doi: 10.1038/s41375-019-0588-4
- García-Ortiz, A., Rodríguez-García, Y., Encinas, J., Maroto-Martín, E., Castellano, E., Teixidó, J., & Martínez-López, J. (2021, January). The Role of Tumor Microenvironment in Multiple Myeloma Development and Progression. *Cancers*, 13(2). Retrieved 2021-02-02, from <https://www.ncbi.nlm.nih.gov/pmc/articles/PMC7827690/> doi: 10.3390/cancers13020217
- Gaur, T., Lengner, C. J., Hovhannisyan, H., Bhat, R. A., Bodine, P. V. N., Komm, B. S., ... Lian, J. B. (2005, September). Canonical WNT signaling promotes osteogenesis by directly stimulating Runx2 gene expression. *The Journal of Biological Chemistry*, 280(39), 33132–33140. doi: 10.1074/jbc.M500608200
- Gentleman. (n.d.). *Bioconductor - BiocViews*. Retrieved 2023-06-09, from <https://bioconductor.org/packages/3.17/BiocViews.html>
- Ghobrial, I. M. (2012, July). Myeloma as a model for the process of metastasis: Implications for therapy. *Blood*, 120(1), 20–30. Retrieved 2022-10-15, from <https://www.ncbi.nlm.nih.gov/pmc/articles/PMC3390959/> doi: 10.1182/blood-2012-01-379024
- Giorgi, F. M., Ceraolo, C., & Mercatelli, D. (2022, April). The R Language: An Engine for Bioinformatics and Data Science. *Life*, 12(5), 648. Retrieved 2024-04-21, from <https://www.ncbi.nlm.nih.gov/pmc/articles/PMC9148156/> doi: 10.3390/life12050648
- Glavey, S. V., Naba, A., Manier, S., Clauser, K., Tahri, S., Park, J., ... Ghobrial, I. M. (2017, November). Proteomic characterization of human multiple myeloma bone marrow extracellular matrix. *Leukemia*, 31(11), 2426–2434. Retrieved 2023-09-05, from <https://www.nature.com/articles/leu2017102> doi: 10.1038/leu.2017.102
- Gomez-Cabrero, D., Abugessaisa, I., Maier, D., Teschendorff, A., Merkenschlager, M., Gisel, A., ... Tegnér, J. (2014, March). Data integration in the era of omics: Current and future challenges. *BMC Systems Biology*, 8(2), I1. Retrieved 2024-03-18, from <https://doi.org/10.1186/1752-0509-8-S2-I1> doi: 10.1186/1752-0509-8-S2-I1
- Gómez-López, G., Dopazo, J., Cigudosa, J. C., Valencia, A., & Al-Shahrour, F. (2019, May). Precision medicine needs pioneering clinical bioinformaticians. *Briefings in Bioinformatics*, 20(3), 752–766. doi: 10.1093/bib/bbx144

- Goodman, S. N., Fanelli, D., & Ioannidis, J. P. A. (2016, June). What does research reproducibility mean? *Science Translational Medicine*, 8(341), 341ps12-341ps12. Retrieved 2024-03-18, from <https://www.science.org/doi/10.1126/scitranslmed.aaf5027> doi: 10.1126/scitranslmed.aaf5027
- Gorelick, M., & Ozsváld, I. (2020). *High Performance Python: Practical Performant Programming for Humans.* "O'Reilly Media, Inc."
- Gosselin, R.-D. (2021, February). Insufficient transparency of statistical reporting in preclinical research: A scoping review. *Scientific Reports*, 11(1), 3335. Retrieved 2024-03-11, from <https://www.nature.com/articles/s41598-021-83006-5> doi: 10.1038/s41598-021-83006-5
- Gramatzki, M., Burger, R., Trautman, U., Marschalek, R., Lorenz, H., Hansen-Hagge, T., ... Kalden, J. (1994). Two new interleukin-6 dependent plasma cell lines carrying a chromosomal abnormality involving the IL-6 gene locus. , 84 Suppl. 1, 173a-173a. Retrieved 2023-03-24, from <https://www.cellosaurus.org/cellopdb/CLPUB00060>
- GraphPad Prism 10 User Guide.* (2024). Retrieved 2024-05-14, from <https://www.graphpad.com/guides/prism/latest/user-guide/multiple-variable-tables.htm>
- Greenstein, S., Krett, N. L., Kurosawa, Y., Ma, C., Chauhan, D., Hideshima, T., ... Rosen, S. T. (2003, April). Characterization of the MM.1 human multiple myeloma (MM) cell lines: A model system to elucidate the characteristics, behavior, and signaling of steroid-sensitive and -resistant MM cells. *Experimental Hematology*, 31(4), 271–282. doi: 10.1016/s0301-472x(03)00023-7
- Gronthos, S., Graves, S. E., Ohta, S., & Simmons, P. J. (1994, December). The STRO-1+ fraction of adult human bone marrow contains the osteogenic precursors. *Blood*, 84(12), 4164–4173.
- Gupta, A., Harrison, P. J., Wieslander, H., Pielawski, N., Kartasalo, K., Partel, G., ... Wählby, C. (2019). Deep Learning in Image Cytometry: A Review. *Cytometry Part A*, 95(4), 366–380. Retrieved 2022-04-08, from <https://onlinelibrary.wiley.com/doi/abs/10.1002/cyto.a.23701> doi: 10.1002/cyto.a.23701
- Gupta, D., Attal, K., & Demner-Fushman, D. (2023, March). A dataset for medical instructional video classification and question answering. *Scientific Data*, 10(1), 158. doi: 10.1038/s41597-023-02036-y
- Hannun, A., Digani, J., Katharopoulos, A., & Collobert, R. (2023). *MLX: Efficient and flexible machine learning on Apple silicon.* Retrieved from <https://github.com/ml-explore>
- Harada, T., Hiasa, M., Teramachi, J., & Abe, M. (2021, September). Myeloma–Bone Interaction: A Vicious Cycle via TAK1–PIM2 Signaling. *Cancers*, 13(17). Retrieved 2024-06-05, from <https://www.ncbi.nlm.nih.gov/pmc/articles/PMC8431187/> doi: 10.3390/cancers13174441
- Harrington, D. P., & Fleming, T. R. (1982). A Class of Rank Test Procedures for Censored Survival Data. *Biometrika*, 69(3), 553–566. Retrieved 2023-08-07, from <https://www.jstor.org/stable/2335991> doi: 10.2307/2335991
- Harris, C. R., Millman, K. J., van der Walt, S. J., Gommers, R., Virtanen, P., Cournapeau, D., ... Oliphant, T. E. (2020, September). Array programming with NumPy. *Nature*, 585(7825), 357–362. Retrieved 2023-08-09, from <https://www.nature.com/articles/s41586-020-2649-2> doi: 10.1038/s41586-020-2649-2
- Hideshima, T., Mitsiades, C., Tonon, G., Richardson, P. G., & Anderson, K. C. (2007, August). Understanding multiple myeloma pathogenesis in the bone marrow to identify new therapeutic targets. *Nature Reviews Cancer*, 7(8), 585–598. Retrieved 2023-02-07, from <https://www.nature.com/articles/nrc2189> doi: 10.1038/nrc2189
- Hose, D., Rème, T., Hielscher, T., Moreaux, J., Messner, T., Seckinger, A., ... Goldschmidt, H. (2011, January). Proliferation is a central independent prognostic factor and target for personalized and risk-adapted treatment in multiple myeloma. *Haematologica*, 96(1), 87–95. doi: 10.3324/haematol.2010.030296
- Hothorn, T., & Lausen, B. (n.d.). *Maximally Selected Rank Statistics in R.* Retrieved from <http://cran.r-project.org/web/packages/maxstat/index.html>.
- Howe, A., & Chain, P. S. G. (2015). Challenges and opportunities in understanding microbial communities with metagenome assembly (accompanied by IPython Notebook tutorial). *Frontiers in Microbiology*, 6, 678. doi: 10.3389/fmicb.2015.00678

- Hu, X., Villodre, E. S., Larson, R., Rahal, O. M., Wang, X., Gong, Y., ... Debeb, B. G. (2021, January). Decorin-mediated suppression of tumorigenesis, invasion, and metastasis in inflammatory breast cancer. *Communications Biology*, 4(1), 72. doi: 10.1038/s42003-020-01590-0
- Huang, S.-Y., Lin, H.-H., Yao, M., Tang, J.-L., Wu, S.-J., Hou, H.-A., ... Tien, H.-F. (2015). Higher Decorin Levels in Bone Marrow Plasma Are Associated with Superior Treatment Response to Novel Agent-Based Induction in Patients with Newly Diagnosed Myeloma - A Retrospective Study. *PloS One*, 10(9), e0137552. doi: 10.1371/journal.pone.0137552
- Hunter, J. D. (2007, May). Matplotlib: A 2D Graphics Environment. *Computing in Science & Engineering*, 9(3), 90–95. Retrieved 2023-11-15, from <https://ieeexplore.ieee.org/document/4160265> doi: 10.1109/MCSE.2007.55
- Huth, J., Buchholz, M., Kraus, J. M., Schmucker, M., von Wichert, G., Krndija, D., ... Kestler, H. A. (2010, April). Significantly improved precision of cell migration analysis in time-lapse video microscopy through use of a fully automated tracking system. *BMC Cell Biology*, 11(1), 24. Retrieved 2024-06-12, from <https://doi.org/10.1186/1471-2121-11-24> doi: 10.1186/1471-2121-11-24
- Inc., P. T. (2015). *Collaborative data science*. Montreal, QC: Plotly Technologies Inc. Retrieved from <https://plot.ly>
- Incerti, D., Thom, H., Baio, G., & Jansen, J. P. (2019, May). R You Still Using Excel? The Advantages of Modern Software Tools for Health Technology Assessment. *Value in Health*, 22(5), 575–579. Retrieved 2024-03-11, from <https://www.sciencedirect.com/science/article/pii/S1098301519300506> doi: 10.1016/j.jval.2019.01.003
- Ioannidis, J. P. A. (2005, August). Why Most Published Research Findings Are False. *PLOS Medicine*, 2(8), e124. Retrieved 2024-04-22, from <https://journals.plos.org/plosmedicine/article?id=10.1371/journal.pmed.0020124> doi: 10.1371/journal.pmed.0020124
- Ito, S., Sato, T., & Maeta, T. (2021, April). Role and Therapeutic Targeting of SDF-1 α /CXCR4 Axis in Multiple Myeloma. *Cancers*, 13(8), 1793. Retrieved 2024-06-10, from <https://www.ncbi.nlm.nih.gov/pmc/articles/PMC8069569/> doi: 10.3390/cancers13081793
- Jansen, B. J. H., Gilissen, C., Roelofs, H., Schaap-Oziemlak, A., Veltman, J. A., Raymakers, R. A. P., ... Adema, G. J. (2010, April). Functional differences between mesenchymal stem cell populations are reflected by their transcriptome. *Stem cells and development*, 19(4), 481–490. doi: 10.1089/scd.2009.0288
- Jung, S.-H., & Lee, J.-J. (2022, April). Update on primary plasma cell leukemia. *Blood Research*, 57(S1), 62–66. doi: 10.5045/br.2022.2022033
- Kaplan, E. L., & Meier, P. (1958, June). Nonparametric Estimation from Incomplete Observations. *Journal of the American Statistical Association*, 53(282), 457–481. Retrieved 2023-08-07, from <http://www.tandfonline.com/doi/abs/10.1080/01621459.1958.10501452> doi: 10.1080/01621459.1958.10501452
- Kastritis, E., Moulopoulos, L. A., Terpos, E., Koutoulidis, V., & Dimopoulos, M. A. (2014, December). The prognostic importance of the presence of more than one focal lesion in spine MRI of patients with asymptomatic (smoldering) multiple myeloma. *Leukemia*, 28(12), 2402–2403. Retrieved 2024-05-23, from <https://www.nature.com/articles/leu2014230> doi: 10.1038/leu.2014.230
- Katz, B.-Z. (2010, June). Adhesion molecules—The lifelines of multiple myeloma cells. *Seminars in Cancer Biology*, 20(3), 186–195. Retrieved 2021-07-04, from <https://linkinghub.elsevier.com/retrieve/pii/S1044579X10000246> doi: 10.1016/j.semcan.2010.04.003
- Kawano, M. M., Huang, N., Tanaka, H., Ishikawa, H., Sakai, A., Tanabe, O., ... Kuramoto, A. (1991, December). Homotypic cell aggregations of human myeloma cells with ICAM-1 and LFA-1 molecules. *British Journal of Haematology*, 79(4), 583–588. doi: 10.1111/j.1365-2141.1991.tb08085.x
- Kazman, R., Bianco, P., Ivers, J., & Klein, J. (2020, December). *Maintainability* (Report). Carnegie Mellon University. Retrieved 2024-03-07, from <https://kilthub.cmu.edu/articles/report/Maintainability/12954908/1> doi: 10.1184/R1/12954908.v1
- Keats, J. J., Chesi, M., Egan, J. B., Garbitt, V. M., Palmer, S. E., Braggio, E., ... Bergsagel, P. L. (2012, August).

- Clonal competition with alternating dominance in multiple myeloma. *Blood*, 120(5), 1067–1076. doi: 10.1182/blood-2012-01-405985
- Kelleher, R. (2024, January). *NVIDIA CEO: ‘This Year, Every Industry Will Become a Technology Industry’*. Retrieved 2024-05-03, from <https://blogs.nvidia.com/blog/nvidia-ceo-ai-drug-discovery-jp-morgan-healthcare-2024/>
- Kelly, B. S., Kirwan, A., Quinn, M. S., Kelly, A. M., Mathur, P., Lawlor, A., & Killeen, R. P. (2023, May). The ethical matrix as a method for involving people living with disease and the wider public (PPI) in near-term artificial intelligence research. *Radiography (London, England: 1995)*, 29 Suppl 1, S103-S111. doi: 10.1016/j.radi.2023.03.009
- Kibler, C., Schermutzki, F., Waller, H. D., Timpl, R., Müller, C. A., & Klein, G. (1998, June). Adhesive interactions of human multiple myeloma cell lines with different extracellular matrix molecules. *Cell Adhesion and Communication*, 5(4), 307–323. doi: 10.3109/15419069809040300
- Kim, D., Langmead, B., & Salzberg, S. L. (2015, April). HISAT: A fast spliced aligner with low memory requirements. *Nature methods*, 12(4), 357–360. Retrieved 2024-04-26, from <https://www.ncbi.nlm.nih.gov/pmc/articles/PMC4655817/> doi: 10.1038/nmeth.3317
- Kluyver, T., Ragan-Kelley, B., Pérez, F., Granger, B., Bussonnier, M., Frederic, J., ... Jupyter Development Team (2016). *Jupyter Notebooks—a publishing format for reproducible computational workflows*. Retrieved 2024-04-20, from <https://ui.adsabs.harvard.edu/abs/2016ppap.book...87K> doi: 10.3233/978-1-61499-649-1-87
- Krekel, H., Oliveira, B., Pfannschmidt, R., Bruynooghe, F., Laugher, B., & Bruhin, F. (2004). *Pytest*. Retrieved from <https://github.com/pytest-dev/pytest>
- Krzywinski, M., & Savig, E. (2013, July). Multidimensional data. *Nature methods*, 10(7), 595. Retrieved 2024-04-22, from <https://www.ncbi.nlm.nih.gov/pmc/articles/PMC6092027/>
- Kundu, S., Jha, S. B., Rivera, A. P., Flores Monar, G. V., Islam, H., Puttagunta, S. M., ... Sange, I. (2022, February). Multiple Myeloma and Renal Failure: Mechanisms, Diagnosis, and Management. *Cureus*, 14(2), e22585. Retrieved 2024-05-23, from <https://www.ncbi.nlm.nih.gov/pmc/articles/PMC8958144/> doi: 10.7759/cureus.22585
- Kuric, M. (2024, April). *Markur4/plotastic*. Retrieved 2024-05-02, from <https://github.com/markur4/plotastic>
- Kuric, M., Beck, S., Schneider, D., Rindt, W., Evers, M., Meißner-Weigl, J., ... Ebert, R. (2024, April). Modeling Myeloma Dissemination In Vitro with hMSC-interacting Subpopulations of INA-6 Cells and Their Aggregation/Detachment Dynamics. *Cancer Research Communications*, 4(4), 1150–1164. Retrieved 2024-05-14, from <https://www.ncbi.nlm.nih.gov/pmc/articles/PMC11057410/> doi: 10.1158/2767-9764.CRC-23-0411
- Kuric, M., & Ebert, R. (2024, March). Plotastic: Bridging Plotting and Statistics in Python. *Journal of Open Source Software*, 9(95), 6304. Retrieved 2024-03-11, from <https://joss.theoj.org/papers/10.21105/joss.06304> doi: 10.21105/joss.06304
- Kyle, R. A. (1997, February). Monoclonal gammopathy of undetermined significance and solitary plasmacytoma. Implications for progression to overt multiple myeloma. *Hematology/Oncology Clinics of North America*, 11(1), 71–87. doi: 10.1016/s0889-8588(05)70416-0
- Lai, T.-Y., Cao, J., Ou-Yang, P., Tsai, C.-Y., Lin, C.-W., Chen, C.-C., ... Lee, C.-Y. (2022, April). Different methods of detaching adherent cells and their effects on the cell surface expression of Fas receptor and Fas ligand. *Scientific Reports*, 12(1), 5713. Retrieved 2023-06-01, from <https://www.nature.com/articles/s41598-022-09605-y> doi: 10.1038/s41598-022-09605-y
- Lakhlfifi, C., Lejeune, F.-X., Rouault, M., Khamassi, M., & Rohaut, B. (2023, April). Illusion of knowledge in statistics among clinicians: Evaluating the alignment between objective accuracy and subjective confidence, an online survey. *Cognitive Research: Principles and Implications*, 8, 23. Retrieved 2024-04-24, from <https://www.ncbi.nlm.nih.gov/pmc/articles/PMC10118231/> doi: 10.1186/s41235-023-00474-1
- Leek, J. T., & Peng, R. D. (2015, April). Statistics: P values are just the tip of the iceberg. *Nature*, 520(7549), 612–612. Retrieved 2024-04-22, from <https://www.nature.com/articles/520612a> doi: 10.1038/520612a

- Li, H., Handsaker, B., Wysoker, A., Fennell, T., Ruan, J., Homer, N., ... 1000 Genome Project Data Processing Subgroup (2009, August). The Sequence Alignment/Map format and SAMtools. *Bioinformatics*, 25(16), 2078–2079. Retrieved 2023-06-09, from <https://doi.org/10.1093/bioinformatics/btp352> doi: 10.1093/bioinformatics/btp352
- Liu, Z., Liu, H., He, J., Lin, P., Tong, Q., & Yang, J. (2020, May). Myeloma cells shift osteoblastogenesis to adipogenesis by inhibiting the ubiquitin ligase MURF1 in mesenchymal stem cells. *Science signaling*, 13(633), eaay8203. Retrieved 2024-06-08, from <https://www.ncbi.nlm.nih.gov/pmc/articles/PMC7376968/> doi: 10.1126/scisignal.aay8203
- Localio, A. R., Goodman, S. N., Meibohm, A., Cornell, J. E., Stack, C. B., Ross, E. A., & Mulrow, C. D. (2018, June). Statistical Code to Support the Scientific Story. *Annals of Internal Medicine*, 168(11), 828–829. Retrieved 2024-04-23, from <https://www.acpjournals.org/doi/10.7326/M17-3431> doi: 10.7326/M17-3431
- Love, M. I., Huber, W., & Anders, S. (2014, December). Moderated estimation of fold change and dispersion for RNA-seq data with DESeq2. *Genome Biology*, 15(12), 550. Retrieved 2024-04-26, from <https://doi.org/10.1186/s13059-014-0550-8> doi: 10.1186/s13059-014-0550-8
- Mai, E. K., Hielscher, T., Kloth, J. K., Merz, M., Shah, S., Raab, M. S., ... Hillengass, J. (2015, June). A magnetic resonance imaging-based prognostic scoring system to predict outcome in transplant-eligible patients with multiple myeloma. *Haematologica*, 100(6), 818–825. Retrieved 2024-05-23, from <https://www.ncbi.nlm.nih.gov/pmc/articles/PMC4450628/> doi: 10.3324/haematol.2015.124115
- Maichl, D. S., Kirner, J. A., Beck, S., Cheng, W.-H., Krug, M., Kuric, M., ... Jundt, F. (2023, September). Identification of NOTCH-driven matrisome-associated genes as prognostic indicators of multiple myeloma patient survival. *Blood Cancer Journal*, 13(1), 1–6. Retrieved 2023-09-05, from <https://www.nature.com/articles/s41408-023-00907-6> doi: 10.1038/s41408-023-00907-6
- Majithia, N., Rajkumar, S.V., Lacy, M.Q., Buadi, F.K., Dispenzieri, A., Gertz, M.A., ... Kumar, S.K. (2016, November). Early relapse following initial therapy for multiple myeloma predicts poor outcomes in the era of novel agents. *Leukemia*, 30(11), 2208–2213. Retrieved 2022-10-15, from <https://www.ncbi.nlm.nih.gov/pmc/articles/PMC5541860/> doi: 10.1038/leu.2016.147
- Mangolini, M., & Ringshausen, I. (2020, February). Bone Marrow Stromal Cells Drive Key Hallmarks of B Cell Malignancies. *International Journal of Molecular Sciences*, 21(4), 1466. Retrieved 2023-05-02, from <https://www.ncbi.nlm.nih.gov/pmc/articles/PMC7073037/> doi: 10.3390/ijms21041466
- Manifesto for Agile Software Development. (2001). Retrieved 2024-05-14, from <http://agilemanifesto.org/>
- Martin, S. K., Diamond, P., Williams, S. A., To, L. B., Peet, D. J., Fujii, N., ... Zannettino, A. C. W. (2010, May). Hypoxia-inducible factor-2 is a novel regulator of aberrant CXCL12 expression in multiple myeloma plasma cells. *Haematologica*, 95(5), 776–784. doi: 10.3324/haematol.2009.015628
- Mateos María-Victoria, Hernández Miguel-Teodoro, Giraldo Pilar, de la Rubia Javier, de Arriba Felipe, Corral Lucía López, ... San Miguel Jesús-F. (2013). Lenalidomide plus Dexamethasone for High-Risk Smoldering Multiple Myeloma. *New England Journal of Medicine*, 369(5), 438–447. Retrieved 2024-05-22, from <https://www.nejm.org/doi/full/10.1056/NEJMoa1300439> doi: 10.1056/NEJMoa1300439
- Mättig, P. (2022, November). Classifying exploratory experimentation – three case studies of exploratory experimentation at the LHC. *European Journal for Philosophy of Science*, 12(4), 66. Retrieved 2024-06-14, from <https://doi.org/10.1007/s13194-022-00496-4> doi: 10.1007/s13194-022-00496-4
- McCall, M. N., McMurray, H. R., Land, H., & Almudevar, A. (2014, August). On non-detects in qPCR data. *Bioinformatics*, 30(16), 2310–2316. Retrieved 2023-04-25, from <https://www.ncbi.nlm.nih.gov/pmc/articles/PMC4133581/> doi: 10.1093/bioinformatics/btu239
- McKay, B. S., Irving, P. E., Skumat, C. M., & Burke, J. M. (1997, November). Cell-cell adhesion molecules and the development of an epithelial phenotype in cultured human retinal pigment epithelial cells. *Experimental Eye Research*, 65(5), 661–671. doi: 10.1006/exer.1997.0374
- McKinney, W. (2010, January). Data Structures for Statistical Computing in Python. In (pp. 56–61). doi: 10.25080/

- Majora-92bf1922-00a
- Mckinney, W. (2011, January). Pandas: A Foundational Python Library for Data Analysis and Statistics. *Python High Performance Science Computer*.
- Mesirov, J. P. (2010, January). Accessible Reproducible Research. *Science*, 327(5964), 415–416. Retrieved 2024-04-22, from <https://www.science.org/doi/10.1126/science.1179653> doi: 10.1126/science.1179653
- Moleiro, A. F., Conceição, G., Leite-Moreira, A. F., & Rocha-Sousa, A. (2017). A Critical Analysis of the Available In Vitro and Ex Vivo Methods to Study Retinal Angiogenesis. *Journal of Ophthalmology*, 2017, 3034953. doi: 10.1155/2017/3034953
- Moñivas Gallego, E., & Zurita Castillo, M. (2024, April). Mesenchymal stem cell therapy in ischemic stroke trials. A systematic review. *Regenerative Therapy*, 27, 301–306. Retrieved 2024-06-10, from <https://www.ncbi.nlm.nih.gov/pmc/articles/PMC11021793/> doi: 10.1016/j.reth.2024.03.026
- Moran, M. (2003). Arguments for rejecting the sequential Bonferroni in ecological studies. *Oikos*, 100(2), 403–405. Retrieved 2024-04-24, from <https://onlinelibrary.wiley.com/doi/abs/10.1034/j.1600-0706.2003.12010.x> doi: 10.1034/j.1600-0706.2003.12010.x
- Morè, S., Corvatta, L., Manieri, V. M., Morsia, E., Poloni, A., & Offidani, M. (2023, November). Novel Immunotherapies and Combinations: The Future Landscape of Multiple Myeloma Treatment. *Pharmaceuticals*, 16(11), 1628. Retrieved 2024-05-22, from <https://www.ncbi.nlm.nih.gov/pmc/articles/PMC10675193/> doi: 10.3390/ph16111628
- Motulsky, H. (2018). *Intuitive Biostatistics: A Nonmathematical Guide to Statistical Thinking*. Oxford University Press.
- Mrozik, K. M., Cheong, C. M., Hewett, D., Chow, A. W., Blaschuk, O. W., Zannettino, A. C., & Vandyke, K. (2015). Therapeutic targeting of N-cadherin is an effective treatment for multiple myeloma. *British Journal of Haematology*, 171(3), 387–399. Retrieved 2024-05-26, from <https://onlinelibrary.wiley.com/doi/abs/10.1111/bjh.13596> doi: 10.1111/bjh.13596
- Muruganandan, S., Roman, A. A., & Sinal, C. J. (2009, January). Adipocyte differentiation of bone marrow-derived mesenchymal stem cells: Cross talk with the osteoblastogenic program. *Cellular and molecular life sciences : CMLS*, 66(2), 236–253. doi: 10.1007/s00018-008-8429-z
- Myers, G. J., Sandler, C., & Badgett, T. (2011). *The art of software testing* (3rd ed.). Wiley Publishing. Retrieved from <https://malenezi.github.io/malenezi/SE401/Books/114-the-art-of-software-testing-3-edition.pdf>
- Nalbant, P., & Dehmelt, L. (2018, August). Exploratory cell dynamics: A sense of touch for cells? *Biological Chemistry*, 399(8), 809–819. Retrieved 2024-06-12, from <https://www.degruyter.com/document/doi/10.1515/hsz-2017-0341/html> doi: 10.1515/hsz-2017-0341
- Narzt, W., Pichler, J., Pirklbauer, K., & Zwinz, M. (1998, January). A Reusability Concept for Process Automation Software..
- Nature Video Content*. (n.d.). Retrieved 2024-06-13, from <https://support.nature.com/en/support/solutions/articles/6000210836-requirements-to-play-video-content-on-the-site>
- Newville, M., Stensitzki, T., Allen, D. B., & Ingargiola, A. (2014, September). *LMFIT: Non-Linear Least-Square Minimization and Curve-Fitting for Python*. Zenodo. Retrieved 2023-05-30, from <https://zenodo.org/record/11813> doi: 10.5281/zenodo.11813
- Niehorster, D. C. (2021, December). Optic Flow: A History. *i-Perception*, 12(6), 20416695211055766. Retrieved 2024-06-14, from <https://www.ncbi.nlm.nih.gov/pmc/articles/PMC8652193/> doi: 10.1177/20416695211055766
- Nilsson, K., Bennich, H., Johansson, S. G., & Pontén, J. (1970, October). Established immunoglobulin producing myeloma (IgE) and lymphoblastoid (IgG) cell lines from an IgE myeloma patient. *Clinical and Experimental Immunology*, 7(4), 477–489.
- Nitta, C. F., Pierce, M., Elia, J., Ruiz, J., Hipol, A.-D., Fong, N., ... Chan, L. L.-Y. (2023, October). A rapid and high-throughput T cell immunophenotyping assay for cellular therapy bioprocess using the Cellaca® PLX image

- cytometer. *Journal of Immunological Methods*, 521, 113538. doi: 10.1016/j.jim.2023.113538
- Nowotschin, S., & Hadjantonakis, A.-K. (2010, August). Cellular dynamics in the early mouse embryo: From axis formation to gastrulation. *Current opinion in genetics & development*, 20(4), 420–427. doi: 10.1016/j.gde.2010.05.008
- Oba, Y., Lee, J. W., Ehrlich, L. A., Chung, H. Y., Jelinek, D. F., Callander, N. S., ... Roodman, G. D. (2005, March). MIP-1alpha utilizes both CCR1 and CCR5 to induce osteoclast formation and increase adhesion of myeloma cells to marrow stromal cells. *Experimental Hematology*, 33(3), 272–278. doi: 10.1016/j.exphem.2004.11.015
- Ocias, L. F., Larsen, T. S., Vestergaard, H., Friis, L. S., Abildgaard, N., Frederiksen, H., & Academy of Geriatric Cancer Research (AgeCare). (2016). Trends in hematological cancer in the elderly in Denmark, 1980–2012. *Acta Oncologica (Stockholm, Sweden)*, 55 Suppl 1, 98–107. doi: 10.3109/0284186X.2015.1115124
- O'Connor, B. P., Raman, V. S., Erickson, L. D., Cook, W. J., Weaver, L. K., Ahonen, C., ... Noelle, R. J. (2004, January). BCMA Is Essential for the Survival of Long-lived Bone Marrow Plasma Cells. *The Journal of Experimental Medicine*, 199(1), 91–98. Retrieved 2024-05-26, from <https://www.ncbi.nlm.nih.gov/pmc/articles/PMC1887725/> doi: 10.1084/jem.20031330
- Okuno, Y., Takahashi, T., Suzuki, A., Ichiba, S., Nakamura, K., Okada, T., ... Imura, H. (1991, February). In vitro growth pattern of myeloma cells in liquid suspension or semi-solid culture containing interleukin-6. *International Journal of Hematology*, 54(1), 41–47.
- Ordak, M. (2023, September). ChatGPT's Skills in Statistical Analysis Using the Example of Allergology: Do We Have Reason for Concern? *Healthcare (Basel, Switzerland)*, 11(18), 2554. doi: 10.3390/healthcare11182554
- Paiva, B., Paino, T., Sayagues, J.-M., Garayoa, M., San-Segundo, L., Martín, M., ... San Miguel, J. F. (2013, November). Detailed characterization of multiple myeloma circulating tumor cells shows unique phenotypic, cytogenetic, functional, and circadian distribution profile. *Blood*, 122(22), 3591–3598. doi: 10.1182/blood-2013-06-510453
- Paiva, B., Pérez-Andrés, M., Vídriales, M.-B., Almeida, J., de las Heras, N., Mateos, M.-V., ... Myeloma Stem Cell Network (MSCNET) (2011, April). Competition between clonal plasma cells and normal cells for potentially overlapping bone marrow niches is associated with a progressively altered cellular distribution in MGUS vs myeloma. *Leukemia*, 25(4), 697–706. doi: 10.1038/leu.2010.320
- Paszke, A., Gross, S., Massa, F., Lerer, A., Bradbury, J., Chanan, G., ... Chintala, S. (2019, December). PyTorch: An Imperative Style, High-Performance Deep Learning Library (No. arXiv:1912.01703). arXiv. Retrieved 2024-03-07, from <http://arxiv.org/abs/1912.01703> doi: 10.48550/arXiv.1912.01703
- Pattarone, G., Acion, L., Simian, M., Mertelsmann, R., Follo, M., & Iarussi, E. (2021, May). Learning deep features for dead and living breast cancer cell classification without staining. *Scientific Reports*, 11, 10304. Retrieved 2024-06-16, from <https://www.ncbi.nlm.nih.gov/pmc/articles/PMC8119670/> doi: 10.1038/s41598-021-89895-w
- Peng, R. D. (2011, December). Reproducible Research in Computational Science. *Science*, 334(6060), 1226–1227. Retrieved 2024-03-18, from <https://www.science.org/doi/10.1126/science.1213847> doi: 10.1126/science.1213847
- Peras, I., Klemenčič Mirazchijski, E., Japelj Pavešić, B., & Mekiš Recek, Ž. (2023, September). Digital versus Paper Reading: A Systematic Literature Review on Contemporary Gaps According to Gender, Socioeconomic Status, and Rurality. *European Journal of Investigation in Health, Psychology and Education*, 13(10), 1986–2005. Retrieved 2024-06-13, from <https://www.ncbi.nlm.nih.gov/pmc/articles/PMC10606230/> doi: 10.3390/ejihpe13100142
- Perez, F., & Granger, B. E. (2007, May). IPython: A System for Interactive Scientific Computing. *Computing in Science & Engineering*, 9(3), 21–29. Retrieved 2024-04-20, from <https://ieeexplore.ieee.org/document/4160251> doi: 10.1109/MCSE.2007.53
- Pérez-Andrés, M., Almeida, J., Martín-Ayuso, M., Moro, M. J., Martín-Nuñez, G., Galende, J., ... Spanish Network of Cancer Research Centers (C03/10) (2005, March). Clonal plasma cells from monoclonal gammopathy of undetermined significance, multiple myeloma and plasma cell leukemia show different expression profiles of molecules involved in the interaction with the immunological bone marrow microenvironment. *Leukemia*, 19(3), 449–455. doi:

- 10.1038/sj.leu.2403647
- Perneger, T. V. (1998, April). What's wrong with Bonferroni adjustments. *BMJ : British Medical Journal*, 316(7139), 1236–1238. Retrieved 2021-11-24, from <https://www.ncbi.nlm.nih.gov/pmc/articles/PMC1112991/>
- Pfaffl, M. W. (2001, May). A new mathematical model for relative quantification in real-time RT-PCR. *Nucleic Acids Research*, 29(9), e45. Retrieved 2024-05-16, from <https://www.ncbi.nlm.nih.gov/pmc/articles/PMC55695/>
- Pittenger, M. F., Mackay, A. M., Beck, S. C., Jaiswal, R. K., Douglas, R., Mosca, J. D., ... Marshak, D. R. (1999). Multilineage Potential of Adult Human Mesenchymal Stem Cells. , 284(April), 143–148. doi: 10.1126/science.284.5411.143
- Podar, K., & Leleu, X. (2021, October). Relapsed/Refractory Multiple Myeloma in 2020/2021 and Beyond. *Cancers*, 13(20), 5154. Retrieved 2024-05-22, from <https://www.ncbi.nlm.nih.gov/pmc/articles/PMC8534171/> doi: 10.3390/cancers13205154
- Polager, S., & Ginsberg, D. (2009, October). P53 and E2f: Partners in life and death. *Nature Reviews Cancer*, 9(10), 738–748. Retrieved 2023-02-14, from <https://www.nature.com/articles/nrc2718> doi: 10.1038/nrc2718
- Price, A., Schroter, S., Clarke, M., & McAneney, H. (2018, September). Role of supplementary material in biomedical journal articles: Surveys of authors, reviewers and readers. *BMJ Open*, 8(9), e021753. Retrieved 2024-06-13, from <https://www.ncbi.nlm.nih.gov/pmc/articles/PMC6157527/> doi: 10.1136/bmjopen-2018-021753
- Purschke, M., Rubio, N., Held, K. D., & Redmond, R. W. (2010, November). Phototoxicity of Hoechst 33342 in time-lapse fluorescence microscopy. *Photochemical & Photobiological Sciences*, 9(12), 1634–1639. Retrieved 2022-03-03, from <https://pubs.rsc.org/en/content/articlelanding/2010/pp/c0pp00234h> doi: 10.1039/C0PP00234H
- Pyvänäinen, J. W., Gómez-de-Mariscal, E., Henriques, R., & Jacquemet, G. (2023, December). Live-cell imaging in the deep learning era. *Current Opinion in Cell Biology*, 85, 102271. Retrieved 2024-06-14, from <https://www.sciencedirect.com/science/article/pii/S0955067423001205> doi: 10.1016/j.ceb.2023.102271
- PyMOL. (2024). Retrieved 2024-04-30, from <https://pymol.org/>
- The Python Language Reference. (2024). Retrieved 2024-03-07, from <https://docs.python.org/3/reference/index.html>
- Qamar, S., Öberg, R., Malyshev, D., & Andersson, M. (2023, October). A hybrid CNN-Random Forest algorithm for bacterial spore segmentation and classification in TEM images. *Scientific Reports*, 13(1), 18758. Retrieved 2024-06-14, from <https://www.nature.com/articles/s41598-023-44212-5> doi: 10.1038/s41598-023-44212-5
- Qasim, W., Zhan, H., Samarasinghe, S., Adams, S., Amrolia, P., Stafford, S., ... Veys, P. (2017, January). Molecular remission of infant B-ALL after infusion of universal TALEN gene-edited CAR T cells. *Science Translational Medicine*, 9(374), eaaj2013. doi: 10.1126/scitranslmed.aaj2013
- Qiang, Y.-W., Barlogie, B., Rudikoff, S., & Shaughnessy, J. D. (2008, April). Dkk1-induced inhibition of Wnt signaling in osteoblast differentiation is an underlying mechanism of bone loss in multiple myeloma. *Bone*, 42(4), 669–680. doi: 10.1016/j.bone.2007.12.006
- Quanbeck, A., Hennessy, R. G., & Park, L. (2022, November). Applying concepts from "rapid" and "agile" implementation to advance implementation research. *Implementation Science Communications*, 3(1), 118. doi: 10.1186/s43058-022-00366-3
- Qureshi, R., Shaughnessy, D., Gill, K. A. R., Robinson, K. A., Li, T., & Agai, E. (2023, April). Are ChatGPT and large language models "the answer" to bringing us closer to systematic review automation? *Systematic Reviews*, 12, 72. Retrieved 2024-05-03, from <https://www.ncbi.nlm.nih.gov/pmc/articles/PMC10148473/> doi: 10.1186/s13643-023-02243-z
- R Core Team. (2018). *R: A language and environment for statistical computing* [Manual]. Vienna, Austria. Retrieved from <https://www.R-project.org/>
- Radford, A., Wu, J., Child, R., Luan, D., Amodei, D., & Sutskever, I. (2019). Language Models are Unsupervised Multitask Learners.. Retrieved 2024-03-07, from <https://www.semanticscholar.org/paper/Language-Models-are>

- Unsupervised-Multitask-Learners-Radford-Wu/9405cc0d6169988371b2755e573cc28650d14dfe
- Rajkumar, S. V., Dimopoulos, M. A., Palumbo, A., Blade, J., Merlini, G., Mateos, M.-V., ... Miguel, J. F. S. (2014, November). International Myeloma Working Group updated criteria for the diagnosis of multiple myeloma. *The Lancet. Oncology*, 15(12), e538–548. doi: 10.1016/S1470-2045(14)70442-5
- Rajkumar, S. V., & Kumar, S. (2020, September). Multiple myeloma current treatment algorithms. *Blood Cancer Journal*, 10(9), 94. Retrieved 2023-07-03, from <https://www.ncbi.nlm.nih.gov/pmc/articles/PMC7523011/> doi: 10.1038/s41408-020-00359-2
- Ramakers, C., Ruijter, J. M., Deprez, R. H., & Moorman, A. F. (2003, March). Assumption-free analysis of quantitative real-time polymerase chain reaction (PCR) data. *Neuroscience Letters*, 339(1), 62–66. Retrieved 2022-11-27, from <https://linkinghub.elsevier.com/retrieve/pii/S0304394002014234> doi: 10.1016/S0304-3940(02)01423-4
- Rayhan, A., & Gross, D. (2023). *The Rise of Python: A Survey of Recent Research*. doi: 10.13140/RG.2.2.27388.92809
- Read the Docs. (2024). Retrieved 2024-05-03, from <https://docs.readthedocs.io/en/stable/index.html>
- Rebl, H., Finke, B., Schroeder, K., & Nebe, J. B. (2010, October). Time-dependent metabolic activity and adhesion of human osteoblast-like cells on sensor chips with a plasma polymer nanolayer. *The International Journal of Artificial Organs*, 33(10), 738–748.
- Ribatti, D., Tamma, R., & Annese, T. (2020, June). Epithelial-Mesenchymal Transition in Cancer: A Historical Overview. *Translational Oncology*, 13(6), 100773. doi: 10.1016/j.tranon.2020.100773
- Richardson, G., Knudby, A., Chen, W., Sawada, M., Lovitt, J., He, L., & Naeni, L. Y. (2023, November). Dense neural network outperforms other machine learning models for scaling-up lichen cover maps in Eastern Canada. *PLOS ONE*, 18(11), e0292839. Retrieved 2024-06-14, from <https://www.ncbi.nlm.nih.gov/pmc/articles/PMC10659193/> doi: 10.1371/journal.pone.0292839
- Rigsby, R. E., & Parker, A. B. (2016, September). Using the PyMOL application to reinforce visual understanding of protein structure. *Biochemistry and Molecular Biology Education: A Bimonthly Publication of the International Union of Biochemistry and Molecular Biology*, 44(5), 433–437. doi: 10.1002/bmb.20966
- Robinson, M. D., McCarthy, D. J., & Smyth, G. K. (2010, January). edgeR: A Bioconductor package for differential expression analysis of digital gene expression data. *Bioinformatics (Oxford, England)*, 26(1), 139–140. Retrieved from <https://www.ncbi.nlm.nih.gov/pubmed/19910308> doi: 10.1093/bioinformatics/btp616
- Robitaille, M. C., Byers, J. M., Christodoulides, J. A., & Raphael, M. P. (2022, November). Self-supervised machine learning for live cell imagery segmentation. *Communications Biology*, 5(1), 1–8. Retrieved 2024-06-14, from <https://www.nature.com/articles/s42003-022-04117-x> doi: 10.1038/s42003-022-04117-x
- Roccaro, A. M., Mishima, Y., Sacco, A., Moschetta, M., Tai, Y.-T., Shi, J., ... Ghobrial, I. M. (2015, July). CXCR4 Regulates Extra-Medullary Myeloma through Epithelial-Mesenchymal-Transition-like Transcriptional Activation. *Cell Reports*, 12(4), 622–635. doi: 10.1016/j.celrep.2015.06.059
- Roukos, V., Pegoraro, G., Voss, T. C., & Misteli, T. (2015, February). Cell cycle staging of individual cells by fluorescence microscopy. *Nature protocols*, 10(2), 334–348. Retrieved 2024-06-16, from <https://www.ncbi.nlm.nih.gov/pmc/articles/PMC6318798/> doi: 10.1038/nprot.2015.016
- Roy, P., Mukherjee, T., Chatterjee, B., Vijayaragavan, B., Banoth, B., & Basak, S. (2017, March). Non-canonical NF κ B mutations reinforce pro-survival TNF response in multiple myeloma through an autoregulatory RelB:p50 NF κ B pathway. *Oncogene*, 36(10), 1417–1429. Retrieved 2024-06-08, from <https://www.nature.com/articles/onc2016309> doi: 10.1038/onc.2016.309
- Roy, P., Sarkar, U., & Basak, S. (2018, May). The NF- κ B Activating Pathways in Multiple Myeloma. *Biomedicines*, 6(2), 59. Retrieved 2021-07-25, from <http://www.mdpi.com/2227-9059/6/2/59> doi: 10.3390/biomedicines6020059
- Rueden, C. T., Schindelin, J., Hiner, M. C., DeZonia, B. E., Walter, A. E., Arena, E. T., & Eliceiri, K. W. (2017, November). ImageJ2: ImageJ for the next generation of scientific image data. *BMC Bioinformatics*, 18(1), 529. Retrieved 2024-04-25, from <https://doi.org/10.1186/s12859-017-1934-z> doi: 10.1186/s12859-017-1934-z

- Ruijter, J. M., Barnewall, R. J., Marsh, I. B., Szentirmay, A. N., Quinn, J. C., van Houdt, R., ... van den Hoff, M. J. B. (2021, June). Efficiency Correction Is Required for Accurate Quantitative PCR Analysis and Reporting. *Clinical Chemistry*, 67(6), 829–842. Retrieved 2023-05-27, from <https://doi.org/10.1093/clinchem/hvab052> doi: 10.1093/clinchem/hvab052
- Ruiz-Villalba, A., Ruijter, J. M., & van den Hoff, M. J. B. (2021, May). Use and Misuse of Cq in qPCR Data Analysis and Reporting. *Life*, 11(6), 496. Retrieved 2023-04-25, from <https://www.ncbi.nlm.nih.gov/pmc/articles/PMC8229287/> doi: 10.3390/life11060496
- Ruksakulpiwat, S., Kumar, A., & Ajibade, A. (2023, May). Using ChatGPT in Medical Research: Current Status and Future Directions. *Journal of Multidisciplinary Healthcare*, 16, 1513–1520. Retrieved 2024-05-03, from <https://www.ncbi.nlm.nih.gov/pmc/articles/PMC10239248/> doi: 10.2147/JMDH.S413470
- Sacchetti, B., Funari, A., Remoli, C., Giannicola, G., Kogler, G., Liedtke, S., ... Bianco, P. (2016). No identical "mesenchymal stem cells" at different times and sites: Human committed progenitors of distinct origin and differentiation potential are incorporated as adventitial cells in microvessels. *Stem Cell Reports*, 6(6), 897–913. Retrieved from <http://dx.doi.org/10.1016/j.stemcr.2016.05.011> doi: 10.1016/j.stemcr.2016.05.011
- Sandve, G. K., Nekrutenko, A., Taylor, J., & Hovig, E. (2013, October). Ten Simple Rules for Reproducible Computational Research. *PLoS Computational Biology*, 9(10), e1003285. Retrieved 2024-03-07, from <https://www.ncbi.nlm.nih.gov/pmc/articles/PMC3812051/> doi: 10.1371/journal.pcbi.1003285
- Santos, B. S., Silva, I., Ribeiro-Dantas, M. d. C., Alves, G., Endo, P. T., & Lima, L. (2020, October). COVID-19: A scholarly production dataset report for research analysis. *Data in Brief*, 32, 106178. doi: 10.1016/j.dib.2020.106178
- Sanz-Rodríguez, F., Ruiz-Velasco, N., Pascual-Salcedo, D., & Teixidó, J. (1999, December). Characterization of VLA-4-dependent myeloma cell adhesion to fibronectin and VCAM-1: VLA-4-dependent Myeloma Cell Adhesion. *British Journal of Haematology*, 107(4), 825–834. Retrieved 2023-04-02, from <http://doi.wiley.com/10.1046/j.1365-2141.1999.01762.x> doi: 10.1046/j.1365-2141.1999.01762.x
- Sarin, V., Yu, K., Ferguson, I. D., Gugliemini, O., Nix, M. A., Hann, B., ... Wiita, A. P. (2020, October). Evaluating the efficacy of multiple myeloma cell lines as models for patient tumors via transcriptomic correlation analysis. *Leukemia*, 34(10), 2754–2765. doi: 10.1038/s41375-020-0785-1
- Seabold, S., & Perktold, J. (2010). Statsmodels: Econometric and Statistical Modeling with Python. In *Python in Science Conference* (pp. 92–96). Austin, Texas. Retrieved 2023-05-29, from <https://conference.scipy.org/proceedings/scipy2010/seabold.html> doi: 10.25080/Majora-92bf1922-011
- Seckinger, A., Delgado, J. A., Moser, S., Moreno, L., Neuber, B., Grab, A., ... Vu, M. D. (2017, March). Target Expression, Generation, Preclinical Activity, and Pharmacokinetics of the BCMA-T Cell Bispecific Antibody EM801 for Multiple Myeloma Treatment. *Cancer Cell*, 31(3), 396–410. Retrieved 2023-07-21, from [https://www.cell.com/cancer-cell/abstract/S1535-6108\(17\)30016-8](https://www.cell.com/cancer-cell/abstract/S1535-6108(17)30016-8) doi: 10.1016/j.ccr.2017.02.002
- Seckinger, A., Hillengass, J., Emde, M., Beck, S., Kimmich, C., Dittrich, T., ... Hose, D. (2018). CD38 as Immunotherapeutic Target in Light Chain Amyloidosis and Multiple Myeloma-Association With Molecular Entities, Risk, Survival, and Mechanisms of Upfront Resistance. *Frontiers in Immunology*, 9, 1676. doi: 10.3389/fimmu.2018.01676
- Shenghui, H., Nakada, D., & Morrison, S. J. (2009). Mechanisms of Stem Cell Self-Renewal. *Annual Review of Cell and Developmental Biology*, 25(1), 377–406. Retrieved from <https://doi.org/10.1146/annurev.cellbio.042308.113248> doi: 10.1146/annurev.cellbio.042308.113248
- Sherina, V. (2020). Multiple imputation and direct estimation for qPCR data with non-detects.
- Siclari, V., Guise, T., & Chirgwin, J. (2007, January). Molecular interactions between breast cancer cells and the bone microenvironment drive skeletal metastases. *Cancer metastasis reviews*, 25, 621–33. doi: 10.1007/s10555-006-9023-1
- Siegel, R. L., Giaquinto, A. N., & Jemal, A. (2024). Cancer statistics, 2024. *CA: A Cancer Journal for Clinicians*, 74(1), 12–49. Retrieved 2024-05-21, from <https://onlinelibrary.wiley.com/doi/abs/10.3322/caac.21820> doi: 10.3322/caac.21820

- Simonyan, K., & Zisserman, A. (2015, April). Very Deep Convolutional Networks for Large-Scale Image Recognition. *arXiv:1409.1556 [cs]*. Retrieved 2022-05-12, from <http://arxiv.org/abs/1409.1556>
- Smith, A. M., Niemeyer, K. E., Katz, D. S., Barba, L. A., Githinji, G., Gymrek, M., ... Vanderplas, J. T. (2018). Journal of Open Source Software (JOSS): Design and first-year review. *PeerJ Preprints*, 4, e147. doi: 10.7717/peerj-cs.147
- Solimando, A. G., Malerba, E., Leone, P., Prete, M., Terragna, C., Cavo, M., & Racanelli, V. (2022, September). Drug resistance in multiple myeloma: Soldiers and weapons in the bone marrow niche. *Frontiers in Oncology*, 12, 973836. Retrieved 2022-10-23, from <https://www.ncbi.nlm.nih.gov/pmc/articles/PMC9533079/> doi: 10.3389/fonc.2022.973836
- Spaepen, P., De Boodt, S., Aerts, J.-M., & Sloten, J. V. (2011). Digital image processing of live/dead staining. *Methods in Molecular Biology (Clifton, N.J.)*, 740, 209–230. doi: 10.1007/978-1-61779-108-6_21
- Sphinx*. (2024). Retrieved 2024-05-03, from <https://docs.readthedocs.io/en/stable/intro/getting-started-with-sphinx.html>
- Sprynski, A. C., Hose, D., Caillot, L., Rème, T., Shaughnessy, J. D., Barlogie, B., ... Klein, B. (2009, May). The role of IGF-1 as a major growth factor for myeloma cell lines and the prognostic relevance of the expression of its receptor. *Blood*, 113(19), 4614–4626. Retrieved 2023-06-29, from <https://www.ncbi.nlm.nih.gov/pmc/articles/PMC2691749/> doi: 10.1182/blood-2008-07-170464
- Standal, T., Seidel, C., Plesner, T., Sanderson, R., Waage, A., Børset, M., & Sundan, A. (2002, November). Osteoprotegerin is bound, internalized, and degraded by multiple myeloma cells. *Blood*, 100, 3002–7. doi: 10.1182/blood-2002-04-1190
- Stock, P., Bruckner, S., Winkler, S., Dollinger, M. M., & Christ, B. (2014, April). Human bone marrow mesenchymal stem cell-derived hepatocytes improve the mouse liver after acute acetaminophen intoxication by preventing progress of injury. *International journal of molecular sciences*, 15(4), 7004–7028. doi: 10.3390/ijms15047004
- Sullivan, G. M., & Feinn, R. S. (2021, August). Facts and Fictions About Handling Multiple Comparisons. *Journal of Graduate Medical Education*, 13(4), 457–460. Retrieved 2024-03-10, from <https://www.ncbi.nlm.nih.gov/pmc/articles/PMC8370375/> doi: 10.4300/JGME-D-21-00599.1
- Tabolacci, C., De Martino, A., Mischiati, C., Feriotto, G., & Beninati, S. (2019, January). The Role of Tissue Transglutaminase in Cancer Cell Initiation, Survival and Progression. *Medical Sciences*, 7(2), 19. Retrieved 2023-03-17, from <https://www.ncbi.nlm.nih.gov/pmc/articles/PMC6409630/> doi: 10.3390/medsci7020019
- Tai, Y.-T., Li, X.-F., Breitkreutz, I., Song, W., Neri, P., Catley, L., ... Anderson, K. C. (2006, July). Role of B-cell-activating factor in adhesion and growth of human multiple myeloma cells in the bone marrow microenvironment. *Cancer Research*, 66(13), 6675–6682. doi: 10.1158/0008-5472.CAN-06-0190
- Tam, P. P., & Beddington, R. S. (1987, January). The formation of mesodermal tissues in the mouse embryo during gastrulation and early organogenesis. *Development (Cambridge, England)*, 99(1), 109–126.
- Taskiran, I. I., Spanier, K. I., Dickmänen, H., Kempynck, N., Pančíková, A., Ekşí, E. C., ... Aerts, S. (2024, February). Cell-type-directed design of synthetic enhancers. *Nature*, 626(7997), 212–220. Retrieved 2024-04-21, from <https://www.nature.com/articles/s41586-023-06936-2> doi: 10.1038/s41586-023-06936-2
- Team, T. P. D. (2020, February). *Pandas-dev/pandas: Pandas*. Zenodo. Retrieved from <https://doi.org/10.5281/zenodo.3509134> doi: 10.5281/zenodo.3509134
- Teoh, G., & Anderson, K. C. (1997, February). INTERACTION OF TUMOR AND HOST CELLS WITH ADHESION AND EXTRACELLULAR MATRIX MOLECULES IN THE DEVELOPMENT OF MULTIPLE MYELOMA. *Hematology/Oncology Clinics of North America*, 11(1), 27–42. Retrieved 2021-01-29, from <http://www.sciencedirect.com/science/article/pii/S0889858805704135> doi: 10.1016/S0889-8588(05)70413-5
- Teramachi, J., Silbermann, R., Yang, P., Zhao, W., Mohammad, K. S., Guo, J., ... Kurihara, N. (2016, February). Blocking the ZZ Domain of Sequestosome1/p62 Suppresses Myeloma Growth and Osteoclast Formation In Vitro and Induces Dramatic Bone Formation in Myeloma-Bearing Bones In Vivo. *Leukemia*, 30(2), 390–398. Retrieved

- 2024-06-08, from <https://www.ncbi.nlm.nih.gov/pmc/articles/PMC4740189/> doi: 10.1038/leu.2015.229
- Terpos, E., Migkou, M., Christoulas, D., Gavriatopoulou, M., Eleutherakis-Papaikovou, E., Kanellias, N., ... Dimopoulos, M. A. (2016, May). Increased circulating VCAM-1 correlates with advanced disease and poor survival in patients with multiple myeloma: Reduction by post-bortezomib and lenalidomide treatment. *Blood Cancer Journal*, 6(5), e428. Retrieved 2021-02-03, from <https://www.ncbi.nlm.nih.gov/pmc/articles/PMC4916305/> doi: 10.1038/bcj.2016.37
- Terpos, E., Ntanasis-Stathopoulos, I., Gavriatopoulou, M., & Dimopoulos, M. A. (2018, January). Pathogenesis of bone disease in multiple myeloma: From bench to bedside. *Blood Cancer Journal*, 8(1), 7. doi: 10.1038/s41408-017-0037-4
- Thompson, S., Dowrick, T., Ahmad, M., Xiao, G., Koo, B., Bonmati, E., ... Clarkson, M. J. (2020, July). SciKit-Surgery: Compact libraries for surgical navigation. *International Journal of Computer Assisted Radiology and Surgery*, 15(7), 1075–1084. doi: 10.1007/s11548-020-02180-5
- Thumallapally, N., Meshref, A., Mousa, M., & Terjanian, T. (2017, January). Solitary plasmacytoma: Population-based analysis of survival trends and effect of various treatment modalities in the USA. *BMC Cancer*, 17, 13. Retrieved 2024-05-21, from <https://www.ncbi.nlm.nih.gov/pmc/articles/PMC5216567/> doi: 10.1186/s12885-016-3015-5
- Trapnell, C., Roberts, A., Goff, L., Pertea, G., Kim, D., Kelley, D. R., ... Pachter, L. (2012, March). Differential gene and transcript expression analysis of RNA-seq experiments with TopHat and Cufflinks. *Nature Protocols*, 7(3), 562–578. doi: 10.1038/nprot.2012.016
- Tsubaki, M., Seki, S., Takeda, T., Chihara, A., Arai, Y., Morii, Y., ... Nishida, S. (2020, October). The HGF/Met/NF- κ B Pathway Regulates RANKL Expression in Osteoblasts and Bone Marrow Stromal Cells. *International Journal of Molecular Sciences*, 21(21), 7905. Retrieved 2024-06-08, from <https://www.ncbi.nlm.nih.gov/pmc/articles/PMC7663721/> doi: 10.3390/ijms21217905
- Turesson, I., Bjorkholm, M., Blimark, C. H., Kristinsson, S., Velez, R., & Landgren, O. (2018, April). Rapidly changing myeloma epidemiology in the general population: Increased incidence, older patients, and longer survival. *European journal of haematology*, 10.1111/ejh.13083. Retrieved 2024-05-22, from <https://www.ncbi.nlm.nih.gov/pmc/articles/PMC6195866/> doi: 10.1111/ejh.13083
- Two new interleukin-6 dependent plasma cell lines carrying a chromosomal abnormality involving the IL-6 gene locus.* Abstract Two plasma cell lines, INA-6 and JK-6, have been initiated and continuously cultured from two patients with malignant plasma cell diseases. Both cell lines are EBNA negative and show morphological and immunophenotypical features of plasma cells. INA-6 expresses the CD39 and CDw75 antigens, JK-6 is strongly positive with CD38 and CD39 antibodies. By flow cytometry they were non-reactive with Ia antibodies and B cell reagents CD19, CD20, CD21, CD22, and CD24. While INA-6 cells are releasing kappa light chains only, JK-6 cells produce IgG kappa. Both cell lines could only be initiated with IL-6 supplemented medium and remained IL-6 responsive throughout continuous culture. INA-6 is strictly dependent on IL-6. No spontaneously secreted IL-6 was found nor could it be induced by IL-1beta /TNFalpha stimulation. Molecular analysis with RT-PCR revealed mRNA for the IL-6 receptor in both lines. No IL-6 mRNA was detectable in INA-6 cells, while in JK-6 minute amounts were observed. Cytogenetic analysis of both lines revealed, among other abnormalities, a deletion (7)(p13). Interestingly, the 7p deletion affects the location of the IL-6 gene. In both cell lines, IL-6 dependent proliferation could be inhibited by IFNalpha. IFNalpha had growth regulatory effects only on JK-6: While high concentrations were inhibitory, low IFNalpha amounts were clearly stimulatory. A wide variety of other cytokines including GM-CSF and IL-11 did not have the capacity to influence proliferation. These plasma cell lines do not only allow to further characterize regulatory events in plasma cell neoplasias but also provide tools to study therapeutic interventions. (n.d.). Retrieved 2023-03-22, from <https://www.cellosaurus.org/cellopdb/CLPUB00060>
- Ullah, I., Subbarao, R. B., & Rho, G. J. (2015). Human mesenchymal stem cells - current trends and future prospective Bioscience Reports. doi: 10.1042/BSR20150025

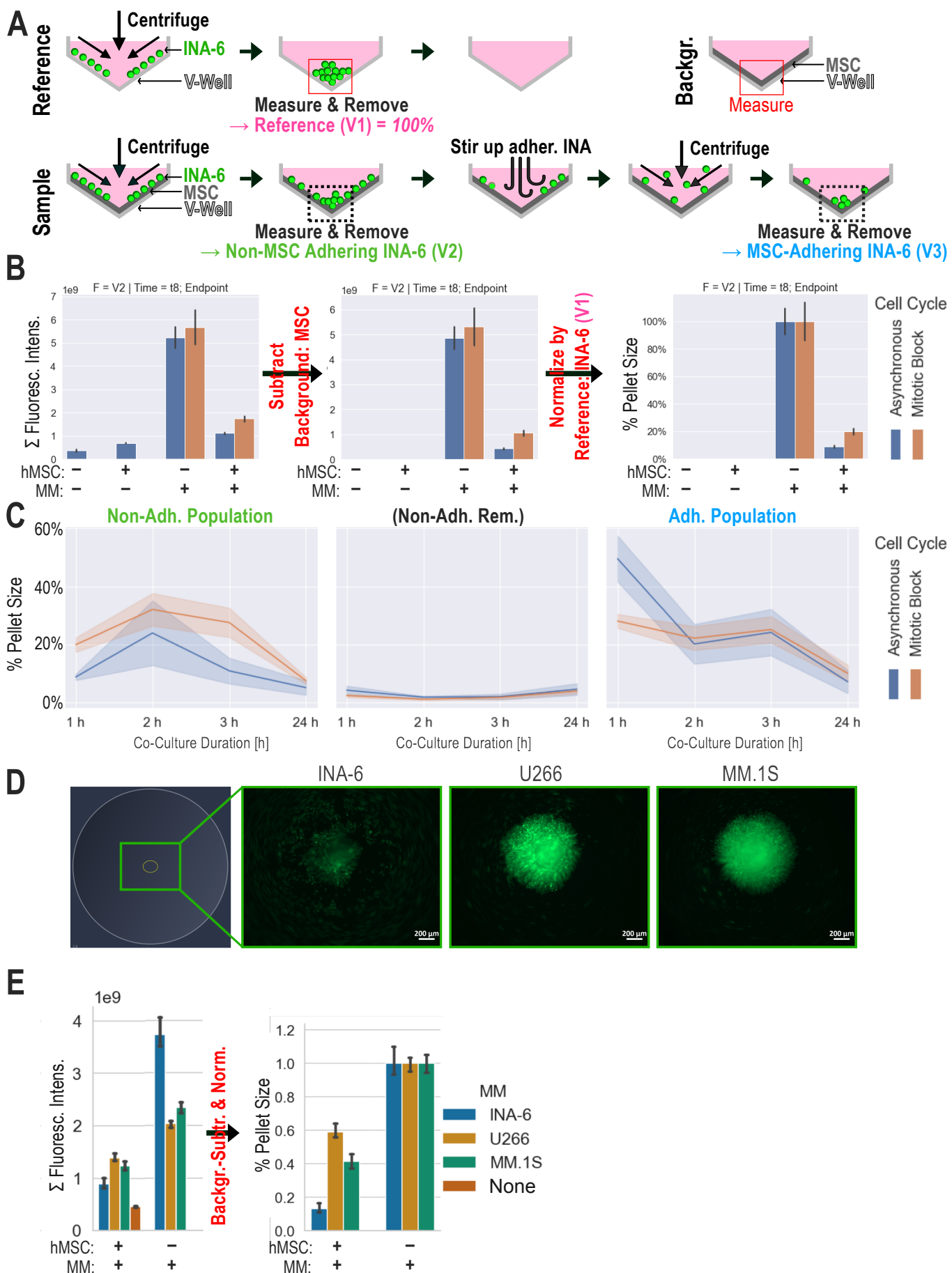
- Ullah, T. R. (2019, August). The role of CXCR4 in multiple myeloma: Cells' journey from bone marrow to beyond. *Journal of Bone Oncology*, 17, 100253. doi: 10.1016/j.jbo.2019.100253
- Urashima, M., Chauhan, D., Uchiyama, H., Freeman, G., & Anderson, K. (1995, April). CD40 ligand triggered interleukin-6 secretion in multiple myeloma. *Blood*, 85(7), 1903–1912. Retrieved 2021-02-01, from <https://ashpublications.org/blood/article/85/7/1903/123565/CD40-ligand-triggered-interleukin6-secretion-in> doi: 10.1182/blood.V85.7.1903.bloodjournal8571903
- Vääänänen, H. K. (1993, August). Mechanism of bone turnover. *Annals of Medicine*, 25(4), 353–359. doi: 10.3109/07853899309147297
- Vallat, R. (2018, November). Pingouin: Statistics in Python. *Journal of Open Source Software*, 3(31), 1026. Retrieved 2023-05-29, from <https://joss.theoj.org/papers/10.21105/joss.01026> doi: 10.21105/joss.01026
- van Rossum, G., Lehtosalo, J., & Langa, L. (2014). PEP 484 – Type Hints / peps.python.org. Retrieved 2024-03-08, from <https://peps.python.org/pep-0484/>
- Vande Broek, I., Vanderkerken, K., Van Camp, B., & Van Riet, I. (2008). Extravasation and homing mechanisms in multiple myeloma. *Clinical & Experimental Metastasis*, 25(4), 325–334. doi: 10.1007/s10585-007-9108-4
- Van Valckenborgh, E., Croucher, P. I., De Raeve, H., Carron, C., De Leenheer, E., Blacher, S., ... Vanderkerken, K. (2004, September). Multifunctional role of matrix metalloproteinases in multiple myeloma: A study in the 5T2MM mouse model. *The American Journal of Pathology*, 165(3), 869–878. doi: 10.1016/S0002-9440(10)63349-4
- Verzella, D., Cornice, J., Arboretti, P., Vecchiotti, D., Di Vito Nolfi, M., Capece, D., ... Franzoso, G. (2022, September). The NF-κB Pharmacopeia: Novel Strategies to Subdue an Intractable Target. *Biomedicines*, 10(9), 2233. Retrieved 2024-06-10, from <https://www.ncbi.nlm.nih.gov/pmc/articles/PMC9496094/> doi: 10.3390/biomedicines10092233
- Wadgaonkar, R., Phelps, K. M., Haque, Z., Williams, A. J., Silverman, E. S., & Collins, T. (1999, January). CREB-binding protein is a nuclear integrator of nuclear factor-kappaB and p53 signaling. *The Journal of Biological Chemistry*, 274(4), 1879–1882. doi: 10.1074/jbc.274.4.1879
- Wang, W., Yang, X., Dai, J., Lu, Y., Zhang, J., & Keller, E. T. (2019, June). Prostate cancer promotes a vicious cycle of bone metastasis progression through inducing osteocytes to secrete GDF15 that stimulates prostate cancer growth and invasion. *Oncogene*, 38(23), 4540–4559. doi: 10.1038/s41388-019-0736-3
- Waskom, M. L. (2021, April). Seaborn: Statistical data visualization. *Journal of Open Source Software*, 6(60), 3021. Retrieved 2023-03-26, from <https://joss.theoj.org/papers/10.21105/joss.03021> doi: 10.21105/joss.03021
- Webster, G. A., & Perkins, N. D. (1999, May). Transcriptional Cross Talk between NF-κB and p53. *Molecular and Cellular Biology*, 19(5), 3485–3495. Retrieved 2023-07-04, from <https://www.ncbi.nlm.nih.gov/pmc/articles/PMC84141/>
- Weetall, M., Hugo, R., Maida, S., West, S., Wattanasin, S., Bouhel, R., ... Friedman, C. (2001, June). A Homogeneous Fluorometric Assay for Measuring Cell Adhesion to Immobilized Ligand Using V-Well Microtiter Plates. *Analytical Biochemistry*, 293(2), 277–287. Retrieved 2022-09-25, from <https://linkinghub.elsevier.com/retrieve/pii/S0003269701951401> doi: 10.1006/abio.2001.5140
- Weiss, C. J. (2022, September). Visualizing protein big data using Python and Jupyter notebooks. *Biochemistry and Molecular Biology Education: A Bimonthly Publication of the International Union of Biochemistry and Molecular Biology*, 50(5), 431–436. doi: 10.1002/bmb.21621
- West, K. (2018, July). Reinventing Research: Agile in the Academic Laboratory / Agile Alliance. Retrieved 2024-05-14, from <https://www.agilealliance.org/resources/experience-reports/reinventing-research-agile-in-the-academic-laboratory/>
- Wickham, H. (2014, September). Tidy Data. *Journal of Statistical Software*, 59, 1–23. Retrieved 2023-11-15, from <https://doi.org/10.18637/jss.v059.i10> doi: 10.18637/jss.v059.i10
- Wilkins, A., Kemp, K., Ginty, M., Hares, K., Mallam, E., & Scolding, N. (2009, July). Human bone marrow-derived mesenchymal stem cells secrete brain-derived neurotrophic factor which promotes neuronal survival in vitro. *Stem*

- cell research*, 3(1), 63–70. doi: 10.1016/j.scr.2009.02.006
- Wilkinson, M. D., Dumontier, M., Aalbersberg, I. J., Appleton, G., Axton, M., Baak, A., ... Mons, B. (2016, March). The FAIR Guiding Principles for scientific data management and stewardship. *Scientific Data*, 3(1), 160018. Retrieved 2024-03-18, from <https://www.nature.com/articles/sdata201618> doi: 10.1038/sdata.2016.18
- Witwer, K. W. (2013, February). Data submission and quality in microarray-based microRNA profiling. *Clinical chemistry*, 59(2), 392–400. Retrieved 2024-04-22, from <https://www.ncbi.nlm.nih.gov/pmc/articles/PMC4037921/> doi: 10.1373/clinchem.2012.193813
- Wong, A. D., & Searson, P. C. (2017, November). Mitosis-mediated intravasation in a tissue-engineered tumor-microvessel platform. *Cancer research*, 77(22), 6453–6461. Retrieved 2023-07-14, from <https://www.ncbi.nlm.nih.gov/pmc/articles/PMC5690825/> doi: 10.1158/0008-5472.CAN-16-3279
- Xu, W., Zhang, X., Qian, H., Zhu, W., Sun, X., Hu, J., ... Chen, Y. (2004, July). Mesenchymal stem cells from adult human bone marrow differentiate into a cardiomyocyte phenotype in vitro. *Experimental biology and medicine (Maywood, N.J.)*, 229(7), 623–631.
- Yang, A., Troup, M., & Ho, J. W. (2017, July). Scalability and Validation of Big Data Bioinformatics Software. *Computational and Structural Biotechnology Journal*, 15, 379–386. Retrieved 2024-03-07, from <https://www.ncbi.nlm.nih.gov/pmc/articles/PMC5537105/> doi: 10.1016/j.csbj.2017.07.002
- Yang, P., Qu, Y., Wang, M., Chu, B., Chen, W., Zheng, Y., ... Qian, Z. (2022, June). Pathogenesis and treatment of multiple myeloma. *MedComm*, 3(2), e146. Retrieved 2024-05-21, from <https://www.ncbi.nlm.nih.gov/pmc/articles/PMC9162151/> doi: 10.1002/mco2.146
- Yang, Y., Macleod, V., Bendre, M., Huang, Y., Theus, A. M., Miao, H.-Q., ... Sanderson, R. D. (2005, February). Heparanase promotes the spontaneous metastasis of myeloma cells to bone. *Blood*, 105(3), 1303–1309. doi: 10.1182/blood-2004-06-2141
- Zeissig, M. N., Zannettino, A. C. W., & Vandyke, K. (2020, December). Tumour Dissemination in Multiple Myeloma Disease Progression and Relapse: A Potential Therapeutic Target in High-Risk Myeloma. *Cancers*, 12(12). Retrieved 2021-02-03, from <https://www.ncbi.nlm.nih.gov/pmc/articles/PMC7761917/> doi: 10.3390/cancers12123643
- Zeiss OAD Feature Extractors*. (n.d.). Retrieved 2024-06-14, from https://github.com/zeiss-microscopy/OAD/blob/master/Machine_Learning/Feature_Extractors/feature_extractors.md
- Zerbino, D. R., Achuthan, P., Akanni, W., Amode, M. R., Barrell, D., Bhai, J., ... Flicek, P. (2018, January). Ensembl 2018. *Nucleic Acids Research*, 46(D1), D754-D761. Retrieved 2023-05-27, from <https://doi.org/10.1093/nar/gkx1098> doi: 10.1093/nar/gkx1098
- Zhou, F., Meng, S., Song, H., & Claret, F. X. (2013, November). Dickkopf-1 is a key regulator of myeloma bone disease: Opportunities and challenges for therapeutic intervention. *Blood reviews*, 27(6), 261–267. Retrieved 2023-02-18, from <https://www.ncbi.nlm.nih.gov/pmc/articles/PMC4133945/> doi: 10.1016/j.blre.2013.08.002
- Zhou, Y., Zhou, B., Pache, L., Chang, M., Khodabakhshi, A. H., Tanaseichuk, O., ... Chanda, S. K. (2019, April). Metascape provides a biologist-oriented resource for the analysis of systems-level datasets. *Nature Communications*, 10(1), 1523. Retrieved 2023-02-09, from <https://www.nature.com/articles/s41467-019-09234-6> doi: 10.1038/s41467-019-09234-6
- Ziemann, M., Eren, Y., & El-Osta, A. (2016, August). Gene name errors are widespread in the scientific literature. *Genome Biology*, 17(1), 177. Retrieved 2024-04-30, from <https://doi.org/10.1186/s13059-016-1044-7> doi: 10.1186/s13059-016-1044-7

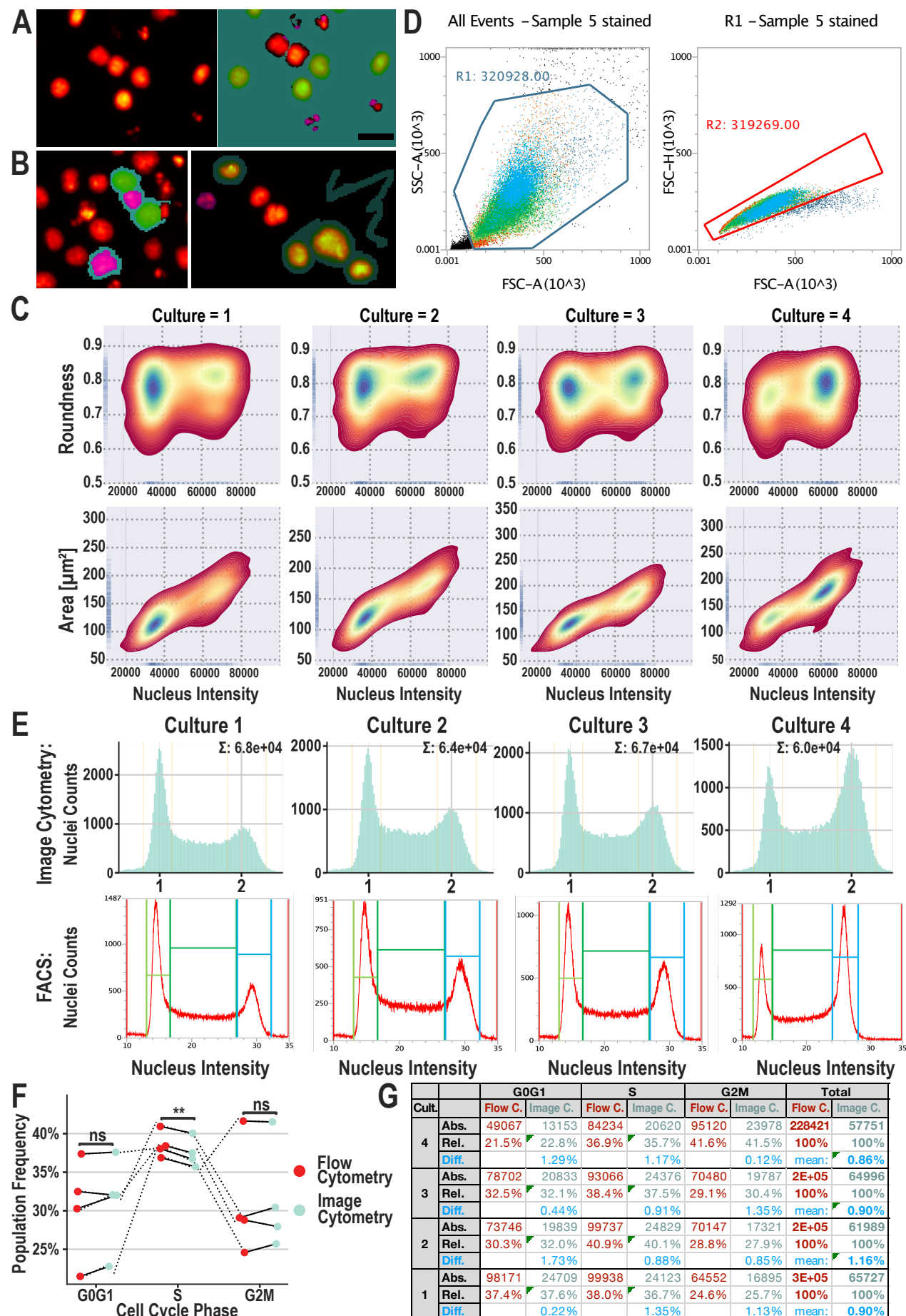
Appendices

A Supplementary Data & Methods

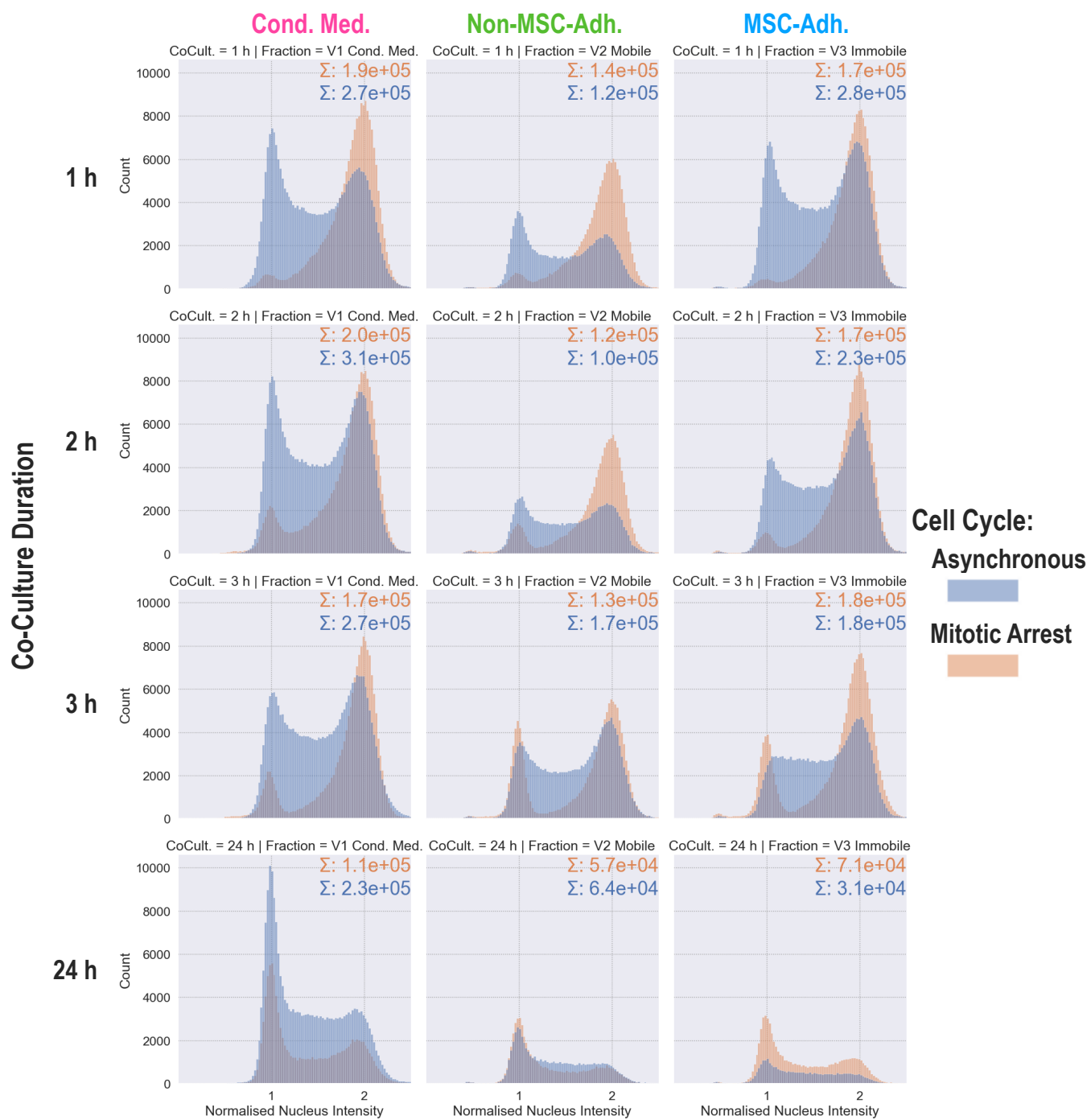
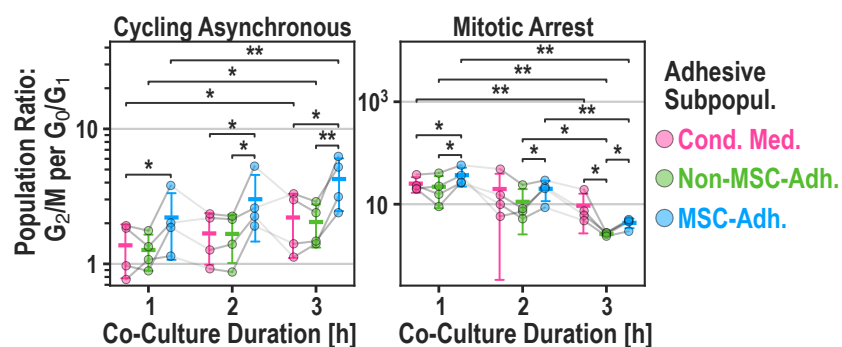
A.1 Figures



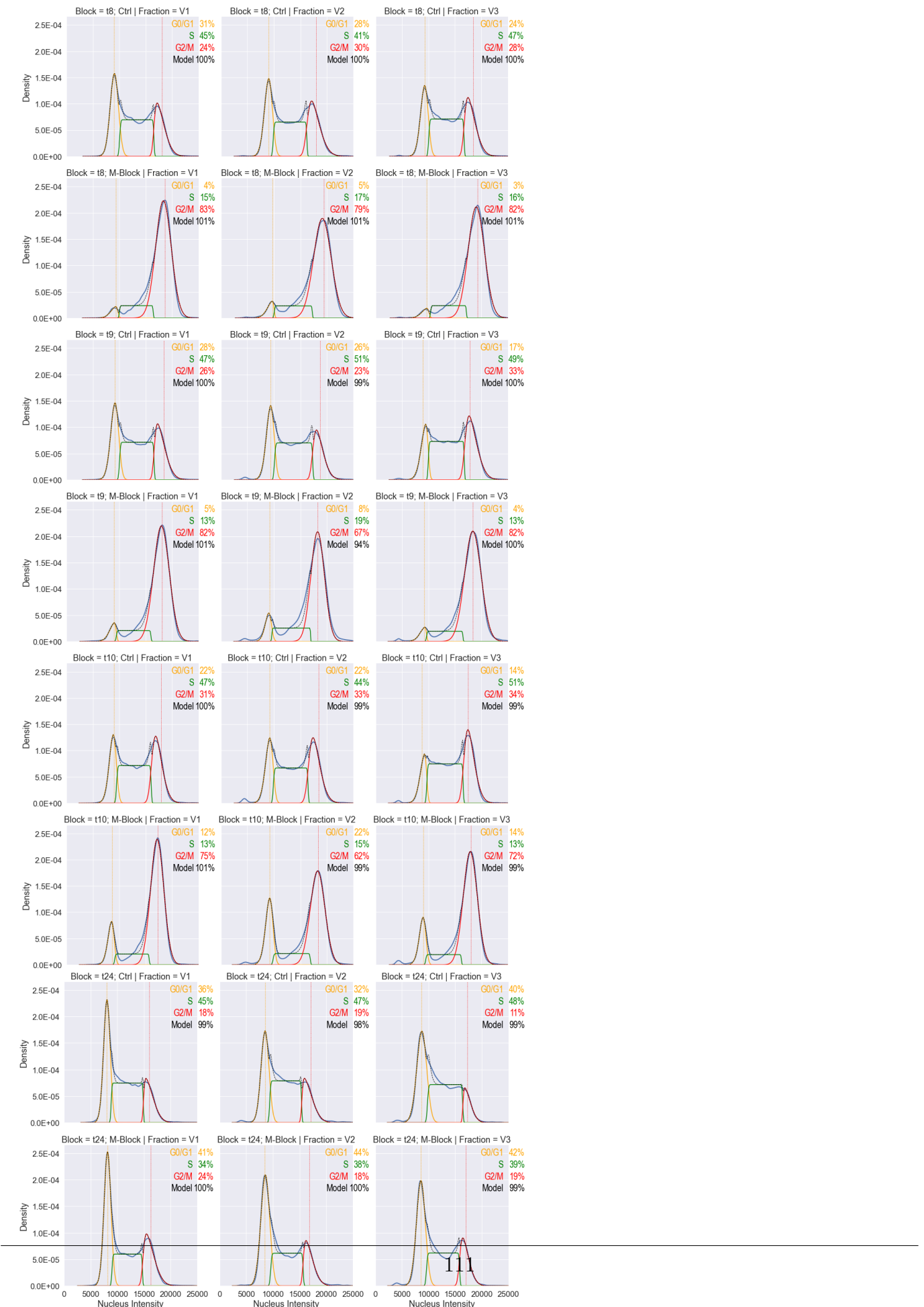
Appendix A Figure 1: Principle and quantification of the V-well adhesion assay of fluorescently labeled myeloma cells adapted by Weetall et al. (2001). **A:** Sample: Subsequent rounds of centrifugation and removal of cell pellet yielded the size of adhesive subpopulations. Fluorescently stained INA-6 cells were added to an hMSC monolayer. Non-adherent INA-6 cells (V2) were pelleted in the well-tip. Pellets were quantified by fluorescence brightness and isolated by pipetting. Immobile INA-6 cells (V3) were manually detached by forceful pipetting. Reference: Omitting adhesive hMSC-layer yielded 100 % non-adherent cells (V1) after the first centrifugation step; Background: hMSC monolayer was used as background signal. **B:** Calculation of the population size relative to total cells starting with pellet intensity. The shown example is the pellet gained by centrifuging mobile subpopulation (V2) after 1 h of co-culture. (see Fig. 3 for context): Intensity values from pellet images were summarized. After subtracting the unlabeled hMSC signal and normalization by a full-size pellet (reference), the resulting values represented the fraction of the adhesive subpopulation. **C:** One of three biological replicates summarized in Fig. 3. Line range shows the standard deviation of four technical replicates. Non.Adh. Rem.: Fluorescence signal after removal of V2. **D:** Example images of myeloma cell lines (INA-6, U266, MM.1S) pelleted in the tip of V-wells. The leftmost image shows the recorded area in a complete V-well. Scale bar = 200 µm. **E:** Results from (D) comparing adhesion strength of three myeloma cell lines to hMSC. Error bars represent technical deviation. MM: Multiple Myeloma.



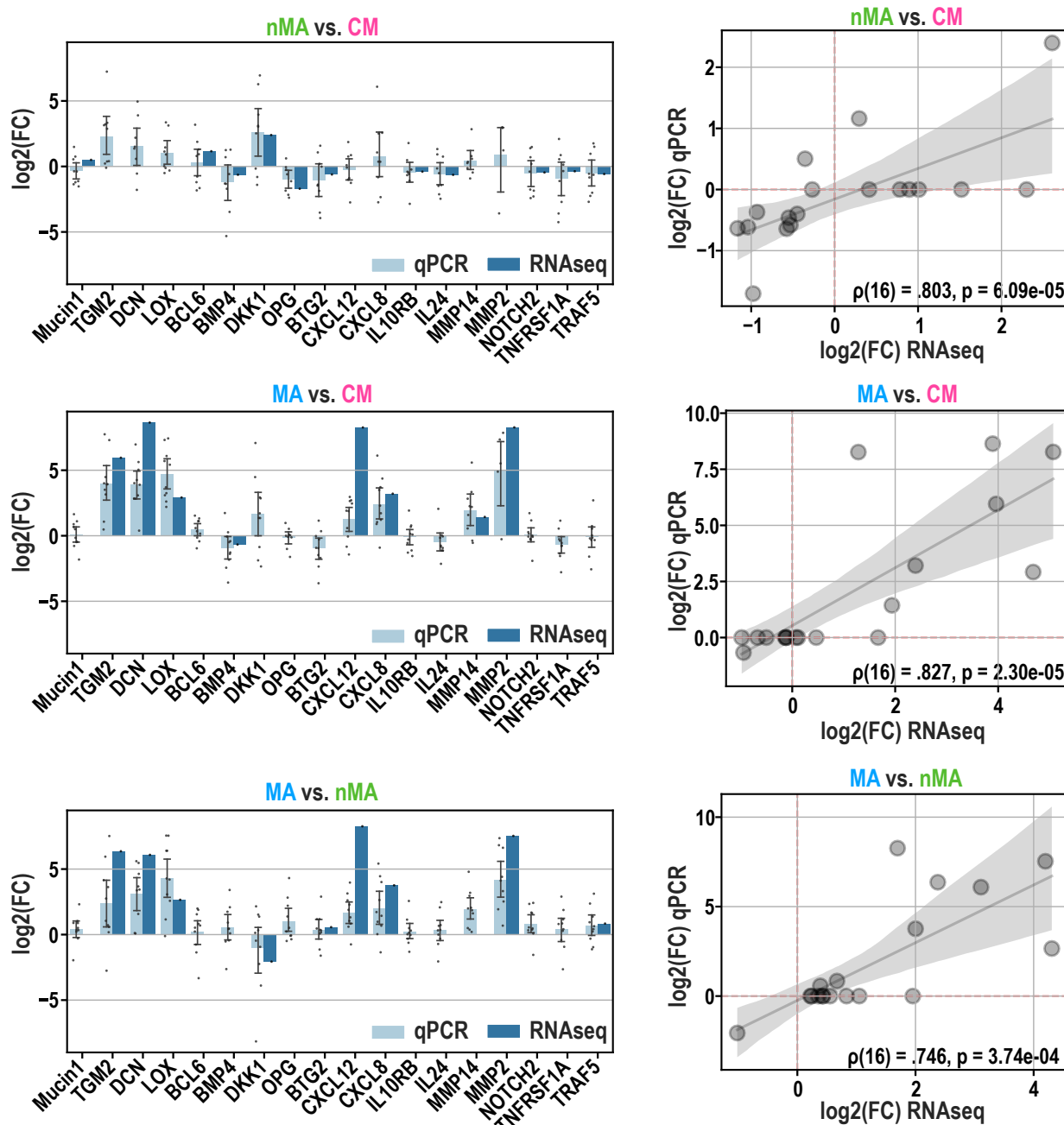
Appendix A Figure 2: Validation of image cytometric analysis of cell cycle in four INA-6 cultures. **A:** Left: Example image cytometric scan: INA-6 cells were stained with Hoechst33342 and scanned by automated fluorescence microscopy. Right: The image was segmented using a convolutional neural network (ZEISS ZEN intellesis) trained to discern healthy nuclei (green) from fragmented ones (magenta). Doublets are excluded by setting an area- and roundness threshold. Scale bar: 20 μm . **B:** Two example images from the training set. **C:** Quality of image cytometric data was ensured by plotting the distribution of nuclei brightnesses vs. the distribution of both nuclei-roundnesses and nuclei-areas. Nuclei with double fluorescence intensity have the same roundness while their area increases, as expected from a cell in G2 phase. **D:** The same samples from (C) were also measured with flow cytometry. Representative example of gating strategy: Left: Dead cells were excluded by setting a minimum threshold for side-scattering (SSC-A). Right: Doublets were excluded by setting a maximum threshold for forward scatter area (FSC-A) (sample “5” represents culture “4” in this figure). **E:** Cell cycle profiles of four independent INA-6 cultures were measured by both image cytometry (top) and flow cytometry (bottom). For both methods, frequencies of G0/G1, S, and G2M were summed up by setting fluorescence intensity thresholds. **F:** Image cytometry yields the same frequencies for G0/G1, S, and G2M when compared to flow cytometry. RM-ANOVA showed that the method has no significant effect on the frequencies of cell cycle populations [$F(1, 3) = 1.421, p\text{-unc} = .32$]. **G:** Results from (F) in tabular form. On average, frequencies for G0/G1, S, and G2M measured by Image cytometry differ by 0.95 percent points compared to flow cytometry measurement. Cult.: Culture; C.: Image cytometry; Abs.: Absolute cell count; Rel.: Relative cell count; Diff.: Difference between relative cell counts determined by flow cytometry and image cytometry.

A**B**

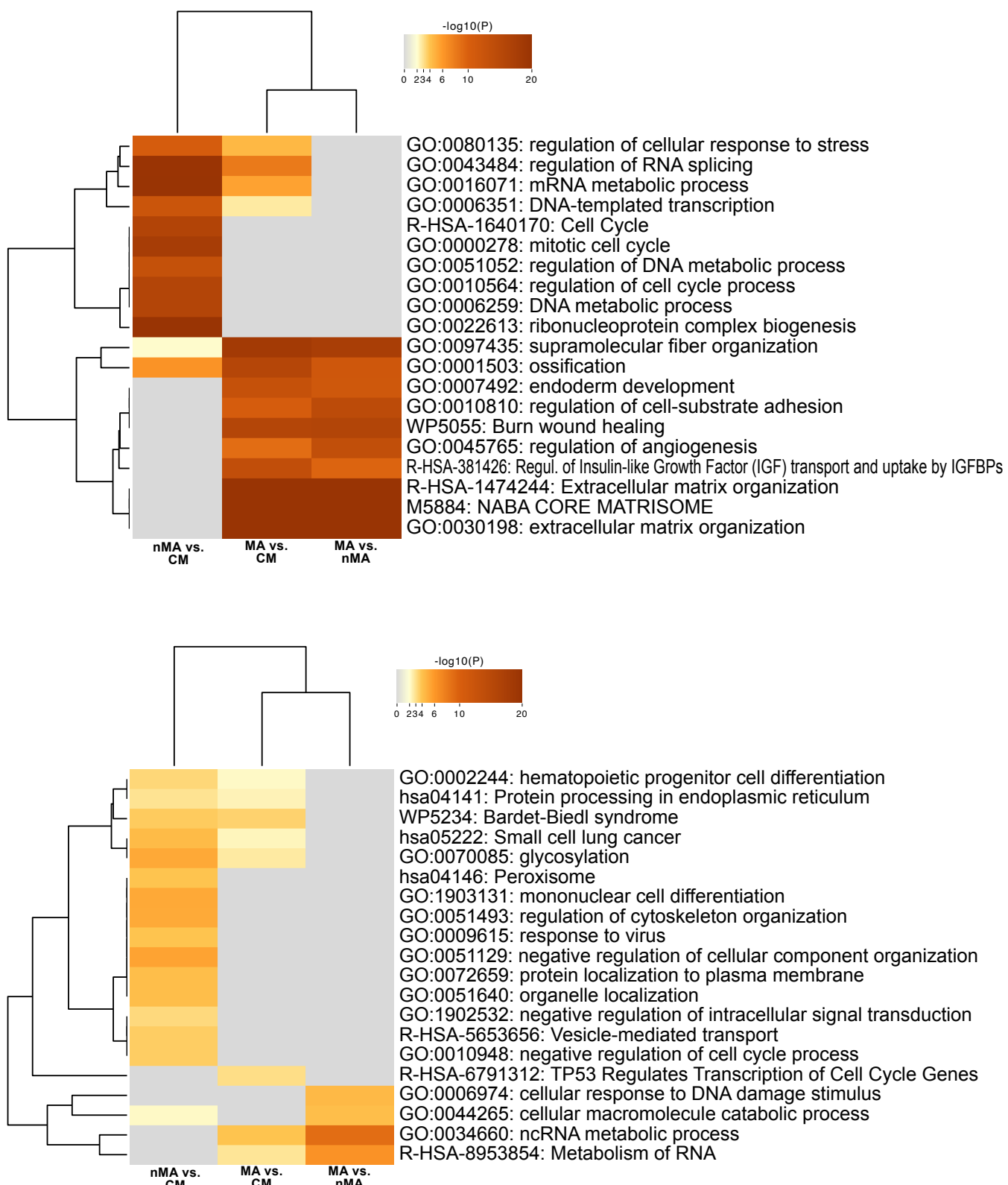
Appendix A Figure 3: Cell cycle analysis of INA-6 pellets gained from V-Well Adhesion assay (Fig. 3). **A:** Cell cycle profiles of MSC-adhering subpopulations. INA-6 cells were synchronized by double thymidine block followed by nocodazole. Cell cycle was released directly before addition to hMSCs. Histograms were normalized and summed up across all biological replicates ($n = 4$). Technical replicates (3) were pooled prior to cell cycle profiling. CoCult. = Co-culture duration. Fraction = Adhesion subpopulations. **B:** Similar figure to Fig. 3C displaying ratio of INA-6 populations (G2/M to G0/G1). **Statistics:** Paired t-test (B).



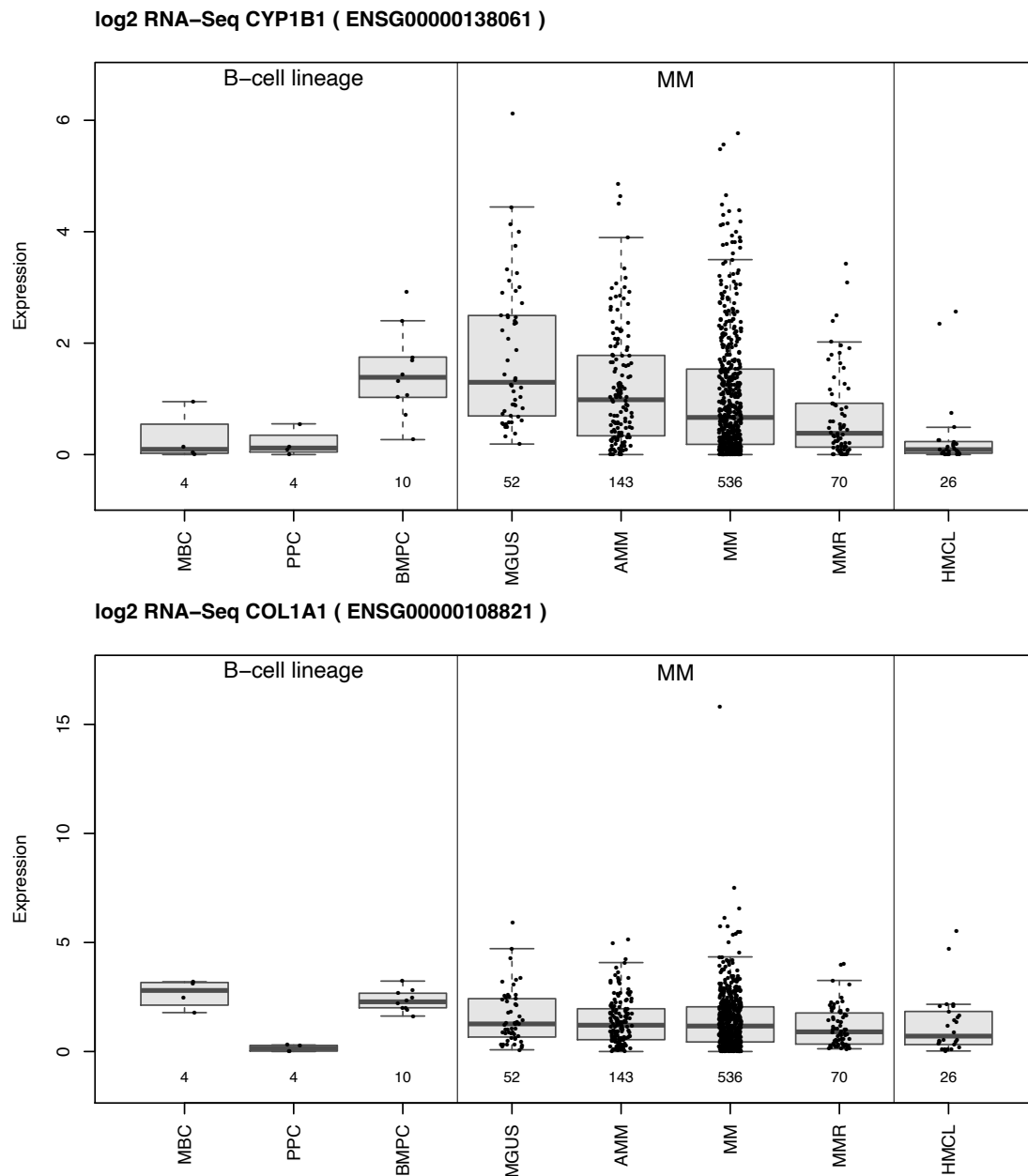
Appendix A Figure 4: Representative (one of the four independent sample sets as seen in Appendix A: Fig. 3) curve fitting analysis of cell cycle profiles generated by Image Cytometry. t8, t9, t10, and t24 refer to 1, 2, 3, and 24 hours after the addition of INA-6 cells to hMSCs.



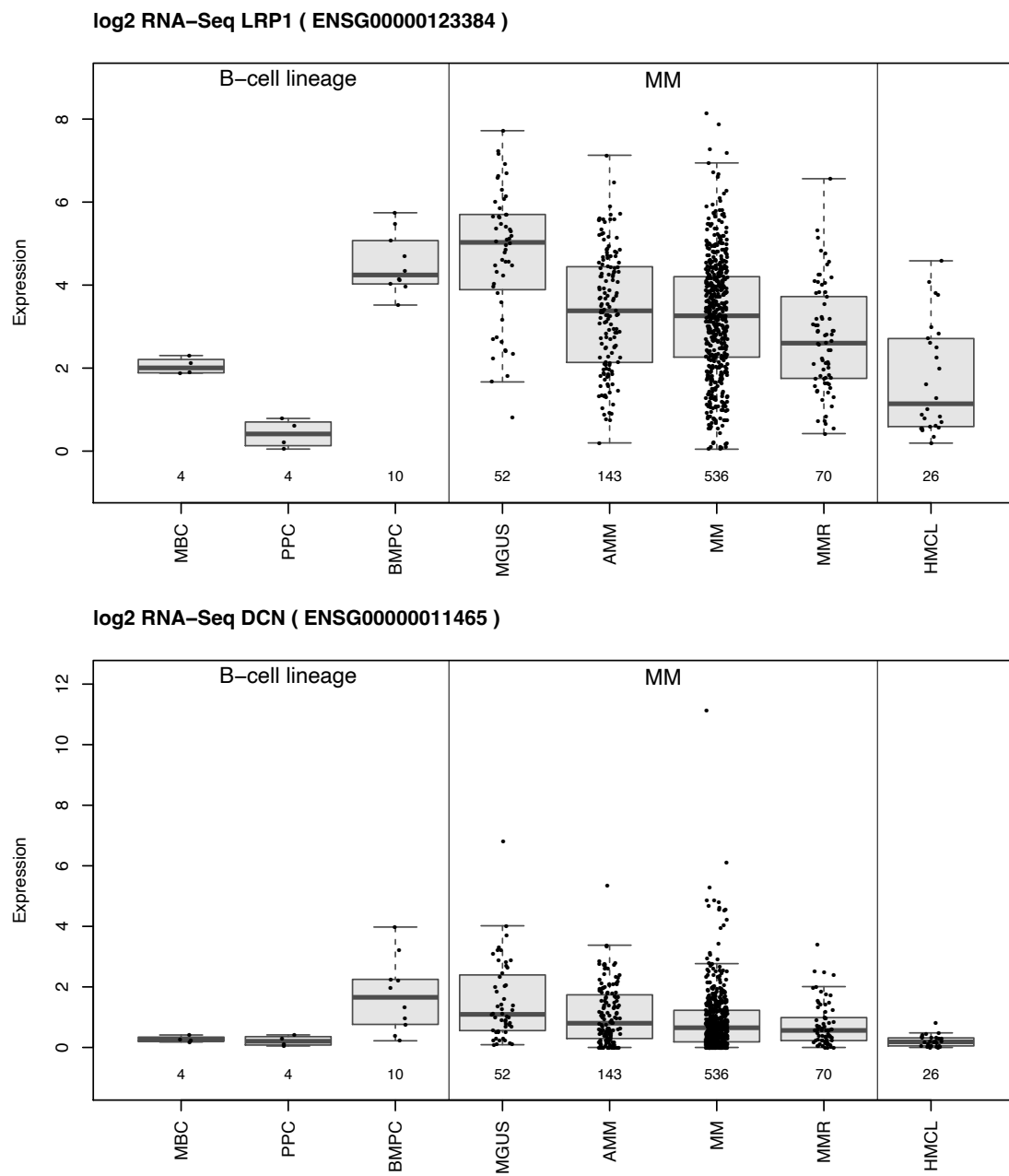
Appendix A Figure 5: Correlation of RNAseq with qPCR Left: Validation of RNAseq results (Fig. 4) with qPCR showing the \log_2 (foldchange expression) of 18 genes. For qPCR, Datapoints each represent one biological replicate ($n = 10$), which is the mean of technical replicates ($n = 3$). Bar height represents mean of biological replicates, error bars show standard deviation of biological replicates. Right: Correlation between qPCR and RNAseq in terms of \log_2 (mean foldchange expression per gene). Each dot represents one gene shown in the barplot to the left. Genes measured with qPCR that showed no differential expression in RNAseq were set to have a $-\log_2(\text{FC}) = 0$. Shaded area shows the confidence interval of linear regression. Correlation coefficient was calculated using Spearman's rank. $N = 18$ genes. FC : Fold change expression.



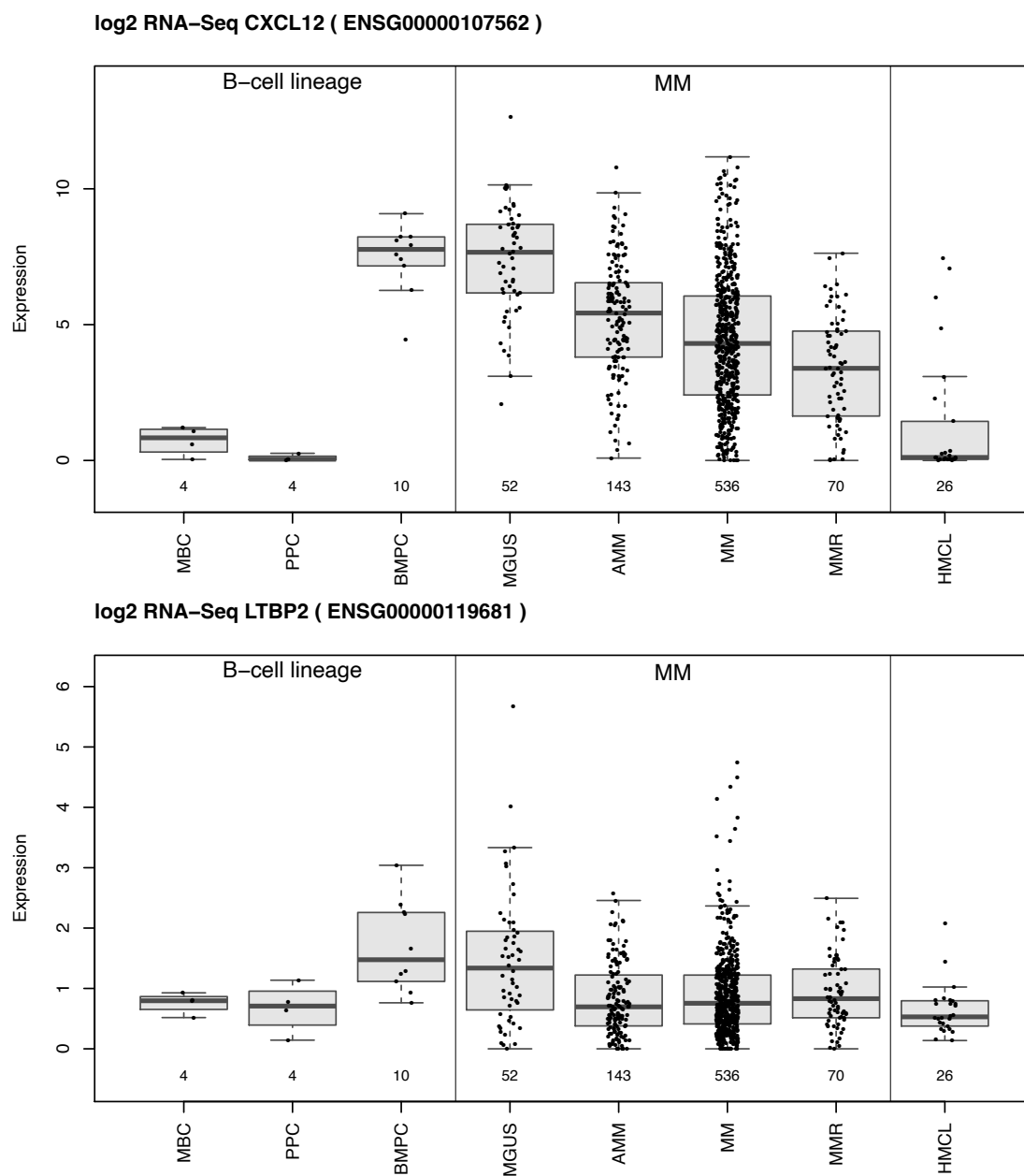
Appendix A Figure 6: Functional enrichment analysis by Metascape using genes that are differentially expressed between MSC-interacting subpopulations. Top: Upregulated genes. Bottom: Downregulated genes.



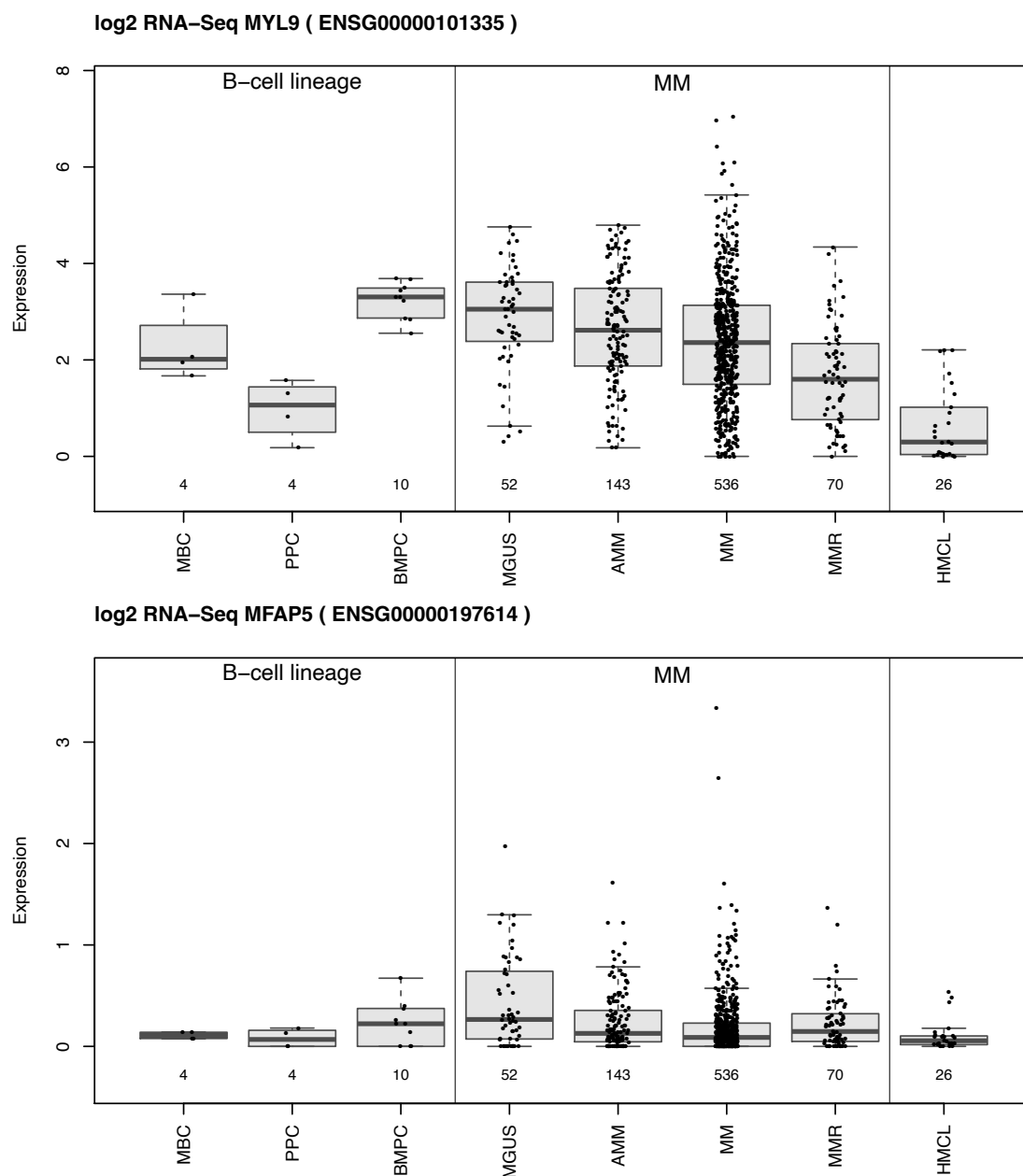
Appendix A Figure 7: Expression levels of adhesion genes that are downregulated and associated with survival ($p < 0.01$). Bone Marrow Plasma Cell (BMPC), Monoclonal Gammopathy of Undetermined Significance (MGUS), Smoldering Multiple Myeloma (sMM), Multiple Myeloma (MM), Multiple Myeloma Relapse (MMR).



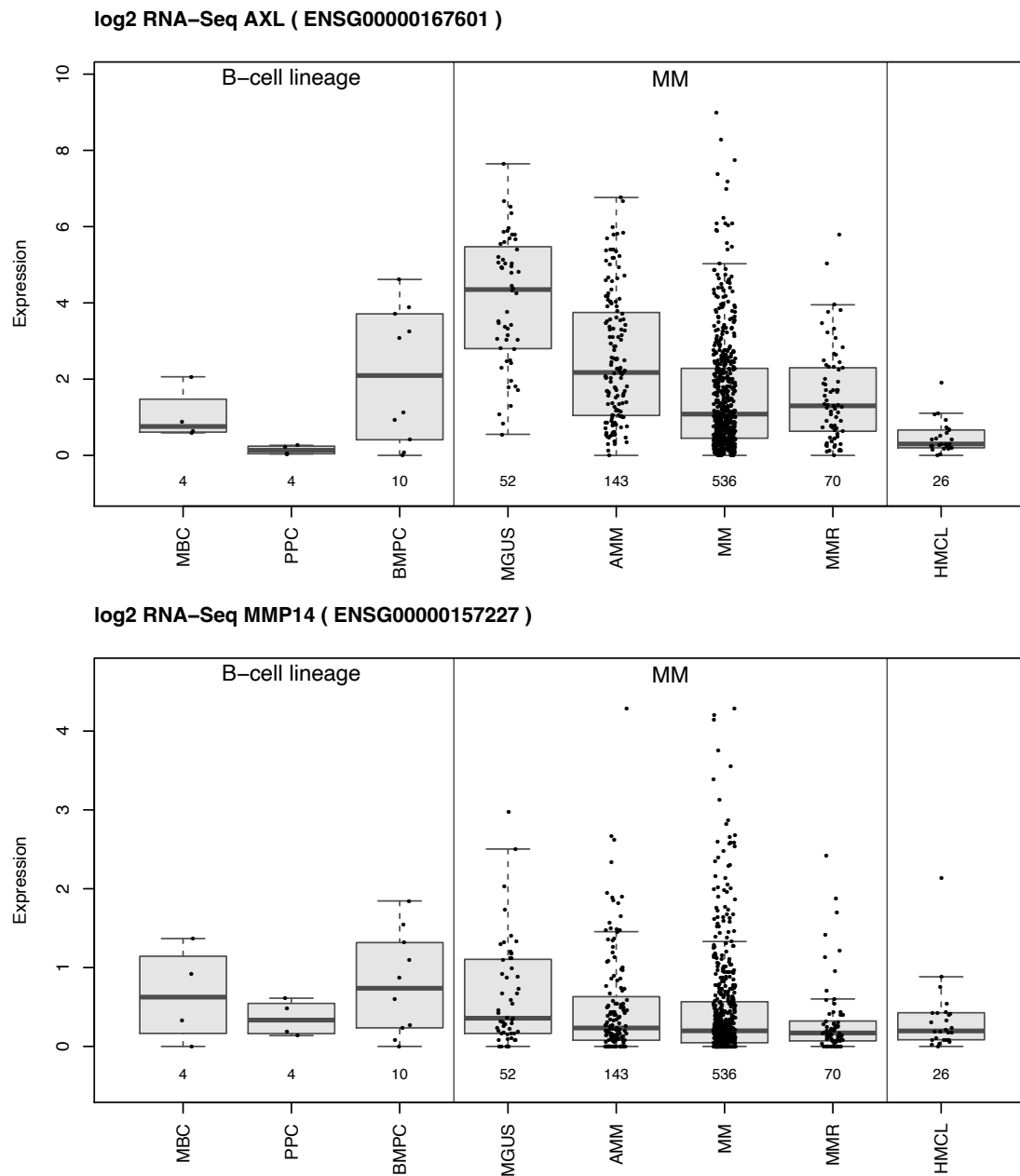
Appendix A Figure 7: continued from previous page



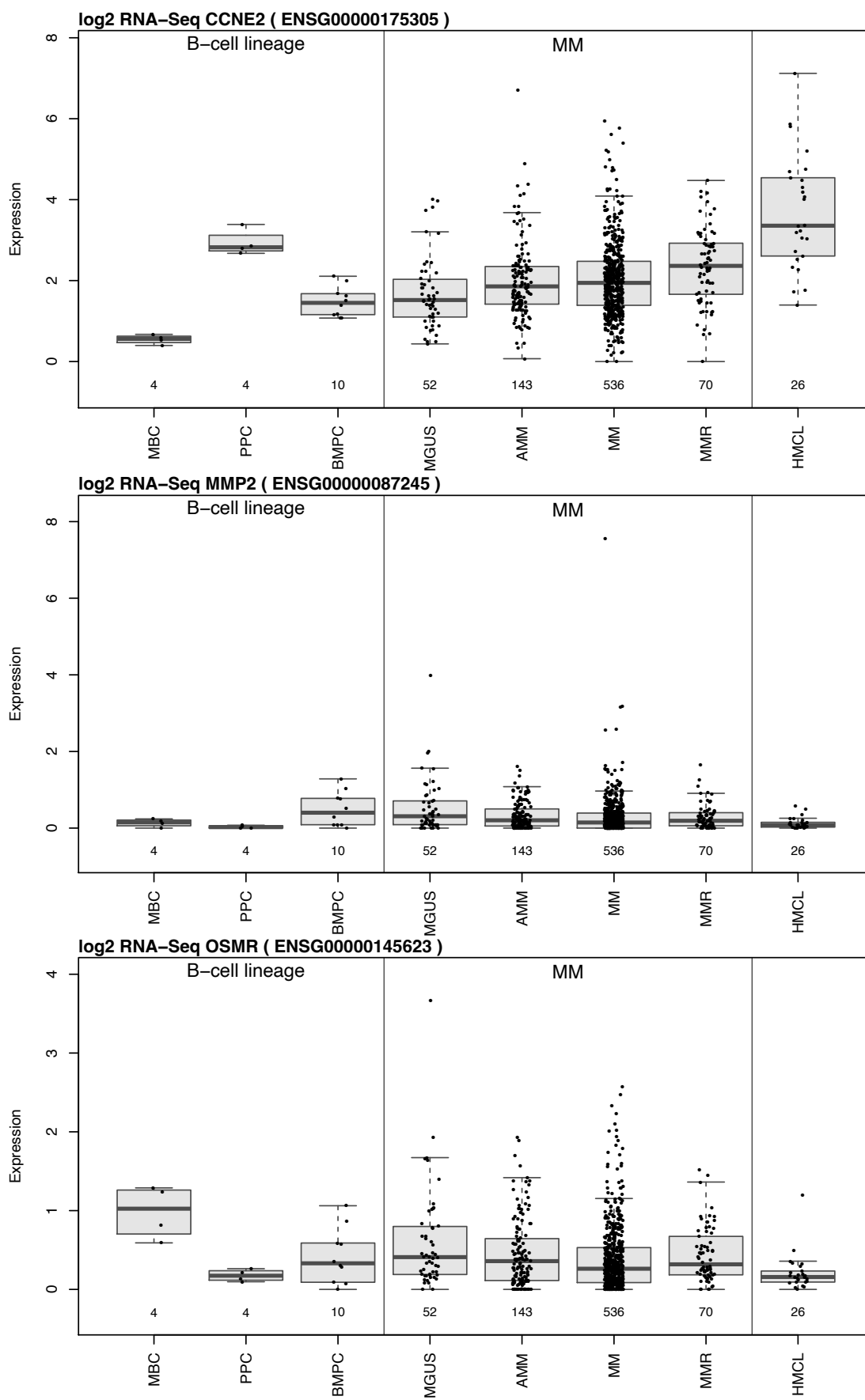
Appendix A Figure 7: continued from previous page



Appendix A Figure 7: continued from previous page



Appendix A Figure 7: continued from previous page



Appendix A Figure 8: Expression levels of adhesion genes that are not downregulated and associated with survival ($p < 0.01$). Bone Marrow Plasma Cell (BMPC), Monoclonal Gammopathy of Undetermined Significance (MGUS), Smoldering Multiple Myeloma (sMM), Multiple Myeloma (MM), Multiple Myeloma Relapse (MMR).

9

A.2 Tables

Appendix A Table 1: List of hMSC donors, myeloma cell lines, and their mycoplasma test status. If no unique donors were available, hMSC donors were used twice for the same experiment at different passages. WPSC: Well plate sandwich centrifugation.

Cell Type	Donor / Line	Donor Ages	Donor Sex	Date of negative Mycoplasma test	Experiment(s)	Figures
Myeloma Cell Line	INA-6	80	m	09.02.22	All	All
	U266			10.10.22	- Validation of V-Well Adhesion Assay	S1E
	MM1.S			24.02.22		
hMSC	1639	49	m	not tested	- Validation of V-Well Adhesion Assay - Time-lapse: INA-6 on dispersed hMSC	S1E 1D; 2[A-E]
	1571	72	m	not tested	- Saturation of hMSCs	1[A-B]
	1573	47	m	not tested		
	1578	82	m	not tested		
	1842	63	m	not tested	- INA-6 Viability dependent on time and hMSC adhesion surface (INA not washed off)	1E right
	1843	60	m	not tested		
	1537	77	f	not tested		
	1794	82	m	not tested	- INA-6 Viability dependent on time and hMSC adhesion surface (INA washed off)	1[C, E left]
	1779	61	m	not tested		
	1849	69	m	not tested		
	1854	80	f	not tested		
	1605	71	f	not tested		
	1650	57	m	not tested	- Time-lapse: INA-6 on dispersed hMSC	1D; 2[A-E]
	1859	64	f	not tested		
	1863	79	f	not tested		
	1861	52	f	not tested	- Time-lapse: INA-6 on confluent hMSC - Cell Cycle Profiling after V-well assay	2[G-I] 3C
	1818	81	f	not tested		
	1824	82	f	not tested		
	1827	56	m	not tested	(Donor measured twice, different passages) - V-well adhesion assay of mitotically blocked INA-6 followed by Cell Cycle Profiling after V-well assay - V-well adhesion assay of mitotically blocked INA-6 followed by Cell Cycle Profiling after V-well assay	3[B,C] 3[B,C]

continued on next page

Appendix A Table 1 – continued from previous page

hMSC	1501	59	m	not tested	<p>- INA-6 AI-assisted count during WPSC (INA-6 stained with celltracker green)</p>	4B
	1643	75	f	not tested		
	1718	67	m	not tested		
	1720	58	m	not tested		
	1653	65	m	not tested		
	1591	78	m	not tested	<p>- WPSC (MACS) followed by RNAseq, Metascape analysis, and qPCR validation</p> <p>- WPSC (Wash) followed by qPCR-Validation and Luminescent Viability assays</p>	4[A,C,D,E]; 5[A-C]
	1654	74	m	not tested	<p>- WPSC (MACS) followed by RNAseq, Metascape analysis, and qPCR validation</p> <p>- WPSC (Wash) followed by qPCR-Validation and Luminescent Viability assays</p>	4[A,C,D,E]; 5[A-C]
	1655	78	f	not tested	<p>- WPSC (MACS) followed by RNAseq, Metascape analysis, and qPCR validation</p>	4[A,C,D,E]; 5[A-C]
	1668	80	f	not tested		
	1670	66	f	not tested		
	1701	81	m	not tested	<p>- WPSC (Wash) followed by qPCR-Validation and Luminescent Viability assays</p>	4[C-E], 4F
	1702	79	f	not tested		
	1600	77	m	not tested		
	1681	56	m	not tested	<p>- WPSC (Wash) followed by Luminescent Viability assays</p>	4F
	1672	65	m	not tested	<p>- WPSC (Wash) followed by qPCR-Validation</p>	4[C-E]

Appendix A Table 2: Adhesion genes (from Fig. 6A) categorized by a continuous downregulation across disease progression. Bone Marrow Plasma Cell (BMPC), Monoclonal Gammopathy of Undetermined Significance (MGUS), Smoldering Multiple Myeloma (sMM), Multiple Myeloma (MM), Multiple Myeloma Relapse (MMR). p-adj. = adjusted p-values (Benj.-Hoch.).

Regulation during disease progression	Gene	Ensemble ID	Progression Free / Overall Survival	Better Prognosis with high/low expression	Association of expression with survival	
					[p-unc]	[p-adj]
False	ADAMTS1	ENSG00000154734	Prog. Free	low	0.031875	0.084719
			Overall	low	0.048755	0.120104
	ADAMTS2	ENSG0000087116	Prog. Free	high	0.63795	0.767059
			Overall	high	0.811174	0.890528
	BGN	ENSG00000182492	Prog. Free	high	0.38065	0.533967
			Overall	high	0.279004	0.426961
	CAVIN1	ENSG00000177469	Prog. Free	high	0.407479	0.548739
			Overall	high	0.210903	0.3492
	CCDC80	ENSG0000091986	Prog. Free	high	0.002038	0.015833
			Overall	high	0.023743	0.077356
	CCN1	ENSG00000142871	Prog. Free	high	0.285568	0.443729
			Overall	low	0.931563	0.961309
	CCN2	ENSG00000118523	Prog. Free	high	0.030562	0.083425
			Overall	high	0.002889	0.024263
	CCNE2	ENSG00000175305	Prog. Free	low	0.012138	0.046195
			Overall	low	0.000534	0.008638
	CDH11	ENSG00000140937	Prog. Free	high	0.413948	0.550115
			Overall	high	0.044627	0.117163
	CEMIP	ENSG00000103888	Prog. Free	high	0.798984	0.877146
			Overall	low	0.287022	0.428378
	COL12A1	ENSG00000111799	Prog. Free	high	0.340978	0.491983
			Overall	low	0.829338	0.900679
	COL16A1	ENSG0000084636	Prog. Free	low	0.281112	0.443629
			Overall	low	0.162895	0.293792
	COL4A1	ENSG00000187498	Prog. Free	high	0.040286	0.098969
			Overall	high	0.009472	0.039863
	COL4A2	ENSG00000134871	Prog. Free	high	0.0124	0.046195
			Overall	high	0.175895	0.3063
	COL5A1	ENSG00000130635	Prog. Free	high	0.368403	0.524066
			Overall	low	0.860512	0.914414
	COL6A3	ENSG00000163359	Prog. Free	low	0.103315	0.208697
			Overall	low	0.197836	0.336625
	COL8A1	ENSG00000144810	Prog. Free	high	0.680745	0.807636
			Overall	high	0.289334	0.428378
	CREB3L1	ENSG00000157613	Prog. Free	low	0.165978	0.310441
			Overall	low	0.047989	0.120104
	EDIL3	ENSG00000164176	Prog. Free	high	0.863476	0.899083
			Overall	low	0.496663	0.611744
	F3	ENSG00000117525	Prog. Free	high	0.091858	0.197397
			Overall	high	0.009177	0.039863
	FBN1	ENSG00000166147	Prog. Free	high	0.472247	0.603376
			Overall	low	0.401546	0.533633
	FLNC	ENSG00000128591	Prog. Free	high	0.18539	0.329735
			Overall	low	0.474071	0.598515
	FN1	ENSG00000115414	Prog. Free	high	0.843432	0.896701
			Overall	low	0.421268	0.552573
	FBN1	ENSG00000166147	Prog. Free	high	0.472247	0.603376
			Overall	low	0.401546	0.533633
	FLNC	ENSG00000128591	Prog. Free	high	0.18539	0.329735
			Overall	low	0.474071	0.598515
	FN1	ENSG00000115414	Prog. Free	high	0.843432	0.896701

continued on next page

Appendix A Table 2 – continued from previous page

		Overall	low	0.421268	0.552573
False	FOSB	ENSG00000125740	Prog. Free	low	0.585138
			Overall	high	0.942273
GJA1		ENSG00000152661	Prog. Free	high	0.333512
			Overall	low	0.34262
GREM1		ENSG00000166923	Prog. Free	high	0.457976
			Overall	low	0.591104
HBEGF		ENSG00000113070	Prog. Free	low	0.145103
			Overall	low	0.051592
HTRA1		ENSG00000166033	Prog. Free	high	0.01203
			Overall	high	0.040407
IGFBP3		ENSG00000146674	Prog. Free	high	0.248011
			Overall	low	0.841566
IGFBP7		ENSG00000163453	Prog. Free	low	0.009533
			Overall	low	0.024942
ITGA11		ENSG00000137809	Prog. Free	high	0.97438
			Overall	low	0.966513
KLF11		ENSG00000172059	Prog. Free	low	0.229416
			Overall	low	0.060892
LAMB1		ENSG00000091136	Prog. Free	high	0.477921
			Overall	high	0.604163
LOX		ENSG00000113083	Prog. Free	low	0.748901
			Overall	low	0.035028
MMP2		ENSG00000087245	Prog. Free	high	2.29E-05
			Overall	high	0.044615
NFKBIZ		ENSG00000144802	Prog. Free	high	0.725256
			Overall	high	0.310216
NR4A1		ENSG00000123358	Prog. Free	high	0.0214
			Overall	high	0.060042
NR4A2		ENSG00000153234	Prog. Free	high	0.275313
			Overall	high	0.11176
OSMR		ENSG00000145623	Prog. Free	high	0.000567
			Overall	high	0.01287
PDGFRB		ENSG00000113721	Prog. Free	high	0.691005
			Overall	high	0.599357
POSTN		ENSG00000133110	Prog. Free	low	0.858041
			Overall	low	0.496348
PTX3		ENSG00000163661	Prog. Free	high	0.020943
			Overall	high	0.045241
PXDN		ENSG00000130508	Prog. Free	low	0.403966
			Overall	low	0.172495
SERPINE1		ENSG00000106366	Prog. Free	low	0.543711
			Overall	high	0.869146
SERPINH1		ENSG00000149257	Prog. Free	low	0.001825
			Overall	low	0.004399
SIX1		ENSG00000126778	Prog. Free	high	0.784446
			Overall	high	0.592089
SMAD3		ENSG00000166949	Prog. Free	low	0.027411
			Overall	low	0.016437
SPARC		ENSG00000113140	Prog. Free	high	0.073989
			Overall	high	0.244069
SPOCK1		ENSG00000152377	Prog. Free	low	0.531524
			Overall	low	0.303273
SULF1		ENSG00000137573	Prog. Free	high	0.190403
			Overall	high	0.388706
THBS2		ENSG00000186340	Prog. Free	low	0.318676
			Overall	high	0.292654
VPS37B		ENSG00000139722	Prog. Free	low	0.1478
			Overall	low	0.199975

continued on next page

Appendix A Table 2 – continued from previous page

True	ACTN1	ENSG0000072110	Prog. Free	high	0.170661	0.313396
			Overall	high	0.007728	0.035478
ADAM12		ENSG00000148848	Prog. Free	high	0.019179	0.062487
			Overall	high	0.081847	0.168704
AEBP1		ENSG00000106624	Prog. Free	high	0.010829	0.046195
			Overall	high	0.057228	0.133697
AXL		ENSG00000167601	Prog. Free	high	0.001496	0.015105
			Overall	high	3.64E-05	0.00184
CD99		ENSG00000002586	Prog. Free	low	0.916833	0.941333
			Overall	low	0.083964	0.169607
COL1A1		ENSG00000108821	Prog. Free	high	0.000303	0.004367
			Overall	high	0.000593	0.008638
COL1A2		ENSG00000164692	Prog. Free	high	0.298023	0.456066
			Overall	high	0.566636	0.673297
COL3A1		ENSG00000168542	Prog. Free	high	0.025985	0.07719
			Overall	high	0.010794	0.042917
COL5A2		ENSG00000204262	Prog. Free	low	0.74501	0.840433
			Overall	low	0.99967	0.99967
COL6A1		ENSG00000142156	Prog. Free	high	0.011972	0.046195
			Overall	high	0.011048	0.042917
COL6A2		ENSG00000142173	Prog. Free	high	0.261528	0.426037
			Overall	high	0.3235	0.447582
CXCL12		ENSG00000107562	Prog. Free	high	0.000116	0.002927
			Overall	high	0.000648	0.008638
CXCL8		ENSG00000169429	Prog. Free	low	0.839416	0.896701
			Overall	high	0.224913	0.366391
CYP1B1		ENSG00000138061	Prog. Free	high	0.008641	0.041735
			Overall	high	0.000684	0.008638
DCN		ENSG0000011465	Prog. Free	high	0.004827	0.030473
			Overall	high	0.000247	0.008327
DUSP1		ENSG00000120129	Prog. Free	high	0.695686	0.807636
			Overall	high	0.454061	0.583718
FBLN1		ENSG0000077942	Prog. Free	high	0.002676	0.019305
			Overall	high	0.003734	0.026138
GNB3		ENSG00000111664	Prog. Free	high	0.003748	0.025234
			Overall	high	0.005734	0.03048
GSTP1		ENSG0000084207	Prog. Free	high	0.972219	0.97438
			Overall	low	0.668091	0.749746
IGFBP4		ENSG00000141753	Prog. Free	high	0.008677	0.041735
			Overall	high	0.007089	0.034093
IL1R1		ENSG00000115594	Prog. Free	high	0.126318	0.250159
			Overall	high	0.256501	0.398563
ITGA5		ENSG00000161638	Prog. Free	high	0.094893	0.19967
			Overall	high	0.159113	0.29219
ITGAX		ENSG00000140678	Prog. Free	high	0.006717	0.036021
			Overall	high	0.003123	0.024263
ITGB5		ENSG0000082781	Prog. Free	low	0.436018	0.57192
			Overall	high	0.539497	0.648681
LAMA4		ENSG00000112769	Prog. Free	high	0.018518	0.062345
			Overall	high	0.104178	0.206314
LAMB2		ENSG00000172037	Prog. Free	high	0.015472	0.053885
			Overall	high	0.001354	0.013865
LOXL2		ENSG00000134013	Prog. Free	high	0.808671	0.878235
			Overall	low	0.933264	0.961309
LRP1		ENSG00000123384	Prog. Free	high	0.006458	0.036021
			Overall	high	0.000434	0.008638
LTBP2		ENSG00000119681	Prog. Free	high	9.03E-05	0.002927
			Overall	high	0.011656	0.043603
LUM		ENSG00000139329	Prog. Free	high	0.05158	0.118399
			Overall	high	0.065084	0.139862

continued on next page

Appendix A Table 2 – continued from previous page

True	MAP3K8	ENSG00000107968	Prog. Free	high	0.000958	0.010755
		Overall	high	0.01617	0.055338	
	MAP4K4	ENSG0000071054	Prog. Free	high	0.041155	0.098969
			Overall	high	0.31743	0.445284
	MFAP5	ENSG00000197614	Prog. Free	high	0.000243	0.004094
			Overall	high	0.004269	0.026138
	MMP14	ENSG00000157227	Prog. Free	high	6.93E-05	0.002927
			Overall	high	0.006691	0.033787
	MXRA5	ENSG00000101825	Prog. Free	high	0.034865	0.088035
			Overall	high	0.033819	0.103505
	MYL9	ENSG00000101335	Prog. Free	high	0.000146	0.00295
			Overall	high	1.56E-05	0.001572
	NRP1	ENSG00000099250	Prog. Free	high	0.001888	0.015833
			Overall	high	0.002212	0.020312
	PAPLN	ENSG00000100767	Prog. Free	high	0.034256	0.088035
			Overall	high	0.159113	0.29219
	TEX14	ENSG00000121101	Prog. Free	high	0.237488	0.399771
			Overall	low	0.518581	0.631044
	TGFBI	ENSG00000120708	Prog. Free	high	0.102621	0.208697
			Overall	high	0.004299	0.026138
	TGM2	ENSG00000198959	Prog. Free	high	0.058634	0.131601
			Overall	high	0.119621	0.227958
	THBS1	ENSG00000137801	Prog. Free	high	0.39286	0.543545
			Overall	high	0.456572	0.583718
	TNC	ENSG00000041982	Prog. Free	high	0.012806	0.046195
			Overall	high	0.004752	0.026663
	TNS1	ENSG00000079308	Prog. Free	high	0.338737	0.491983
			Overall	high	0.757617	0.840872
	TPM1	ENSG00000140416	Prog. Free	high	0.029263	0.0821
			Overall	high	0.001373	0.013865
	TUBA1A	ENSG00000167552	Prog. Free	low	0.006776	0.036021
			Overall	low	0.042929	0.117163
	TUBB6	ENSG00000176014	Prog. Free	low	0.186088	0.329735
			Overall	low	0.060071	0.133697
	VCAN	ENSG0000038427	Prog. Free	high	0.042782	0.100487
			Overall	high	0.080757	0.168704
	ZFP36L1	ENSG00000185650	Prog. Free	high	0.922693	0.941333
			Overall	high	0.24957	0.393852

Appendix A Table 3: List of primers. Some primers required a melting step to be performed before fluorescent readout to remove byproducts.

Primer	Sequence 5' - 3'	base pairs [bp]	annealing temp. [°C]
36B4_s	tgcattcgtacccattctatcat	122	60
36B4_as	aggcagatggatcagccaaga		
BCL6_s	tagagcccataaaacggtcctcat	221	55 + Melting Step at 77 °C
BCL6_as	cgc当地attgagccgagatgtgt		
BMP4_s	tacatgcggatcttaccg	132	58
BMP4_as	atgttcttcgtggtggaagc		
BTG2_s	gtattcttgttaggccgacactaa	264	60 + Melting Step at 78 °C
BTG2_as	tcttaaggtattcggtttggaa		
CXCL8_s	actgagagtgattgagagtggacc	251	55 + Melting Step at 77 °C
CXCL8_as	ccctacaacagacccacacaatac		
CXCL12_s	gattctcgaaagccatgttgcga	119	56
CXCL12_as	caatgcacacttgtctgttgttgc		
DCN_s	caacaacaagcttaccagagtacct	160	57
DCN_as	tgaaaagactcacacccgaaataaga		
DKK1_s	gcactgtgagttactgcgttag	129	56
DKK1_as	ttttgcagtaattccggggc		
IL10RB_s	gagtggcctgtctgtgagcaa	139	55
IL10RB_as	cttggtaaacgcaccacagcaag		
IL24_s	caaacagttggacgtagaagcagc	149	55
IL24_as	tgaaatgacacagggaaacaaacca		
LOX_s	ctgctcagattccccaaag	125	57
LOX_as	tggcatcaagcaggtcatag		
MMP2_s	ttgtatgtatggcatgcgtcaga	155	56
MMP2_as	cgtataccgcataatctttccg		
MMP14_s	cgacaagattgtatgcgtc	140	57
MMP14_as	tccctcccagactttgatg		
MUC1_s	gcagccctctcgatataacctg	200	58
MUC1_as	gtagggtgggtactcgctca		
NOTCH2_s	gtgcgttgtgaacacttgtgcc	185	55
NOTCH2_as	cactgcatactgttatccaccaatg		
OPG_s	no sequence available (Proprietary primers from Qiagen: QT00014294 TNFRSF11B_1_SG)		60
OPG_as			
PRICKLE1_s	cagaggatatcatgaaggacggc	102	56
PRICKLE1_as	gtccacaccaaatgttcccccac		
TGM2_s	caacccattctcatcgagttcccg	100	58
TGM2_as	tcatccacgactccacccag		
TNFRSF1A_s	ctccttcaccgcttcagaaaacc	153	55
TNFRSF1A_as	ttcactccaataatgcccgtactg		
TRAF5_s	tgc当地ctgttagataaagaggtcatca	177	56
TRAF5_as	aacactgcacaggttcaaataagc		

A.3 Materials & Methods

Isolation and Culturing of Primary Human Bone Marrow-Derived Mesenchymal Stromal Cells

Primary human Mesenchymal Stromal Cells (MSCs) were obtained from the femoral head of patients (Appendix A: Tab. 1) undergoing elective hip arthroplasty. Material was collected with written informed consent of all patients and the procedure was approved by the local Ethics Committee of the University of Würzburg (186/18). In brief, bone marrow was washed with MSC-medium (Dulbecco's modified Eagle's medium (DMEM/F12, Thermo Fisher Scientific, Darmstadt, Germany) supplemented with 10 % Fetal Calf Serum (FCS, Bio&Sell GmbH, Feucht, Germany, Fernandez-Rebollo et al. (2017)), 100 U/ml penicillin, 0.1 mg/ml streptomycin (Thermo Fisher Scientific), 50 µg/ml ascorbate and 100 nmol/l sodium selenite (both Sigma-Aldrich GmbH, Munich, Germany)) and centrifuged at 250 g for 5 min. The pellet was washed four times with MSC-medium and resulting supernatants containing released cells were collected. Cells were pelleted and cultured at a density of 1×10^9 cells per 175 cm² culture flask. After two days non-attached cells were washed away and adherent ones were cultivated in MSC-medium until confluence. Then, they were either frozen in liquid nitrogen or directly utilized for experiments. hMSC cultures were sustained for a maximum of two passages. All cells were cultured at 37 °C and at 5 % CO₂.

Culturing of Myeloma Cell Lines

The plasmacytoma cell line INA-6 [*RRID:CVCL_5209*; DSMZ, Braunschweig, Germany, authenticated by DSMZ in 2014 (Burger, Guenther, et al., 2001; Gramatzki et al., 1994)] was cultivated in RPMI1640 medium (Thermo Fisher Scientific) supplemented with 20 % (v/v) FCS, 100 µg/ml gentamicin, 2 mmol/l L-glutamine (both Thermo Fisher Scientific), 1 mmol/l sodium pyruvate, 100 nmol/l sodium selenite (both Sigma Aldrich GmbH) and 2 ng/ml recombinant human interleukin-6 (IL-6; Miltenyi Biotec, Bergisch Gladbach, Germany). INA-6 were passaged three times per week by diluting them to 1×10^5 cells/ml, 2×10^5 cells/ml, or 4×10^5 cells/ml for 3, 2, and 1 days of culturing, respectively. MM.1S [*RRID:CVCL_8792*] (Greenstein et al., 2003), and U266 cells [*CVCL_0566*] (Nilsson et al., 1970) were propagated and cultivated in RPMI1640 medium comprising 10 % (v/v) FCS, 100 U/ml penicillin, 100 µg/ml streptomycin, 2 mmol/l L-glutamine, and 1 mmol/l sodium pyruvate. All cells were cultured at 37 °C and at 5 % CO₂.

Co-Culturing of Primary hMSCs and INA-6 and MSC-Conditioning of Medium

For each co-culture, hMSCs were seeded out 24 h prior to INA-6 addition to generate MSC-conditioned medium (CM). CM from different donors was collected separately and used immediately when adding INA-6. To ensure that CM was free of hMSCs, it was strained (40 µm) and centrifuged for 15 min at 250 g. INA-6 cells were washed with PBS (5 min, 1200 rpm), resuspended in MSC-medium and added

to hMSCs such that co-culture comprised 33% (v/v) of CM gathered directly from the respective hMSC-donor. Co-cultures did not contain IL-6 (Chatterjee et al., 2002).

Collagen I Coating

Collagen I solution (isolated from rat tail, Corning, NY, USA) was diluted 1:2 (75 ng/mL) in acetic acid (0.02 N), applied to 96-well plates (30 µL in each well) and incubated for 2 h at room temperature. Acetic acid was removed and wells were washed once with 100 µL of PBS. Coated plates were stored dry at 4 °C.

Fluorescent Staining of Cells

For each live staining, cells were strained (70 µm) to remove clumps and washed (5 min, 250 g) once with the respective media (without FCS) and then resuspended in staining reagents. For *Cell-Tracker™Green CMFDA Dye* and *CellTracker™Deep Red Dye* (Thermo Fisher Scientific) staining, 1 mL staining solution for a maximum of 1×10^6 cells was prepared. Staining was done at room temperature (RT) for 15 min using 5 µM CMFDA (5-Chlormethyl-fluoresceindiacetat) and 5 min of 1–2 µM DeepRed. To reduce background, stained cells were pelleted, resuspended in cell medium (containing FCS), incubated for 30 min (37 °C, 5% CO₂), washed in cell medium, resuspended in 100–1000 µL and counted.

For PKH26 staining (Sigma Aldrich GmbH), a maximum of 1×10^4 cells was resuspended in 500 µL diluent C before swiftly adding 500 µL of staining solution (1 µL diluted in 500 µL diluent C) and incubating cells for 5 min at RT. The staining reaction was stopped by adding 1 mL of FCS-containing medium and adding 3 mL of FCS-free medium. Cells were washed with 10 mL of FCS-containing medium, resuspended in 100–1000 µL cell medium, and counted.

For Calcein-AM (Calcein-O,O -diacetat-tetrakis-(acetoxymethyl)-ester) (Thermo Fisher Scientific) staining, end concentrations of 0.5 µM were used. 12.5 µL of diluted stock solution (2.5 µM) was carefully added to 50 µL of the co-culture and incubated for 10 min at 37 °C.

For Hoechst 33342 staining, cells were washed once with PBS, resuspended in a maximum of 500 µL of PBS, and fixed with 5 mL of ice-cold ethanol (70% v/v) by vigorously pipetting up and down to dissociate aggregates. Cells were washed once with PBS and stained with 2.5 µg/mL Hoechst 33342 (Thermo Fisher Scientific) diluted in PBS for 1 hour at 37 °C.

Automated Fluorescence Microscopy

To remove clumps for microscopic applications, we cultured cells in 40 µm strained medium containing FCS. To reduce background fluorescence and phototoxicity, we used phenol-red free versions of the

respective medium, if available.

All microscopy equipment was acquired from ZEISS. The microscope was an *Axio Observer 7* with confocal *ApoTome.2* equipped with a motorized reflector revolver and motorized scanning table (130×100 mm). The microscope was mounted on an Antivibrations-Set (Axio Observer (D)) with two antivibration carrier plates, each equipped with two vibration dampening feet. The light source was a *microLED 2* for transmission light and (for fluorescence) *Colibri 7* (R[G/Y]B-UV) for five channels of incident light (385 nm, 475 nm, 555 nm, 590 nm and 630 nm). For excitation (EX) and emission (EM) light filtering and beam splitting (BS) we used the following reflectors: *96 HE BFP shift free* (E) (EX: 390 / 40 nm, BS: 420 nm, EM: 450 / 40 nm), *43 HE Cy 3 shift free* (E) (EX: 550 / 25 nm, BS: 570 nm, EM: 605 / 70 nm), *38 HE eGFP shift free* (E) (EX: 470 / 40 nm, BS: 495 nm, EM: 525 / 50 nm) and *90 HE LED* (E) (EX: 385 + 475 + 555 + 630 nm, BS: 405 + 493 + 575 + 653 nm, EM: 425/30 + 514/30 + 592/30 + 709/100 nm). We used the black and white camera *Axiocam 506 mono* (D) and if not stated otherwise, 2×2 binning was used for fluorescence imaging. For mosaic acquisitions (“tiles”) we used a tiling overlap of 8–10 % and image tiles were not stitched. Images were magnified 5x and 10x (*Fluar 5x/0.25 M27* and *EC Plan-Neofluar 10x/0.3 Ph1 M27*).

Cell Viability and Apoptosis Assay

To examine cell viability and apoptosis, cells were seeded in a 96-well plate (1×10^4 cells per well) to be measured inside culture wells after respective incubation time immediately. ATP-amount and Caspase 3/7 activity were used as a proxy for viability and apoptosis rates, respectively. They were assessed using the *CellTiter-Glo Luminescent Cell Viability Assay* and the *Caspase-Glo 3/7 Assay*, respectively (Promega GmbH, Mannheim, Germany), according to the manufacturer’s instructions. Luminescence was measured with an Orion II Luminometer (Berthold Detection Systems, Pforzheim, Germany).

Microscopic Characterization of hMSC Saturation

For saturating hMSC with INA-6, hMSCs were stained with *CellTracker Green*, plated out on 384-well plates (Greiner Bio-One GmbH, Frickenhausen, Germany) at 5×10^3 hMSC/cm² and cultured for 24 h. INA-6 cells were stained with *CellTracker DeepRed*, resuspended in MSC-medium, added to adhering hMSCs in different amounts (5×10^3 INA6/cm², 1×10^3 INA6/cm², 2×10^3 INA6/cm²) and co-cultured for 24 h and 48 h. The complete co-culture was scanned and the number of INA-6 cells adhering to one hMSC was counted manually for 100 MSCs for each technical replicate. Fluorescent images were digitally re-stained (INA-6 green, hMSC inverse black).

Analysis of INA-6 Survival and Aggregation Depending on hMSC Confluence

To describe aggregate growth and survival of INA-6 depending on hMSC density, unstained hMSCs were seeded out into 96-well plates (white, clear bottom, Greiner) at different densities (see Seeding Table). To ensure nutrient supply, we used lower cell densities for longer co-culturing durations while maintaining constant ratios of INA-6 to adhesion surface provided by hMSCs. Those plates that were to be assessed after 72 h of co-culturing received an additional 100 μL of fresh MSC-medium after 24 h of co-culturing (total volume of 300 μL), and after 48 h of co-culturing, 100 μL was gently removed from the co-culture and carefully replaced with fresh MSC-medium without disturbing the co-culture on the bottom.

To describe aggregate growth, complete wells were scanned using 10x magnification, phase contrast, 2×2 binning, and autofocus focusing on each tile both before and after harvesting. Afterwards, INA-6 cells were harvested for measuring viability and apoptosis.

Seeding Table: Seeding densities for describing growth and survival of INA-6 depending on hMSC density. Co-cult. dur.: Co culturing duration; MSC-adh. surface: adhesion surface provided by hMSCs; vol.: volume.

Co-cult. dur. [h]	hMSC density [1000 hMSC/cm ²]	INA-6 density [1000 INA6/cm ²]	Ratios INA : MSC (adh. surface)	Seeding vol. [μL]	End vol. [μL]
24	2, 10, 40	10	1:0.2, 1:1, 1:confluent	200	200
48	1, 5, 40	5	1:0.2, 1:1, 1:confluent	200	200
72	1, 5, 40	5	1:0.2, 1:1, 1:confluent	200	300 [after 24 h: +100], [after 48 h: exchange 100]

For luminescent assessment of cell survival, INA-6 cells were harvested by removing co-culture medium, adding 150 μL of MSC-medium, and then stirred by strongly pipetting up and down twice while aiming the pipette tip at the upper corner, lower left, and lower right of the well bottom ('Mercedes star'). Washing and stirring was repeated once before washing wells again with 150 μL MSC-medium. Harvested INA-6 cells were strained (40 μm filter), pelleted, and resuspended in 200 μL MSC-medium. Cells were counted using Neubauer chambers, re-distributed into 96-well plates (white, clear bottom) with 1×10^5 INA-6 cells per well, and then subjected to viability and apoptosis assays.

To minimize the loss of sensitive apoptotic cells, another approach was used to measure viability and apoptosis without harvesting INA-6 cells. hMSCs and INA-6 were seeded out individually in parallel to the co-cultures. Prior to measuring viability and apoptosis, culture volume was adjusted to 150 μL by removing 50 μL or 150 μL for the timepoints 48 h or 72 h, respectively (carefully not to stir up culture on bottom). 100 μL of luminescent reagents were then added directly to 150 μL of co-culture. The fold change of viability or apoptosis that is due to MSC interaction ($FC_{\text{MSC interaction}}$) was then calculated using the following formula, with L being the mean of four technical replicates measured in relative luminescent units per seconds [RLU/s], and $L_{\text{Co Culture}}$, L_{MSC} , L_{INA6} the luminescence

measured in the co-culture, hMSCs alone, and INA-6 alone, respectively.

$$FC_{\text{MSC Interaction}} = \frac{L_{\text{Co Culture}}}{L_{\text{MSC}} + L_{\text{INA-6}}}$$

Time-Lapse Characterization of INA-6 Aggregation, Detachment and Division

In order to record the aggregation and detachment of INA-6 in contact with hMSCs, hMSCs (5×10^3 cells/cm 2) were fluorescently stained with PKH26 and plated onto 8-well μ -Slides (ibidi, Gräfelfing, Germany). hMSCs were incubated for 24 h before being placed into an ibidi Stage Top Incubation System and were equilibrated to the incubation system for a minimum of 3 h (80 % humidity and 5 % CO₂). INA-6 cells (2×10^4 cells/cm 2) were washed and resuspended in 33 % (v/v) MSC-conditioned medium before adding them directly before acquisition start in a small volume (10 μ L). Brightfield and fluorescence images of 13 mm 2 of co-culture were acquired every 15 minutes for 63 h. Movement speed of the motorized table was adjusted to the lowest setting that allows acquisition of the complete region within 15 minutes.

Respective events of interest were analyzed manually and categorized into defined event parameters. Events were binned across the time axis using these boundaries: [0.0, 12.85, 25.7, 38.55, 51.4, 64.25]. We collected a minimum of events per recording and analysis so that each time bin contained at least 5 values, except when analyzing detachment events, since these did not appear before 20 h of incubation for some replicates. For each recording and event parameter, the event count was normalized by dividing by the total number of events per time bin.

We determined the frequency and the cause of aggregation by looking for two interacting INA-6 cells and went backward in time to see if they were two daughter cells or if two independent INA-6 cells had collided. We determined the frequency of aggregates with detaching cells by tracing their growth across the complete time-lapse and looking for detachment events. We picked random 100 aggregates by including aggregates from both the border and center of the well.

We characterized detachment events by noting multiple parameters manually: Time point of detachment, aggregate size (at the time of detachment), the last interaction partner, and the number of detaching INA-6 cells.

For characterizing cell division events, we recorded a new set of time-lapse videos using unstained hMSCs that were grown to confluence for 24 h (4×10^4 hMSCs/cm 2) to provide for unlimited adhesion surface. We categorized daughter cells in terms of their mobility (mobility being the speed of putative movements or “rolling”). The mobility criteria were met if one INA-6 daughter cell moved farther than half a cell radius within one frame (15 min) relative to the MSC-adherent INA-6 cell which was required to stand still in-between respective frames. We measured the “rolling” duration by subtracting the time point of the last perceived movement from the time point of division. We

excluded those division events from the measurement of rolling duration if INA-6 cells underwent apoptosis shortly after division.

Cell Cycle Synchronization at M-Phase

INA-6 cells were arrested at mitosis by double thymidine (2 mM) treatments followed by 5 h of nocodazole (500 ng/mL) incubation. In detail: 3×10^5 cells/mL INA-6 in 4 mL were treated with 2 mM thymidine (Sigma Aldrich GmbH) for 16.5 h. Cells were released by washing them in INA-6 medium once and allowed to cycle for 9 h before treating them with 2 mM thymidine for 18 h a second time. Afterwards, cells were released and allowed to cycle for 2 h before treating them with 100 ng/mL nocodazole (Sigma Aldrich GmbH) for 5 h. Arrested INA-6 were released by washing them once and resuspending them in MSC-medium with 33 % MSC-conditioned medium. Cell cycle profile was checked using image cytometry (Appendix A: Fig. 2).

V-Well Adhesion Assay

This assay was modified from (Weetall et al., 2001). 96 v-well plates were coated with collagen I (rat tail, Corning). Collagen coating ensures that confluent hMSCs withstand centrifugation even after hMSCs in the well tip were removed. hMSCs (4×10^4 cells/cm²) were seeded out and grown to confluence for 24 h in collagen-coated v-well plates. To ensure that only INA-6 are pelleted in the v-well tip, hMSCs were removed from the well-tip by touching the well-ground with a 10 μ L pipette and roughly pipetting hMSCs away.

Arrested INA-6 (1×10^4 cells/cm²) were released by washing them once in PBS and resuspending them in 33 % (v/v) MSC-conditioned medium before adding them on top of confluent hMSCs. INA-6 adhered for 1, 2, 3, and 24 h before the complete co-culture was stained with 0.5 μ M Calcein-AM (10 min at 37 °C). Non-adherent INA-6 were pelleted by centrifugation using a Hettich 1460 rotor ($r = 124$ mm) at 2000 rpm (555 g) for 10 min.

The well tip was imaged by fluorescence microscopy with 5x magnification, 96 HE emission filter, autofocus configured for maximum signal intensity, 2 \times 2 binning and 14 bit grayscale depth. Pellet brightness was analyzed in ZEN 2.6 (Zeiss) by summing up pixel brightnesses across the complete pellet image. Background brightness was acquired from a cell culture with only hMSCs. Reference brightness was acquired from a cell culture with only INA-6, defining 100 % pellet brightness without adhesion. Background intensity was subtracted before normalizing by reference. Outliers were removed from technical replicates ($n = 4$) if their z-score was larger than 1.5 σ technical variation.

After measuring pellet brightnesses, the cell pellet was removed by pipetting 10 μ L from the well tip. Pellets of the same technical replicates were pooled, washed in PBS, resuspended in 200 μ L PBS, added to 1.8 mL ice-cold 70 % ethanol, and stored at -20 °C. Remaining non-MSC-adhering INA-6

cells were removed by replacing culture medium with 100 μ L of medium. MSC-adherent INA-6 were manually detached by rapid pipetting and equally pelleted, analyzed, and isolated.

Cell Cycle Profiling

INA-6 cells were fixed in 70 % ice-cold ethanol, washed, resuspended in PBS, distributed in 96-well plates, and stained with Hoechst 33342 (2.5 μ g/mL in PBS) for 1 h at 37 °C. For image cytometric cell cycle profiling, plates were scanned completely using automated fluorescence microscopy with 5x magnification, 96 HE emission filter, 1 \times 1 binning, 14 bit depth, and an illumination time that fills 70 % of the grayscale range. The autofocus was configured to re-adjust every second tile. A pre-trained convolutional neural network (“DeepFeatures 2 reduced”, *Intellesis*, Zeiss) was fine-tuned to segment scans into background, single nuclei, and fragmented nuclei. Nuclei were filtered to exclude fragmented nuclei and those nuclei with extreme size (within the range of 50–500 μm^2) and roundness (within the range of 0.4–1.0). Cell cycle profiles were normalized by the mode of the nucleus intensities within the G0/G1 peak. To retrieve frequencies of cells cycling in G0/G1, S, and G2 phase, the brightness distribution of all single nuclei was fitted to the sum of three Gaussian curves (“Skewed Gaussian Model” for G0G1 and G2 phase, and “Rectangle Model” for S phase) using the python package LMFIT (Newville et al., 2014) (Appendix A: Fig. 4). The Gaussian curves were used to calculate the cell frequencies for each cell cycle phase by integration using the composite trapezoidal rule implemented by numpy.trapz (Harris et al., 2020).

For validation of image cytometry, 5 mL of INA-6 stock culture was removed and ethanol fixed as described above. Flow cytometry analyses were performed using an *Attune Nxt Flow Cytometer* (Thermo Fisher Scientific). Data analyses were performed using FlowJo V10 software (TreeStar, USA).

Protocol: Well Plate Sandwich Centrifugation (WPSC)

96-well plates (flat bottom, clear) were coated with collagen I (rat tail, Corning) to ensure that confluent hMSCs withstand centrifugation and repeated washing. hMSCs (2×10^4 cells/cm 2) were seeded out and grown to confluence for 72 hours in collagen-coated 96-well plates. To remove aggregates from the medium and prevent clogging of magnetic columns, any FCS-containing fluid was strained with a 40 μm cell strainer.

- **Collect MSC-Conditioned Medium and Add INA-6:**

1. Collect hMSC-conditioned medium (CM) from the well plates and replace it with 100 μ L of fresh hMSC medium. Collect CM from different donors separately.
2. Strain CM (40 μm) and centrifuge for 15 minutes at 250 g to ensure that CM does not contain hMSCs.

3. Dilute CM by mixing 2 parts of CM with 1 part of MSC-medium (dilute 1.5 fold).
4. Count INA-6 cells and retrieve enough cells to fill all 96 wells with 2×10^4 INA6/cm² (6.8×10^4 cells per well, covering approximately 65 % of the well bottom).
5. Centrifuge INA-6 (5 minutes, 250 g) and resuspend them in a volume of diluted CM to reach a concentration of 6.8×10^5 INA6/mL.
6. Add 100 µL INA-6 suspension to hMSCs (end volume: 200 µL; end concentration: 33 % (v/v) hMSC-conditioned medium).
7. Incubate for 24 hours at 37 °C and 5 % CO₂.

- **Prepare CM-INA6 Reference:**

8. Add 100 µL of fresh MSC-medium into each well of an empty 96-well plate (not coated).
9. Add 100 µL of INA-6 suspension (6.8×10^5 INA-6/mL in diluted CM).
10. Incubate for 24 hours at 37 °C and 5 % CO₂.

- **Collect CM-INA6 and nMA-INA6:**

11. Pre-warm well plate centrifuge to 37 °C.
12. Prepare a counter-weight by filling 200 µL of water into all wells of an empty 96-well plate.
13. Prepare well-plate sandwiches:
 - a. Turn an empty 96-well plate (“catching plate”) upside down and place one on top of the co-culture-plate, the CM-INA6 reference plate, and the counter-weight so that all well openings align.
 - b. Fix well plates using tape with reusable adhesive (e.g., *Leukofix*).
14. Turn both plates around. Medium will spill from the co-culture plate into the catching plate.
15. Centrifuge plate for 40 seconds at 1000 rpm with the catching plate facing the ground.
16. Remove the adhesive tape and the co-culture plate.
17. Turn the co-culture plate around and add 30 µL of washing medium (MSC-medium 0% FCS, 3 mM EDTA) gently by touching the wall of each well and pressing the pipette slowly.
 - a. Work quickly to ensure that co-culture does not dry. We recommend using a multipette (Eppendorf).
 - b. Many nMA-INA6 are removed by physical force applied by adding 30 µL of medium and not just by centrifugation. Hence, it is critical to apply the same dispensing technique across all replicates. We recommend using a multipette (Eppendorf) that can apply 30 µL with controllable pressure, since its push-button retains a long pushing path even for dispensing small volumes, unlike push-buttons from the usual 100 µL pipettes that reduce the pushing-path for smaller volumes.
 - c. Centrifugation minimizes technical variability by replacing one step of manual pipetting. Also, it ensures that confluent MSCs remain unharmed. Manual pipetting on the other hand would require touching the well-bottom to remove all fluids which damages the adhesive hMSC layer.
18. Turn the co-culture plate upside down, place it onto the catching plate and re-apply

- adhesive tape to fix the well plate sandwich.
19. Repeat steps 14-18 two more times until the catching plate contains 290 µL of medium in each well.
 20. Pool CM-INA6 from the catching plate that was fixed to the reference plate.
 21. Pool nMA-INA6 from the catching plate that was fixed to the co-culture plate.
 22. Collect remaining INA-6 by adding 100 µL of PBS into each well of the catching plates, collect and pool with CM-INA6 or nMA-INA6.
 23. Strain CM-INA6 and nMA-INA6 using 40 µm cell strainer.
 24. Isolate MA-INA6 by continuing with either accutase dissociation or rough pipetting.
- **Collect MA-INA6 by Accutase Dissociation Followed by MAC Sorting:**
 25. Block 2 mL tubes with sorting buffer (PBS, 2 mM EDTA, 1% BSA) for 1 hour at 4 °C.
 26. Dilute accutase (Sigma Aldrich GmbH) (400 to 600 units/mL) 4-fold in cold PBS. Always keep accutase on ice, since accutase loses activity at room temperature.
 27. Add 50 µL of cold accutase (directly after the last centrifugation step) and incubate co-culture plate for 5 minutes at 37 °C.
 28. Place a co-culture plate onto a shaker and shake for 1 minute at 300 rpm.
 29. Collect cell suspension from wells and stop the reaction by adding 500 µL of FCS to pooled cell suspension.
 30. Evaluate presence of adherent INA-6 cells and the integrity of confluent hMSCs under the microscope.
 31. Repeat steps 27-30 until all INA-6 cells have dissociated or until confluent hMSCs start to tear.
 32. Strain cell suspension (30 µm). This yields MA-INA6.
 33. Pellet MA-INA6, nMA-INA6, and CM-INA6 (1200 rpm, 10 minutes).
 34. Resuspend MA-INA6 in 86 µL sorting buffer (PBS, 2 mM EDTA, 1 percent BSA).
 35. Resuspend CM-INA6 and nMA-INA6 in 300 µL cold diluted accutase and incubate for 3 minutes at 37 °C to ensure equal treatment for all samples.
 36. Stop accutase by adding 200 µL of FCS (100 percent).
 37. Pellet CM-INA6 and nMA-INA6 (1200 rpm, 10 minutes) and resuspend in 86 µL sorting buffer (PBS, 2 mM EDTA, 1 percent BSA).
 38. Transfer samples into 2 mL tubes that were blocked with sorting buffer.
 39. Add 10 µL of CD45 coated magnetic beads (Miltenyi Biotec B.V. & Co. KG, Bergisch Gladbach).
 40. Place tubes into rotator and incubate for 15 minutes at 4 °C.
 41. Continue with MAC sorting according to the manual. Use an MS column and wash 3 times.
 42. Improve purity of eluted MA-INA6 by straining eluate (30 µm) (wash strainer using 1 mL of sorting buffer) and applying it onto an MS column a second time. Wash three times.
 43. Collect 20 µL per eluate and apply it onto a 96 well plate to evaluate purity.
 - a. Incubate plate for 24 hours.

- b. Count the number of adherent cells (hMSCs) per INA-6 using phase contrast microscopy.
 - c. We reached a mean purity of 3.2×10^{-4} ($\pm 2.2 \times 10^{-4}$) hMSCs per MA-INA6.
 - d. hMSC contamination did not have an impact on RNAseq, since those genes that are highly expressed in hMSCs (VCAM1, ALPL, FGF5, FGFR2), did not appear as differentially expressed in MA-INA6 (data not shown). RNAseq detected 0.44 ± 0.16 CPM-normalized counts of VCAM1 transcripts in MA-INA6, however, it was excluded like all genes with less than 1 count in at least 2 of 5 replicates.
44. Count cells using a Neubauer chamber.
45. Pellet samples (250 g for 5 minutes).
46. Resuspend in respective medium or lysis buffer (e.g., RA1 for RNA extraction).
- **Collect MA-INA6 by Rough Pipetting (No MAC Sorting):**
47. After the last centrifugation step, add hMSC-medium to each well of the co-culture plate to reach a volume of 150 μ L.
- a. Since the yield of MA-INA6 was large, we dissociated MA-INA6 cells from hMSCs by vigorous pipetting (for further samples after RNAseq, see Supplementary Table 1). Since no enzymatic digestion is used, we reckoned that there would be no need for MAC sorting. Confluent hMSCs withstand this procedure and don't dissociate as single cells, which can be removed by straining cells (30 μ m). We reached similar purities as for MAC-sorting (data not shown).
48. Using a multi-channel pipette (100 μ L), gently raise 90 μ L into the tips.
49. Lean pipette tip on the upper well-border and roughly pipette up and down once.
50. Repeat step 48 at the lower right and lower left well border (Total of 3 pipetting steps “Mercedes Star”).
51. Attach a catching plate onto the co-culture and centrifuge for 40 seconds at 500 rpm (28 g).
52. Repeat steps 46-50 until a sufficient amount of MA-INA6 is removed.
53. Control purity of MA-INA6 by placing out aliquot onto an empty 96 well plate.
54. Collect MA-INA6 from catching plate.
55. Remove hMSCs by straining cell suspension (30 μ m).
56. Count cells using a Neubauer chamber.
57. Pellet MA-INA6 (250 g for 5 minutes).
58. Resuspend in respective medium or lysis buffer.

Centrifugal Force: We used a Hettich 1460 rotor ($r = 124$ mm) (Hettich GmbH & Co. KG, Tuttlingen, Germany). For calculating the centrifugal force that acts onto the co-culture within well plate sandwiches, we subtracted the height of the catching plate (14.4 mm, Greiner 96-well plate) and the depth of each well (10.9 mm). This yields a radius of 98.7 mm, which translates to the following centrifugal forces: 500 rpm: 28 g; 1000 rpm: 110 g; 2000 rpm: 441 g.

Washing medium containing EDTA: Washing medium containing EDTA: EDTA removes

calcium from integrins, which are required for adhesion. It is not strong enough to dissociate INA-6 from hMSCs, but could help with removing INA-6 from other INA-6. For generating samples for RNAseq, we added 3 mM of EDTA to the washing medium. For further samples, we did not add EDTA to the washing medium, since we found that it does not increase yield for all biological replicates consistently (data not shown). We suspect that integrin-mediated adhesion depends on hMSC donor or internal variance of INA-6. We recommend using 3 mM of EDTA, however, this requires further optimizations like including an incubation time at 37 °C after the addition of washing medium to account for biological variance. However, this could take long incubation times of up to 60 minutes (Lai et al., 2022).

Track Cell Number During WPSC

To track the cell count during WPSC, INA-6 cells were stained with *CellTracker green*, and both co-culturing and catching plates were scanned after each centrifugation step. For each round of centrifugation, an empty catching plate was used. A pre-trained convolutional neural network (*Intellesis*, Zeiss) was fine-tuned to segment the scans into background, cells, and cell borders. Single cells were counted, and the cumulative sum for each catching plate was calculated.

Sub-Culturing After WPSC of MSC-Interacting INA-6 Subpopulations

After CM-INA6, nMA-INA6, and MA-INA6 were isolated, they were counted with a Neubauer chamber using all nine quadrants and diluted to 1×10^5 cells/mL in MSC-medium (10% FCS, no IL-6 except for control). 100 µL of cell suspension was applied to 96-well plates, incubated for 48 hours at 37 °C and 5 % CO₂, and then subjected to viability and apoptosis assays.

RNA Isolation

Total RNA was isolated from INA-6 cells using the *NucleoSpin RNA II Purification Kit* (Macherey-Nagel, Düren, Germany) according to the manufacturer's instructions.

RNAseq, Differential Expression and Functional Enrichment Analysis of INA-6 cells

FASTQ files were merged to the respective sample. The quality of FASTQ files was assessed with FastQC (Andrews, 2010) and a joint report was created with MultiQC (Ewels et al., 2016). FASTQ files were aligned with STAR (Dobin et al., 2013) to the GRCh38 reference genome build (Zerbino et al., 2018). Quality and alignment statistics of final BAM files were assessed with samtools stats (Li et al., 2009), and a joint report with FastQC reports by MultiQC was generated.

Raw read counts were generated with HTSeq (Anders et al., 2015) using the union method. HTSeq runs internally in STAR. Differential gene expression analysis was performed with edgeR (Robinson et al., 2010) in R 3.6.3 (R Core Team, 2018), according to the edgeR manual.

Counts were merged and genes with zero counts in all samples were removed (number of genes: 36380). The whole count table was annotated with R Bioconductor (Gentleman, n.d.) human annotation data package org.Hs.eg.db (Carlson, 2016). A DGEList Element was created with the raw counts, gene information, i.e., Ensembl GeneIDs, HUGO Symbol, Genename, and ENTREZ GeneIDs and a sample grouping metadata table.

```
1 y <- DGEList(counts=ct2[,-1:4], group=meta.data$group, genes=ct2[,1:4])
```

Counts were filtered to keep only those genes which have at least 1 read per million in at least 2 samples (number of genes: 14136). Afterwards, normalization factors were recalculated.

```
1 keep <- rowSums(cpm(y)>1) >=2
2 y <- y[keep, , keep.lib.size=FALSE]
3 y1 <- calcNormFactors(y)
```

A design matrix was created with the grouping factor by treatment condition (group=F1, F2, F3, which are abbreviations for CM-INA6, nMA-INA6, MA-INA6, respectively)

```
1 design = model.matrix(~0+group)
```

Dispersion was estimated, the resulting coefficient of biological variation (BCV) is 0.135, i.e., BCV expression values vary up and down by 13.5% between samples.

```
1 y1.1 <- estimateDisp(y1, design)
2 BCV <- sqrt(model.F$y1.1$common.dispersion)
```

A generalized linear model (glmQLFit function) was fitted.

```
1 fit <- glmQLFit(y1.1, design)
```

and pairwise comparisons were made, e.g.

```
1 F1vsF2 <- glmQLFTest(fit, contrast=makeContrasts(groupF1 - groupF2, levels=design))
2 DE.F1vsF2 <- topTags(F1vsF2, n=nrow(F1vsF2), p.value=0.05)
```

Afterwards, gene list of differentially expressed genes were used for functional enrichment analysis with Metascape (Y. Zhou et al., 2019).

RT-qPCR

For cDNA synthesis, 1 µg of total RNA was reverse transcribed with Oligo(dT)15 primers and Random Primers (both Promega GmbH) and *Superscript IV* reverse transcriptase (Thermo Fisher Scientific) according to the manufacturer's instructions. For quantitative PCR, the cDNA was diluted 1:10, and

qPCR was performed in 20 µL using 2 µL of cDNA, 10 µL of *GoTaq qPCR Master Mix* (Promega GmbH), and 5 pmol of sequence-specific primers obtained from biomers.net GmbH (Ulm, Germany) or Qiagen GmbH (Hilden, Germany) (see Supplementary Table 3 for primer sequences and PCR conditions). qPCR conditions were as follows: 95 °C for 3 minutes; 40 cycles: 95 °C for 10 seconds; respective annealing temperature for 10 seconds; 72 °C for 10 seconds; followed by melting curve analysis for the specificity of qPCR products using an *TOptical Gradient 96 PCR Thermal Cycler* (Analytik Jena AG, Jena, Germany). Samples that showed unspecific byproducts were discarded. Ct values were measured in three technical replicates (triplicates). Non-detects were discarded. One of three technical replicates was treated as an outlier and excluded if its z-score crossed 1.5 σ technical variation. We normalized expression by the housekeeping gene *36B4*. Efficiencies were determined in each reaction by linear regression of log-transformed amplification curves (Ramakers et al., 2003). Differential expression was calculated based on a modified $\Delta\Delta Ct$ formula that separated exponents to apply individual efficiencies to each *Ct* value:

$$\begin{aligned} \text{Fold Change} &= \frac{E_{\text{tar}}^{\Delta Ct_{\text{tar}(co - treated)}}}{E_{\text{ref}}^{\Delta Ct_{\text{ref}(co - treated)}}} \\ &= \frac{E_{\text{tar},\text{co}}^{Ct_{\text{tar},\text{co}}} \div E_{\text{tar},\text{treated}}^{Ct_{\text{tar},\text{treated}}}}{E_{\text{ref},\text{co}}^{Ct_{\text{ref},\text{co}}} \div E_{\text{ref},\text{treated}}^{Ct_{\text{ref},\text{treated}}}} \end{aligned}$$

- $E_{\text{tar},\text{co}}$ = Efficiency of the target gene measured in the control sample
- $Ct_{\text{tar},\text{co}}$ = Ct value of the target gene measured in the control sample
- *tar* = Target Gene
- *ref* = Reference Gene
- *treated* = Treated sample
- *co* = Control Sample

Fold change expression was normalized by the median of CM-INA6 (and not sample-wise, as commonly used in $\Delta\Delta Ct$) since some genes were not expressed without direct hMSC contact (e.g., *MMP2*), and also in order to display variation of CM-INA6 next to nMA-INA6 and MA-INA6.

Statistics

For molecular analyses, each data point represents one biological replicate, defined as the mean of all technical replicates of co-cultures seeded from the same batch of hMSCs and/or INA-6 cells on the same day. For analyses of time-lapse recordings, each data point represents the normalized event count from one co-culture recording. Unique hMSCs were prioritized for each biological replicate or recording (see Appendix A: Tab. 1). Bars and lines represent the mean, and error bars represent the standard deviation of all hMSC donors or recordings (= all biological replicates).

Metric, normally distributed, dependent data were analyzed using factorial RM-ANOVA and paired Student's t-tests. Results of RM-ANOVA are reported as follows

$$[F(df_1, df_2) = F; p = p\text{-value}],$$

where df_1 is the degrees of freedom of the observed effect, df_2 is the degrees of freedom of the error,

and F is the F-statistic (Vallat, 2018). If sphericity was met, p -values were not corrected using the Greenhouse-Geisser method (p -unc).

$$\begin{aligned} df_1 &= k - 1 & (k = \text{number of groups}) \\ df_2 &= (k - 1)(n - 1) & (n = \text{number of samples in each group}) \\ F &= \frac{SS_{\text{Effect}}/df_1}{SS_{\text{Error}}/df_2} & (\text{SS} = \text{Sums of squares for effect or error}) \end{aligned}$$

If data points within dependent sample pairs were missing, such pairs were excluded from paired t-tests while others from the same subject remained.

Metric non-normal distributed, independent data was analyzed using the Kruskal-Wallis H-test and Mann–Whitney U tests. Results of the Kruskal-Wallis H-test are reported as

$$H(df) = H$$

, with df being the degrees of freedom and H being the Kruskal-Wallis H statistic, corrected for ties (Vallat, 2018).

Metric bivariate non-normal distributed data was correlated using Spearman’s rank correlation and reported as:

$$\rho(df) = \rho, p = p\text{-value}$$

, where ρ is Spearman’s rank correlation coefficient. df is calculated as

$$df = n - 2 \quad (n = \text{number of observations})$$

These tests were applied using Python (3.10) packages `pingouin` (0.5.1) and `statsmodels` (0.14.0) (Seabold & Perktold, 2010; Vallat, 2018). Data was plotted using `seaborn` (Waskom, 2021) and `plotastic` (Kuric & Ebert, 2024). Sphericity was ensured by Mauchly’s test. Normality was checked with the Shapiro-Wilk test for $n > 3$.

Data points were log10 transformed to convert the scale from multiplicative (“fold change”) to additive, or to fulfill sphericity requirements. P -values derived from patient survival data were corrected using the Benjamini-Hochberg procedure. For other post-hoc analyses, p -values were not adjusted for family-wise error rate in order to minimize type I errors. To prevent type II errors, the same conclusions were validated by different experimental setups and through varying hMSCs donors across experiments (see Appendix A: Tab. 1).

Significant p -values from pairwise tests were annotated as stars between data groups

$$p\text{-value} = 0.05 > * > 0.01 > ** > 10^{-3} > *** > 10^{-4} > ****.$$

If too many significant pairs were detected, only those pairs of interest were annotated.

No power calculation was performed to determine sample size since samples were limited by availability of primary hMSC donors. Experiments were repeated until a minimum of three biological replicates were gathered.

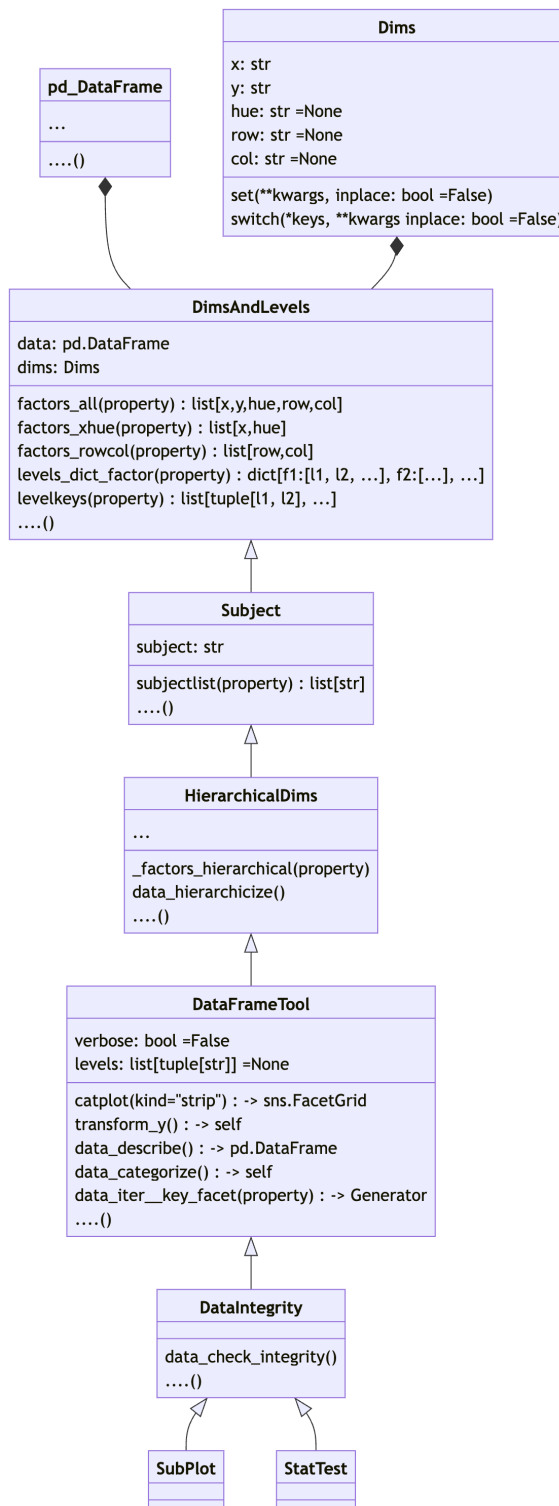
Patient Cohort, Analysis of Survival and Expression

Patient samples ($n = 873$) were collected at the University Hospital Heidelberg and processed as described (Seckinger et al., 2017, 2018), and are available at the European Nucleotide Archive (ENA) via accession numbers PRJEB36223 and PRJEB37100. Consecutive patients with monoclonal gammopathy of unknown significance (MGUS) ($n = 62$), asymptomatic ($n = 259$), symptomatic, therapy-requiring ($n = 764$), and relapsed/refractory myeloma ($n = 90$), as well as healthy donors ($n = 19$) as comparators were included in the study approved by the ethics committee (#229/2003, #S-152/2010) after written informed consent.

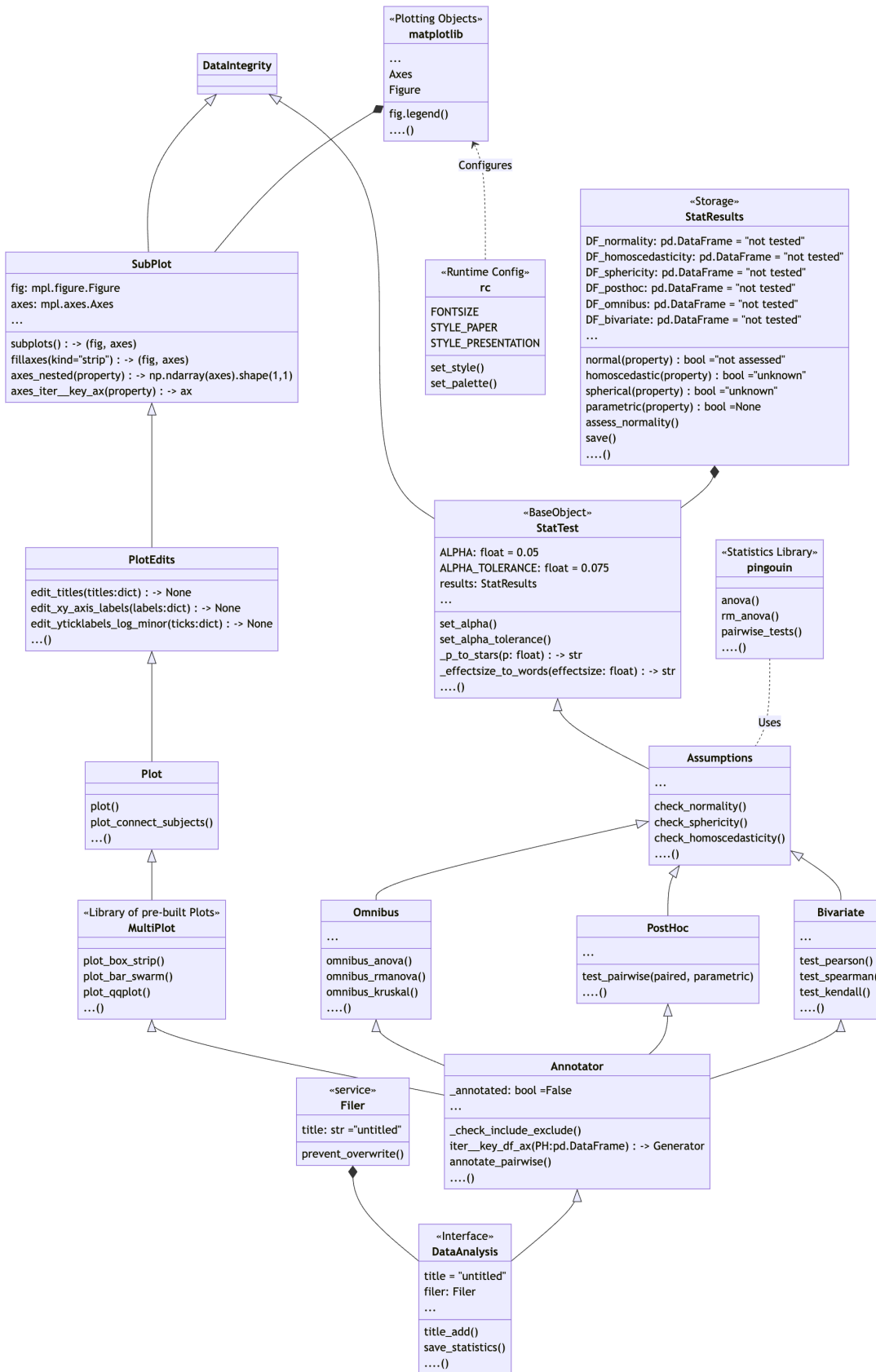
Gene expression was measured by RNA sequencing as previously described (Seckinger et al., 2018). Gene expression is defined as the \log_2 transformed value of normalized counts + 1 (as pseudocount). Progression-free (PFS) and overall survival (OS) were analyzed for the subset of previously untreated symptomatic myeloma patients. For delineating “high” and “low” expression of target adhesion ($n = 101$) and cell cycle ($n = 173$) genes, thresholds per gene were calculated with maximally selected rank statistics by the `maxstat` package in R (Hothorn & Lausen, n.d.). PFS and OS were analyzed for high vs. low expression with the Kaplan-Meier method (Kaplan & Meier, 1958). Significant differences between the curves were analyzed with log-rank tests (Harrington & Fleming, 1982). P -values were corrected for multiple testing by the Benjamini-Hochberg method. Analyses were performed with R version 3.6.3 (R Core Team, 2018).

B Documentation of `plotastic`

B.1 Class Diagram



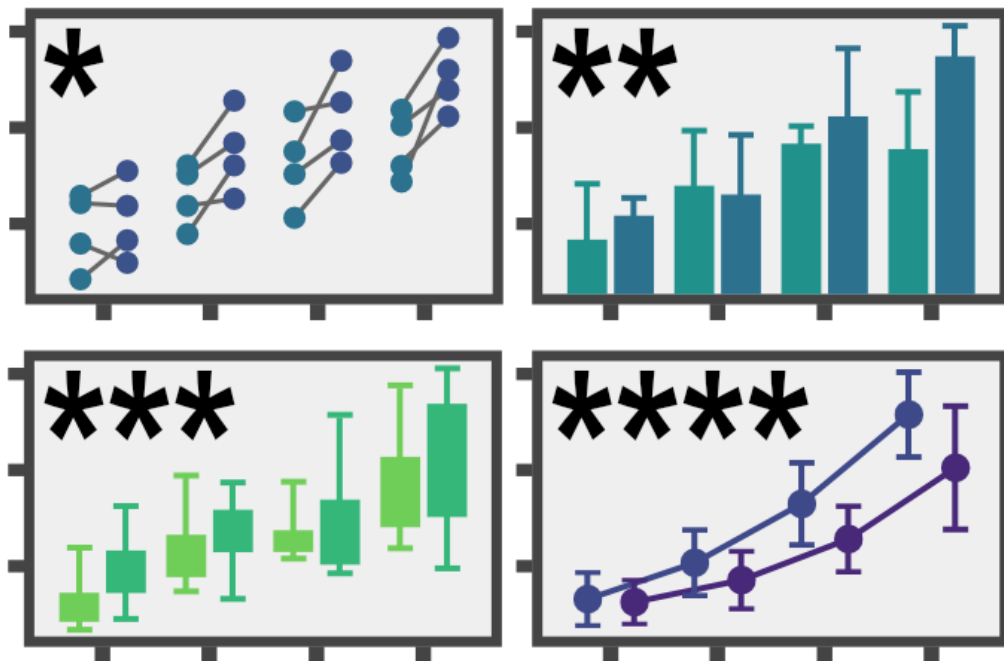
Appendix B Figure 1: Class diagram of plotastic (upper part): The architecture of plotastic begins with classes that are related to handling a pandas.DataFrame object which stores the data, and defining dimensions to group the data (y, x, hue, col, row). This diagram ends with the classes SubPlot and StatTest and is continued on the next page. Arrow shapes follow the UML (unified modeling language): A hollow triangle indicates inheritance (“*is a*”) and a filled diamond indicates composition (“*has a*”).



Appendix B Figure 1: *continued from previous page* The architecture of plotastic continues after the class DataIntegrity with classes for plotting (SubPlot) and statistical testing (StatTest) and ends with the class DataAnalysis, which serves as the main user interface. Arrow shapes follow the UML (unified modeling language): A hollow triangle indicates inheritance (“*is a*”) and a filled diamond indicates composition (“*has a*”).

B.2 Readme

The following pages are the README.md of plotastic found in the Python Package Index (PyPi) (pypi.org/project/plotastic), and on GitHub (github.com/markur4/plotastic).



[code style](#) [black](#) [codecov](#) [79%](#) [JOSS](#) [10.21105/joss.06304](#)

plotastic: Bridging Plotting and Statistics

Installation

Install from PyPi:

```
pip install plotastic
```

Install from GitHub: (experimental, check CHANGELOG.md)

```
pip install git+https://github.com/markur4/plotastic.git
```

Requirements

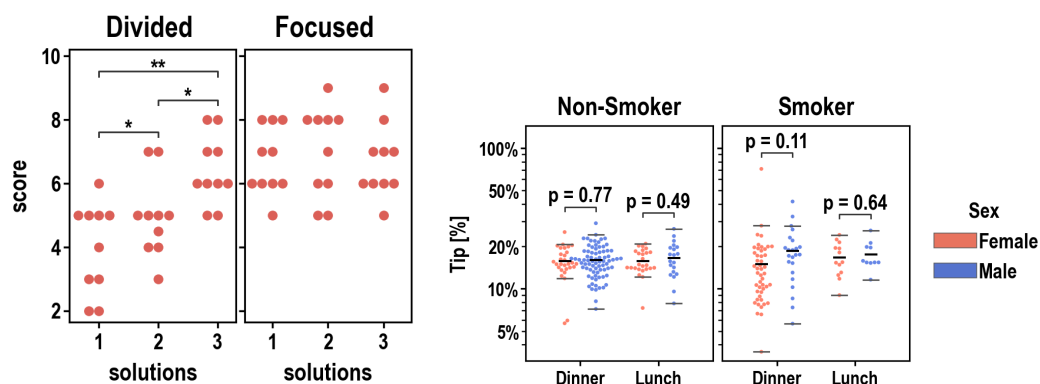
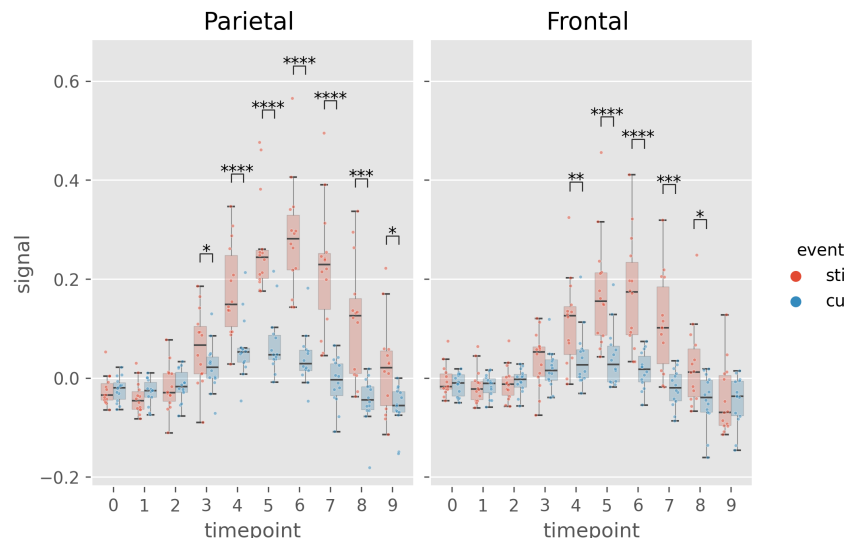
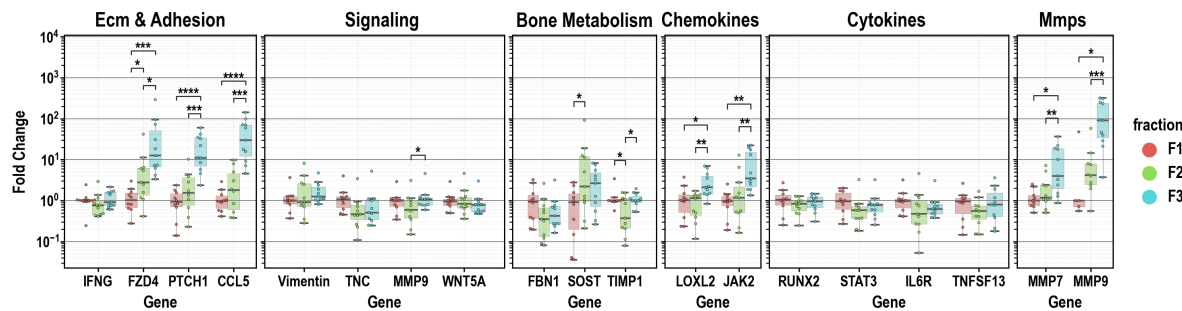
- Python >= 3.11 (*not tested with earlier versions*)

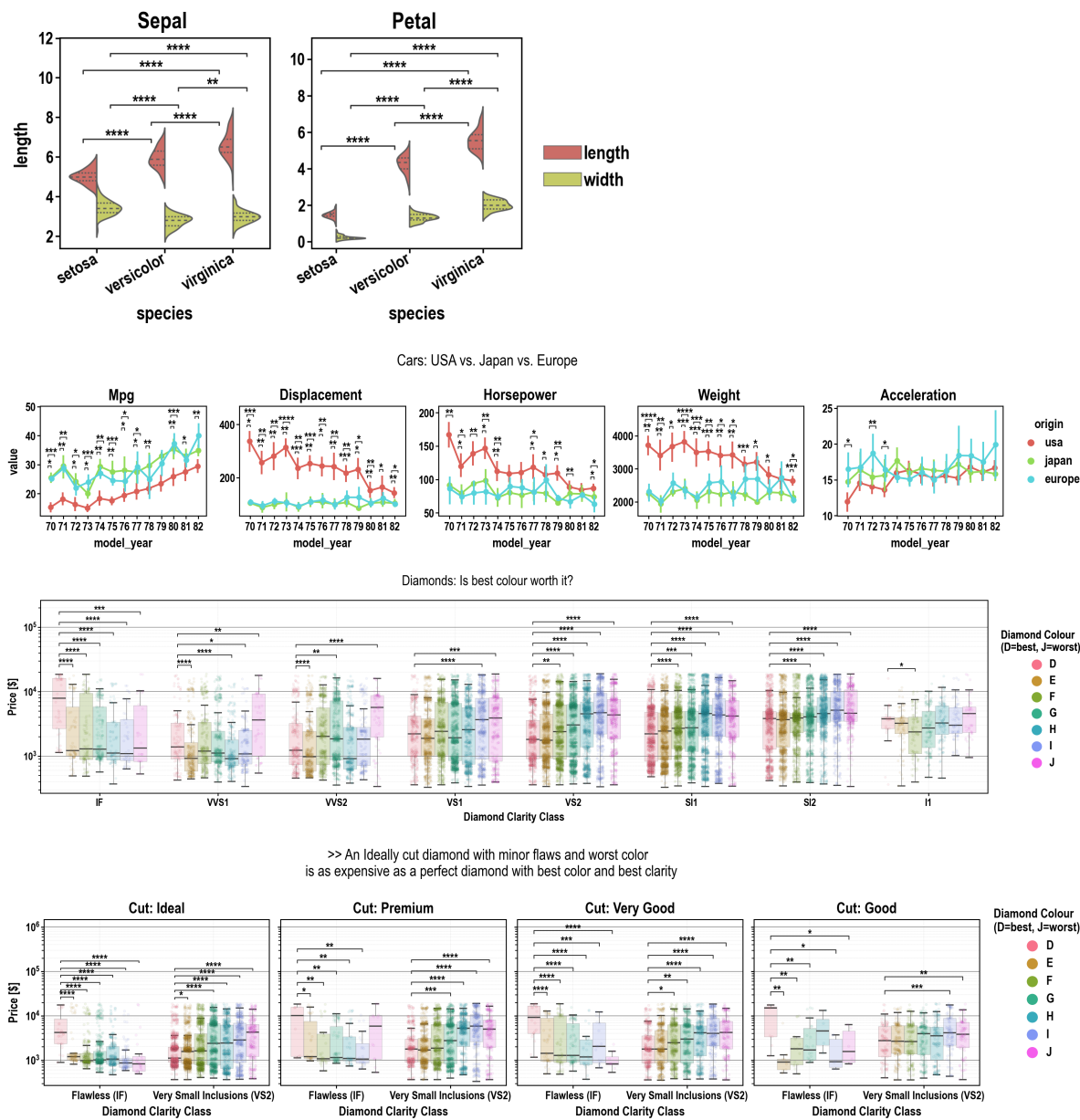
- pandas == 1.5.3 (*pingouin needs this*)
- seaborn <= 0.12.2 (*later versions reworked hue*)

Example Gallery

► (click to unfold)

 Click on Images for Code! 





>About plotastic

▶ 🧑 Summary

plotastic addresses the challenges of transitioning from exploratory data analysis to hypothesis testing in Python's data science ecosystem. Bridging the gap between **seaborn** and **pingouin**, this library offers a unified environment for plotting and statistical analysis. It simplifies the workflow with a user-friendly syntax and seamless integration with familiar **seaborn** parameters (`y`, `x`, `hue`, `row`, `col`). Inspired by **seaborn**'s consistency, **plotastic** utilizes a **DataAnalysis** object to intelligently pass parameters to **pingouin** statistical functions. The library systematically groups the data according to the needs of statistical tests and plots, conducts visualisation, analyses and supports extensive customization options. In essence, **plotastic** establishes a protocol for configuring statical analyses through plotting parameters.

This approach streamlines the process, translating `seaborn` parameters into statistical terms, providing researchers and data scientists with a cohesive and user-friendly solution in python.!

Workflow:

1. Import & Prepare your pandas DataFrame

- We require a long-format pandas dataframe with categorical columns
- If it works with seaborn, it works with plotastic!

2. Make a DataAnalysis Object

- `DataAnalysis(DataFrame, dims={x, y, hue, row, col})`
- Check for empty data groups, differing samplesizes, NaN-count, etc. automatically

3. Explore Data

- Check Data integrity, unequal samplesizes, empty groups, etc.
- Quick preliminary plotting with e.g. `DataAnalysis.catplot()`

4. Adapt Data

- Categorize multiple columns at once
- Transform dependent variable
- Each step warns you, if you introduced NaNs without knowledge!
- etc.

5. Perform Statistical Tests

- Check Normality, Homoscedasticity, Sphericity
- Perform Omnibus tests (ANOVA, RMANOVA, Kruskal-Wallis, Friedman)
- Perform PostHoc tests (Tukey, Dunn, Wilcoxon, etc.) based on `pg.pairwise_tests()`

6. Plot figure

- Use pre-defined and optimized multi-layered plots with one line (e.g. strip over box)!
- Annotate statistical results (p-values as *, **, ***, etc.) with full control over which data to include or exclude!

7. Save all results at once!

- One DataAnalysis object holds:
 - One DataFrame in `self.data`
 - One Figure in `self.fig, self.axes`
 - Multiple statistical results: `self.results`
- Use `DataAnalysis.save_statistics()` to save all results to different sheets collected in one .xlsx filesheet per test

► Translating Plots into Statistics!

In Principle:

- Categorical data is separable into `seaborn`'s categorization parameters: `x, y, hue, row, col`. We call those "*dimensions*".
- These dimensions are assigned to statistical terms:
 - `y` is the **dependent variable (DV)**
 - `x` and `hue` are **independent variables (IV)** and are treated as **within/between factors** (categorical variables)
 - `row` and `col` are **grouping variables** (categorical variables)
 - A `subject` may be specified for within/paired study designs (categorical variable)

- For each level of **row** or **col** (or for each combination of **row-** and **col** levels), statistical tests will be performed with regards to the two-factors **x** and **hue**

Example with ANOVA:

- Imagine this example data:
 - Each day you measure the tip of a group of people.
 - For each tip, you note down the **day**, **gender**, **age-group** and whether they **smoke** or not.
 - Hence, this data has 4 categorical dimensions, each with 2 or more *levels*:
 - **day**: 4 levels (*monday, tuesday, wednesday, Thursday*)
 - **gender**: 2 levels (*male, female*)
 - **smoker**: 2 levels (*yes, no*)
 - **age-group**: 2 levels (*young, old*)
- Each category is assigned to a place of a plot, and when calling statistical tests, we assign them to statistical terms (in comments):

```

◦ # dims is short for dimensions
dims = dict(           # STATISTICAL TERM:
    y = "tip",         # y-axis, dependent variable
    x = "day",          # x-axis, independent variable (within-
    subject factor)
    hue = "gender",     # color, independent variable (within-
    subject factor)
    col = "smoker",     # axes, grouping variable
    row = "age-group"   # axes, grouping variable
)

```

- We perform statistical testing groupwise:
 - For each level-combinations of **smoker** and **age-group**, a two-way ANOVA will be performed (with **day** and **gender** as **between** factors for each datagroup):
 - 1st ANOVA assesses datapoints where **smoker=yes** AND **age-group=young**
 - 2nd ANOVA assesses datapoints where **smoker=yes** AND **age-group=old**
 - 3rd ANOVA assesses datapoints where **smoker=no** AND **age-group=young**
 - 4th ANOVA assesses datapoints where **smoker=no** AND **age-group=old**
 - Three-way ANOVAs are not possible (yet), since that would require setting e.g. **col** as the third factor, or implementing another dimension (e.g. **hue2**).

► ! Disclaimer about Statistics

This software was inspired by ...

- ... ***Intuitive Biostatistics*** - Fourth Edition (2017); Harvey Motulsky
- ... ***Introduction to Statistical Learning with applications in Python*** - First Edition (2023); Gareth James, Daniela Witten, Trevor Hastie, Robert Tibshirani, Jonathan Taylor
- ... talking to other scientists struggling with statistics

 **plotastic** can help you with...

- ... gaining some practical experience when learning statistics
- ... quickly gain statistical implications about your data without switching to another software
- ... making first steps towards a full statistical analysis
- ... plotting publication grade figures (check statistics results with other software)
- ... publication grade statistical analysis **IF** you really know what you're doing OR you have back-checked your results by a professional statistician
- ... quickly test data transformations (log)

🚫 **plotastic** can NOT ...

- ... replace a professional statistician
- ... teach you statistics, you need some basic knowledge (but is awesome for practicing!)
- ... test for multicollinearity (Absence of multicollinearity is required by ANOVA!)
- ... perform stringent correction for multiple testing (e.g. bonferroni), as statistical tests are applied to sub-facets of the whole dataframe for each axes, which depends on the definition of x, hue, col, etc. Hence, corrected p-values might over-estimate the significance of your results.

🟡 Be critical and responsible with your statistical analysis!

- **Expect Errors:** Don't trust automated systems like this one!
- **Document your work in ridiculous detail:**
 - Include the applied tests, the number of technical replicates and the number of biological/independent in each figure legend
 - State explicitly what each datapoint represents:
 - 1 datapoint = 1 Technical replicate?
 - 1 datapoint = The mean of all technical replicate per independent replicate/subject?
 - State explicitly what the error-bars mean: Standard deviation? Confidence interval?
 - (Don't mix technical with biological/independent variance)
 - Report if/how you removed outliers
 - Report if you did or did not apply correction methods (multiple comparisons, Greenhouse Geyser, etc.) and what your rationale is (exploratory vs. confirmatory study? Validation through other methods to reduce Type I error?)
- **Check results with professionals:**
 - "Here is my data, here is my question, here is my analysis, here is my interpretation. What do you think?"

► ✅ Feature List

- ✅ : Complete and tested
- 👍 : Complete
- 📅 : Planned or unfinished (no date)
- 🧑‍💨 : Maybe..? (Rather not...)
- 🚫 : Not planned, don't want
- 😢 : Help Please..?

▼ Plotting

- 👍 Make and Edit Plots: Implemented ✅

- All (non-facetgrid) seaborn plots should work, not tested
- QQ-Plot
- Kaplan-Meyer-Plot
- Interactive Plots (where you click stuff and adjust scale etc.)
 - That's gonna be a lot of work!
- Support for `seaborn.FacetGrid`
 - Why not? - `plotastic` uses `matplotlib` figures and fills its axes with `seaborn` plot functions. In my opinion, that's the best solution that offers the best adaptability of every plot detail while being easy to maintain
- Support for `seaborn.objects` (same as Facetgrid)
 - Why not? - I don't see the need to refactor the code
- NEED HELP WITH: The hidden state of `matplotlib` figures/plots/stuff that gets drawn:
 - I want to save the figure in `DataAnalysis.fig` attribute. As simple as that sounds, `matplotlib` does weird stuff, not applying changes after editing the plot.
 - It'd be cool if I could control the changes to a `DataAnalysis` object better (e.g. using `inplace=True` like with `pd.DataFrame`). But I never figured out how to control `matplotlib` figure generation, even with re-drawing the figure with `canvas`. It's a mess and I wasted so much time already.

▼ Multi-Layered Plotting

- Box-plot + swarm
- Box-plot + strip
- Violin + swarm/strip

▼ Statistics

- Assumption testing
 - Normality (e.g. Shapiro-Wilk)
 - Homoscedasticity (e.g. Levene)
 - Sphericity (e.g. Mauchly)
- Omnibus tests
 - ANOVA, RMANOVA, Kruskal-Wallis, Friedman
 - Mixed ANOVA
 - Annotate Results into Plot
- PostHoc
 - `pg.pairwise_tests()`
 - Works with all primary options. That includes all parametric, non-parametric, paired, unpaired, etc. tests (*t-test*, paired *t-test*, *MWU*, *Wilcoxon*, etc.)
 - Annotate Stars into plots (*, **, etc.)
 - Specific pairs can be included/excluded from annotation
 - Make correction for multiple testing go over complete DataFrame and not Facet-wise:
- Bivariate
 - Find and Implement system to switch between numerical and categorical x-axis
 - Function to convert numerical data into categorical data by binning?
 - Pearson, Spearman, Kendall

▼ Analysis Pipelines

Idea: Put all those statistical tests into one line. I might work on this only after everything's implemented and working confidently and well!

- 🐦 `between_samples(parametric=True)`: ANOVA + Tukey (if Normality & Homoscedasticity are given)
- 🐦 `between_samples(parametric=False)`: Kruskal-Wallis + Dunn
- 🐦 `within_samples(parametric=True)`: RM-ANOVA + multiple paired t-tests (if Normality & Sphericity are given)
- 🐦 `within_samples(parametric=False)`: Friedman + multiple Wilcoxon



How To Use

Documentations

1. Example Gallery

1. Quick Example: FMRI
2. qPCR (paired, parametric)
3. Cars (unpaired, non-parametric)
4. Diamonds (unpaired, non-parametric)
5. Attention (paired/mixed, parametric)
6. Iris (unpaired, parametric)
7. Tips (unpaired, parametric)

2. Data

1. Set/Switch Dimensions

3. Plotting

1. Quick & Simple: MultiPlots
2. Constructing Plots
3. Legends
4. Styles

Quick Example

Import plotastic and example Data

```
import matplotlib.pyplot as plt
import plotastic as plst

# Import Example Data (Long-Format)
DF, _dims = plst.load_dataset("fmri", verbose = False)
DF.head()
```

Assign each column to a dimension (**y**, **x**, **hue**, **col**, **row**):

```
dims = dict(
    y = "signal",      # y-axis, dependent variable
    x = "timepoint",   # x-axis, independent variable & within-subject
    factor
    hue = "event",     # color, grouping variable & within-subject factor
    col = "region"     # axes, grouping variable
)
```

Initialize DataAnalysis Object

```
DA = plst.DataAnalysis(
    data=DF,           # Dataframe, long format
    dims=dims,         # Dictionary with y, x, hue, col, row
    subject="subject", # Datapoints are paired by subject (optional)
    verbose=False,     # Print out info about the Data (optional)
)
```

Perform Statistics

No arguments need to be passed, although `**kwargs`, are passed to respective `pingouin` functions.

```
DA.check_normality() # Normal Distribution?
DA.check_sphericity() # Sphericity?
DA.omnibus_rm_anova() # Repeated Measures ANOVA
DA.test_pairwise() # Post-hoc tests
```

Save Results:

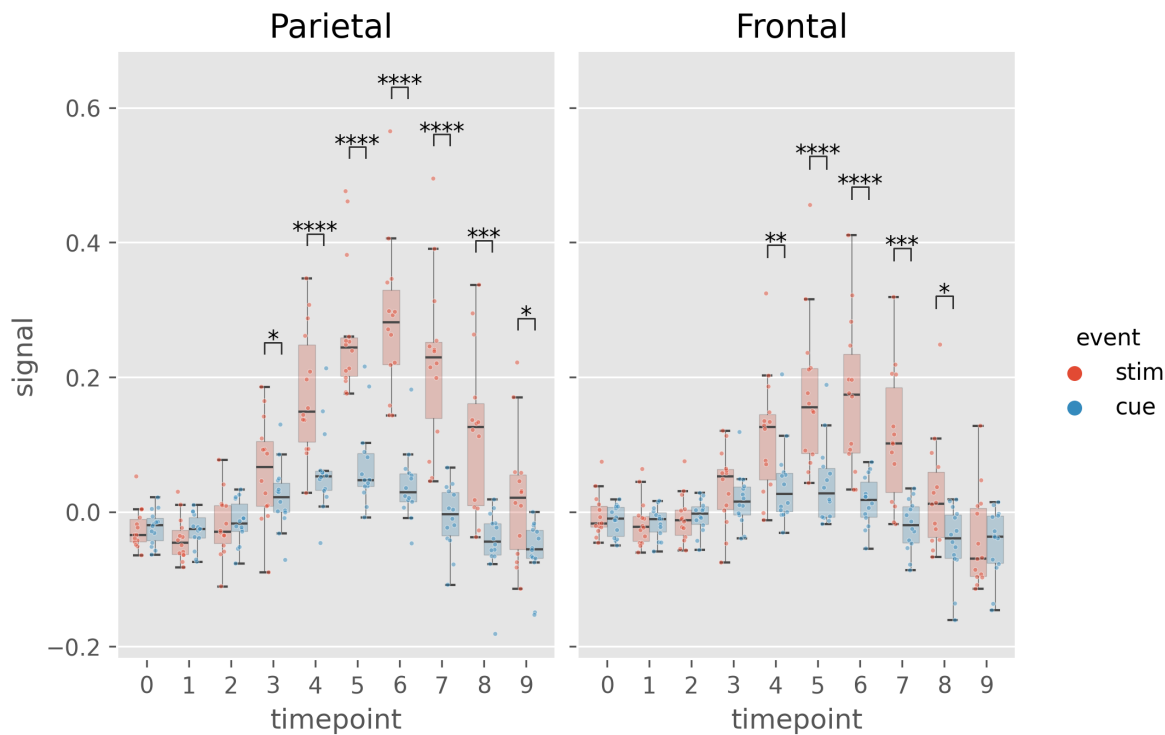
Output is one excel file containing results of all performed tests (normality, anova, t-tests, etc.) in different sheets

```
DA.save_statistics("example.xlsx")
```

Annotate post-hoc results into plot:

```
(DA
    .plot_box_strip() # Pre-built plotting function initializes plot
    .annotate_pairwise( # Annotate results from DA.test_pairwise()
        include="__HUE" # Use only significant pairs across each hue
    )
)
```

```
# Saving the plot like matplotlib!
plt.savefig("example.png", dpi=200, bbox_inches="tight")
```



🧪 Testing

▶ (click to unfold)

- Download/Clone repository
- Install development tools `pip install .[dev]`
- Run tests
 - Run `pytest ./tests`
 - To include a coverage report run `pytest ./tests -cov--cov-report=html` and open `./htmlcov/index.html` with your browser.

🤝 Community Guidelines

▶ (click to unfold)

When interacting with the community, you must adhere to the [Code of Conduct](#)

Contribute

I am grateful for [pull requests!](#)

- Make sure to understand the code (e.g. see Class diagram in this Readme)
- Run tests before submitting a pull request

Reporting Issues & Problems

If you need help, please open an [issue](#) on this repository.

- Please provide a minimal example to reproduce the problem.

Support

If you need help, please open an [issue](#) on this repository.

✍ Cite These!

► **(click to unfold)**

Kuric et al., (2024). plotastic: Bridging Plotting and Statistics in Python. *Journal of Open Source Software*, 9(95), 6304, <https://doi.org/10.21105/joss.06304>

Vallat, R. (2018). Pingouin: statistics in Python. *Journal of Open Source Software*, 3(31), 1026, <https://doi.org/10.21105/joss.01026>

Waskom, M. L., (2021). seaborn: statistical data visualization. *Journal of Open Source Software*, 6(60), 3021, <https://doi.org/10.21105/joss.03021>.

```
@article{Kuric2024,
  doi = {10.21105/joss.06304},
  url = {https://doi.org/10.21105/joss.06304},
  year = {2024}, publisher = {The Open Journal},
  volume = {9},
  number = {95},
  pages = {6304},
  author = {Martin Kuric and Regina Ebert},
  title = {plotastic: Bridging Plotting and Statistics in Python},
  journal = {Journal of Open Source Software}
}

@article{Waskom2021,
  doi = {10.21105/joss.03021},
  url = {https://doi.org/10.21105/joss.03021},
  year = {2021},
  publisher = {The Open Journal},
  volume = {6},
  number = {60},
  pages = {3021},
  author = {Michael L. Waskom},
  title = {seaborn: statistical data visualization},
  journal = {Journal of Open Source Software}
}

@article{Vallat2018,
  title = "Pingouin: statistics in Python",
  author = "Vallat, Raphael",
  journal = "The Journal of Open Source Software",
  volume = 3,
```

```
number    = 31,  
pages     = "1026",  
month     = nov,  
year      = 2018  
}
```

B.3 Example Analysis “qpcr”

The following pages are a jupyter notebook from an example analysis using `plotastic`. This notebook and further analyses examples are found on GitHub (github.com/markur4/plotastic). The qPCR dataset was derived from the experiments described in Chapter 1 Fig. 4 and was changed into a public test dataset by exchanging the original gene names with random ones while preserving gene classes and quantitative fold changes.

qPCR

April 9, 2024

```
[ ]: import plotastic as plst
import matplotlib.pyplot as plt
import seaborn as sns
import pandas as pd

[ ]: # Set Plot Style
plst.set_style("paper")
# plst.set_palette("hls", verbose=True)
plst.set_palette(["#db5f57", "#91db57", "#57d3db"])

#! You chose this color palette: ['#db5f57', '#91db57', '#57d3db', '#db5f57',
'#91db57', '#57d3db', '#db5f57', '#91db57']

['#db5f57',
 '#91db57',
 '#57d3db',
 '#db5f57',
 '#91db57',
 '#57d3db',
 '#db5f57',
 '#91db57']
```

1 Example Analysis: qPCR

Raw Data: https://github.com/markur4/plotastic/tree/main/src/plotastic/example_data/data

Original Source: (unpublished)

```
[ ]: # Import Example Data
DF, _dims = plst.load_dataset("qPCR", verbose=False)
dims = dict(
    y="fc",
    x="gene",
    hue="fraction",
    # col= 'method',
    row="class",
)
DA = plst.DataAnalysis(DF, dims, subject="subject", verbose=False)
```

```
[ ]: DA.transform_y("log10", inplace=True) # Log transform
DA.check_normality() # -> Only few groups are not normal -> parametric
```

[]:

				W	pval	normal	n
	class	gene	fraction				
Bone Metabolism		F1	FBN1	0.936873	0.518768	True	10
			SOST	0.880395	0.131862	True	10
			TIMP1	0.745494	0.004807	False	9
		F2	FBN1	0.954764	0.705148	True	11
			SOST	0.967810	0.863610	True	11
			TIMP1	0.914325	0.274168	True	11
		F3	FBN1	0.915247	0.281020	True	11
			SOST	0.923112	0.345415	True	11
			TIMP1	0.937230	0.488505	True	11
Chemokines		F1	LOXL2	0.930358	0.451421	True	10
			JAK2	0.897331	0.204749	True	10
		F2	LOXL2	0.874630	0.088876	True	11
			JAK2	0.960025	0.772006	True	11
		F3	LOXL2	0.943678	0.564652	True	11
			JAK2	0.878406	0.099301	True	11
Cytokines		F1	RUNX2	0.947142	0.634825	True	10
			STAT3	0.933422	0.482382	True	10
			IL6R	0.927258	0.421472	True	10
			TNFSF13	0.907481	0.264130	True	10
		F2	RUNX2	0.915611	0.283765	True	11
			STAT3	0.907354	0.226836	True	11
			IL6R	0.985709	0.989621	True	11
			TNFSF13	0.958855	0.757330	True	11
		F3	RUNX2	0.924060	0.353917	True	11
			STAT3	0.932663	0.438418	True	11
			IL6R	0.826181	0.020798	False	11
			TNFSF13	0.970421	0.890746	True	11
ECM & Adhesion		F1	IFNG	0.715267	0.001349	False	10
			FZD4	0.981633	0.973303	True	10
			PTCH1	0.911578	0.292008	True	10
			CCL5	0.969121	0.882582	True	10
		F2	IFNG	0.899109	0.180269	True	11
			FZD4	0.979590	0.963841	True	11
			PTCH1	0.986610	0.990734	True	10
			CCL5	0.925780	0.407685	True	10
		F3	IFNG	0.905665	0.216509	True	11
			FZD4	0.923819	0.351743	True	11
			PTCH1	0.957827	0.744318	True	11
			CCL5	0.940093	0.521596	True	11
MMPs		F1	MMP7	0.955749	0.752957	True	9
			MMP9	0.675286	0.005186	False	5
		F2	MMP7	0.926078	0.372552	True	11

		MMP9	0.971128	0.901100	True	10
	F3	MMP7	0.924886	0.361455	True	11
		MMP9	0.913554	0.268549	True	11
Signaling	F1	Vimentin	0.919696	0.354424	True	10
		TNC	0.928589	0.434161	True	10
		NOTCH1	0.922084	0.374662	True	10
		WNT5A	0.903581	0.239742	True	10
	F2	Vimentin	0.957763	0.743507	True	11
		TNC	0.959813	0.769352	True	11
		NOTCH1	0.977556	0.951045	True	11
		WNT5A	0.937156	0.487661	True	11
	F3	Vimentin	0.910924	0.250109	True	11
		TNC	0.884194	0.117578	True	11
		NOTCH1	0.779982	0.005132	False	11
		WNT5A	0.812114	0.013581	False	11

[]: DA.check_sphericity()

		spher	W	chi2	dof	pval	\
class	fraction						
Bone Metabolism	F1	0	True	0.592922	3.658847	2	0.160506
	F2	0	True	0.703252	3.168356	2	0.205116
	F3	0	True	0.832864	1.645964	2	0.439120
Chemokines	F1	0	True	NaN	NaN	1	1.000000
	F2	0	True	NaN	NaN	1	1.000000
	F3	0	True	NaN	NaN	1	1.000000
Cytokines	F1	0	True	0.629185	3.577934	5	0.614197
	F2	0	False	0.262747	11.657816	5	0.040987
	F3	0	False	0.210032	13.610980	5	0.019012
ECM & Adhesion	F1	0	True	0.486690	5.560987	5	0.354712
	F2	0	True	0.295164	8.202615	5	0.149255
	F3	0	True	0.297080	10.586623	5	0.061736
MMPs	F1	0	True	NaN	NaN	1	1.000000
	F2	0	True	NaN	NaN	1	1.000000
	F3	0	True	NaN	NaN	1	1.000000
Signaling	F1	0	True	0.536227	4.812474	5	0.442437
	F2	0	True	0.554009	5.151113	5	0.400336
	F3	0	False	0.117602	18.669462	5	0.002375
		group	count	n per group			
class	fraction						
Bone Metabolism	F1	0	3	[10, 10, 9]			
	F2	0	3	[11, 11, 11]			
	F3	0	3	[11, 11, 11]			
Chemokines	F1	0	2	[10, 10]			
	F2	0	2	[11, 11]			
	F3	0	2	[11, 11]			

Cytokines	F1	0	4	[10, 10, 10, 10]
	F2	0	4	[11, 11, 11, 11]
	F3	0	4	[11, 11, 11, 11]
ECM & Adhesion	F1	0	4	[10, 10, 10, 10]
	F2	0	4	[10, 11, 11, 10]
	F3	0	4	[11, 11, 11, 11]
MMPs	F1	0	2	[9, 5]
	F2	0	2	[11, 10]
	F3	0	2	[11, 11]
Signaling	F1	0	4	[10, 10, 10, 10]
	F2	0	4	[11, 11, 11, 11]
	F3	0	4	[11, 11, 11, 11]

```
[ ]: # Default is (paired) t-test, and since DA has subject: paired=True
DA.test_pairwise()
```

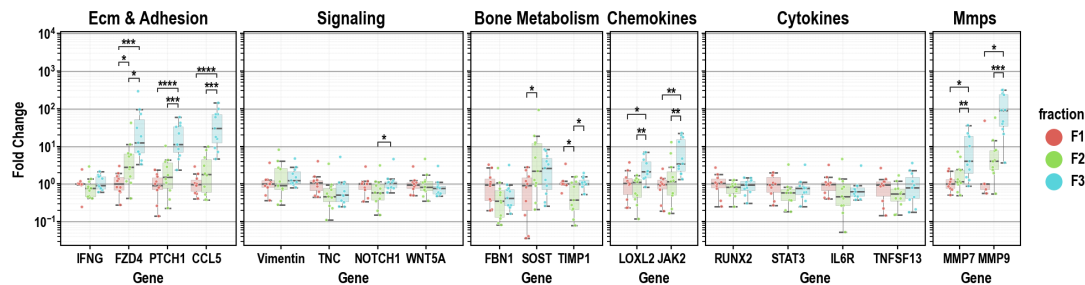
			gene	A	B	mean(A)	\
	class	fraction Contrast					
ECM & Adhesion	-	gene	-	CCL5	FZD4	0.591713	
		gene	-	CCL5	IFNG	0.591713	
		gene	-	CCL5	PTCH1	0.591713	
		gene	-	FZD4	IFNG	0.622994	
		gene	-	FZD4	PTCH1	0.622994	
..			
MMPs	NaN	gene * fraction	MMP9	F1	F3	0.256111	
		gene * fraction	MMP9	F2	F3	0.677357	
	F1	fraction * gene	NaN	MMP7	MMP9	0.032549	
	F2	fraction * gene	NaN	MMP7	MMP9	0.185211	
	F3	fraction * gene	NaN	MMP7	MMP9	0.742060	
			std(A)	mean(B)	std(B)	Paired	\
	class	fraction Contrast					
ECM & Adhesion	-	gene	0.253752	0.622994	0.266747	True	
		gene	0.253752	-0.026656	0.149430	True	
		gene	0.253752	0.469495	0.330886	True	
		gene	0.266747	-0.026656	0.149430	True	
		gene	0.266747	0.469495	0.330886	True	
..			
MMPs	NaN	gene * fraction	0.802159	1.845550	0.600687	True	
		gene * fraction	0.546148	1.845550	0.600687	True	
	F1	fraction * gene	0.228544	0.256111	0.802159	True	
	F2	fraction * gene	0.361750	0.677357	0.546148	True	
	F3	fraction * gene	0.567249	1.845550	0.600687	True	
			Parametric		T	dof	\
	class	fraction Contrast					
ECM & Adhesion	-	gene	True	-0.327586	10.0		

		gene	True	7.882620	10.0	
		gene	True	1.320783	10.0	
		gene	True	7.532512	10.0	
		gene	True	2.105924	10.0	
..			
MMPs	NaN	gene * fraction	True	-3.513968	4.0	
		gene * fraction	True	-5.680475	9.0	
	F1	fraction * gene	True	-0.543884	4.0	
	F2	fraction * gene	True	-3.811156	9.0	
	F3	fraction * gene	True	-15.767066	10.0	
			alternative		p-unc	BF10 \
class		fraction Contrast				
ECM & Adhesion -		gene	two-sided	7.499799e-01		0.312
		gene	two-sided	1.339935e-05		1643.947
		gene	two-sided	2.160003e-01		0.598
		gene	two-sided	1.987311e-05		1165.781
		gene	two-sided	6.146203e-02		1.461
..			
MMPs	NaN	gene * fraction	two-sided	2.458360e-02		3.686
		gene * fraction	two-sided	3.016844e-04		111.751
	F1	fraction * gene	two-sided	6.154168e-01		0.448
	F2	fraction * gene	two-sided	4.145762e-03		12.636
	F3	fraction * gene	two-sided	2.163081e-08		4.845e+05
			hedges	**p-unc	Sign.	\
class		fraction Contrast				
ECM & Adhesion -		gene	-0.115597	ns	False	
		gene	2.856874	****	signif.	
		gene	0.398765	ns	False	
		gene	2.890772	****	signif.	
		gene	0.491362	0.061	toler.	
..			
MMPs	NaN	gene * fraction	-2.179426	*	signif.	
		gene * fraction	-2.024511	***	signif.	
	F1	fraction * gene	-0.255634	ns	False	
	F2	fraction * gene	-0.939861	**	signif.	
	F3	fraction * gene	-1.817138	****	signif.	
				pairs	cross	
class		fraction Contrast				
ECM & Adhesion -		gene		(CCL5, FZD4)	x	
		gene		(CCL5, IFNG)	x	
		gene		(CCL5, PTCH1)	x	
		gene		(FZD4, IFNG)	x	
		gene		(FZD4, PTCH1)	x	
..				

MMPs	NaN	gene * fraction	((MMP9, F3), (MMP9, F1))	hue
		gene * fraction	((MMP9, F3), (MMP9, F2))	hue
	F1	fraction * gene	((MMP9, F1), (MMP7, F1))	x
	F2	fraction * gene	((MMP9, F2), (MMP7, F2))	x
	F3	fraction * gene	((MMP9, F3), (MMP7, F3))	x

[167 rows x 19 columns]

```
[ ]: # Plot
(
  DA.switch("row", "col", verbose=False)
  .set(y="fc", inplace=False) # set y back to fc to display non-log values
  .plot_box_strip(
    subplot_kws=dict(
      figsize=(10, 2.5),
      width_ratios=[4, 5, 3, 2, 5, 2],
    ),
    strip_kws=dict(alpha=0.8),
  )
  .edit_grid()
  .edit_y_scale_log(10)
  .edit_xy_axis_labels(y_leftmost_col="Fold Change", x="Gene")
  .annotate_pairwise(include="__HUE")
)
plt.savefig("qpcr1.png", dpi=300, bbox_inches="tight")
```



C Submission Forms & Documents

C.1 Author Contributions



Statement of individual author contributions and of legal second publication rights to manuscripts included in the dissertation

Manuscript 1: Research Article (submitted, under revision)

Martin Kuric (MK), Susanne Beck, Doris Schneider, Wyonna Rindt, Marietheres Evers, Jutta Meißner-Weigl, Sabine Zeck, Melanie Krug, Marietta Herrmann, Tanja Nicole Hartmann, Ellen Leich, Maximilian Rudert, Denitsa Docheva, Anja Seckinger, Dirk Hose, Franziska Jundt, Regina Ebert (RE) (2024): Keep it Together: Describing Myeloma Dissemination *in vitro* with hMSC-Interacting Subpopulations and their Aggregation/Detachment Dynamics, **Cancer Research Communications**

Participated in	Author Initials , Responsibility decreasing from left to right				
Study Design	<u>MK</u>	Regina Ebert	Wyonna Rindt		
Methods Development	<u>MK</u>	Doris Schneider			
Data Collection	<u>MK</u>	Doris Schneider			
Data Analysis and Interpretation	<u>MK</u>	Susanne Beck	Regina Ebert		
Manuscript Writing Writing of Introduction Writing of Materials & Methods Writing of Discussion Writing of First Draft	<u>MK</u>	Regina Ebert			

Explanations: The content of this publication exceeds the usual scope (~29 pages Supplemental). It includes not only research findings but also survival data and protocols of new, established methods and their validations. The contribution of Martin Kuric was pivotal and predominant in all aspects of this work. Doris Schneider assisted in the experimental procedures. Susanne Beck analyzed the raw data from RNAseq and survival data, which were interpreted, depicted, and summarized by Martin Kuric.

Manuscript 2: Data Analysis Software (submitted, passed peer-review, under revision)

Martin Kuric (MK), Regina Ebert (2024): plotastic: Bridging Plotting and Statistics in Python, **Journal of Open Source Software**

Participated in	Author Initials , Responsibility decreasing from left to right				
Idea, Architectural Design	<u>MK</u>				
Software Development Feature Implementation Testing	<u>MK</u>				
Distribution of Software Documentation Version Control (GitHub) Deployment (PyPi)	<u>MK</u>				
Manuscript Writing Writing of Statement of Need Writing of Example Writing of Overview	<u>MK</u>	Regina Ebert			

Explanations: The software was entirely created by Martin Kuric, comprising more than 8000 total lines (including ~2000 testable lines) and is comparable in size to a typical web application. The release of this software involved version control using GitHub, packaging and deployment on PyPi. Regina Ebert gave feedback on submitted manuscript.

Manuscript 3: Research Letter (published)

Daniela Simone Maichl, Julius Arthur Kirner, Susanne Beck, Wen-Hui Cheng, Melanie Krug, Martin Kuric (MK), Carsten Patrick Ade, Thorsten Bischler, Franz Jakob, Dirk Hose, Anja Seckinger, Regina Ebert & Franziska Jundt (2023): Identification of NOTCH-driven matrisome-associated genes as prognostic indicators of multiple myeloma patient survival, **Blood Cancer Journal 13:134**

Participated in	Author Initials , Responsibility decreasing from left to right				
Study Design Methods Development	Daniela Simone		Franziska Jundt		
Data Collection	Daniela Simone		Franziska Jundt		
Data Analysis and Interpretation	Daniela Simone	Susanne Beck	Franziska Jundt	<u>MK</u>	
Manuscript Writing Writing of Introduction Writing of Materials & Methods Writing of Discussion Writing of First Draft	Daniela Simone		Franziska Jundt	<u>MK</u>	

Explanations: This co-authorship is not a chapter in this dissertation. Martin Kuric produced figures of processed but complex-to-visualize data and gave feedback on submitted manuscript.

Manuscript 4: Research Paper (under peer-review)

Wyonna Rindt, Melanie Krug, Shuntaro Yamada, Franziska Sennefelder, Louisa Belz, Wen-Hui Cheng, Azeem Muhammad, Martin Kuric (MK), Marietheres Evers, Ellen Leich, Tanja Nicole Hartmann, Ana Rita Pereira, Marietta Herrmann, Jan Hansmann, Mohammed Ahmed Yassin, Kamal Mustafa, Regina Ebert, and Franziska Jundt (2024): A 3D bioreactor model to study osteocyte differentiation and mechanobiology under perfusion and compressive mechanical loading, **Acta Biomaterialia**

Participated in	Author Initials , Responsibility decreasing from left to right				
Study Design Methods Development	Wyonna Rindt	Franziska Jundt		<u>MK</u>	
Data Collection	Wyonna Rindt	Franziska Jundt		<u>MK</u>	
Data Analysis and Interpretation	Wyonna Rindt	Franziska Jundt		<u>MK</u>	
Manuscript Writing Writing of Introduction Writing of Materials & Methods Writing of Discussion Writing of First Draft	Wyonna Rindt	Franziska Jundt		<u>MK</u>	

Explanations: This co-authorship is not a chapter in this dissertation. Martin Kuric contributed by counseling during weekly meetings in tight collaboration with Franziska Jundt's group, assisting Wyonna Rindt during laboratory experiments, image analysis and giving feedback on submitted manuscript.

Manuscript 5: Research Paper (under revision)

Marietta Herrmann, Jutta Schneidereit, Susanne Wiesner, Martin Kuric (MK), Maximilian Rudert, Martin Lüdemann, Mugdha Srivastava, Norbert Schütze, Regina Ebert, Denitsa Docheva, Franz Jakob (2024): Peripheral blood cells enriched by adhesion to CYR61 are heterogenous myeloid modulators of tissue regeneration with early endothelial progenitor characteristics, **European Cells and Materials**

Participated in	Author Initials , Responsibility decreasing from left to right				
Study Design Methods Development	Marietta Herrmann				
Data Collection	Marietta Herrmann			<u>MK</u>	

Data Analysis and Interpretation	Marietta Herrmann				
Manuscript Writing Writing of Introduction Writing of Materials & Methods Writing of Discussion Writing of First Draft	Marietta Herrmann			<u>MK</u>	

Explanations: This co-authorship is not a chapter in this dissertation. Martin Kuric contributed by establishing and measuring large automated microscopy scans of stained cells for quantifying osteogenic differentiation and giving feedback on submitted manuscript.

Manuscript 6: Research Letter (published)					
Participated in	Author Initials, Responsibility decreasing from left to right				
Study Design Methods Development	Marietheres Evers				
Data Collection	Marietheres Evers				
Data Analysis and Interpretation	Marietheres Evers			<u>MK</u>	
Manuscript Writing Writing of Introduction Writing of Materials & Methods Writing of Discussion Writing of First Draft	Marietheres Evers			<u>MK</u>	

Explanations: This co-authorship is not a chapter in this dissertation. Martin Kuric contributed by counseling during regular meetings with Ellen Leich's group and giving feedback on submitted manuscript.

If applicable, the doctoral researcher confirms that she/he has obtained permission from both the publishers (copyright) and the co-authors for legal second publication.

The doctoral researcher and the primary supervisor confirm the correctness of the above mentioned assessment.

Würzburg

Doctoral Researcher's Name	Date	Place	Signature
----------------------------	------	-------	-----------

Würzburg

Primary Supervisor's Name	Date	Place	Signature
---------------------------	------	-------	-----------



Statement of individual author contributions to figures/tables of manuscripts included in the dissertation

Manuscript 1: Research Article (submitted, under revision)

Martin Kuric (MK), Susanne Beck, Doris Schneider, Wyonna Rindt, Marietheres Evers, Jutta Meißner-Weigl, Sabine Zeck, Melanie Krug, Marietta Herrmann, Tanja Nicole Hartmann, Ellen Leich, Maximilian Rudert, Denitsa Docheva, Anja Seckinger, Dirk Hose, Franziska Jundt, Regina Ebert1 (2024): Keep it Together: Describing Myeloma Dissemination *in vitro* with hMSC-Interacting Subpopulations and their Aggregation/Detachment Dynamics, **Cancer Research Communications**

Figure	Author Initials , Responsibility decreasing from left to right				
1	<u>MK</u>	Doris Schneider			
2	<u>MK</u>	Doris Schneider			
3	<u>MK</u>	Doris Schneider	Sabine Zeck	Wyonna Rindt	Melanie Krug
4	<u>MK</u>	Doris Schneider	Susanne Beck		
5	<u>MK</u>	Susanne Beck			
6	<u>MK</u>	Susanne Beck			
7	<u>MK</u>				
S1	<u>MK</u>	Doris Schneider	Sabine Zeck	Wyonna Rindt	Melanie Krug
S2	<u>MK</u>	Doris Schneider	Marietta Herrmann		
S3	<u>MK</u>	Doris Schneider	Sabine Zeck		
S4	<u>MK</u>				
S5	<u>MK</u>				
S6	<u>MK</u>	Susanne Beck			
Table	Author Initials , Responsibility decreasing from left to right				
1	<u>MK</u>	Susanne Beck			
2	<u>MK</u>	Susanne Beck			
S1	<u>MK</u>	Doris Schneider			
S2	<u>MK</u>	Susanne Beck			
S3	<u>MK</u>				
S4	<u>MK</u>	Doris Schneider			

Manuscript 2: Data Analysis Software (submitted, passed peer-review, under revision)

Martin Kuric, Regina Ebert (2024): plotastic: Bridging Plotting and Statistics in Python, **Journal of Open Source Software**

Figure	Author Initials , Responsibility decreasing from left to right				
1	<u>MK</u>				
Table	Author Initials , Responsibility decreasing from left to right				
1	<u>MK</u>				
2	<u>MK</u>				

Documentation	Author Initials , Responsibility decreasing from left to right				
README	<u>MK</u>				
Example Gallery	<u>MK</u>				
Features	<u>MK</u>				
Testing	Author Initials , Responsibility decreasing from left to right				
Test-Code (Pytest)	<u>MK</u>				
Continuous Integration	<u>MK</u>				

Explanations: All files are available on GitHub (<https://github.com/markur4/plotastic>) and installable via pypi.com. Documentations are found in the Readme, including example gallery and feature explanation. Software tests was written using pytest. Coverage of code by tests is reviewable with codecov (<https://app.codecov.io/gh/markur4/plotastic>). Continuous Integration is implemented using GitHub actions.

Manuscript 3: Research Letter (published)

Daniela Simone Maichl, Julius Arthur Kirner, Susanne Beck, Wen-Hui Cheng, Melanie Krug, Martin Kuric, Carsten Patrick Ade, Thorsten Bischler, Franz Jakob, Dirk Hose, Anja Seckinger, Regina Ebert & Franziska Jundt (2023): Identification of NOTCH-driven matrisome-associated genes as prognostic indicators of multiple myeloma patient survival, **Blood Cancer Journal** **13:134**

Figure	Author Initials , Responsibility decreasing from left to right				
1 a	Daniela Simone			Susanne Beck	
1 b	Daniela Simone			Susanne Beck	
1 c	Daniela Simone			Susanne Beck	<u>MK</u>
1 d	Daniela Simone			Susanne Beck	<u>MK</u>
Table	Author Initials , Responsibility decreasing from left to right				
1	Daniela Simone				

Explanations: Martin Kuric plotted multidimensional diagrams using python and fine-adjusted them using professional design software (Affinity Publisher, Serif Ltd).

Manuscript 4: Research Paper (under peer-review)

Wyonna Rindt, Melanie Krug, Shuntaro Yamada, Franziska Sennefelder, Louisa Belz, Wen-Hui Cheng, Azeem Muhammad, Martin Kuric (MK), Marietheres Evers, Ellen Leich, Tanja Nicole Hartmann, Ana Rita Pereira, Marietta Hermann, Jan Hansmann, Mohammed Ahmed Yassin, Kamal Mustafa, Regina Ebert, and Franziska Jundt (2024): A 3D bioreactor model to study osteocyte differentiation and mechanobiology under perfusion and compressive mechanical loading, **Acta Biomaterialia**

Figure	Author Initials , Responsibility decreasing from left to right				
1	Wyonna Rindt				<u>MK</u>
2	Wyonna Rindt				
3	Wyonna Rindt				
4	Wyonna Rindt				
5	Wyonna Rindt				<u>MK</u>
6	Wyonna Rindt				<u>MK</u>
7	Wyonna Rindt				<u>MK</u>

Explanations: Martin Kuric contributed by counseling on experimental procedures and data analysis, such as quantifying normalized fluorescence intensity of immunohistochemistry and qPCR.

Manuscript 5: Research Paper (under revision)

Marietta Herrmann, Jutta Schneidereit, Susanne Wiesner, Martin Kuric (MK), Maximilian Rudert, Martin Lüdemann, Mugdha Srivastava, Norbert Schütze, Regina Ebert, Denitsa Docheva, Franz Jakob (2024): Peripheral blood cells enriched by adhesion to CYR61 are heterogenous myeloid modulators of tissue regeneration with early endothelial progenitor characteristics, **European Cells and Materials**

Figure	Author Initials , Responsibility decreasing from left to right				
1	Marietta Herrmann				
2	Marietta Herrmann				
3	Marietta Herrmann				
4	Marietta Herrmann				
5	Marietta Herrmann				
6	Marietta Herrmann				
7	Marietta Herrmann				<u>MK</u>

Explanations: Martin Kuric scanned osteogenically differentiated MSCs in Fig. 7 for quantification of alizarin red staining.

Manuscript 6: Research Letter (published)

Marietheres Evers, Martin Schreder, Thorsten Stühmer, Franziska Jundt, Regina Ebert, Tanja Nicole Hartmann, Michael Altenbuchinger, Martina Rudelius, Martin Kuric (MK), Wyonna Darleen Rindt, Torsten Steinbrunn, Christian Langer, Sofia Catalina Heredia-Guerrero, Hermann Einsele, Ralf Christian Bargou, Andreas Rosenwald, Ellen Leich (2023): Prognostic value of extracellular matrix gene mutations and expression in multiple myeloma, **Blood Cancer J. 13(1):43**

Figure	Author Initials , Responsibility decreasing from left to right				
1	Marietheres Evers				
2	Marietheres Evers				

Explanations: Martin Kuric contributed indirectly through counseling and feedback on submitted manuscript.

I also confirm my primary supervisor's acceptance.

Doctoral Researcher's Name

Date

Place

Signature

C.2 Affidavit

Affidavit

I hereby confirm that my thesis entitled "Development and Semi-Automated Analysis of an in vitro Model for Myeloma Cells Interacting with Mesenchymal Stromal Cells" is the result of my own work. I did not receive any help or support from commercial consultants. All sources and / or materials applied are listed and specified in the thesis.

Furthermore, I confirm that this thesis has not yet been submitted as part of another examination process neither in identical nor in similar form.

Würzburg
Place, Date

Signature

Eidesstattliche Erklärung

Hiermit erkläre ich an Eides statt, die Dissertation "Entwicklung und semi-automatisierte Analyse eines in vitro-Modells für Myelomzellen in Interaktion mit mesenchymalen Stromazellen" eigenständig, d.h. insbesondere selbstständig und ohne Hilfe eines kommerziellen Promotionsberaters, angefertigt und keine anderen als die von mir angegebenen Quellen und Hilfsmittel verwendet zu haben.

Ich erkläre außerdem, dass die Dissertation weder in gleicher noch in ähnlicher Form bereits in einem anderen Prüfungsverfahren vorgelegen hat.

Würzburg
Ort, Datum

Unterschrift

C.3 Usage of Generative AI and Other Software

Erklärung zur Nutzung von ChatGPT, GitHub Copilot und sonstiger Software

Als Grundlage dieses Schreibens nennt der Autor die Eidesstattliche Erklärung (*Affidavit*), welche zur Angabe von Hilfsmitteln auffordert, aber nicht explizit die Nutzung von Hilfsmitteln als Einschränkung der Eigenständigkeit des Autors betrachtet. Ebenso wird auf die *Stellungnahme des Präsidiums der Deutschen Forschungsgemeinschaft (DFG) zum Einfluss generativer Modelle für die Text- und Bilderstellung auf die Wissenschaften und das Förderhandeln der DFG* (September 2023) verwiesen: Der Einsatz generativer Modelle wie ChatGPT soll nicht ausgeschlossen werden, sondern erfordert transparente und nachvollziehbare Dokumentation, um wissenschaftliche Integrität zu gewährleisten. Wissenschaftler müssen offenlegen, ob und wie sie generative Modelle verwendet haben, und sicherstellen, dass keine Verletzung geistigen Eigentums oder wissenschaftliches Fehlverhalten vorliegt. Diese Stellungnahme wurde, laut Telefonat vom 24.05.2024 mit Dr. Jennifer Ritzer, als Grundlage zum Umgang mit KI bei der Graduate School of Life Sciences (GSLS), Universität Würzburg, festgelegt.

Die KI-generierten Chat-Verläufe sind in der digitalen Version dieser Arbeit einsehbar und dienen als Beweis zur Einhaltung der hier genannten Prinzipien. Dem ist hinzuzufügen, dass die in den Chat-Verläufen generierten Texte einen weiteren manuellen Bearbeitungsverlauf nicht dokumentieren, weswegen auch ignorierte oder auch vollständig vom Autor umgeschriebene Abschnitte in den Chat-Verläufen enthalten sind.

Der Autor bemerkte selbstständig folgende Mängel generativer KI-Modelle:

- Unzuverlässigkeit bei der Korrektheit wissenschaftlicher Fakten
- Starke Tendenz, die Meinung des Nutzers zu bestätigen
- Mangel an Präzision und Nutzung abstrakter Formulierungen
- Halluzinieren von nicht existierenden wissenschaftlichen Quellen

Der Autor entschied sich, auch zur Wahrung wissenschaftlicher Integrität, dass KI keinen entscheidenden Einfluss auf die Kernaussagen der bearbeiteten Abschnitte ausüben sollte. Um dies sicherzustellen, wurden **generative KI-Modelle** für folgende Zwecke nicht genutzt:

1. Sammlung oder Überprüfung wissenschaftlicher Fakten.
2. Erweiterung des Informationsgehalts der Arbeit: Die in den Vorgaben (*prompt*) enthaltene Information wurde nicht durch KI-generierte Inhalte erweitert. Konkret bedeutet dies, dass ChatGPT nicht zur Sammlung von Ideen oder wissenschaftlichen Fragestellungen verwendet wurde, welche die Einleitung, Ergebnisse und/oder Diskussion maßgeblich beeinflusst hätten.
3. Übernahme KI-generierter Texte ohne nachfolgender Überarbeitung durch den Autor.
4. Datenanalyse und Statistik

ChatGPT (Versionen 3.5, 4 und 4o) wurde für folgende Zwecke benutzt:

1. Ausformulierung kohärenter Textabschnitte basierend auf manuell erstellten rohen Textabschnitten und Stichpunkten.
2. Iterative Verbesserung der Formulierungen: Erstellen einer Erstfassung ausgehend von einer Rohfassung, Ausgabe einer durch ChatGPT verbesserten Version, Abänderung durch den Autor, etc.
3. Erstellung von zusammenfassenden Abschnitten (z.B.: *Summary, Aims, Conclusion*) mit nachfolgender Überarbeitung.
4. Übersetzen der Summary von Englisch auf Deutsch
5. Programmierhilfe zur Formatierung in LaTeX.
6. Suche nach weiteren Quellen zu bereits erarbeiteten Inhalten, falls vorhanden.

GitHub Copilot (Version 1.198.0) ist als Programmierhilfe spezialisiert und wurde genutzt, um begonnene Sätze oder code zu vervollständigen und bugs zu beheben.

Aus diesen Grundsätzen ist ersichtlich, dass generative KI Modelle ausschließlich als Programmier-, Phrasierungs- und Zusammenfassungshilfe genutzt wurde, vergleichbar mit als unbedenklich geltende Tools wie *Grammarly*. Dem entsprechend hätte diese Arbeit problemlos ohne ChatGPT oder GitHub Copilot angefertigt werden können, was die Eigenständigkeit des Autors sicherstellt.

Ebenso wurde folgende **sonstige Software** verwendet:

- Visual Studio Code (VS Code) als code und LaTeX Editor, einschließlich Plugins (z.B. zur Korrektur von Grammatik)
- LaTeX (MacTeX Distribution)
- Zotero zur Zitation von Quellen und automatisierten Erstellung des Quellenverzeichnisses einschließlich Plugins (ZotFile, Better BibTeX, etc.)
- Affinity Publisher zur Montage von Abbildungen

Ort, Datum und Unterschrift folgen auf der nächsten Seite der englischen Version.

Declaration of ChatGPT, GitHub Copilot, and Other Software Usage

The basis of this declaration is the Affidavit, which requires the disclosure of aids but does not explicitly consider the use of aids as a limitation on the author's independence. Additionally, the *statement by the Presidium of the German Research Foundation (DFG) on the influence of generative models for text and image creation on the sciences and DFG funding* (September 2023) is referenced: The use of generative models like ChatGPT should not be excluded but requires transparent and comprehensible documentation to ensure scientific integrity. Scientists must disclose whether and how they used generative models and ensure that no intellectual property is violated or scientific misconduct occurs. This statement was established as the basis for dealing with AI at the Graduate School of Life Sciences (GSLS) University of Würzburg, according to a phone call with Dr. Jennifer Ritzer on 24.05.2024.

The AI-generated chat logs are accessible in the digital version of this work and serve as proof of compliance with the principles outlined here. It should be noted that the texts generated in the chat logs do not document subsequent manual revision, which is why ignored or also completely rewritten sections by the author are included in the chat logs.

The author independently noticed the following deficiencies of generative AI models:

- Unreliability in the accuracy of scientific facts
- Strong tendency to confirm the user's opinion
- Lack of precision and use of abstract formulations
- Hallucination of non-existent scientific sources

The author decided to ensure scientific integrity by ensuring that AI should not have a decisive influence on the core statements of the processed sections. To ensure this, **generative AI models** were not used for the following purposes:

- Collection or verification of scientific facts
- Expansion of the content of the work: The information contained in the prompts was not expanded by AI-generated content. Specifically, this means that ChatGPT was not used to gather ideas or scientific questions that would significantly influence the introduction, results, and/or discussion.
- Adoption of AI-generated texts without subsequent revision by the author
- Data analysis and statistics

ChatGPT (versions 3.5, 4, and 4.0) was used for the following purposes:

- Formulation of coherent text sections based on manually created raw text sections and notes
- Iterative improvement of formulations: Creating a first draft based on a raw draft, generating a version improved by ChatGPT, revising by the author, etc.
- Creation of summarizing sections (e.g., *Summary, Aims, Conclusion*) with subsequent revision
- Translating the Summary from English to German
- Programming assistance for formatting in LaTeX
- Searching for additional sources for already developed content, if available

GitHub Copilot (version 1.198.0) is specialized as a programming aid and was used to complete started sentences or code and to fix bugs.

From these principles, it is evident that generative AI models were used exclusively as programming, phrasing, and summarizing aids, comparable to tools such as *Grammarly*, which are considered unobjectionable. Accordingly, this work could have been completed without ChatGPT or GitHub Copilot, ensuring the author's independence.

The following **other software** was also used:

- Visual Studio Code (VS Code) as code and LaTeX editor, including plugins (e.g., for grammar correction)
- LaTeX (MacTex distribution)
- Zotero for citation of sources and automated creation of the bibliography, including plugins (ZotFile, Better BibTex, etc.)
- Affinity Publisher for image montage

Würzburg,

Place, Date

Signature of Author

C.4 Curriculum Vitae

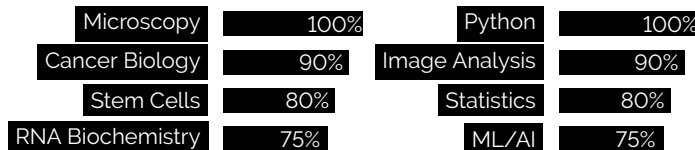
MARTIN KURIC

Cell Biologist | Data Scientist



WHO AM I?

As a cancer cell biologist with a strong passion for data analysis and machine learning, I am seeking a position where I can utilize my creativity to automate tasks, solve complex problems or handle big data.



SELECTED PROJECTS

2024	Python Software “ImageP” Accelerates batch processing of images of different sizes and types by >100%. <code>numpy</code> / <code>skimage</code> / <code>scipy</code>	GitHub Repository ⚡
2020-2024	Python Software “plotastic” Published a statistical library that self-configures based on intuitive plotting parameters. <code>pandas</code> / <code>matplotlib</code> / <code>pingouin</code> / <code>seaborn</code>	Journal of Open Source Software GitHub Repository ⚡
2018-2024	Cancer Research Project Worked in a team with up to three technical assistants and published a list of genes with relevance for survival of myeloma patients (under peer-review). <code>Time-Lapse Microscopy</code> / <code>RNAseq</code> / <code>Analysis of Patient Survival</code>	Journal: Cancer Research Communications
26.05.2022	Deep-Learning Assisted Image Cytometry Measurement of per-cell parameters from large automated microscopy scans. <code>Convolutional Neural Networks</code> / <code>Image Segmentation</code>	Poster at "Achilles Conference"

EDUCATION

28.01.2019 – 2024	Dr. rer. nat. in Biomedicine Research focus: Dissemination of multiple myeloma & mesenchymal stromal cell interactions	Prof. Dr. Regina Ebert University of Würzburg
01.04.2017 – 2024 parallel to M.Sc. & PhD	Elite Biological Physics Interdisciplinary & international study program for exceptional students of physics or biology.	University of Bayreuth
01.10.15 – 15.08.18	M.Sc. in Biochemistry & Molecular Biology Research focus: RNA biochemistry, small RNAseq, stem cells & piRNAs in <i>S. mediterranea</i>	Prof. Dr. Claus-D. Kuhn University of Bayreuth
01.10.12 – 14.12.15	B.Sc. in Biochemistry Research focus: Cell biology, mitochondrial inheritance in <i>S. cerevisiae</i>	Prof. Dr. Benedikt Westermann University of Bayreuth

LANGUAGES

German, English - C2
 Slovakian - passive
 French, Spanish - A2

SOFT SKILLS

Quality Management
 Project Management
 Violent Free Communication

HOBBIES

Coding - Python
 Music - Piano & Guitar
 Gym - Lift. Grow. Repeat

Würzburg

05.03.2024

Location

Date

Martin Kuric

Signature